CAPACI OCCASIO
FOUNDED 1894

SAIMM

JOURNAL OF THE SOUTHERN AFRICAN INSTITUTE OF MINING AND METALLURGY

VOLUME 117 NO. 8 AUGUST 2017

‘Green’ standards

The latest equipment for the mining and minerals-processing industry manufactured by MIP Process Technologies of Sandton, Johannesburg has been designed to comply with the pending 2018 South African emissions-control regulation of 30 mg/m^3 of particulates.

This is an indication of the OEM’s high level of innovation and commitment to ongoing technological development and product improvement, Managing Director **Philip Hoff** comments. Equipment manufactured ranges from attrition scrubbers to clarifiers and thickeners, linear screens, flocculant plants, mixers and agitators.

“Not only do we design all of our equipment to comply with the latest standards and regulations, but we also offer smaller companies a continuous plan to improve their dust-extraction emissions. Our approach is to collaborate closely with our clients to lower their total cost of ownership by optimising their equipment,” Hoff explains.

The OEM is currently manufacturing linear screens and a clarifier for an Australian customer in Panama at its factory in Springs, Gauteng. In South Africa, it is building three thickeners for a major platinum producer in Marikana. Other local projects include a range of flocculant and reagent plants for various customers.

Indeed, such is the quantity of work being derived locally at present that 75% of its business is located outside South Africa, as opposed to as little as 25% about a year ago. He adds that there has also been an upsurge in the chrome-mining industry due to rising commodity prices. “All in all, it looks like it will be a good year for us, and the future is bright.”

However, the OEM continues to expand globally, with agents as far afield as South America, Mexico, and Australia. “These regions are similar to South Africa in the sense of the size and scope of the mining projects that they are undertaking. Our minerals-processing equipment has a design life in excess of 30 years. Taken together, our pricing and quality mean we are still highly competitive compared to Asian and Chinese manufacturers,” Hoff points out.

Hence Hoff remains optimistic about the future and the OEM’s ongoing growth, spurred on largely by its 10 000 m^2 local manufacturing facility, which allows it to remain cost-competitive. “It also means we are able to design robust equipment matched to African operating conditions. Indeed, our experience has resulted in us supplying equipment from Russia to Egypt and North America.”

The OEM continues to enjoy a competitive edge in the marketplace due to its philosophy of manufacturing equipment “faster, better quality, quicker, and at a lower total cost. The quicker we can meet a customer’s order, the faster the equipment can be installed, so the project can be up and running and contributing to the bottom line as soon as possible. This also gives our project team in particular a bit of a window to look at the next project in the pipeline.” Hence the OEM has built a solid reputation for being responsive to customer requirements.

“We are working on a lot of coal-mining projects and platinum projects for junior mining companies,” Hoff confirms.

“We are looking at developing a more cost-effective product range specifically for this sector, as wastewater is a lighter-duty application than minerals-processing slurries. “

mip | PROCESS TECHNOLOGIES

MIP Process Technologies (Pty) Ltd. | P.O. BOX 677, Kelvin 2054 |
Tel: +27 (0) 11 234 1007 | Fax: +27 (11) 86 682 2394 |
E mail: sales@mipprocess.com | Website: www.mipprocess.com |
MIP House, 4A Coombe Place, Rivonia, 2128

Smart drilling

Improve production, productivity and profitability with the ground-breaking Atlas Copco SmartROC down-the-hole drill rig. Equipped with smart technology, the SmartROC sets the industry benchmark in intelligent, powerful and efficient high-precision drilling. Optimise drilling and blasting, improve accuracy, extend machine availability and life-cycle, reduce fuel consumption, and enhance operator safety and performance.

www.atlascopco.co.za

Sustainable Productivity

Atlas Copco

The Southern African Institute of Mining and Metallurgy

OFFICE BEARERS AND COUNCIL FOR THE 2016/2017 SESSION

Honorary President
Mike Teke
President, Chamber of Mines of South Africa

Honorary Vice-Presidents
Mosebenzi Zwane
Minister of Mineral Resources, South Africa

Rob Davies
Minister of Trade and Industry, South Africa

Naledi Pandor
Minister of Science and Technology, South Africa

President
C. Musingwini

President Elect
S. Ndlovu

Senior Vice-President
A.S. Macfarlane

Junior Vice-President
M.I. Mthenjane

Immediate Past President
R.T. Jones

Honorary Treasurer
J.L. Porter

Co-opted Member
Z. Botha

Ordinary Members on Council

V.G. Duke
I.J. Geldenhuys
M.F. Handley
W.C. Joughin
M. Motuku
D.D. Munro
G. Njowa
A.G. Smith
M.H. Solomon
M.R. Tlala
D. Tudor
D.J. van Niekerk
A.T. van Zyl

Past Presidents Serving on Council

N.A. Barcza
R.D. Beck
J.R. Dixon
M. Dworzanowski
H.E. James
G.V.R. Landman
J.C. Ngoma
S.J. Ramokgopa
M.H. Rogers
D.A.J. Ross-Watt
G.L. Smith
W.H. van Niekerk
R.P.H. Willis

Branch Chairpersons

Botswana	L.E. Dimbungu
DRC	S. Maleba
Johannesburg	J.A. Luckmann
Namibia	N.M. Namate
Northern Cape	C.A. van Wyk
Pretoria	P. Bredell
Western Cape	C.G. Sweet
Zambia	D. Muma
Zimbabwe	S. Matutu
Zululand	C.W. Mienie

Corresponding Members of Council

Australia:	I.J. Corrans, R.J. Dippenaar, A. Croll, C. Workman-Davies
Austria:	H. Wagner
Botswana:	S.D. Williams
United Kingdom:	J.J.L. Cilliers, N.A. Barcza
USA:	J-M.M. Rendu, P.C. Pistorius

PAST PRESIDENTS

*Deceased

* W. Bettel (1894–1895)
* A.F. Crosse (1895–1896)
* W.R. Feldtmann (1896–1897)
* C. Butters (1897–1898)
* J. Loevy (1898–1899)
* J.R. Williams (1899–1903)
* S.H. Pearce (1903–1904)
* W.A. Caldecott (1904–1905)
* W. Cullen (1905–1906)
* E.H. Johnson (1906–1907)
* J. Yates (1907–1908)
* R.G. Bevington (1908–1909)
* A. McA. Johnston (1909–1910)
* J. Moir (1910–1911)
* C.B. Saner (1911–1912)
* W.R. Dowling (1912–1913)
* A. Richardson (1913–1914)
* G.H. Stanley (1914–1915)
* J.E. Thomas (1915–1916)
* J.A. Wilkinson (1916–1917)
* G. Hildick-Smith (1917–1918)
* H.S. Meyer (1918–1919)
* J. Gray (1919–1920)
* J. Chilton (1920–1921)
* F. Wartenweiler (1921–1922)
* G.A. Watermeyer (1922–1923)
* F.W. Watson (1923–1924)
* C.J. Gray (1924–1925)
* H.A. White (1925–1926)
* H.R. Adam (1926–1927)
* Sir Robert Kotze (1927–1928)
* J.A. Woodburn (1928–1929)
* H. Pirow (1929–1930)
* J. Henderson (1930–1931)
* A. King (1931–1932)
* V. Nimmo-Dewar (1932–1933)
* P.N. Lategan (1933–1934)
* E.C. Ranson (1934–1935)
* R.A. Flugge-De-Smidt (1935–1936)
* T.K. Prentice (1936–1937)
* R.S.G. Stokes (1937–1938)
* P.E. Hall (1938–1939)
* E.H.A. Joseph (1939–1940)
* J.H. Dobson (1940–1941)
* Theo Meyer (1941–1942)
* John V. Muller (1942–1943)
* C. Biccard Jeppe (1943–1944)
* P.J. Louis Bok (1944–1945)
* J.T. McIntyre (1945–1946)
* M. Falcon (1946–1947)
* A. Clemens (1947–1948)
* F.G. Hill (1948–1949)
* O.A.E. Jackson (1949–1950)
* W.E. Gooday (1950–1951)
* C.J. Irving (1951–1952)
* D.D. Stitt (1952–1953)
* M.C.G. Meyer (1953–1954)
* L.A. Bushell (1954–1955)
* H. Britten (1955–1956)
* Wm. Bleloch (1956–1957)
* H. Simon (1957–1958)
* M. Barcza (1958–1959)
* R.J. Adamson (1959–1960)
* W.S. Findlay (1960–1961)
* D.G. Maxwell (1961–1962)
* J. de V. Lambrechts (1962–1963)
* J.F. Reid (1963–1964)
* D.M. Jamieson (1964–1965)
* H.E. Cross (1965–1966)
* D. Gordon Jones (1966–1967)
* P. Lambooy (1967–1968)
* R.C.J. Goode (1968–1969)
* J.K.E. Douglas (1969–1970)
* V.C. Robinson (1970–1971)
* D.D. Howat (1971–1972)
* J.P. Hugo (1972–1973)
* P.W.J. van Rensburg (1973–1974)
* R.P. Plewman (1974–1975)
* R.E. Robinson (1975–1976)
* M.D.G. Salamon (1976–1977)
* P.A. Von Wielligh (1977–1978)
* M.G. Atmore (1978–1979)
* D.A. Viljoen (1979–1980)
* P.R. Jochens (1980–1981)

G.Y. Nisbet (1981–1982)
A.N. Brown (1982–1983)

* R.P. King (1983–1984)

J.D. Austin (1984–1985)
H.E. James (1985–1986)
H. Wagner (1986–1987)

* B.C. Alberts (1987–1988)

C.E. Fivaz (1988–1989)
O.K.H. Steffen (1989–1990)

* H.G. Mosenthal (1990–1991)

R.D. Beck (1991–1992)

* J.P. Hoffman (1992–1993)
* H. Scott-Russell (1993–1994)

J.A. Cruise (1994–1995)
D.A.J. Ross-Watt (1995–1996)
N.A. Barcza (1996–1997)

* R.P. Mohring (1997–1998)

J.R. Dixon (1998–1999)
M.H. Rogers (1999–2000)
L.A. Cramer (2000–2001)

* A.A.B. Douglas (2001–2002)

S.J. Ramokgopa (2002-2003)
T.R. Stacey (2003–2004)
F.M.G. Egerton (2004–2005)
W.H. van Niekerk (2005–2006)
R.P.H. Willis (2006–2007)
R.G.B. Pickering (2007–2008)
A.M. Garbers-Craig (2008–2009)
J.C. Ngoma (2009–2010)
G.V.R. Landman (2010–2011)
J.N. van der Merwe (2011–2012)
G.L. Smith (2012–2013)
M. Dworzanowski (2013–2014)
J.L. Porter (2014–2015)
R.T. Jones (2015–2016)

Honorary Legal Advisers
Scop Incorporated

Auditors
Messrs R.H. Kitching

Secretaries
The Southern African Institute of Mining and Metallurgy
Fifth Floor, Chamber of Mines Building
5 Hollard Street, Johannesburg 2001 • P.O. Box 61127, Marshalltown 2107
Telephone (011) 834-1273/7 • Fax (011) 838-5923 or (011) 833-8156
E-mail: journal@saimm.co.za

Typeset and Published by
The Southern African Institute of Mining and Metallurgy
P.O. Box 61127
Marshalltown 2107
Telephone (011) 834-1273/7
Fax (011) 838-5923
E-mail: journal@saimm.co.za

Printed by
Camera Press, Johannesburg

Advertising Representative
Barbara Spence
Avenue Advertising
Telephone (011) 463-7940
E-mail: barbara@avenue.co.za

The Secretariat
The Southern African Institute of Mining and Metallurgy

ISSN 2225-6253 (print)
ISSN 2411-9717 (online)

SAIMM
JOURNAL OF THE SOUTHERN AFRICAN INSTITUTE OF MINING AND METALLURGY

VOLUME 117 NO. 8 AUGUST 2017

Contents

HYDROMETALLURGY CONFERENCE 2016

SAIMM
JOURNAL OF THE SOUTHERN AFRICAN INSTITUTE OF MINING AND METALLURGY
VOLUME 117 NO. 8 AUGUST 2017

Hydrometallurgy Conference 2016

'Sustainable Hydrometallurgical Extraction of Metals'

This edition of the *Journal* features papers that were presented at the Hydrometallurgy Conference, which was held from 31 July to 3 August 2016. The theme of the conference was 'Sustainable Hydrometallurgical Extraction of Metals' and it was attended by 150 delegates from around the world. The conference was organized in collaboration with the Western Cape Branch of the SAIMM.

The conference was preceded by a workshop on 'Test work and its importance in metallurgical design'. Topics presented at the workshop included a review of existing models for process and project development, process test work, flow sheet selection, simulation models, and case studies. The workshop was very well attended by industry delegates, academics, and students.

There were five keynote addresses. Professor Kwado Osseo-Asare from Penn State University, USA gave a very interesting talk on the fundamentals of hydrometallurgy, linking solid solution and nanoscience. Dr Frank Crundwell from CM Solutions, South Africa, discussed the linkages between corrosion, hydrometallurgy, and flotation. Professor Mike Nicol from Murdoch University, Australia, discussed the ineffectiveness of oxygen as an oxidant in hydrometallurgical processes. Professor Markus Reuter from Helmholtz Institute Freiberg for Resource Technology, Germany, gave a very stimulating presentation on the role of hydrometallurgy in a circular economy. Professor Bhargava from RMIT University in Australia covered a topic that resonated with most researchers; innovative research during hard times in the minerals industry. The keynote addresses were all of high quality, were very stimulating, complemented all aspects of the conference, but above all, had take-home messages for industry delegates, students, and researchers alike.

The papers presented at the conference highlighted the fact that although hydrometallurgical extraction of metals is still largely based on primary resources there is also a large amount of metal-containing waste material being generated in the metal production and manufacturing industries that has potential to act as a secondary source of metals. It was clear that global academic and industrial research into metal recovery from such secondary metal resources has become a focal point. The hydrometallurgy of copper was a hot topic as usual; a large number of papers were dedicated to copper processing and these sessions had a high attendance rate. It was particularly heartening to see the enthusiastic participation of many young and emerging mining and minerals professionals; they are the key enablers for the future of our industry.

The overwhelming interest shown in uranium processing suggested that there was a need for a focused event on this topic, and this was subsequently validated by the decision of the Technical Programme Committee – Metallurgy to hold a uranium conference in Namibia in the second half of 2017.

The contributions from the eleven companies that sponsored the Conference and the funding provided by the DST/NRF are gratefully acknowledged.

S. Ndlovu
Chairperson of the Organizing Committee

SAIMM
THE SOUTHERN AFRICAN INSTITUTE OF MINING AND METALLURGY

SAIMM *Journal* Management

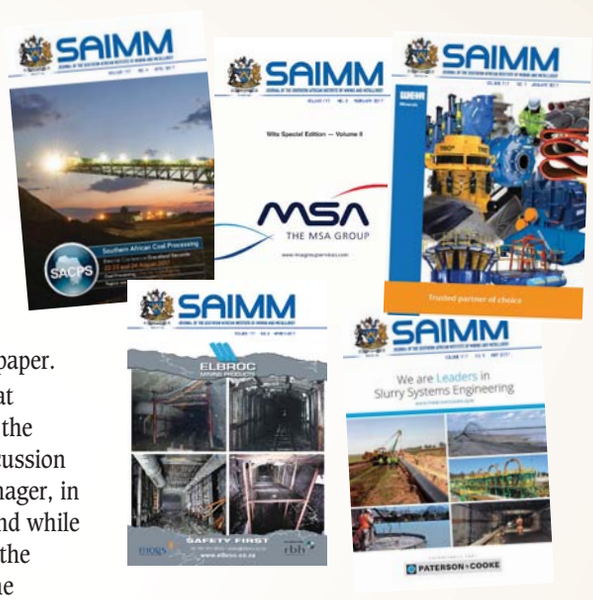

The SAIMM is adopting a new system to manage the publication of the *Journal*. The Open *Journal* System (OJS) for journal management is a free, web-based platform that has been developed by the Public Knowledge Project [https://pkp.sfu.ca] at the Simon Fraser University in British Columbia through its federally funded efforts to expand and improve access to research.

Our present system of handling the submissions to the *Journal*, the refereeing process, and the iteration that takes place between authors, reviewers, the *Journal* Coordinator, and proofreader is by e-mail, telephone, and paper.

With a view to improving the mechanics of the way that submissions to the *Journal* are processed and speeding up the approval for publication, we undertook an exploratory discussion with Aries Systems Corporation, who market Editorial Manager, in June 2015. An on-line demonstration was well received, and while Editorial Manager could do what was required, the cost of the system at $8000 pa was deemed to be prohibitive under the prevailing economic constraints. Similarly 'ScholarOne', which is marketed by Thomson Reuters and was introduced to us in June 2016, has very similar features and costs as Editorial Manager.

In February 2017 Dave Tudor attended a workshop hosted by the Academy of Science of South Africa (ASSAf) in Pretoria which detailed the OJS, the set-up, and management.

Ina Smith, the Project Manager: African Open Science Platform at ASSAf, has been instrumental in the development of the OJS in Africa. Ina gave a tutorial to Sam Moolla, Kelly Mathee, and Dave Tudor on 13 June 2017 which included a comprehensive introduction to the system and set-up.

While the set-up, which can be viewed at http://www.saimmjournal.co.za , can be added to and refined, the important business of establishing the procedures for submissions and review is nearing completion. An important first step is to contact each one of the referees on our database and request them to register as a reviewer on the OJS system.

There will be a period of time during which the new OJS process will be run in parallel with the existing 'manual' system until this system is cleared.

D. Tudor
Editorial Consultant

The last 100 days in the office of the SAIMM Presidency

When presidents or leaders are elected, it is often customary to expect them to deliver a speech when they attain their first 100 days in office. Barack Hussein Obama was inaugurated on 20 January 2009 as the 44th President of the United States, and gave a speech on his first 100 days in office on 29 April 2009. As is normal, his speech met with mixed reactions. Critics felt it was as vague as his campaign message, while supporters believed he was delivering on his campaign promises. It is during their first 100 days in office that presidents are scrutinized and watched particularly closely. Fortunately, in the SAIMM we have a rich tradition of leadership succession. Before one becomes President, one must have served at least two years on the SAIMM Council, followed by a year of co-option as an Office Bearer before successively becoming Junior Vice-President, Senior Vice-President, President-Elect, and President; After the term as President, one becomes Immediate Past-President and finally retires back onto Council as a Past President. There are therefore no campaign promises you need to make, as you become accustomed early on to the SAIMM's strategic direction, which you then continue to drive during your one-year Presidential term. I therefore found it prudent to write on my last 100 days in office.

The past 100 days have been quite busy, but I also had time to pause and reflect. The SAIMM has weathered the prevailing tough economic times, closely watching our revenue and expenditure streams to ensure that we survive the short-term. However, our long-term strategy remains a robust one of making the Institute a great Institute that we, the members, can all continue to be proud of. For example, support for the Young Professionals Council (YPC) and regional branches has been maintained, because these are critical for growing our membership base into the future. We have managed to grow our membership base to just above the 5000 mark.

However, despite the progress we have made, we cannot afford to be complacent because we are not out of the woods yet. The tough economic times are still upon us. My last 100 days have instilled confidence in me that the SAIMM will be around for a very long time to come, but we still need to do more. We still need to organize many viable quality conferences. We need to draw more into our membership ranks. We still need to continue to publish a quality *Journal*. We still need to continue to encourage each other in volunteering to serve on committees that drive the key activities of the SAIMM. We still need to continually motivate and support our office staff, who carry out the back-office work that ensures we can deliver the quality services that our membership mandates us to provide. There are many in our rank-and-file who can help, and they are encouraged to come forward to keep the wheels turning.

The past 100 days have also been an opportunity for me to look back at my experiences as President and share these with future presidents. My broad advice resonates with that of Jeff Immelt, former CEO of General Electric, when he stepped down after 16 years of service and handed over the leadership baton to John Flannery. Jeff said that in his advice to John 'I gave him maybe the most important advice for incoming CEOs, and that is: every job looks easy when you're not the one doing it.' My advice is that it is going to be tough being President, but it is always gratifying when you give of your best. Leadership is about building a strong team. What I have learnt is this: a good leader humbles himself, asks the right questions, listens to advice, is of service to others, and above all, is willing to learn. My last 100 days have taught me to be a better person and I am grateful to the SAIMM for the opportunity of serving you as President. I leave office with a great sense of hope for the future of the SAIMM.

C. Musingwini
President, SAIMM

Ivanplats, CanPro, and 'Maru A Mokopane' digitally activate communities

For South Africa's communities to become economically active, it is essential that they have access to information and communication technology (ICT).

The long-lamented 'digital divide' remains alive and well, but an increasing number of companies are realizing the benefit of fast-tracking digital access for their workforce and neighbouring communities.

CanPro, a provider of digital workplace development and monitoring solutions, recently assisted mining company Ivanplats to do just that. Ivanplats' Platreef platinum, gold, and nickel mining project is based in Mokopane, in South Africa's Limpopo Province. Its operations are at the heart of a large community marked by socioeconomic challenges such as youth unemployment.

Ivanplats had sought permission from the Department of Mineral Resources (DMR) to develop and implement a multi-faceted 'Youth Digital Communication Project' in Mokopane Municipality as part of its Social and Labour Plan. This aims to digitally activate the external mining communities, local businesses, and youth enterprises as well as Ivanplats' internal workforce to facilitate meaningful social and economic participation.

A spin-off for local unemployed youth is the opportunity to become providers of digital services in the area. With phase one in progress, 17 local youth enterprises have already trained over 3000 community members to connect to locally-provided free WiFi and utilize online services via a zero-rated community portal aptly named *Maru A Mokopane, or Clouds of Mokopane*.

Maru A Mokopane offers zero-rated access to opportunities, news, a local business directory, a feedback section, eLearning, and online banking as well as 300 MB daily to search any other sites.

Managing Director of Ivanplats, Dr Patricia Makhesha, describes some of the strategic goals of the project: 'We aim to build a common platform from which our internal and external communities can communicate and collaborate and have access to information such as news and alerts about matters that are important to them or present opportunities. At the same time, the community will have constant access to employment and procurement information at Ivanplats.'

Key stakeholders have expressed their enthusiasm for the project, which officially launched on Youth Day this year. Mogalakwena Municipality Acting Mayor, Councillor Pheladi Olifant says: 'The internet connection Ivanplats will be providing to our villages will become an essential resource in today's modern economy that none of us can afford to live without.'

Liesel Kirsten, Managing Director of CanPro, says: 'Ivanplats is the most recent manifestation of our solution that is designed to help companies bridge the digital divide with meaningful, user-friendly, and accessible digital services delivered via customized community portals. As our network of clients expands, we are also in a better position to foster collaboration between communities and engage other companies who wish to add value in particular locations by investing in digital services for their stakeholders.'

Sheryl Thiel Consulting

http://dx.doi.org/10.17159/2411-9717/2017/v117n8a1

Physical and chemical transformations of gangue materials during leaching of copper sulphides, and their influence on copper leaching kinetics

by T. Vargas*, F. Rojas*, C. Bahamondez*, R. Castro*, C.F. Ihle*, M. Caraballo*, and E. Widzyk-Capehart*

Synopsis

This work reports preliminary results from investigations of the chemical and physical transformations of gangue materials during ferric leaching of a copper sulphide ore in sulphuric acid solutions, and their effect on copper leachability. Experiments were conducted with sulphide ore containing 0.6% Cu, consisting mainly of chalcopyrite, chalcocite, and covellite particles in the size range -3/8 +1/4 inches (6.3–9.5 mm). Leaching was conducted on small flooded ore beds using solutions containing 10 g/L H_2SO_4 and 3 g/L Fe^{3+}. Leaching solutions were maintained at a constant pH (pH = 1) and at a constant Eh (0.75 V/NHE) during the experiments. Leaching progress was monitored through analysis of Cu, Fe, Si, Al, Ca, and Mg in solution. Chemical transformations in the ore were characterized by XRD and changes in the internal porosity of ore particles were characterized by measuring nitrogen adsorption with a sorptometer. The results showed a fivefold increase in internal porous area of the ore particles due to selective leaching of gangue species under acid attack. Variation in ore porosity influences the kinetics of copper dissolution, presumably due to the liberation of sulphide particles occluded in the gangue.

Keywords
ferric leaching, copper sulphide, porosity, gangue minerals.

Introduction

Heap leaching is a well-established technology that enables the economic processing of various types of low-grade ores in the copper industry, which could not otherwise be exploited (Ghorbani *et al.*, 2011; Watling, 2006). In the case of secondary sulphide copper ores, heap leaching can offer a process alternative that is economically more attractive than the conventional concentration and smelting route. Compared to other extractive technologies, heap leaching is unique in that relatively large particles sizes are treated, typically 12–25 mm top size for crushed and agglomerated ores and larger for run-of mine dump leaching operations or *in-situ* leaching. Accordingly, despite much progress since it was first applied in recent times, the process remains limited by low recoveries and long extraction times.

The rate of copper leaching and the extent of final copper recovery from heaps, dumps, and *in situ* operations are to a great extent limited by the limited access of leaching solutions to copper sulphide particles occluded in the gangue (Watling *et al.*, 2014). Increased access of the solution to the copper sulphides can be gained by further reducing the ore particle size by crushing, when economically acceptable. In fact, a relationship between the percentage of copper minerals exposed with respect to particle size can provide a good basis for predicting copper recovery for a known particle size distribution (Miller *et al.*, 2003; Dhawan *et al.*, 2012). It would be economically advantageous to find ways of improving the leaching rate of copper minerals that remain occluded in the gangue without further reduction in particle size. The leaching rate is very slow as it depends on the diffusion of lixiviant and soluble products through gangue materials that encapsulate the copper minerals, and which can present very low natural porosity (Watling *et al.*, 2014). Leaching improvements have been obtained by utilizing crushing techniques such as the high-pressure grinding roll (HPGR), which induces a high level of microfracturing that increases diffusion rates in the gangue (Ghorbani *et al.*, 2013). The influence of microfracturing produced by blasting on copper leaching recoveries has been also investigated (Parra *et al.*, 2015).

It is well known that during leaching there is an important degree of gangue dissolution under acid attack (Hiskey, 1992). This is shown by the incorporation of a wide variety of ions into the pregnant leach solution (Crundwell, 2015). However, little research has been done to study the influence that this dissolution process could have on the structure of the gangue and, eventually, on the mechanism of dissolution of copper mineral particles. The present work is part of a research programme aimed at identifying chemical and biological routes to improve the

* *Advanced Mining Technology Center (AMTC), University of Chile, Santiago, Chile.*
 This paper was first presented at the Hydrometallurgy Conference 2016 'Sustainable Hydrometallurgical Extraction of Metals', *1–3 August 2016, Belmont Mount Nelson Hotel, Cape Town.*

access to and leachability of mineral particles occluded in the ore. Experimental results so far obtained have enabled the quantification of the porosity created by acid attack on gangue materials during ferric leaching of copper sulphide ores, and led to investigations of the influence of acid pretreatment on copper leaching rate.

Experimental

Leaching experiments were conducted on a copper ore sample with particle size in the range -3/8 +1/4 inches (6.3–9.5 mm). The ore contained 0.6% Cu, 6.1% Fe, 5.6% S, 51.8% Si, 21% Al, 6.8% Ca, and 2.5% Mg. Cu was mainly present in chalcopyrite, chalcocite, and covellite. The contents of the main species present in the ore, obtained from X-ray diffraction analysis, are listed in Table I. Leaching experiments were conducted in a system of flooded differential ore columns, which consisted of small ore beds with a mass of about 600 g completely immersed in about 3 L of leaching solution. The solution was gently stirred during the leaching experiment to circulate it inside the ore bed and prevent the formation of internal concentration gradients of reactants (see Figure 1).

Three different experiments were conducted. In experiment A the ore was leached for 288 hours with a solution containing 10 g/L H_2SO_4 and 3 g/L Fe^{+3}; in experiment B, which was an acid pre-treatment, the ore was leached for 288 hours with a solution containing only 10 g/L of H_2SO_4; in experiment C the same ore initially leached in Experiment B was leached for a further 264 hours with a solution containing 10 g/L H_2SO_4 and 3 g/L Fe^{+3}. Experiments were conducted at 30°C under iso-pH conditions (pH 1), maintained by periodical addition of H_2SO_4, and under iso-Eh conditions (0.75 V/NHE), maintained by periodical additions of peroxide. Leaching progress was monitored by analysis of Cu, Fe, Al, Ca, Si, and Mg in the leaching solution. Chemical transformations of the ore in experiment A were characterized by XRD analysis of the initial and leached ore samples. Changes of internal porosity of ore particles in experiment A were characterized by analysis of the initial and leached samples with a sorptometer (Micromeritics ASAP 2010), which measured the internal area of the particles by adsorption of nitrogen by the BET method (Brunauer, Emmett, and Teller, 1938).

Table I

Mineralogy of the copper sulphide ore from X-ray diffraction analysis

Species	Formula	Content (%)
Quartz	SiO_2	18.37
Anhydrite	$Ca(SO_4)$	3.11
Anorthite	$CaAl_2Si_2O_8$	49.54
Chalcocite	Cu_2S	0.71
Chalcopyrite	$CuFeS_2$	0.68
Augite	$Ca(Mg_{0.85}Al_{0.15})(Si_{1.70}Al_{0.30})O_6$	1.45
Esseneite	$Ca(Fe_{1.4}Al_{0.6})SiO_6$	0.1
Covellite	CuS	0.48
Rutile	TiO_2	0.15
Illite	$(K,H_3O)Al_2Si_3AlO_{10}(OH)_2$	15.59
Phlogopite	$KMg_3(Si_3Al)O_{10}(OH)_2$	7.15
Clinochlore	$(Mg,Al,Fe)_6(Si,Al)_4O_{10}(OH)_8$	2.69

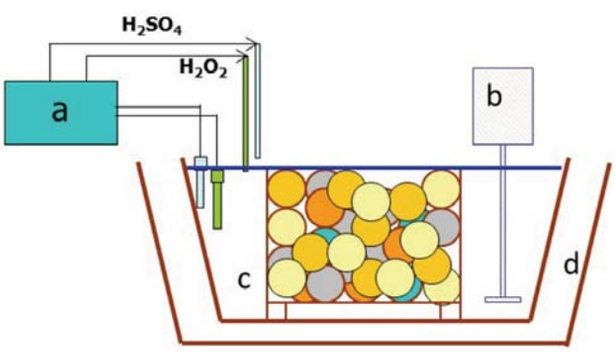

Figure 1—Schematic of the leaching experimental apparatus. (a) pH, Eh sensors, (b) stirrer, (c) flooded ore column, (d) thermostatic bath

Results and discussion

The dissolution results for experiment A, which corresponds to ferric leaching of the ore, are shown in Figure 2. Copper reached a maximum concentration of 27 mg/L in solution, which corresponds to 2.3% recovery. Solution concentrations of elements associated with gangue minerals were 664 mg/L Ca (5.0% recovery), 210 mg/L Mg (4.3% recovery), 223 mg/L Al (0.54 % recovery), and 321 mg/L Si (0.32 % recovery). The presence of gangue elements in solution can in principle be attributed to dissolution of clinochlore, phlogopite, augite, and anhydrite, the contents of which were drastically reduced in the leach residue. However, the percentage of dissolved calcium cannot be explained solely on these grounds, and indicates that a fraction of the anorthite was also dissolved.

Table II shows the results of porosity measurements of the copper ore before and after leaching in experiment A. The leaching greatly increased the surface area of the ore, from 0.593 to 3.51 m^2/g, which represents an increase of about six times. The porosity of the leached residue was 2.6 times greater than in the untreated ore. The average pore diameter in the leached sample, however, was smaller than in the untreated ore sample, and varied from 81.8 to 40.8 Å. This indicates that the newly created porosity consisted of a network of pores much smaller than those originally present in the ore.

The porosity increase observed in experiment A can be in principle related to partial dissolution of gangue minerals under acid attack, as observed from the amounts of Al, Ca, Mg, and Si dissolved. In order to assess the potential effect of the porosity increase on copper leaching, a series of experiments was designed in which copper dissolution was measured during ferric leaching of an ore sample after acid pretreatment. Accordingly, the fresh ore was initially leached in a solution containing only 10 g/L of H_2SO_4 (experiment B) and immediately thereafter was further leached in a solution containing 3 g/L Fe^{+3} and 10 g/L H_2SO_4 (experiment C).

Figure 3 shows the dissolution results for experiment B. Comparison of Figures 2 and 3 shows that the rate of dissolution of Ca, Al, Si, and Mg was very similar in both experiments, confirming that these ions originate from the dissolution of gangue minerals by H_2SO_4, which was at the same concentration in both experiments. The copper extraction in experiment A (2.32%) was about three times

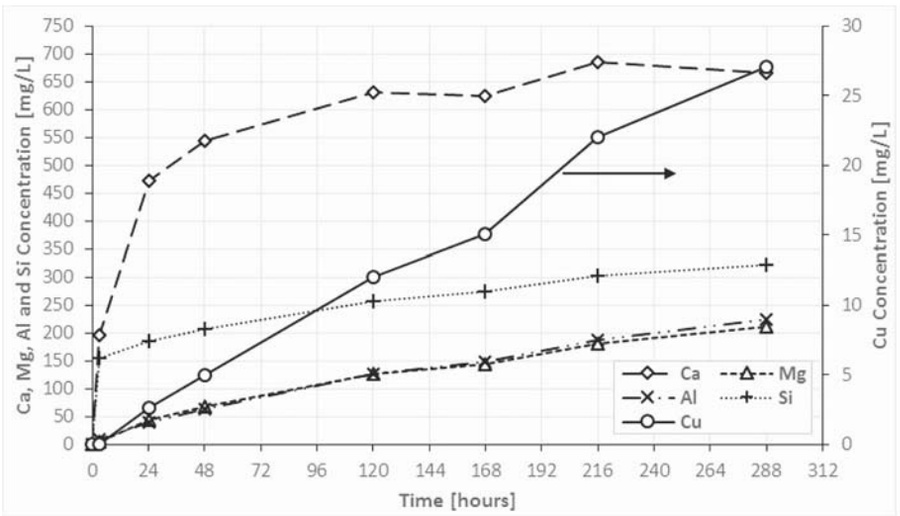

Figure 2—Dissolution of Ca, Mg, Al, Si, and Cu in experiment A

Table II

Porosity and surface area measurements by BET

	Pre-leach	Post-leach	Difference
Pore area (m^2/g)	0.4793 0.7074	3.137 3.883	- -
Average	**0.593**	**3.51**	**5.9 times (+500%)**
Pore volume (cm^3/g)	0.001352 0.001045	0.003332 0.003716	- -
Average	**0.001199**	**0.003224**	**2.6 times (+260%)**
Pore diameter (Å)	76.4223 87.2117	34.3264 47.3816	- -
Average	**81.817**	**40.854**	**0.5 times (-50%)**

that observed in experiment B (0.89%). This difference is consistent with the presence of 3 g/L of Fe^{+3} in the leaching solution of experiment A, which triggers ferric leaching of copper sulphides. Copper dissolution in experiment B under acid leaching is unexpectedly high, considering that the sample did not contain copper oxides. Copper leaching in this case can be explained in part as the result of the oxidative leaching of copper sulphides by ferric ions released during the dissolution of iron-containing gangue species such as clinochlore, and partial oxidation by dissolved oxygen. It is also possible that it originates from acid dissolution of chalcocite.

Figure 4 shows the copper dissolution for experiments A, B, and C. Copper dissolution in experiment C started slowly, probably due to the initial depletion of sulphide particles directly exposed on the surfaces of the ore particles, which were presumably leached during the acid pretreatment step. However, after 72 hours of leaching, the copper dissolution rate in experiment C began to increase continually. In fact, after 264 hours of leaching in experiment C, copper dissolution exceeded that obtained in the same leaching time in experiment B, by ferric leaching without acid pretreatment.

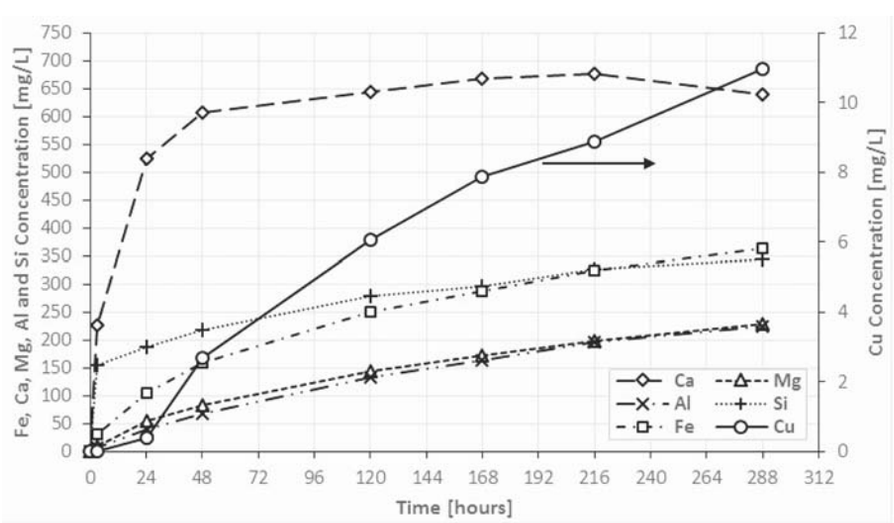

Figure 3—Dissolution of Fe, Ca, Mg, Al, Si, and Cu in experiment B

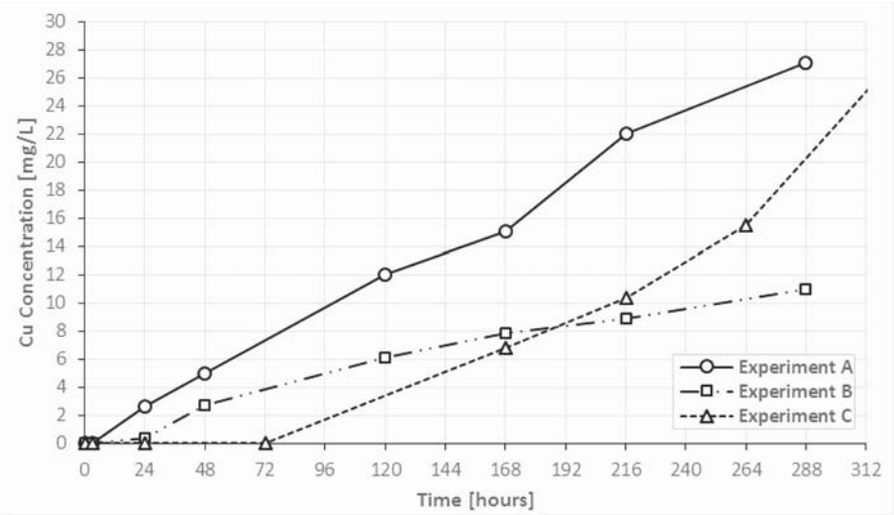

Figure 4—Copper dissolution in experiments A, B, and C

It has been reported that in porphyry copper ores, copper sulphides can be associated with quartz, feldspars, and some types of mica (Watling *et al.*, 2014). In the ore used in the current study, it is very likely that an important fraction of the copper sulphides is associated with anorthite, a feldspar that constitutes about 50% of the gangue (Table I). It is well known that feldspars are subject to acid attack during heap leaching, which causes accumulation of potassium, sodium, aluminium, and silica in processing circuits (Crundwell, 2015). Therefore, the increase in copper leaching rate observed here is presumably due to the liberation of copper sulphide particles by partial dissolution of anorthite under acid attack.

Conclusions

Secondary sulphidic copper ores subjected to ferric leaching with 3 g/L Fe^{+3} in 10 g/L sulphuric acid solutions underwent a dramatic increase in internal porosity. Pretreatment of the ore with acid leaching confirmed that the porosity increase was related to selective dissolution of gangue minerals under acid attack. The increase in gangue porosity influences the rate of copper leaching, suggesting that acid attack of the gangue contributes to liberation of some sulphide particles occluded in the gangue.

Further research is necessary to identify the mechanism of porosity formation under acid attack and quantify its influence on the copper leaching rate.

Acknowledgements

Financial support from Conicyt Basal Project FB0809 is gratefully acknowledged.

References

Brunauer, S., Emmett, P.H., and Teller, E. 1938. Adsorption of gases in multimolecular layers. *Journal of the American Chemical Society*, vol. 60. pp. 309–319.

Crundwell, F.K. 2015. The mechanism of dissolution of the feldspars: Part I. Dissolution at conditions far from equilibrium. *Hydrometallurgy*, vol. 151. pp. 151–162

Dhawan, N., Safarzadeh, M.S., Miller, J.D., Moats, M.S., Rajamani, R.K., and Lin, C-L. 2012. Recent advances in the application of X-ray computed tomography in the analysis of heap leaching systems. *Minerals Engineering*, vol. 35. pp. 75–86.

Ghorbani, Y., Becker, M., Mainza, A., Franzidis, J-P., and Petersen, J. 2011. Large particle effects in chemical/biochemical heap leach processes – a review. *Minerals Engineering*, vol. 24. pp. 1172–1184.

Ghorbani, Y., Mainza, A.N., Petersen, J., Becker, M., Franzidis, J-P., and Kalala, J.T. 2013. Investigation of particles with high crack density produced by HPGR and its effect on the redistribution of the particle size fraction in heaps. *Minerals Engineering*, vol. 43–44. pp. 44–51.

Hiskey, J.B., Oner, G., and Collins, D.W. 1992. Recent trends in copper in situ leaching. *Mineral Processing and Extractive Metallurgy Review*, vol. 8. pp. 1–16.

Miller, J.D., Lin, C.L., Garcia, C., and Arias, H. 2003. Ultimate recovery in heap leaching operations as established from mineral exposure analysis by X-ray microtomography. *International Journal of Mineral Processing*, vol. 72. pp. 331–340.

Parra, H., Onederra, I., Michaux, S., Kuhar, L., McFarlane, A., and Chapman, N. 2015. A study of the impact of blast induced conditioning on leaching performance. *Minerals Engineering*, vol. 74. pp. 1–12.

Watling, H.R. 2006.The bioleaching of sulphide minerals with emphasis on copper sulphides — a review. *Hydrometallurgy*, vol. 84. pp. 81–108.

Watling, H.R., Shiers, D.W., Li, J., Chapman, N.M., and Douglas, G.B. 2014. Effect of water quality on the leaching of a low-grade copper sulfide ore. *Minerals Engineering*, vol. 58. pp. 39–51. ◆

http://dx.doi.org/10.17159/2411-9717/2017/v117n8a2

Extraction of rare earths from iron-rich rare earth deposits

by K. Bisaka*, I.C. Thobadi*, and C. Pawlik*

Synopsis

Rare earth metals are classified as critical metals by the United Nations, as they have found wide application in the fabrication of magnets, particularly those used in green energy technologies which mitigate global warming.

Processing of ores containing rare earth elements is complex, and differs according to the nature of each ore. In the conventional process, run of mine (ROM) ores are processed in a physical separation plant to produce a concentrate from which rare earth elements are extracted via a hydrometallurgical route. To extract rare earth elements economically, multiple sequential physical and chemical separation steps are used to produce a mixture of rare earth salts, followed by purification and production of metals and alloys.

Large iron-rich rare-earth-bearing deposits exist in China, Southern Africa, Canada, and Australia. Although these deposits carry significant reserves of rare earth elements, a number of them are not exploited as no economically viable process exists to do so. The mineralogy of the difficult deposits is complex, with rare earth minerals of particle size less than 20 μm disseminated in a matrix of iron oxide such as haematite, magnetite, or goethite. A process comprising fine milling for liberation of rare earth minerals, and physical upgrading of the resulting materials, would be technically challenging, inefficient, and not economically viable. Globally, research efforts are directed towards the development of novel methods and new reagents to overcome these difficulties.

PyEarth™ is a novel process currently under development at Mintek, that is aimed at achieving efficient extraction of rare earths from the mineralogically complex iron-rich, rare-earth-bearing ores. The process incorporates a preliminary smelting step to reduce the iron to the metallic state and concentrate the rare earths into the slag phase, followed by leaching of the slag and recovery of the rare earths from the leach liquor. Tests at the laboratory scale on samples from deposits originating from Southern Africa have proved that the extraction of rare earths from iron-rich, rare-earth-bearing ores using this process is technically feasible, robust, and viable.

Keywords

PyEarth™, iron-rich rare-earth-bearing ore, direct smelting, rare-earth-rich slag, hydrochloric leaching, rare earth.

Introduction

The rare earths are listed amongst the strategic metals by the United Nations because of their properties and increasing usage (Long *et al.*, 2010). Among many possible applications, rare earths are used to sustain today's lifestyle through the manufacture of magnets, catalysts, weaponry, production of green electricity, *etc.*

Current global production is about 130 kt/a of rare earth oxides (REO), with about 90% of this coming from China. Consumption of rare earths is projected to increase at a rate of 6–10% per annum and could reach 200 kt/a in the very near future (Long *et al.*, 2010; Haque *et al*, 2014; Wang *et al.*, 2015; Li and Yang, 2014). More than 50% of today's global consumption of rare earths is currently located in China.

The proven global rare earth reserves are estimated at about 110 Mt of REO (Wang *et al.*, 2015). China's resources of rare earths are the largest and are estimated at about 48 Mt of REO or about 43% of the global reserves. Other rare earth resources are located in Russia (17.3%), the USA (11.8%), Australia, India, Brazil, and Greenland (Gupta and Krishnamurthy, 2004). Placer deposits of ilmenite as well as phosphate deposits are also considered to some extent as resources of rare earths. Placer deposits that predominantly contain monazite are mainly found in Australia, India, South Africa, Mozambique, Kenya, and Malawi. Historically, rare earths have been produced in South Africa and (sporadically) in the Democratic Republic of Congo. As reported by Gupta and Krishnamurthy (2004), Namibia has the second largest reserve worldwide with about 20 Mt REOs, and South Africa has about 1 Mt. Despite the existence of large deposits, Africa's contribution to the global supply of rare earths is insignificant.

Production of rare earths from ores involves a complex process that is designed according to the nature and mineralogy of each ore deposit. Basically, run-of-mine rare-earth-bearing ores are beneficiated by physical methods into a concentrate that is leached to extract the rare earth species. In very few situations, an *in-situ* leaching process (also

* *Mintek, Randburg, South Africa.*
 ISSN 2225-6253. This paper was first presented at the Hydrometallurgy Conference 2016 'Sustainable Hydrometallurgical Extraction of Metals', *1–3 August 2016, Belmont Mount Nelson Hotel, Cape Town.*

called solution mining) is carried out in which the leaching reagent is injected into wells drilled in the orebody to selectively leach the rare earth species, and the leachate is collected, thus minimizing environmental pollution (Li and Yang, 2014). Rare earths are extracted from the leachate and transformed into pure rare earth oxides, chlorides, or halides by hydrometallurgical means. Pure rare earth metals and rare-earth-metal alloys are produced by direct reduction of rare earth oxides, reduction of anhydrous chlorides and fluorides, and fused salt electrolysis of rare earth chlorides or oxide-fluoride mixtures. Pure rare earth oxides may be prepared by selective oxidation, selective reduction, fractional crystallization, ion exchange, and solvent extraction. Chlorides and fluorides are produced by transformation of rare earth oxides (Gupta and Krishnamurthy, 2004; Mishra and Anderson, 2014).

A rare earth deposit is valuable only when the metal values can be extracted in a cost-effective, efficient, sustainable, and environmentally responsible manner. Although a large number of deposits have been explored worldwide, only a few are mined for rare earths. The most prominent rare earth mining operations are Bayan Obo in China, Mount Weld in Australia, and Mountain Pass in the USA, which has been on care and maintenance since 2015 (Haque *et al.*, 2014; Li and Yang, 2014).

Bayan Obo is the largest exploited iron-rich rare earth deposit. The ore contains up to 6% REO and 35% Fe. More than 90% of the rare earth elements (REE) in the ore exist as independent minerals, and about 4–7% of the total rare earth minerals are disseminated in the iron oxide minerals. The Bayan Obo deposit contains bastnaesite and monazite, with magnetite and haematite as the dominant iron ore minerals. This ore is upgraded to a 65% REO concentrate with an overall rare earth recovery of about 61% via a complex beneficiation process. The milled ore, 90–95% passing 74 μm, is submitted to low-intensity magnetic separation (LIMS) and high-intensity magnetic separation (HIMS) to produce a mixed concentrate containing about 9.78–12% REO. The mixed concentrate is subjected to a HIMs cleaner stage to separate the haematite, which is recovered by reverse flotation, while the HIMS cleaner tails, containing most of the rare earth minerals, are beneficiated by flotation to obtain a high- (60% REO) and a low- (>30% REO) grade concentrate. This is followed by selective flotation to separate bastnaesite and monazite. Higher recoveries of up to 75% can be achieved at a lower concentrate grade (Li and Yang, 2014).

The Mount Weld mine, which was opened in 2011, exploits one of the world's highest grade rare earth deposits, with an average REO grade of 15.4%. Mount Weld has been described as a secondary rare-earth phosphate deposit, but the phosphates (most likely monazite) are encapsulated in iron oxide minerals (Haque *et al.*, 2014). Mount Weld produces a rare earth concentrate and an iron ore concentrate for further beneficiation.

Upgrading of some of the rare earth ores is challenging, due to the complexity of the mineralogy. This was the case for two specific iron-rich rare earth deposits in the Southern African region. Milling was not able to liberate the rare earth minerals from the iron mineral matrix. In this paper we present the results of an investigation into the processing of iron-rich rare-earth-bearing ores from the Southern African region.

Process overview – iron-rich rare-earth-bearing ores from Southern Africa

Brief mineralogy and implications

Two samples of iron-rich rare-earth-bearing ore from two deposits in Southern Africa were evaluated. In both samples, the bulk of the REE are contained in monazite minerals less than 20 μm in size. Rare earth mineralization occurs as coatings on haematite/goethite or as grains disseminated in the haematite/goethite matrix. The ores also contain bastnaesite, synchysite, ancylite, pyrochlore, REE-apatite, and rhabdophane. Quartz, jarosite, svanbergite, apatite, barite, mica, clays, crandallite, gorceixite, carbonates, and nordite are present as gangue minerals. Monazite and ancylite often occur as submicroscopic inhomogeneous grains in association with Fe-oxyhydroxides. Ancylite is associated with calcite and apatite. The main Fe-carbonate minerals are dolomite/ankerite, with minor calcite and Fe-oxyhydroxides. The gangue contains REE minerals less than 10 μm in size.

Fine milling to below 20 μm to liberate the rare earth minerals in order to selectively separate them (principally from haematite or goethite) was extensively investigated by Mintek's Mineral Processing Division. Most of the conventional physical separation techniques were found to be inefficient.

Globally, research efforts are directed towards the development of novel methods and new reagents to overcome these difficulties. Bulk leaching of these ores to extract rare earths inevitably solubilizes iron minerals and increases acid consumption. Removal of the iron from the leachate requires excessive amounts of reagents such as lime. This, in addition to the discarding of the iron precipitate, increases the cost of the process, usually beyond economic viability. Methods for extracting rare earths without affecting the value of the iron minerals are required to improve the economics of processing these ores.

High-temperature processing of iron-rich rare earth ores

Separation of iron and rare earths is theoretically possible by carbothermic reduction and could be an alternative to physical upgrading of the ore. As shown in the Ellingham diagram for pure oxides (Figure 1), iron oxide can be selectively reduced over rare earth oxides. However, in the present case, smelting would be required to enable efficient separation of iron metal from the rare-earth oxide bearing slag. Rare earth oxides are stable under the iron smelting conditions generally described by the temperature and oxygen partial pressure, therefore they will report to the slag phase while the iron will report to the metal phase. However, the most important step is the extraction of the rare earths from the slag. Hydrometallurgical methods were investigated for this purpose.

In practice, smelting of the ore and solubilization of the rare earth oxides through acid leaching is affected by the ore mineralogy and impurities. The mineralogy of the ore affects the kinetics of both smelting and leaching.

Principle of the PyEarth process

The 'PyEarth' process flow sheet, as presented in Figure 2, incorporates the smelting of ore, leaching of rare earths from

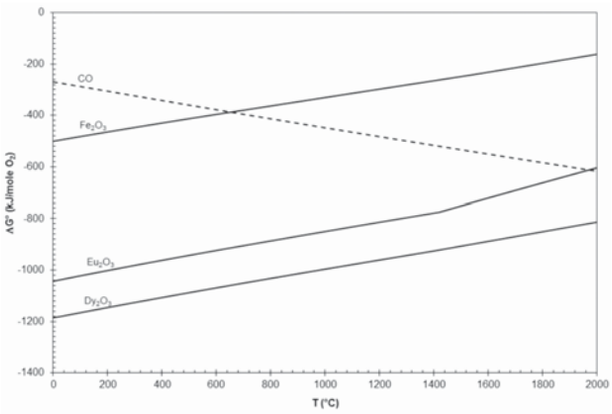

Figure 1—Ellingham diagram for pure oxides

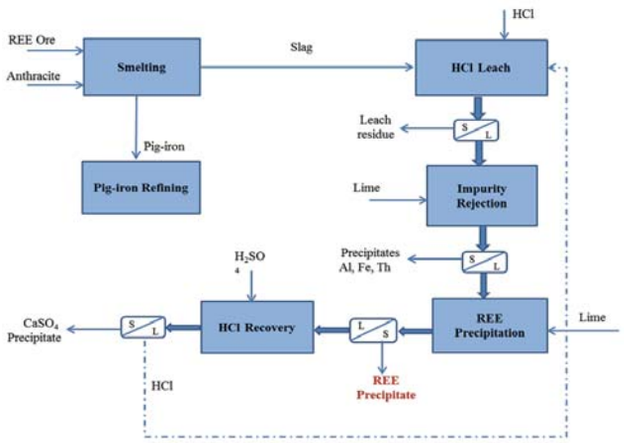

Figure 2—Proposed flow sheet for the PyEarth™ process

the resulting slag, and recovery of the rare earths from the leach liquor. Smelting of the ore to a slag in which the REE are concentrated, as well as a metal product, followed by leaching of the slag, constitute the main critical steps of this process. In practice, there is more than one option/technique available for smelting, leaching, and recovery of rare earths from the solution. However, for simplicity, the flow sheet considers the use of a DC open-arc furnace to smelt the ore, leaching in a hydrochloric medium, precipitation of impurities, precipitation of the rare earths, and recovery of HCl. As opposed to other smelting reactors such as blast furnaces and submerged-arc electric furnaces, the DC open-arc furnace is able to process ore fines without prior preparation and the complex nature of the mineralogy is easily managed by way of temperature control. This reactor would be an appropriate option for the smelting of the mineralogically complex iron-rich, rare-earth-bearing ores.

Upgrading of the slag prior to leaching to remove constituents other than REOs is not included in the basic flow sheet presented in this paper. However, this option may improve the efficiency of the subsequent hydrometallurgical operations if physical upgrading (such as electrostatic and magnetic concentration, froth flotation, and gravity concentration) is introduced post-taphole.

The results of preliminary smelting and leaching tests are presented and discussed in the following sections.

Smelting

Raw materials

A sample of iron-rich rare-earth-bearing ore from a Southern African deposit was subjected to series of laboratory tests. The bulk chemical composition was determined by simultaneous inductively coupled plasma–optical emission spectrometry (ICP-OES) (Varian Vista-PRO CCD), and the morphological and phase chemical compositions were determined by scanning electron microscopy (SEM) (Zeiss MA15 with energy-dispersive spectrometry (EDS) (Bruker) and X-ray diffractometry (XRD) (Bruker D8 Advance), respectively. The chemical composition of the ore is given in Table I, and the proximate analysis of the anthracite used as reductant is given in Table II. High-purity CaO was used as a fluxing agent to improve the smelting process, particularly to decrease the slag liquidus temperature and viscosity, constraints that are exacerbated at small scale.

Table I

Summary of the bulk chemical composition of the iron-rich rare earth ore

	MgO (%)	Al_2O_3 (%)	SiO_2 (%)	CaO (%)	TiO_2 (%)	V_2O_5 (%)	Cr_2O_3 (%)	MnO (%)	FeO(OH) (%)	S/A	S/M	P_2O_5 (%)
Ore 1	1.13	6.48	6.08	2.06	3.87	0.109	0.073	9.09	46.9	0.94	5.38	1.77

	La (mg/kg)	Ce (mg/kg)	Pr (mg/kg)	Nd (mg/kg)	Sm (mg/kg)	Eu (mg/kg)	Gd (mg/kg)	Dy (mg/kg)	Er (mg/kg)	TREE (%)	Th (mg/kg)	U (mg/kg)
Ore 1	6060	10200	921	3900	478	145	435	166	99.8	2.34	221	71.6

TREE: Total rear earth elements
Ho, Tm, Lu, Yb : REE with concenterations less than 100 ppm
S/A: ratio of silica to alumina
S/M: ratio of silica to MgO

Table II

Summary of the bulk chemical composition of the anthracite (mass %)

Ash	Volatile	Fixed carbon	Total sulphur
4.74	6.19	89.1	0.56

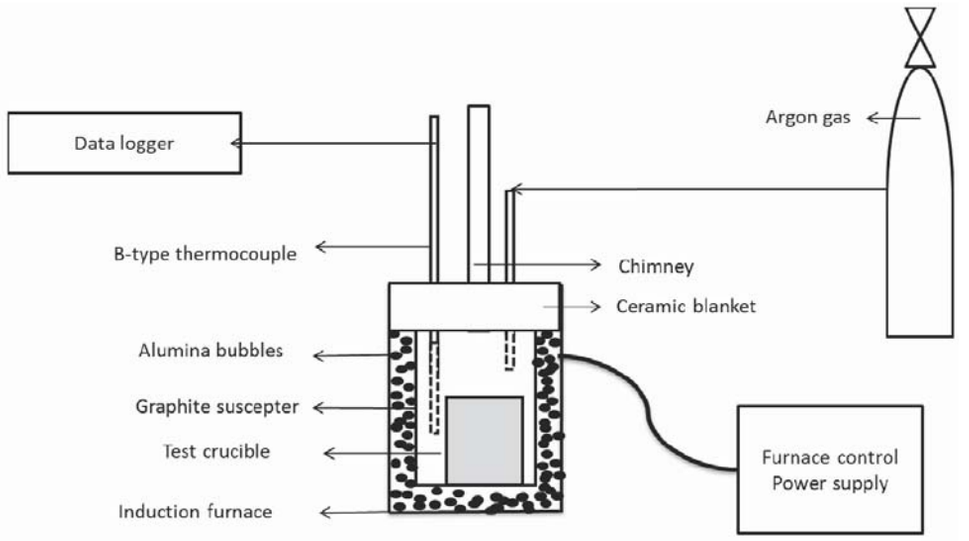

Figure 3—Schematic of the induction furnace experimental set-up

Experimental procedure

Laboratory smelting tests were conducted in 30 kW and 60 kW induction furnaces. Figure 3 shows a schematic of the induction furnace set-up.

The raw material components for the test conditions specified in Table III were blended and packed in a graphite crucible. Tests 1 and 2 were unfluxed tests conducted at stoichiometric anthracite addition and different temperatures. In this particular case, the anthracite amount was calculated so as to fully reduce the iron and manganese oxides. Tests 3 and 4 were fluxed with 0.5% CaO with stoichiometric anthracite addition, and conducted at two different operating temperatures.

Table III

Conditions for laboratory smelting tests

Test	Anthracite (%)	CaO (%)	Temperature (°C)
1	100	0	1700
2	100	0	1800
3	100	0.5	1700
4	100	0.5	1600

The packed crucible was placed at the centre of the graphite susceptor in the induction furnace. A B-type thermocouple was secured next to the crucible, and argon gas was purged into the furnace to create an inert environment. The power was switched on and manually increased to attain a heating rate of 20–50°C/min until the target temperature was reached. The crucible was held for about 30 minutes at the target temperature. The furnace power was then switched off and the crucible was left to cool in the Ar gas atmosphere inside the furnace. The cold crucible was removed, weighed, and then broken down to separate the metal and slag phases. The metal and slag samples were subjected to chemical and mineralogical analysis.

Smelting results and discussion

The mass balances for each smelting test, including the metal and slag masses, are given in Table IV. The smelting target was to achieve a slag with the highest REO grade as well as a clean separation between the slag and metal products.

Slag produced per unit of ore smelted and total REO grade of the slag product

The mass of slag generated per kilogram of ore smelted varied between 210 and 300 g. On average, a mass of about

Table IV

Mass balances for the smelting tests

Test	Ore (g)	Anthracite (g)	CaO (g)	Total mass (g)	Products (g)				Total mass out (g)	*T* (°C)
					Alloy+slag	Alloy	Slag	Gas / LOI		
1	400.0	60.0	0	460.0	265.0	158.0	107.0	192.0	457.0	1700
2	400.0	60.0	0	460.0	249.0	164.0	85.0	211.0	457.0	1800
3	100.0	16.0	0.5	116.5	66.3	44.3	22.0	50.2	116.5	1700
4	100.0	16.0	0.5	116.5	70.8	42.1	28.7	45.7	116.5	1600

250 g was produced per kilogram of ore smelted. As with a physical method such as flotation, smelting is here used principally as a concentration step. Applying flotation terminology to this case, the slag product may be termed a concentrate and the metal tailings—although it is expected that the metal product may in fact have substantial economic value on its own merit. The mass pull, expressed in mass per cent, is the mass of concentrate produced per unit of ore processed. In this smelting case, a mass pull of 25% is achievable, depending on the ore composition, particularly the iron, manganese, and chromium contents, the loss on ignition, and the extent of smelting-reduction. The value of 25% can be considered as a baseline for concentration by smelting for this particular ore. The chemical analyses of the slags produced in the smelting tests are given in Table V and Table VI.

A slag with a total rare earth oxide (TREO) grade at least five times greater than that of the ore was achieved; which is a significant upgrading ratio. Slags containing up to 13.8% TREO were produced from ore with 2.5% TREO. A higher grade of TREO in the slag is desirable as this will decrease the amount of feed to the leaching process and thus improve the process economics. Of course, this needs to be balanced against the cost of the smelting step.

The smelting conditions were optimized at laboratory scale with regard to the contents of FeO and MnO in the slag and ultimately the amount of slag generated. This had an impact on the slag TREO grade. Within the scope of this test work, the optimal slag TREO grade of 13.6% was produced by smelting the ore at the highest temperature of about 1800°C. However, addition of 0.5% lime to the smelting recipe produced a slightly higher slag grade of 13.8% TREO at a lower temperature of about 1700°C. Operation at lower temperature as would result in furnace electricity savings.

Alloy quality

The compositions of the carbon-saturated iron-manganese alloys produced in these smelting tests are shown Table VII. Table VIII presents the rare earth contents of the alloys.

Other results (not presented here) indicated that the alloy composition is strongly related to manganese reduction. An increase in the extent of manganese reduction increases the manganese content of the alloy, while it decreases its iron concentration by dilution. Manganese oxide in the slag is deleterious as it increases the acid consumption in the subsequent leaching step. Therefore, its reduction to the alloy in the smelting step is desirable.

The reduction of manganese oxide is driven by a combination of the reductant addition, temperature, and slag basicity. The preferred alloy composition produced from ore 1 was 79–84% Fe, 10–12.5% Mn, 2–4% C, 3–6% Si, and 0.7–1.3% P. This alloy composition falls within the composition range of commercial manganese steel, which consists of 11–13% Mn. The alloy may require P removal.

Recovery of REO to the slag

The recovery of TREO to the slag was calculated as the portion of the REO in the ore that reported to the slag phase. The highest content of total rare earth elements (TREE) in the metal was about 600 ppm, while the highest slag TREO was about 13.8%. Within the scope of the present test work, and considering the above values, a recovery of rare earths to the slag of more than 95% was achieved. This confirmed that rare earth oxides are stable at the smelting conditions tested and fully reported to the slag phase, irrespective of the final slag grade.

Smelting energy requirement

The theoretical amount of energy required by a large-scale smelting process was calculated using FactSage software. FactSage predicted a furnace energy consumption in the range of 1.0–1.2 MWh per ton of ore. An electric arc furnace will be used to produce the rare-earth-rich slag and the iron alloy. The plant finances may be structured in such a way that the smelting energy cost is entirely covered by the sale of the alloy.

Table V

REE content of the slags

Test	La (mg/kg)	Ce (mg/kg)	Pr (mg/kg)	Nd (mg/kg)	Sm (mg/kg)	Eu (mg/kg)	Gd (mg/kg)	Dy (mg/kg)	Ho (mg/kg)	Er (mg/kg)
1	21601	42805	4328	19338	2327	829	1416	972	170	380
2	29459	49500	5444	19144	2685	727	2420	1048	173	456
3	28970	57197	5232	15077	2335	603	1816	785	153	364
4	19429	32083	3569	12516	1756	550	1654	698	113	292

Test	Tm (mg/kg)	Yb (mg/kg)	Lu (mg/kg)	Y (mg/kg)	Tb (mg/kg)	Th (mg/kg)	U (mg/kg)	REE (%)	RE_2O_3 (REO) (%)
1	50.4	257	45.3	3904	139	-	-	**9.86**	**11.6**
2	58.3	362	49.9	4547	275	863	210	**11.60**	**13.6**
3	53.6	321	44.6	5015	210	986	256	**11.80**	**13.8**
4	38.8	234	32.5	2536	195	862	452	**7.57**	**8.87**

Table VI

Other metal oxides in the slags, with total REO

Test	MgO	Al_2O_3	SiO_2	CaO	TiO_2	V_2O_5	Cr_2O_3	MnO	FeO	BI	S/A	S/M	REE	RE_2O_3 (REO)
	%	%	%	%	%	%	%	%	%				%	%
1	5.24	24.4	24.9	9.97	10.5	0.10	0.08	5.81	3.16	0.31	1.02	4.75	**9.86**	**11.6**
2	7.74	29.6	18.3	13.6	4.40	0.108	0.089	4.69	1.39	0.45	0.62	2.36	**11.6**	**13.6**
3	6.82	25.8	13.2	14.1	5.10	0.089	0.073	1.67	3.04	0.54	0.51	1.94	**11.8**	**13.8**
4	5.74	19.9	22.8	10.1	11.4	0.089	0.073	5.24	4.64	0.37	1.15	3.97	**7.57**	**8.87**

Traces amounts of CoO, NiO, CuO, ZnO, PbO <0.01% S=SiO_2; A=Al_2O_3; M=MgO

Table VII

Alloy analyses

Test	Si (%)	Ti (%)	V (%)	Mn (%)	Cr (%)	Cu (%)	Ni (%)	Ca (%)	Fe (%)	Mg (%)	Al (%)	P (%)	C (%)
1	3.30	0.35	0.10	10.1	0.05	0.05	0.05	0.05	81.2	0.05	0.14	0.83	3.77
2	0.78	0.67	0.11	12.0	0.08	0.03	0.04	0.19	83.9	0.09	0.34	0.73	4.09
3	4.56	0.37	0.10	12.4	0.05	0.05	0.05	0.10	79.2	0.05	0.26	1.26	1.57
4	1.72	0.39	0.13	11.4	0.04	0.05	0.04	0.09	81.5	0.04	0.26	0.69	3.68

Table VIII

REE analyses of selected alloys

Test	Ce (p)pm	Dy (ppm)	Er (ppm)	Gd (ppm)	La (ppm)	Nd (ppm)	Pr (ppm)	Sc (ppm)	Sm (ppm)	Tm (ppm)	Y (ppm)	Yb (ppm)	Th (ppm)	U (ppm)
1	250	5.26	1.96	15.9	143	123	31.3	17.8	1.32	10.7	1.18		6.95	50.10
3	155	2.80	1.49	7.00	98.9	59.2	18.3	66.4	8.22	1	15.4	1	8.65	31.5

Table IX

Chemical analysis of the slag

Element	Concentration	Unit
La	25 120	mg/kg
Ce	49 509	mg/kg
Pr	5 022	mg/kg
Nd	18 387	mg/kg
Sm	2 722	mg/kg
Eu	986	mg/kg
Gd	1 671	mg/kg
Dy	1118	mg/kg
Er	428	mg/kg
TREE	*10.5*	% (w/w)
Th	738	mg/kg
U	234	mg/kg
Mg	2.63	% (w/w)
Al	13.0	% (w/w)
Si	6.43	% (w/w)
Ca	6.32	% (w/w)
Ti	5.09	% (w/w)
Mn	3.03	% (w/w)
Fe	7.39	% (w/w)

Table X

Process conditions for direct HCl leach

Test number	Solids content % (m/m)	Acid dosage kg/kg of slag	Acid dosage kg/kg of TREE
5	20	708	6.4
6	10	861	7.8
7	20	2201	20
8	10	3445	31
9	10	3445	31

Temperature: 60°C
Residence time: 2 h
Grind size: 80% <35 µm

Table XI

Summary of actual operating conditions and extractions of REE and impurities

Test	5	6	7	8	9
Final temperature, °C	61	61	59	59	59
Residence time, h	2	2	2	2	2
Solids content, mass %	20.0	9.4	20.0	8.9	8.9
Final pH	1.00	0.00	0.07	0.00	0.00
Final Eh	131	-144	-102	298	298
Acid dosage, kg/t of slag	708	861	2201	3445	3445
Acid dosage, kg/kg of TREE	6.4	7.8	20.0	31.3	31.3
Mass loss, %	44.7	55.6	56.2	53.7	57.2
Grind size, % <35 µm	80	80	80	80	80
Solid-based metal extraction, mass %					
Mg	27.0	46.1	46.7	40.5	44.9
Al	57.6	69.7	69.5	66.6	69.4
Si	<1	<1	<1	<1	<1
Ca	79.2	90.9	86.1	86.7	87.7
Ti	27.6	45.1	49.1	44.9	49.3
Mn	38.1	64.5	61.7	60.6	63.1
Fe	93.4	95.7	94.5	95.4	95.4
Th	N/D	93.2	90.0	91.2	92.3
U	N/D	95.3	94.0	93.2	94.8
La	93.8	96.8	95.1	95.9	96.1
Ce	94.4	97.0	95.4	96.2	96.4
Pr	93.5	96.6	94.8	95.6	95.9
Nd	93.8	96.7	95.0	95.8	96.0
Sm	94.1	97.0	95.4	95.9	96.2
Gd	90.3	95.7	93.2	94.2	94.4
Dy	93.7	97.4	95.8	96.3	96.4
Ho	94.0	97.5	96.1	96.4	96.5
Er	92.5	96.9	95.2	95.5	95.7
TREE	**93.8**	**96.8**	**95.1**	**95.9**	**96.1**

N/D: not determined

REE recovery from slag by leaching

Selection of leach procedure

Initially, two classical treatment routes that are commonly used for REE recovery, namely caustic cracking followed by leaching of the REE with hydrochloric acid, and a sulphuric acid bake followed by a water leach, were evaluated for treating the slag (Gupta and Krishnamurthy, 2004).

The TREE extractions were relatively poor, yielding 49% recovery for the caustic cracking route at a reagent dosage of 2000 kg NaOH per ton of slag, and 41% at a reagent dosage of 2200 kg H_2SO_4 per ton of slag for the sulphuric acid bake route.

A third leaching option, a direct hydrochloric acid leach, was then evaluated and subsequently selected as it yielded the best results, which are discussed in more detail below.

Slag characteristics

The slag produced in Test 1 was used as the feed for direct hydrochloric leaching tests. The concentrations of REE and major impurities are listed in Table IX. Minor REE are omitted.

Experimental procedure for direct HCl leaching process

The slag was milled to 80% <35 µm prior to leaching. The milled slag was leached under four different process conditions at various acid dosages and pulp densities. Table X summarizes the various leaching conditions. Leaching was conducted by pulping the slag in HCl solution at 60ºC with agitation. Operating parameters such as redox potential, temperature, and pH were recorded at regular intervals. After a leach duration of 2 hours, the pulp was filtered. The filter cake was washed thoroughly and subsequently dried, weighed, and analysed. The solution volumes were measured prior to analysis of the product liquors.

Results and discussion

The actual operating conditions as well as the solid-based leach extractions for REE and impurities are summarized in Table XI. The TREE leach efficiencies ranged between 94% and 97%, and seemed largely insensitive to either pulp density or acid addition. At the lowest acid addition of 708 kg/t slag, the REE recovery was lowest (94%); however, the co-extraction of some impurities was also markedly depressed.

Nonetheless, due to the co-extraction of deleterious impurities such as Al, Ti, Mn, Fe, Th, and U, further treatment of the liquor prior to REE separation would be required. Although the TREE recovery was slightly lower, the results of the test conducted at 20% (w/w) pulp density at an acid addition of 708 kg/t slag could be considered the most favourable. This is due not only to the lower lixiviant addition and associated lower lixiviant costs, but also to decreased neutralizing reagent requirements downstream for both the residual free acid as well as for impurities. In addition, a higher pulp density would allow a smaller equipment size and thus reduce the capital costs for this step.

Mineralogy of slag and slag leach residue

The REE were predominantly detected in the Ca silicate phases, with traces in the Ba-Ca-Al silicate phase and the Ba-Ca silicate phase in the leach feed. Figure 4 shows the related backscattered electron image and EDS analysis.

Figure 5 shows the backscattered electron image and EDS analysis of the direct HCl leach residue. Residual REE, albeit at low concentrations, were detected in Ca-Ti silicate phases and in Ca-Al silicate phases Rare-earth-rich Ca silicate phases, which were the main REE-bearing phases in the slag prior to leaching, were not detected in the leach residue. The REE-bearing Ba-Ca-Al silicate phases were also not detected in the leach residue, which suggests that these phases are also amenable to attack by hydrochloric acid.

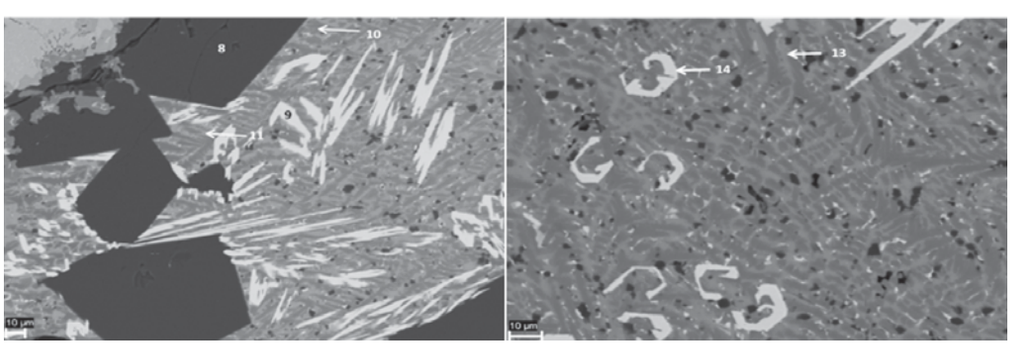

Spectrum	O	Mg	Al	Si	S	Ca	Ba	La	Ce	Nd	Phase
11	36.4		14.8	16.3		2.7	29.8				Ba-Al silicate
10	39.1		17.0	12.3		20.4	2.1	3.0	6.2		REE Ba-Ca-Al silicate
13	36.9	1.0	15.4	13.3	0.3	9.8	16.5		6.7		REE Ba-Ca-Al -silicate
9	26.4			10.5	1.5	7.5		15.9	26.8	11.5	REE-Ca silicate
14	26.1			10.4	1.3	7.1	0.0	16.5	26.6	11.9	REE-Ca silicate
8	44.7	19.4	35.9								Spinel

Figure 4—Backscattered electron image and EDS analysis for test 1, graphite crucible slag at 1700°C

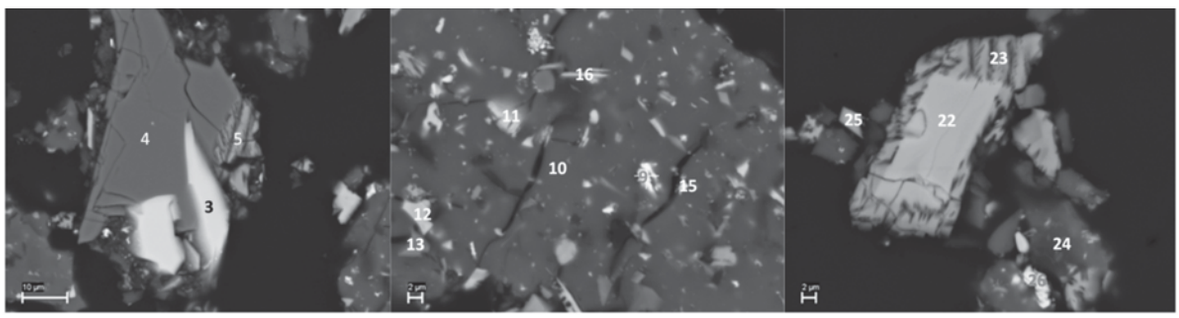

Phase	Analysis	O	Na	Mg	Al	Si	P	Ca	Ti	Mn	Fe	Zr	Ba	Ce	Nd
Ba silicate	3	38.3	0.36		15.1	18.8		0.26					27.2		
	1	32.2		4.60	11.9	10.9				7.60			31.6		
	11	37.1		3.46	8.7	18.9				9.70			20.7		
	15	42.7			0.7	22.9		0.35					24.7		
REE Ca-Al silicate	2	41.8		4.10	14.1	14.6		14.2	3.81	2.35		0.67		2.82	1.47
	5	43.0		4.73	12.4	17.4		14.5	2.51	3.80		0.81		0.82	
	22	41.7		3.69	13.3	14.3		14.3	5.95	2.28		0.68		2.45	1.40
	23	42.7		4.32	12.5	17.4		15.6	1.75	4.13		0.42		0.81	0.34
	25	42.8		4.17	12.2	18.3		13.7	1.37	4.74		0.91		1.29	0.57
REE Ca-Ti silicate	9	38.0	1.56		1.96	9.55		9.30	28.8					7.92	2.94
Low-REE silica	10	52.5	0.01		0.63	43.8	0.22	0.20	2.48					0.12	0.02
	24	51.6		0.35	0.97	42.1		0.49	2.59	0.63		1.12		0.15	0.00
REE-Ti silicate	16	46.1		2.65	5.59	24.5	0.19	0.17	12.21	4.49				2.70	
Spinel	18	41.3		12.32	31.3				2.50	12.63					
	4	43.4		16.75	34.4		0.04		0.57	4.81					

Figure 5—Backscattered electron image and EDS analysis of unfluxed test 1 leach residue

Conclusions

The PyEarth™ process was developed by Mintek to recover rare earth elements from iron-rich rare-earth-bearing carbonatite ores of complex mineralogy from Southern Africa.

The PyEarth process comprises two critical steps, namely smelting, which typically produces an Fe-Mn alloy as a potential saleable by-product and concentrates the rare earth oxides in the resulting slag, followed by leaching of the slag to recover the rare earths using hydrochloric acid.

The investigation successfully demonstrated that the smelting process can be operated as a pre-concentration step for REE. In addition, the Fe and Mn are converted into a potentially saleable by-product, whereas in the classical treatment routes large quantities of these would have to be discarded as tailings, with economic and environmental implications.

In the smelting step, close to full recovery of the rare earths to the slag is achieved, regardless of the REO grade of the final slag. A rare earth recovery in excess of 94% to the pregnant leach solution was attained using this process. Although some deleterious impurities are co-extracted from the slag, these would be removed downstream by conventional hydrometallurgical means. Process optimization is required, and future plans include test work at the pilot plant scale.

The laboratory test work showed that the PyEarth process is indeed a technically feasible, robust, and viable process for the extraction of rare earths from the mineralogically complex iron-rich rare-earth-bearing ores from the Southern African region.

Acknowledgements

This paper is published with the permission of Mintek.

References

Gupta, C.K. and Krishnamurthy, N. 2004. Extractive Metallurgy of Rare Earths. CRC Press, Boca Raton, FL.

Haque, N., Hughes, A., Lim, S., and Vernon, C. 2014. Rare earth elements: overview of mining, mineralogy, uses, sustainability and environmental impact. *Resources*, vol. 3. pp. 614–635.

Li, L.Z. and Yang, X. 2014. China's rare earth ore deposits and beneficiation techniques. *Proceedings of the 1st European Rare Earth Resources Conference*, Milos, Greece, 4–7 September 2014. pp. 28–39.

Long, K.R., van Gosen, B.S., Foley, N.K., and Cordier, D. 2010. The principal rare earth elements deposits of the United States. *Scientific Investigations Report* 2010–5220. US Geological Survey.

Mishra, B. and Anderson, A. 2014. Extraction and recovery of rare-earth metals: challenges in processing. *Proceedings of the 1st European Rare Earth Resources Conference*, Milos, Greece, 4–7 September 2014. pp. 20–27.

Wang, X., Lei, Y., Ge, J., and Wu, S. 2015. Production forecast of China's rare earths based on Generalized Weng model and policy recommendations. *Resources Policy,* vol. 3, no. 4. pp. 11–18. ◆

WITS UNIVERSITY, JOHANNESBURG

JCI Chair – Mineral Resources and Reserves

The School of Mining Engineering at the University of the Witwatersrand, Johannesburg, is an internationally recognised Mining School, with about 600 and 200 registered undergraduate and postgraduate students, respectively. About 15% of the students are international students.

The University is seeking a suitably qualified person to fill the position of Professor for the JCI Chair in Mineral Resources and Reserves.

The School of Mining Engineering provides quality education towards the bachelor's degree in Mining Engineering. It also has a particularly strong postgraduate coursework programme including courses on the evaluation of mineral resources and mineral reserves.

The School has an active Mineral Resources and Reserves Evaluation Research Programme. The research programme has both full-time and part-time research students. The part-time students generally are working full-time in the mining industry and often carry out research relevant to their employer organisations.

Qualifications and Experience: An earned doctoral degree in the field of mineral resources and reserves evaluation; professional registration or eligibility for professional registration; suitable teaching experience; a good publications track record; high national and/or international standing in the area of mineral resources and reserves evaluation.

Duties: Contribute to the development of the professional discipline; lecturing at both undergraduate and postgraduate levels; conduct research and supervise postgraduate students; fund-raise to sustain the Chair's research activities; contribute to the administrative functioning of the School and perform other duties as assigned by the Head of School.

Remuneration: A competitive university package with excellent benefits are offered, commensurate with the level of appointment.

Enquiries: Professor Cuthbert Musingwini, Head of the School of Mining Engineering, Tel no. +27 11 717 7412; Fax no. +27 11 339-8295; E-mail: Cuthbert.Musingwini@wits.ac.za

To apply: Submit a covering letter of motivation, a detailed CV with names, current e-mail addresses and contact numbers of 3 referees, certified copies of qualifications, academic transcripts and South African ID (copy of Passport if not a South African Citizen). External applicants are invited to apply by registering on the Wits i-Recruitment platform located at https://irec.wits.ac.za. Internal employees may apply directly on Oracle Self–Service on the Wits Intranet by selecting "Apply for a job".

Closing date for applications: 31st August 2017

The University is committed to employment equity. Preference may be given to appointable applicants from the under-represented designated groups in terms of the relevant employment equity plans and policies of the University. The University reserves the right to verify all information provided by candidates. Please note that correspondence will only be entered into with short-listed candidates. The University reserves the right not to make an appointment nor to re-advertise.

http://dx.doi.org/10.17159/2411-9717/2017/v117n8a3

The FLSmidth® Rapid Oxidative Leach (ROL) process: a mechano-chemical approach and industrial applications for rapid metal sulphide dissolution

by M. Mulligan*, D. Chaiko*, F. Baczek*, S. Rocks*, C. Eyzaguirre*, C. Dickinson*, and R. Klepper*

Synopsis

The leaching of primary copper concentrates using acidic ferric sulphate lixiviants is known to suffer from slow kinetics and poor copper recoveries. A number of processes have been developed over the years to improve the leach kinetics and copper recoveries, and while many are effective, they have high CAPEX and/or OPEX. FLSmidth is developing a mechano-chemical approach that confers significant process efficiencies by taking advantage of the enhanced reactivity of transitory, surface-defect structures generated during particle fracture. The patent-pending FLSmidth® Rapid Oxidative Leach (ROL) process uses a stirred media reactor (SMRt) to achieve copper recoveries of more than 97% in less than 6 hours under atmospheric conditions. The mechano-chemical approach overcomes many of the surface passivation problems that have hindered other atmospheric leach processes. Results of batch leach tests and new insights to leach mechanisms are presented.

During the life-cycle of many orebodies, the mineralogy transitions from oxides to secondary and primary sulphides, ore grades decrease, and the ore become more difficult to process. Cost-efficient leach processes will be required to maintain copper production at existing mines or take advantage of new orebodies, particularly those containing arsenic-rich minerals like enargite. To date, the majority of the FLSmidth work has been on primary chalcopyrite concentrates, with a minor amount of work done on enargite and arsenopyrite concentrates. Brownfield and greenfield industry applications are reviewed for potential use of the FLSmidth® ROL process, primarily looking at copper recovery from chalcopyrite and enargite. We also include a discussion on applications to other metals, like refractory gold, nickel, and zinc.

Keywords

chalcopyrite, enargite, refractory gold, atmospheric leaching, stirred media reactor, mechano-chemical processing.

Introduction

The hydrometallurgical production of copper dates from the late 1960s, when copper-selective solvent extraction (SX) reagents were commercially introduced by BASF (General Mills at the time) in response to the need for a more economical and cost-efficient process to recover copper from oxide leach solutions other than cementation on scrap iron. With the progressive introduction of more stable and selective reagent/diluent systems, copper SX technology has matured to become a cost-effective, large-scale technology that is used throughout the world. It is now used to recover copper from pregnant leach solutions (PLS) containing 2–20 g/L copper produced by either heap leaching of oxide ores or atmospheric tank leaching of secondary sulphide ores. Currently, about 20% of the world's copper production uses the combination of SX and electrowinning (EW). Heap leaching and atmospheric tank leaching technologies are now accepted as state-of-the-art for processing oxides and secondary sulphides.

Pressure oxidation (POX) autoclave technology, operating at temperatures of 140–225°C, offers acceptable dissolution kinetics and recoveries for primary copper sulphide concentrates, but suffers from relatively high CAPEX and OPEX. At the higher operating temperatures, total oxidation of sulphide to sulphuric acid consumes oxygen in excess of that required for copper dissolution. In the absence of an accompanying oxide heap leach process, the relatively dilute acid produced by POX requires neutralization and disposal. Thus, unique project circumstances are necessary to produce acceptable economics.

The CESL process, owned by TECK, is a chloride-catalysed autoclave process that operates at 140°C with partial sulphur oxidation. The Salobo demonstration plant in Brazil, owned by Vale, was built and operated to demonstrate the CESL technology for copper recovery. The CESL process is currently under consideration for treating arsenic-rich copper concentrates.

A partial list of processes that have been considered for leaching primary sulphide copper concentrates during the last 25 years is given below, along with the current owners:

- Activox® process—Norilsk Nickel, formerly LionOre Mining International Ltd
- Albion™ process—XT of Glencore, formerly Xstrata Technologies

* *FLSmidth, USA.*

 This paper was first presented at the Hydrometallurgy Conference 2016 'Sustainable Hydrometallurgical Extraction of Metals', *1–3 August 2016, Belmont Mount Nelson Hotel, Cape Town.*

- CESL Process—TECK, formerly Cominco Engineering Services Ltd
- Dynatec—Sherritt International
- Galvanox™—University of British Columbia
- HydroCopper®—Outotec
- Placer Dome/Phelps Dodge—Freeport McMoRan.

Efforts have been made to commercialize all of these processes, but either process- or chemistry-related problems have been encountered that resulted in unacceptable technical risk and return on investment.

FLSmidth has identified a simple process that will leach copper sulphide concentrates, with chalcopyrite as the predominant copper-bearing mineral, at 80°C and under atmospheric pressure. Over the past two years, more than 150 batch leach tests have been completed in 14-litre reactors, using more than ten copper concentrates from different sources. The data confirms that the process is robust and can attain 97% to >99% copper dissolution in less than 6 hours. The rapid leach kinetics and high copper recoveries place the process economics on par with stirred-tank leaching of secondary copper sulphide concentrates. The key to process performance is the use of very low-energy, interstage and/or intrastage attrition/grinding to enhance the selective dissolution of copper-bearing minerals by a mechano-chemical process. In this paper we present representative results of batch leach tests and some new insights into potential industrial applications.

Methodology

Concentrate processing

Numerous copper concentrates, from different mine sites, were used in the leach testing. Chalcopyrite was either the major or the sole copper-bearing mineral. In all cases, pyrite and quartz comprised the bulk of the gangue mineralogy in the high-grade concentrates. A low-grade concentrate, containing 20% chalcopyrite and 7.6 wt% Cu was also tested. In this sample, the majority of the gangue minerals were layered silicates, pyrite, and quartz.

Also, three enargite-containing concentrates, which contained secondary copper sulphides and layered silicates, were used in a limited number of leach tests (see Table I for the copper mineralogy).

The as-received concentrates were slurry-split, and individual 1 kg samples were pressure filtered, then vacuum sealed under argon for later use in leach testing. In certain cases, chalcopyrite concentrates were fine-milled to a D_{80} of 17 μm using a FLSmidth VXP laboratory-scale fine grinding mill. The enargite concentrate was tested as-received with a D_{80} of 47 μm. Concentrate samples were analysed for moisture, particle size distribution, Rietveld XRD mineralogy, and elemental composition by inductively coupled plasma (ICP). Mineralogy and elemental analysis were also determined on the leach residues.

Table I

Composition of an enargite concentrate—copper-bearing minerals

Mineral	wt%
Enargite	29.2
Chalcocite	20.0
Bornite	3.8
Covellite	2.8
Chalcopyrite	2.1

Atmospheric leaching

A jacketed 14 L (operating at 10 L volume) glass leach vessel was coupled to an Eppendorf BioFlo 310 control unit, which enabled precise monitoring of temperature, pH, Eh, agitation rate, redox control via modulation of oxygen sparging, instantaneous gas flow, and cumulative gas flow.

Flotation concentrates were leached in a stirred reactor with the assistance of a stirred media reactor (SMRt), in acidic ferric sulphate media at 80°C. The slurry was continuously recirculated between the two reactor types as shown in Figure 1a. Oxygen was sparged into the stirred reactor to maintain a minimum redox set-point of 650 mV (SHE). The applied mixing power in the stirred reactor was approximately 1–5 kW/m^3, and 15–20 kW/m^3 in the SMRt reactor.

A larger, heat-blanketed 120 L stainless steel leach vessel was coupled to a LabVIEW® control unit, and the same SMRt reactor was used with the same methodology as with the 14 L unit. The 120 L vessel was operated with a 50 L volume.

Pressurized leaching

A limited number of pressurized leach tests were performed using a model 4520—2 L stainless steel Parr reactor fitted with a Teflon insert. A model 4848 Parr controller was used to adjust the temperature within ± 2°C accuracy, and a Parr magnetic drive, modified to house three impellers, was used to provide agitation. To simulate the mechano-chemical properties of the SMRt unit at higher temperatures and pressures, the Teflon insert contained ceramic media similar to that used in the SMRt reactor. Two of the impellers were located below the media level and the third impeller remained halfway up the remaining slurry level (Figure 1b).

The pulp density in the reactor was typically 7 wt% solids in a solution of sulphuric acid and iron sulphate salts. The system was then closed and brought to temperature. Pure oxygen gas was allowed to freely flow into the reactor as needed to maintain the targeted oxygen partial pressure. The flow of oxygen and total oxygen consumption were measured by an Aalborg gas flow unit during leach testing.

Results and discussion

The FLSmidth® Rapid Oxidative Leach (ROL) process—14 L vessel

The FLSmidth® Rapid Oxidative Leach (ROL) process utilizes a series of stirred media reactors (SMRts) placed in tandem with conventional, stirred leach tanks to achieve copper recoveries of 97% to >99% in 6 hours or less from primary sulphide concentrates. The interstage or intrastage placement of the SMRts, shown in Figures 2a and 2b, gives the advantage of mechano-chemical activation processes with only a minimal addition to baseline processing costs. Processing costs are further reduced by optimizing the volume ratio between the stirred leach tanks and the SMRts.

The FLSmidth® Rapid Oxidative Leach (ROL) process

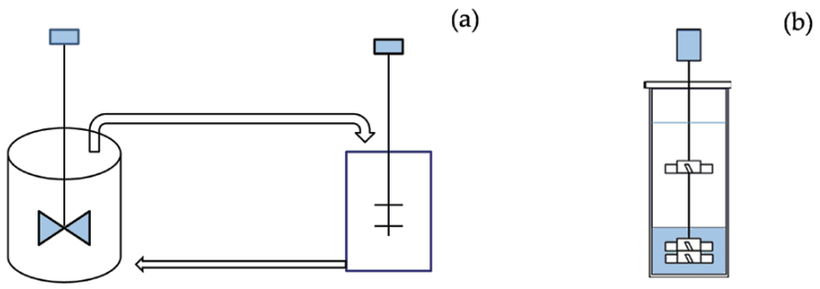

Figure 1—(a) Batch leach configuration with continuous slurry recirculation between the stirred reactor and the SMRt. (b) Batch leach configuration of the autoclave apparatus with ceramic media

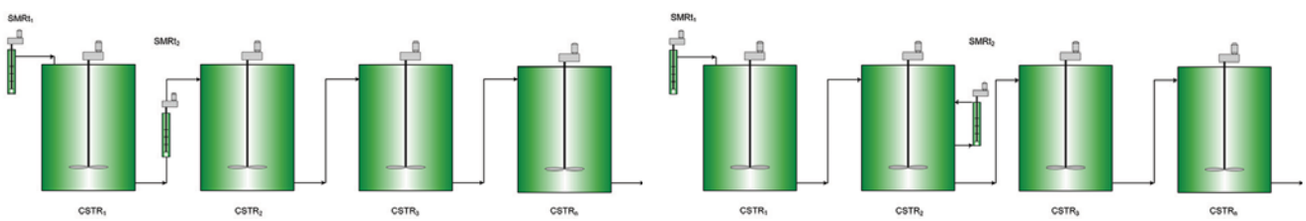

Figure 2—Continuous leach circuit configuration with stirred media reactors (SMRts) placed (a) interstage between continuous stirred tank reactors (CSTRs); (b) intrastage between the CSTRs with variable recycle. Note that the SMRt placement will depend on the mineral leach kinetics, and generally not all positions require a SMRt. For example, chalcopyrite only requires an initial SMRt operated at 50% solids to feed CSTR1

As a point of reference, the full-scale ROL processing costs are estimated to be only marginally above those for the stirred-tank leaching of secondary copper sulphides. Minimum concentrate grades of approximately 7 wt% copper would be economically viable.

The concept of combining mechanical and chemical processes has received significant interest within the chemical process industry (*e.g.* Hickenboth *et al.*, 2007; Stellacci *et al.*, 2009), and has been shown to offer potential benefits to hydrometallurgical applications (*e.g.* Balaz and Achimovicova, 2006; Cobble, Jordan, and Rice, 1993). However, the concept has not caught on commercially due to either the prohibitively high mixing energies that have been employed or the use of equipment not amenable to scaling to reach commercially relevant throughputs for copper production. In addition, the leaching of metal sulphides is a special application as the sulphur product layer can complicate the process if not accounted for in mechano-chemical reactor designs. In its current configuration, the FLSmidth® SMRt is purposefully tuned for metal sulphide leaching, and is designed to promote mechano-chemical activation with specific power densities much lower than previous systems (discussed in more detail below).

Atmospheric chalcopyrite leaching

Representative copper recovery curves for low- and high-grade chalcopyrite concentrates (7.6 and 22 wt% Cu, respectively) using the FLSmidth® ROL process under batch conditions, are presented in Figure 3a. The process is capable of leaching chalcopyrite concentrates within 6 hours, regardless of grade, and readily handles common gangue materials such as layered silicates without adverse effects on copper recoveries. While the initial and final leach rates are virtually identical, the low-grade concentrate actually responds better than the high-grade concentrate.

Leach data from two low-grade (7.6 wt% Cu) chalcopyrite concentrates differing only in particle size distribution are presented in Figure 3b. As expected, the smaller particle size led to a faster initial leach rate. However, both concentrates leached within approximately 5.5 hours despite the large difference in particle size distributions. It is hypothesised that the removal of passivating product layers and the generation of active species on the mineral surfaces within the SMRt enables the rapid leaching of chalcopyrite concentrates. Thus, rapid leach rates and high metal recoveries are possible even for low-grade concentrates and without fine grinding.

Figure 3a also shows the effect of specific mixing power on chalcopyrite dissolution. In the ROL system, the time to reach 80% copper recovery was unaffected by reducing the specific power in the SMRt from 20 to 11.4 kW/m^3. During the early 1990s, studies were conducted by the US Bureau of Mines (USBM) on the effects of turbomilling during ferric sulphate leaching of chalcopyrite. In that system (the optimum leach recovery value is denoted by ▲ in Figure 3a), leaching was confined exclusively to the turbomill. Thus, while the optimum specific power density was fairly low in batch leach tests (*e.g.*, 1048 kWh/t Cu leached at 80% Cu recovery), inefficiencies inherent to the configuration of the USBM leach circuit resulted in the consumption of over 1800 kWh/t Cu leached at 90% copper recovery. Significantly more energy would have been required to reach 95–98% recoveries, making the approach of using only attrition mills in the leach process uneconomical. In contrast, the reactor configuration of the ROL process (Figure 2) results in an estimated total mixing energy for the combination of all SMRts and CSTRs of about 550 kWh/t Cu leached. Of this total, the contribution from the SMRt reactors is approximately 130 kWh/t Cu leached.

In addition to controlling the power density of the SMRt, further gains in process efficiency can be realized by varying the volumetric ratio between the CSTRs and the SMRts (CSTR:SMRt). A reactor volume ratio of between 40:1 and 80:1 represents a good balance between the mean residence times within the two reactor types.

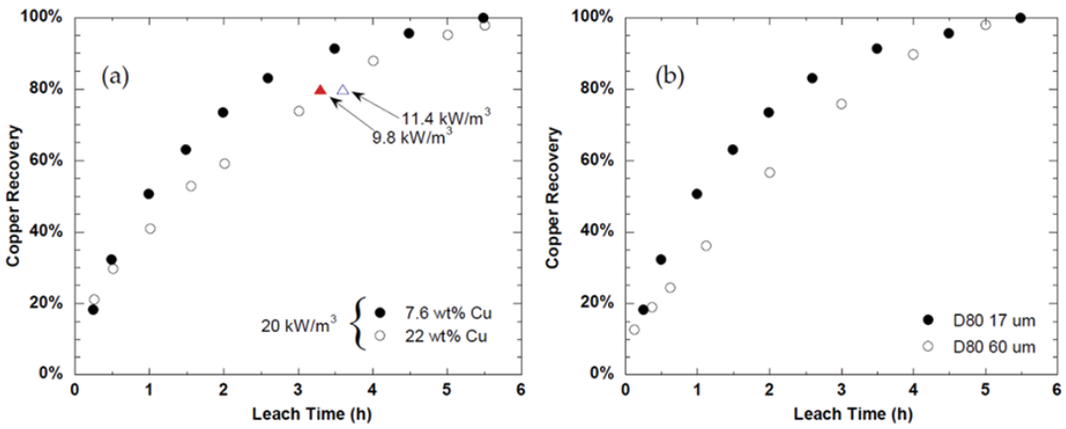

Figure 3—(a) Copper recovery curves for high-grade (22 wt% Cu, ○) and low-grade (7.6 wt% Cu, •) concentrates with *D*80s of 17 um; (b) copper recovery curves from two low-grade (7.6 wt% Cu) chalcopyrite concentrates with *D*80s of 17 um (•) and 60 um (○). Concentrates were leached using the FLSmidth® ROL process at 80°C, 20 g/L Fe, and a mixing power density of approximately 20 kW/m^3 in the SMRt. Leaching tests conducted at 11.4 kW/m^3 (FLSmidth, Δ) and 9.8 kW/m^3 (Cobble, Jordan, and Rice, 1993; ▲) fall on the same leach curve as the 20 kW/m^3, suggesting that a power density of 20 kW/m^3 is more than sufficient

Atmospheric enargite leaching

While the primary focus has been on the leaching of chalcopyrite concentrates, preliminary leach results from an arsenic-rich concentrate are presented to illustrate the process's ability to handle a wide range of refractory minerals (see Table I for the feed Cu mineralogy). Leach conditions were identical to those used in leaching chalcopyrite, and it should be understood that further process optimization is needed. The leach was conducted at 80°C, with 30 g/L initial Fe, 50 g/L initial H_2SO_4, and with continuous slurry recirculation between a SMRt and a stirred tank reactor. A summary of the leach results is provided in Table II. The total copper recovery reached 97% within 12 hours, and complete dissolution of all secondary sulphides and chalcopyrite was noted. The leach resulted in a 55% mass loss due to dissolution of the copper and iron sulphides. While the enargite concentration in the leach residue was 5.7 wt%, this equates to only 9% of the initial enargite remaining unleached. Arsenic remained soluble during the test and there was no evidence of scorodite formation, although it should be noted that no attempt was made to produce scorodite during the leach test. An advantage of producing soluble arsenic during the copper leach is the opportunity of selectively removing arsenic from the PLS and the leach residue.

Table II

Copper-bearing mineralogy of an enargite leach residue. 'BD' denotes phases present in the concentrate but which were below the XRD detection limit in the leach residue

Mineral	wt%	% leached
Enargite	5.7	91.3
Chalcocite	BD	>99
Covellite	BD	>99
Chalcopyrite	BD	>99
Bornite	BD	>99

Pressurized ROL leach

Heat and mass balance models of a continuous, multi-stage ROL process indicate that autogenous heating of the slurry to slightly above 100°C can be expected in the initial leach stages of a full-scale system. In addition, the advantages of operating a leach process at moderate temperatures (80–105°C) with above-atmospheric O_2 pressures (200–500 kPa) have been noted (Richmond and Dreisinger, 2003). These potential advantages include somewhat faster Cu dissolution kinetics; more efficient oxidation of ferrous to ferric—thereby ensuring that the required redox potential is readily maintained during the leach process; and higher oxygen utilization efficiencies. Normally, mechano-chemical processes would not be expected to show temperature sensitivity, as the mechanical action supplies the necessary activation energy to drive a chemical reaction (Ma *et al.*, 2014). To determine if the ROL process would benefit from operating under slightly higher temperatures and pressures, a limited number of leach tests were conducted in a pressurized SMRt at 105°C and 140°C. Because of the complications of leaching at or above the melt temperature of elemental sulphur (Marsden, Wilmot, and Hazen, 2007), we report here a representative summary of leach results for 105°C only.

Interestingly, and contrary to expectations, the combination of slightly higher leach temperature and elevated O_2 pressure dramatically altered metal sulphide leach behaviour. Increasing the temperature from 80 to 105°C (517 kPa O_2 overpressure) substantially enhanced O_2 mass transfer by approximately 50–55 times during the initial 15 minutes (see Figure 4). Not surprisingly, the higher O_2 overpressure resulted in a slightly higher redox potential. The higher O_2 mass transfer was accompanied by enhanced chalcopyrite and pyrite dissolution (see Table III). At the end of 2 hours, the Cu extraction yield from chalcopyrite was 90%, compared to 59% for the same period at 80°C. While the Cu leach rate was faster, chalcopyrite dissolution rates at 80°C are, nevertheless, quite acceptable.

Operating the mechano-chemical leach process above 100°C, but below the melting temperature of elemental sulphur, significantly enhanced the dissolution of pyrite. X-ray analysis of the leach residues indicated that 84% of the

Table III

Comparison of chalcopyrite leaching by the ROL process at 80°C and 105°C, 517 kPa O_2 overpressure

Description	Leach time (min)	Eh (mV)	$CuFeS_2$ S° recovery (%)	$CuFeS_2$ Dissolution (%)	$CuFeS_2$ FeS_2 dissolution (%)
ROL, 105 °C	120	730	46	90	84
*ROL, 80 °C	120	635	43	59	12
*ROL, 80 °C	330	673	68	>99	24

*Values from same test – a sample was collected at 120 minutes and solid mineralogy, solution [Cu], and Eh measured. Test was completed by 330 minutes

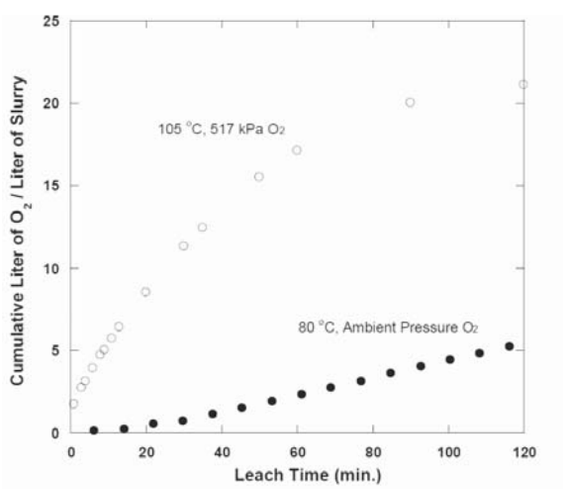

Figure 4—Normalized oxygen consumption curves for the ROL process at ambient O_2 pressure, 80°C (•), and 517 kPa O_2 partial pressure, 105°C (○). During the initial 10 minutes, O_2 consumption at 105°C was approximately 55 times higher than at 80°C

pyrite was leached at 105°C, compared with only 24% at 80°C. High pyrite oxidation yields are expected to occur in autoclaves at much higher temperatures (*e.g.* 190–230°C), as routinely observed in the pretreatment of refractory gold ores (Rusanen, Aromaa, and Forsen, 2013). That this level of pyrite reactivity was observed at only 105°C is unique and may open new opportunities in precious metals recovery. One of the disadvantages of high-temperature POX is the high oxygen consumption which accompanies the near-complete oxidation of sulphide to sulphuric acid (McDonald and Muir, 2007). An advantage of both the low- and high-temperature ROL processes is the fact that the oxidation of sulphide to sulphate during metal dissolution is limited. Elemental sulphur recoveries were approximately 68% at 80°C and 46% at 105°C.

While the atmospheric ROL process is fully capable of leaching chalcopyrite, pressurized ROL leaching offers the advantage of simultaneously generating acid and iron from pyrite. The lower operating temperatures provide an advantage over POX autoclaves for those instances where a source of iron is needed, as for example in the leaching of secondary copper sulphides and copper arsenic sulphides (*e.g.* enargite).

Scale-up of the FLSmidth® Rapid Oxidative Leach (ROL) Process

50 L batch leaching

A few leach tests have been performed with a concentrate containing 26 wt% copper in a scaled-up 50 L system using the FLSmidth® ROL process, and included an activation step of 4% chalcopyrite conversion. The activation step is a rapid pretreatment of chalcopyrite with soluble copper that improves copper leach kinetics by producing a lattice-strained, iron- and sulphide-depleted copper sulphate (Chaiko *et al*, 2015a, 2015b). The leach was conducted at 80°C, 20 g/L Fe, and a mixing power density of approximately 20 kW/m^3 in the SMRt. Figure 5 shows that copper recoveries of greater than 95% were achieved in 6 hours' residence time, and greater than 99% in 7 hours' residence time. It is believed that following some minor improvements to the system, the leach results will be on a par with those from the 14 L tests.

Continuous pilot plant

A pilot plant facility (Figure 6) has been constructed at FLSmidth's technology centre in Salt Lake City, USA and was

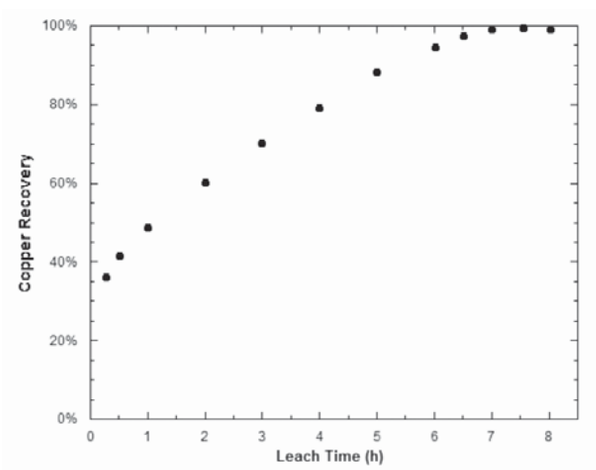

Figure 5—Copper recovery curve for high-grade (26 wt% Cu, •) concentrate. Concentrate was leached using the FLSmidth® ROL process, 80°C, 20 g/L Fe, and a mixing power density of approximately 20 kW/m^3 in the SMRt

Figure 6—FLSmidth's pilot plant facility under construction in the technology centre in Salt Lake City, USA

commissioned in Q2 2016. It includes four 14 L reactors and four 50 L reactors, and a number of SMRts that will be able to operate in interstage and/or intrastage arrangements. Each reactor is instrumented for measurement and control of temperature, pH, Eh, and oxygen addition, and is linked to a data recording system. This pilot plant facility will enable continuous operation of the ROL process on a larger scale. Following the demonstration of the FLSmidth® ROL process in the pilot plant, countercurrent decantation (CCD), solvent extraction (SX), electrowinning (EW), and impurity removal stages will be added to demonstrate a fully integrated circuit.

Potential industrial applications

Copper industry

Sustained SX-EW copper production – oxide to sulphide transition

There are a number of copper hydrometallurgical facilities around the world with SX-EW plants where the oxide orebodies are being depleted, and the mines will start moving into transitional and sulphide zones. These transitional zones are either secondary sulphides with underlying primary sulphides, or a mix of oxide and primary sulphides. This is resulting in a drop in heap leach recoveries and thus a lower PLS copper tenor, leading to lower copper cathode production.

With the FLSmidth® ROL process, a grinding circuit with bulk flotation can be added upstream of the existing SX-EW plant. A bulk concentrate can be leached using the FLSmidth® ROL process, followed by CCD with the resulting PLS fed to the existing SX-EW facility. The higher copper tenor PLS can either (a) be blended with the lower copper tenor PLS from the existing heap leach facility; or (b) be fed directly into the existing SX-EW plant.

Due to the brownfield nature of the transitional zone and the subsequent move into the primary sulphide zone, scenarios need to be carefully studied for each plant to ensure that the existing SX-EW facility is properly utilized to sustain copper cathode production, and in some cases additional EW capacity would need to be added.

Low- to medium-grade concentrates

Some copper concentrator plants have to process feed with decreasing copper grades, resulting in concentrates with a low copper grade. This leads to high penalties charged by the smelter, which significantly impact the profitability of the mine. In some cases, the copper mine becomes uneconomic and is either put on care and maintenance or permanently closed.

The FLSmidth® ROL process can be used in a number of scenarios for these low- to medium-grade concentrates.

- Where pockets of low- to medium-grade feed material are mined, the ROL process can be used to selectively leach copper concentrate that does not meet acceptable smelter grades, and produce copper cathode from a new SX-EW facility. When high-grade concentrate is produced, this is still sold to the smelter with no penalty charges
- If the feed grade is consistently low, the ROL process can be used to leach all of the concentrate, and copper cathode produced in a new SX-EW facility. Either a rougher bulk concentrate, with the additional benefit of higher overall copper recovery, or a cleaner concentrate can be leached using the ROL process, and analysis of the particular project would be required to assess economics
- Some historical greenfield projects have not progressed due to the concentrate being too low a grade to sustain the project. Some of these projects could become economically viable with the FLSmidth® ROL process, and should be studied to assess the current economics.

Arsenic-rich concentrates

The FLSmidth® ROL process makes it possible to develop mineral deposits containing arsenic (*e.g.* enargite) for recovery of copper, gold, and silver, while complying with stringent environmental regulations. As the FLSmidth® ROL process operates at atmospheric pressure, a concentrate can be treated at the mine site with complete control over the arsenic-bearing leach residues. This makes it possible to avoid the potential of arsenic contamination of the environment while transporting concentrate from the mine to the smelter.

Many existing mines have stockpiles of copper concentrate containing more than 0.5% arsenic, which is too high for smelting. The FLSmidth® ROL process can be used to treat these high-arsenic concentrates, and even makes it possible to develop new mineral deposits high in arsenic.

Electrorefinery and smelter materials

The FLSmidth® ROL technology can integrate within existing electrorefinery and smelter operations to supplement and/or increase copper cathode production. The enabling feature of the technology is the use of an FLSmidth® SMRt in which metallic materials such as anode scrap and blister copper are rapidly and selectively dissolved into dilute sulphuric acid (1–2 M H_2SO_4). The dissolution process is exothermic and produces a concentrated copper sulphate electrolyte that can be used to increase existing electrorefinery output while simultaneously eliminating the need to recycle anode scrap back to the smelter. Alternatively, the process has the potential to eliminate the pyrometallurgical refining step altogether by processing blister copper directly for cathode production by electrowinning.

Other mineral sectors

While the copper industry has been the main area of focus for the FLSmidth® ROL technology, there are other industries that could also use the ROL technology. No FLSmidth® ROL leach test work has been performed in any of these other sectors; however, they are perceived as constituting potential areas for application.

Gold industry

Refractory gold ores yield poor gold recoveries in conventional cyanide leaching circuits, even if the ore is finely ground. This can be either due to the gold being finely disseminated and physically 'locked' in the sulphide minerals, or to the presence of naturally occurring preg-robbing carbonaceous materials. The finely disseminated gold is often enclosed within pyrite and arsenopyrite (FeAsS), and rimming of pyrite with arsenic-rich assemblages as well as arsenopyrite-marcasite-pyrite associations is common (*e.g.* Aylmore and Jaffer, 2012). Preliminary studies presented in this paper indicate that pyrite can be readily leached

mechano-chemically at more moderate temperatures and pressures than those used in existing refractory ore treatment options.

Nickel industry

Nickel sulphides are processed via a variety of routes, for example pyrometallurgical, high-pressure acid leach (HPAL), and the Caron process. A number of atmospheric leach technologies have been tested, such as Albion™ and Activox®, but none have been applied commercially at a large scale. The FLSmidth® ROL technology is another atmospheric leaching technology that has potential to be used in the nickel industry.

Zinc industry

Zinc is often separated from polymetallic ores via flotation processes. The FLSmidth® ROL technology could rapidly leach sphalerite, thus providing an alternative processing route to zinc smelting. The zinc PLS solution can then be further processed via SX-EW, which is well-proven hydrometallurgical technology.

Conclusions

The FLSmidth® Rapid Oxidative Leach (ROL) process provides chalcopyrite leach rates and Cu recoveries that are comparable to secondary copper sulphide leach processes operated under atmospheric conditions. The key to achieving this performance is the coupling of stirred media reactors (SMRts) in tandem with continuous stirred tank reactors (CSTRs). The concept is equally applicable for retrofitting to existing secondary copper sulphide tank leach circuits. The power density of the SMRts is controlled to balance the rates of mechanical and chemical processes within the reactors. Incremental mixing costs related to the use of the SMRts are further minimized by specifying reactor volume ratios within the range of 40:1 to 80:1. For mineral systems with slow leach kinetics, such as enargite, the reactor volume ratio can be advantageously increased to within the range of 50:1 to 100:1, thereby further reducing mixing costs. Leach times as low as 6 hours are sufficient to reach Cu recoveries from 97% to > 99% from chalcopyrite concentrates. The process can also be readily adapted to operate at temperatures close to the melting point of elemental sulphur. This has the added advantage of using pyrite as a source of iron for the leaching of secondary sulphides and enargite, thereby eliminating the need for high-temperature POX autoclaves.

There are many potential industrial applications for the FLSmidth® ROL technology. The copper industry is the current focus for implementation, and the technology has progressed from 14 L leach reactor to a 50 L leach reactor tests. A continuous pilot plant was constructed to prove the technology on a larger, continuous level, following which a fully integrated pilot plant will be completed with a CCD, SX-EW, and waste treatment sections.

A short- to medium-term application of the technology is the sustaining of copper SX-EW facilities that are transitioning from oxide orebodies to sulphide orebodies. This will allow existing facilities to continue operating with minimal CAPEX investment, and to continue using existing SX-EW facilities to produce copper cathode. The ability to process low- to medium-grade concentrates has the potential to significantly improve the economics of existing operations where concentrate grades are falling, and also for new greenfield projects that will be more viable if the economics can be improved. Arsenic-rich concentrates are continually becoming a greater problem, particularly in countries like Chile, and the FLSmidth® ROL technology has the potential to process these concentrates economically and in an environmentally acceptable manner. A newer potential area of application is in the use of ROL to process metallic materials, such as anode scrap and blister copper, to produce a concentrated copper sulphate electrolyte stream to increase existing electrorefinery output while simultaneously eliminating the need to recycle anode scrap back to the pyrometallurgical refiner.

Acknowledgements

The authors wish to thank the staff of FLSmidth's analytical services laboratory for XRD and elemental analysis of process samples. We would also like to thank the staff of FLSmidth's Dawson Laboratory for processing the flotation concentrates used in the leach studies.

References

Aylmore, M. and Jaffer, A. 2012. Evaluating process options for treating some refractory ores. *Proceedings of the ALTA 2012 International Gold Conference*, Perth, Australia, 31 May–1 June 2012.

Baláž, P. and Achimovičová, M. 2006. Mechano-chemical leaching in hydrometallurgy of complex sulphides. *Hydrometallurgy*, vol. 84. pp. 60–68.

Chaiko, D.J., Baczek, F., Rocks, S.S., Walters, T. and Klepper, R. 2015a. The FLSmidth® Rapid Oxidative Leach (ROL) process. Part I: mechano-chemical process for treating chalcopyrite', *Proceedings of the Conference of Metallurgists, Hydrometallurgical Processing and Technologies, Lucy Rosato Memorial Symposium*, Toronto, Canada, 23–26 August.

Chaiko, D.J., Rocks, S.S., Walters, T., Asihene, S., Klepper, R., Baczek, F., and McMahon, G. 2015b. The FLSmidth® Rapid Oxidative Leach (ROL) process. Part II: a new chemical activation process for chalcopyrite. *Proceedings of the Conference of Metallurgists, Hydrometallurgical Processing and Technologies, Lucy Rosato Memorial Symposium*, Toronto, Canada, 23-26 August.

Cobble, J.R., Jordan, C.E., and Rice, D.A. 1993. Hydrometallurgical production of copper from flotation concentrates., *Report of Investigations* RI 9472. US Bureau of Mines.

Eyzaguirre C., Rocks S., Klepper R., Baczek F., and Chaiko, D. 2015. The FLSmidth® Rapid Oxidative Leach (ROL) Process: A mechano-chemical approach for rapid metal sulfide dissolution. *Proceedings of Hydroprocess 2015*, Antofagasta, Chile, 22–24 July. Gecamin Ltda, Santiago.

Hickenboth, C.R., Moore, J.S., White, S.R., Sottos, N.R., Baudry, J., and Wilson, S.R. 2007. Biasing reaction pathways with mechanical force. *Nature*, vol. 446. pp. 423–427.

Ma, X., Yuan, W., Bell, S.E.J., and James, S.L. 2014. Better understanding of mechanochemical reactions: Raman monitoring reveals surprisingly simple 'pseudo-fluid' model for a ball milling reaction. *Chemical Communications*, vol. 50. pp. 1585–1587.

McDonald, R.G. and Muir, D.M. 2007. Pressure oxidation of chalcopyrite. Part I. Comparison of high and low temperature reaction kinetics and products. *Hydrometallurgy*, vol. 86. pp. 191–205.

Marsden, J.O., Wilmot, J.C., and Hazen, N. 2007. Medium-temperature pressure leaching of copper concentrates – Part I: Chemistry and initial process development'. *Preprint* MMP-07-027. Society for Mining, Metallurgy and Exploration Inc., Littleton, CO.

Richmond, G. and Dreisinger, D.B. 2003. Processing copper sulphide ores. US patent 6,537,440.

Rusanen, L., Aromaa, J., and Forsen, O. 2013. Pressure oxidation of pyrite-arsenopyrite refractory gold concentrate. *Physicochemical Problems of Mineral Processing*, vol. 49, no. 1. pp. 101–109.

Stellacci, P., Liberti, L., Notarnicola, M., and Bishop, P.L. 2009. Valorization of coal fly ash by mechano-chemical activation Part II. Enhancing pozzolanic reactivity. *Chemical Engineering Journal*, vol. 149. pp. 19–24. ◆

The Southern African Institute of Mining and Metallurgy (SAIMM) in cooperation with the International Atomic Energy Agency (IAEA), the Canadian Institute for Mining, Metallurgy and Petroleum (CIM), the Namibian Uranium Institute, and the Namibia University of Science and Technology (NUST) is proud to host the

URANIUM 2017 INTERNATIONAL CONFERENCE

Extraction and Applications of Uranium — Present and Future

11 September 2017—Short Courses and Technical Visit
12–13 September 2017—Conference
14 & 15 September 2017—Technical Visits
Swakopmund Hotel, Swakopmund, Namibia

BACKGROUND

Namibia is currently ranked the fifth-largest producer of uranium in the world and is set to become the world's second-largest producer once Swakop Uranium's Husab Mine is fully operational. This will undoubtedly position Namibia as a major uranium mining hub and will see the industry playing a more significant role in the national and regional economies.

Uranium as a material, and its applications, are often controversial. Yet, nuclear reactors are still being built despite the growth in energy generation through renewable sources and despite highly publicised nuclear accidents. Several countries are pursuing uranium enrichment programmes. Although prices are currently subdued, it is highly likely that there will be continued and sustained demand for uranium for the foreseeable future.

This conference aims to bring together professionals in the uranium industry. A broad range of topics will be discussed, ranging from mining to some of the applications of uranium, and including safety, and post-operations closure and remediation issues. Innovations in the extraction and applications of uranium are constantly being made, and this conference provides a platform for the discussion of advances and for generating new ideas.

It is fitting that the conference takes place in Swakopmund, Namibia. Not only do Namibia and this town have much to offer in scenic beauty, but Swakopmund (apart from being a favourite seaside resort) is also the centre of uranium extraction in the country. Most mines are located in the Namib Desert, within easy driving distance of the conference venue. The oldest uranium mine, Rössing Uranium, celebrated its 40th anniversary last year, having commenced operations in 1976. Pre- and post-conference visits are available.

The Uranium 2017 Conference will bring together internationally and locally recognized experts, operating personnel, engineering providers, policy makers, R&D establishments, academia, as well as students, to explore how future uranium extraction technologies can:

- Assist in sustainable uranium extraction
- Lower energy costs
- Minimize the impact on the environment
- Play an enhanced role in the medical field

EXHIBITION/SPONSORSHIP

Sponsorship opportunities are available. Companies wishing to sponsor or exhibit should contact the Conference Co-ordinator.

SAIMM THE SOUTHERN AFRICAN INSTITUTE OF MINING AND METALLURGY

CIM ICM

NAMIBIAN URANIUM INSTITUTE

NAMIBIA UNIVERSITY OF SCIENCE AND TECHNOLOGY

IAEA International Atomic Energy Agency

www.facebook.com/TheSAIMM/

https://www.linkedin.com/company/saimm---the-southern-african-institute-of-mining-and-metallurgy

https://twitter.com/SAIMM1

FOR FURTHER INFORMATION PLEASE CONTACT:
Camielah Jardine • Head of Conferencing · SAIMM • Tel: +27 (0)11 834-1273/7 • E-mail: camielah@saimm.co.za • Website: http://www.saimm.co.za

Conference Announcement

http://dx.doi.org/10.17159/2411-9717/2017/v117n8a4

Evaluation of ozonation technology for gold recovery and cyanide management during processing of a double refractory gold ore

by V. Bazhko* and V. Yahorava*

Synopsis

The depletion of conventional gold resources around the world has resulted in mining companies and research institutions exploring the recovery of gold from refractory and double refractory ores. However, conventional gold processing routes are not feasible for such deposits due to the low gold recoveries and higher reagent consumptions. A number of technologies have been developed to overcome refractoriness, one of which is ozonation. The unique chemical properties of ozone have been tested successfully on a laboratory scale for the pre-oxidation of refractory ores as well as for the detoxification of cyanide effluent streams. However, ozonation has never been implemented on a commercial scale due to the high capital and operating costs associated with ozone generation. Recent developments in ozone generation and contactor systems have revived interest in ozonation as a technology for the processing of refractory ores and the recycling and detoxification of cyanide streams.

In order to demonstrate the viability of these new developments and to evaluate their impact on the entire cyanide management cycle, it is important to quantify the performance of ozonation technology on a double refractory ore. The effect of pH on sulphide, cyanide, and thiocyanate oxidation as well as the decomposition of the preg-robbing component was evaluated. Pre-oxidation of the material with ozone in an acidic medium (pH 1–2) resulted in the oxidation of sulphides and the liberation of gold. Partial destruction of the preg-robbing component was also observed. This resulted in increased gold recoveries during the subsequent cyanidation step. It was also established that ozone in an alkaline medium can oxidize more than 99% of CN^- and SCN^- within 30 minutes. Moreover, ozonation was found to be efficient for treatment of both filtrates and slurries. In an acidic medium (pH 2), 60% of the thiocyanate was converted to cyanide. This reaction can potentially be utilized for cyanide regeneration from thiocyanate formed during cyanidation of sulphide minerals.

It is thus concluded that ozonation could be incorporated at different stages of gold processing in order to improve gold recovery, reduce operating costs by recycling cyanide, and minimize the environmental impact by efficient detoxification of the effluent streams.

Keywords

refractory gold, gold recovery, pre-oxidation, ozonation, cyanide detoxification.

Introduction

Gold deposits that can be treated by conventional cyanidation/carbon-in-pulp (CIP) processes are becoming exhausted around the world (González-Anaya, Nava-Alonso, and Pecina-Treviño, 2011). Mining companies have thus shifted their focus to the processing of refractory and double refractory gold ores. Commonly, in these types of ores, the gold is associated with sulphide minerals. The presence of sulphides can affect gold recovery via cyanidation due to encapsulation or passivation of the gold, thereby increasing reagent consumption. In the case of double refractory ores, gold recovery is further limited due to the presence of carbonaceous materials as well as sulphides. Carbonaceous material can encapsulate and/or adsorb gold from cyanide solution, thus competing with activated carbon added (the so-called preg-robbing effect).

A number of approaches have been developed for the treatment of refractory/double refractory gold ores. In order to overcome refractoriness associated with sulphides the partial or complete destruction of sulphides (and sometimes carbon) via chemical or biological processes, pressure oxidation, or roasting is typically considered. In the case of refractoriness associated with carbonaceous material, resin-in-pulp (RIP) technology, sometimes with the addition of blinding reagents, is used or alternative lixiviants to cyanide are applied.

Ozone can potentially be utilized for pre-oxidation of refractory ores, thus improving gold recovery and lowering subsequent cyanide consumption. The unique chemical properties of ozone can also potentially be utilized at other stages of gold processing. Ozone can be used for the destruction of free and weak acid dissociable (WAD) cyanide, thiocyanate (SCN), and (partially) strong acid dissociable (SAD) cyanide. Ozone has also been found to show potential for cyanide regeneration from thiocyanate formed during cyanidation of sulphur-containing materials (Botz, 2001).

The current paper presents results from a study conducted to evaluate ozonation

* *Mintek, Randburg, South Africa.*

 ISSN 2225-6253. This paper was first presented at the Hydrometallurgy Conference 2016 'Sustainable Hydrometallurgical Extraction of Metals', *1–3 August 2016, Belmont Mount Nelson Hotel, Cape Town.*

technology for processing of a South African double refractory ore sample which yields a low gold recovery via conventional cyanidation.

Background theory

Ozone is a powerful oxidant with a high standard oxidation potential in both acidic and alkaline media (Lurje, 1971):

$$O_3 + 2H^+ + 2e^- \rightarrow H_2O^- + O_2 \qquad E^0 = 2.07\ V \qquad [1]$$

$$O_3 + H_2O + 2e^- \rightarrow 2OH^- + O_2 \qquad E^0 = 1.24\ V \qquad [2]$$

and which readily reacts with species containing multiple bonds such as C=C, C=N, and N=N, as well as. ions such as S^{2-} with the formation of SO_4^{2-} ions.

Ozone has a limited solubility in water, which depends on a number of parameters such as ozone concentration in the gas phase, temperature, and pH. Henry's Law describes the linear correlation between the concentration of ozone in the gas (O_{3g}) and aqueous (O_{3s}) phases (Lenntech, 1998):

$$Hc = O_{3g} / O_{3s} \qquad [3]$$

The Henry's Law constant (Hc) is a function of temperature, pH, and ionic strength of the liquid phase.

The negative effect of temperature on ozone solubility in 'pure' water is described by Equation [4] (Bin, 2006):

$$H_c = a \exp(bt) \qquad [4]$$

where $a = 1.599 \pm 0.0164$;
$b = 0.0473 \pm 0.0004$ in the temperature range from 0 to 60°C
t is temperature in °C.

An increase in pH value and ionic strength generally decreases ozone solubility, as shown in Figure 1 and Figure 2, respectively.

Ozone reacts with hydroxyl ions via multiple steps involving the formation of $^{\bullet}OH$, $^{\bullet}O_2^-$, $^{\bullet}O_3^-$ and $HO_2^{\bullet}$ radicals. The depletion is a chain process and has been described by different mechanisms (Ershov, 2009; Langlais, 1991).

At high pH values, the ozone decomposition rate is essential as shown in Figure 3.

If easily oxidized compounds are present in water, larger amounts of ozone will dissolve to satisfy the demand. A common problem associated with ozonation (especially in laboratory-scale oxidation tests) is the poor mass transfer of ozone into the aqueous phase and the loss of ozone to the overlying headspace. In practical applications, ozone passing through the solution does not have sufficient contact time to reach equilibrium conditions, thereby resulting in lower solubilities than predicted from Henry's Law (Barlow, n.d.).

Additionally, the size of the gas bubbles has a significant effect on ozone distribution between the gas and liquid phases as well as its solubility. Large bubbles cause poor distribution since they tend to rise to the surface rapidly and release the ozone-air mixture into the headspace, whereas smaller bubbles promote intimate mixing and better lateral distribution through the saturated zone (Kollmeier, 2002).

The following parameters can affect the size of gas bubbles and therefore ozone dissolution (OzoneLab™ Instruments, n.d.):

- Type of gas-introducing system
- Type of impeller
- Agitation speed
- Gas flow rate.

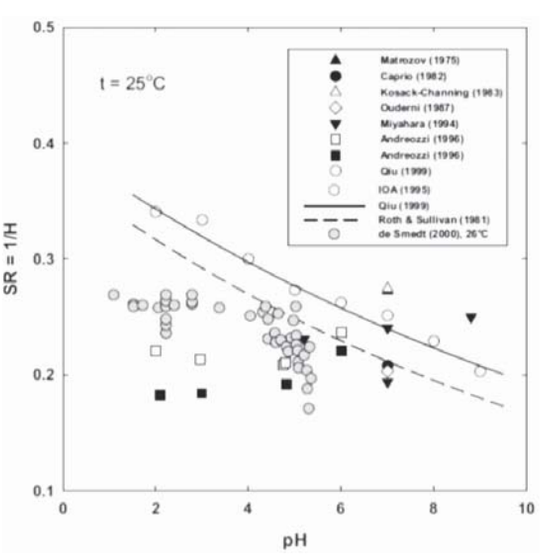

Figure 1—Effect of pH on ozone solubility ratio (SR=1/H) (Bin, 2006)

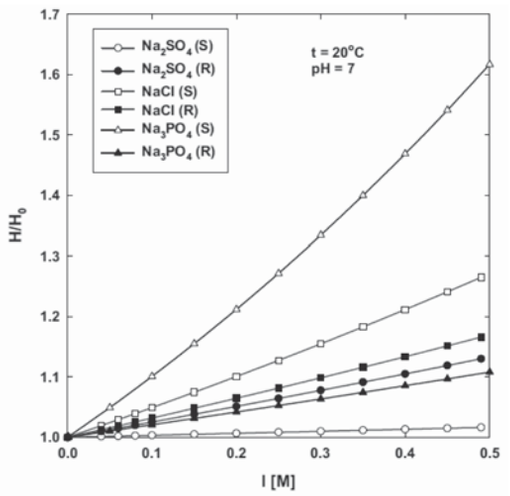

Figure 2—Effect of ionic strength on the ratio of Henry's Law constants in salt solutions (H) and in water (H0) (Bin, 2006)

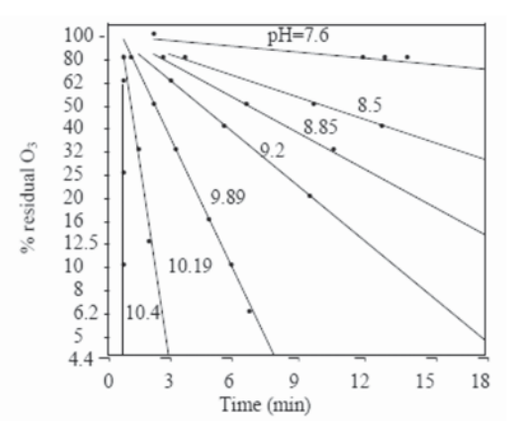

Figure 3—Effect of pH on the decomposition of ozone at 15°C (Grima, 2009)

Usually, higher gas flow rates increase the mass transfer coefficient and the amount of soluble ozone. However, increasing the volume of the carrier gas (O_2 or air) may result in the formation of larger bubbles which have poorer diffusion characteristics. An increase in mixing rate influences the gas-liquid transfer positively (Rodríguez-Rodríguez, 2014).

Experimental approach

Chemical analysis

The feed material was analysed for Au by standard fire assay, with Au finish using atomic absorption spectrometry (AAS) with a detection limit of 0.001 g/t. Base metals and Si were determined by inductively coupled plasma-optical emission spectrometry (ICP-OES) with a detection limit of 0.05%. Additionally, S and C speciation were determined by a combustion technique with detection limits 0.01–0.2% (depending on the species analysed).

Mineralogical analysis

A portion of the feed material was pulverized and subjected to X-ray diffraction (XRD) analysis to identify the crystalline phases present and to determine their relative abundance. It should be noted that amorphous phases cannot be identified by this technique, and only crystalline phases present in amounts greater than approximately 3 mass% are usually detectable.

Polished sections were prepared from a further portion of the feed material for bulk mineralogy, base metal sulphides (BMS) search, and for the gold deportment study on an automated scanning electron microscope (AutoSEM).

Diagnostic leach procedure

The diagnostic leach procedure involved the sequential dissolution of minerals associated with Au, commencing with the least stable, and then extracting the associated Au by cyanidation/resin-in-leach (RIL). The test conditions are specified in Table I.

Ozonation set-up

The experimental set-up consisted of a 2 L glass baffled reactor, stirred mechanically with a slanted blade impeller. The reactor was equipped with electrodes for pH and Eh measurements. Ozone was produced from oxygen with a CD 2000P ozonator; the gas was fed into the reactor through a borosilicate glass sparger with a sintered filter candle with a porosity of four (10–16 μm). The concentration of ozone in the gas outlet was determined by a BMT 964 ozone analyser.

All tests were conducted at the following conditions:

- Oxygen pressure of 10 psi (68.9 kPa)
- Oxygen flow rate of 10 cfh or 283 L/h
- Ozone concentration in the inlet gas (read off the BMT analyser) an average 40 g/Nm^3, which corresponded to an ozone output of 19 g/h
- Agitation speed controlled at 400 r/min.

Pre-treatment of the ore

Eight tests were conducted to evaluate the effect of pH, Eh, temperature, and oxidation time on pre-oxidation efficiency of the gold ore. Pre-treatment was conducted at 30% solids. Operating parameters such as Eh and ozone concentration in the gas phase were monitored. The test pH was adjusted to the required value by the addition of sulphuric acid.

Table I

Diagnostic leach conditions

Step	Test	Sample	Leach conditions	Gold association
1	Direct cyanidation	Feed sample	30% solids, 10 kg/t NaCN, pH 11, 24 h leach	Free and exposed Au
2	Resin-in-leach (RIL)	Feed sample	20% solids, 10 kg/t NaCN, 50 ml/L Minix resin, pH 11, 24 h leach	Au preg-robbed (by difference)
3	Hydrochloric acid leach (HCl) followed by RIL	Step 2 residue after RIL test	20% solids, 2.5 M HCl at 70°C (till completion) followed by RIL	Au associated with minerals soluble in HCl
4	Nitric acid leach (HNO_3) followed by RIL	Step 3 residue after HCl/RIL leach	20% solids, 50%(v/v) HNO_3 at 70°C (till completion) followed by RIL	Au associated with the more stable sulphides and mica
5	Roasting	Step 4 residue after HNO_3 /RIL leach	2-3 h at 850°C followed by RIL	Au associated with carbonaceous minerals
6	Calculation			Au is assumed to be locked in gangue minerals

Cyanidation/RIL

A sub-sample of the ore ('as is' or pre-treated with ozone) was slurried to 30% (m/m) solids using Rand Water Board water. The pH of the slurry was adjusted to 10.5 by the addition of dry hydrated lime (AR grade). Exactly 2 kg/t sodium cyanide and 50 mL/L of the Minix® resin (in the case of RIL) were added. After 24 hours' residence time, the resin was screened, the slurry was filtered, and the solids were washed three times by re-pulping with deionized water, dried, and subjected to gold analysis by fire assay. The resin was eluted with 20 BV of acidic thiourea solution (1 M TU in 1 M HCl) at 60°C and the eluates analysed for Au by AAS with detection limit of 0.08 mg/L.

Detoxification

Test work was conducted on a sample of the slurry and filtrate generated during cyanidation of the sample. 1 L slurry and 700 mL solution were used for the test work. The filtrate contained 500 mg/L WAD CN and 350 mg/L SCN. The pH of the sample was maintained at a value of 10.5 by the addition of 1 M NaOH and the samples were treated with ozone. Solutions were analysed for CN species using segmented flow injection analysis (SFIA).

Cyanide regeneration

Three tests were done at different pH values. The test work was done on the PLS generated during cyanidation of the sample pre-oxidized with ozone at pH 2. A 350 mL sample of the liquor containing 1500 mg/L SCN was acidified to pH values of 2, 3, and 4 prior to ozonation. Agitation was very slow to minimize liberation of HCN gas. The solutions were sparged with ozone and analysed for CN species using SFIA.

Results

Sample characterization

A sample of the double refractory ore originating from a greenstone belt in South Africa was used for this study. The sample was milled to 80% -75 µm and the gold content determined in triplicate by fire assay at 3.03 g/t. The sample contained a significant amount of sulphides (4.17%) and 1.12% organic carbon, which can contribute to refractoriness through preg-robbing.

The chemical analysis of the sample is listed in Table II, and Figure 4 presents the bulk modal mineralogical analysis.

The bulk modal analysis presented in Figure 4 indicated that the sample contained about 20% sulphide minerals, of which 15% was pyrrhotite (which can cause refractoriness of the ore), 54% silicates, 20% carbonates, and 1% organic carbon (potential preg-robber).

Gold in the ore was present as native gold (12 mass%) and electrum (AuAg, 88 mass%) with majority of particles within the 0-4 µm size class. Approximately 6% of the gold had free surface, while 82% was associated with pyrite, 5% with pyrrhotite, and 6% with silicate. From these results, the expected gold recovery via direct cyanidation of the ore was low.

The sample was subjected to a gold diagnostic leach, the main outcomes of which are presented graphically in Figure 5.

The sample can be characterized as follows.

- Only 10% of the gold could be recovered via direct cyanidation
- Addition of the resin to the cyanide leach increased the gold recovery to 23%, indicating the presence of a preg-robbing component

Table II

Chemical composition of the sample

Constituent	Value, % m/m
Mg	2.24
Al	3.27
Si	23.00
Ca	3.39
Ti	0.15
Fe	14.7
Zn	0.11
Cr	0.052
Mn	0.36
As	0.30
Sulphide	4.17
Sulphate	4.90
Elemental S	0.13
Carbonate	11.92
Organic C	1.12
Au	3.03 g/t

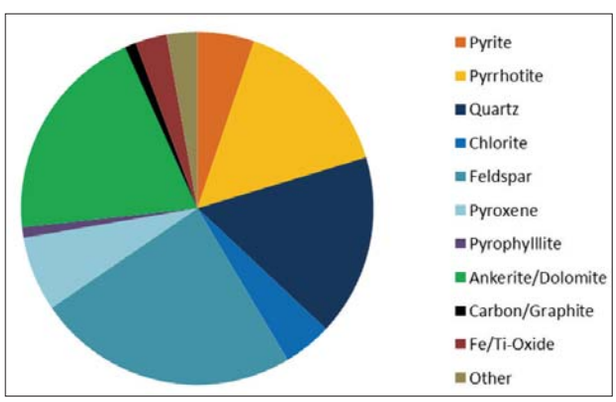

Figure 4—Mineralogical composition of the sample

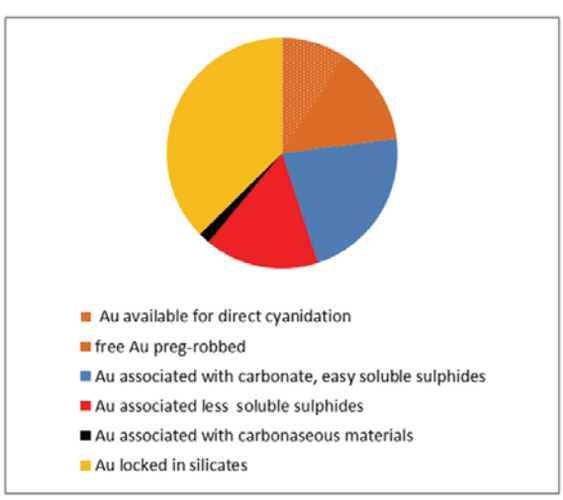

Figure 5—Gold association with different mineral phases

- A significant portion of gold (22%) was locked in carbonates and easily soluble sulphides
- Around 16% of the gold was recovered after treatment of the sample with 5 M HNO_3 (this gold was associated with less soluble sulphide minerals)
- Roasting of the sample was targeted at the destruction of organic carbon in order to liberate gold associated with it. This fraction of the gold accounted for approximately 1.6% of the total gold present in the sample
- The rest of the gold in the sample (38%) was not available for leaching and was probably locked in the silicate minerals.

Ore pre-treatment via ozonation

Eight pre-treatment tests were conducted at different conditions. The main outcomes are listed in Table III. Continuous acid addition was required to control the pH as the sample contained a significant amount of carbonates. Consequently, substantial amounts of Mg and Ca was leached, although Ca was simultaneously precipitated as gypsum for tests 1, 2, and 6–8. Additionally, relatively high amounts of Fe, Mg, Mn, Zn, and As were solubilized at pH ≤3.

At low pH values, oxidation of sulphides occurred according to the following reaction (González-Anaya, Nava-Alonso, and Pecina-Treviño, 2011):

$$2FeS_2 + 5O_3 + 2H_2O \rightarrow 2Fe^{3+} + 4SO_4^{2-} + 2H^+ \quad [5]$$

The mineralogical analysis of the leach residues (Figure 6) indicated that mostly pyrrhotite was leached, while pyrite was unreactive under the conditions tested.

For the tests conducted at pH 6 and 7, negligible amounts of Ca, Mg, and sulphate were detected in the solutions. At high pH very little or no carbonate dissolution was observed, and ferric ions produced from sulphide minerals according to Equation [5] were hydrolysed to form ferric hydroxide.

Test 5, which was conducted at natural pH, indicated that acid was generated during ozonation as the pH decreased from 7.6 to 7.1 after 60 minutes of ozonation, presumably due to the occurrence of reaction [5].

In order to evaluate the effects of pre-acidification and ozonation separately, test 6 was conducted at pH 2 but without ozone addition. Treatment with acid only resulted in similar or lower dissolutions of Fe, As, Zn, and Mn, with a significant portion of the pyrrhotite dissolving. It was noted that the acid consumption during pre-acidification was higher than in test 2, when ozone was added, *i.e.* 218 *vs* 140 kg/t. The difference in acid consumptions proved that during ozonation, acid was generated by the oxidation of sulphides.

With an extended oxidation time and increased temperature applied during ozonation at pH 2 (tests 7 and 8, respectively), the acid consumption, as well as the extraction of base metals and arsenic, increased.

Gold recovery after pre-treatment

The residues generated in the pre-oxidation experiments were subjected to cyanidation and resin-in-leach (RIL) tests

Table III

Extraction of the elements during pre-treatment

Test	Targeted pH	H_2SO_4 consumption, kg/t	Dissolution, %				
			Fe	Mg	Mn	Zn	As
1	1	238	17	43	61	30	14
2	2	140	16	33	51	32	20
3	3	27	1	8	15	17	0
4	6	4.4	0	2	0	3	0
5	Natural (7)	0	0	1	0	0	0
6	2 (no O_3)	218	17	48	64	11	2
7	2 (180 min)	160	21	45	62	34	31
8	2 (240 min, 45°C)	212	28	62	87	65	47

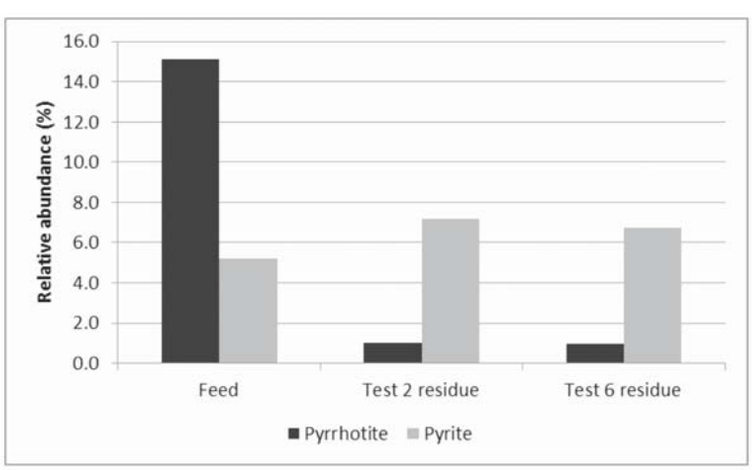

Figure 6—Effect of pre-treatment of sulphide minerals in the sample

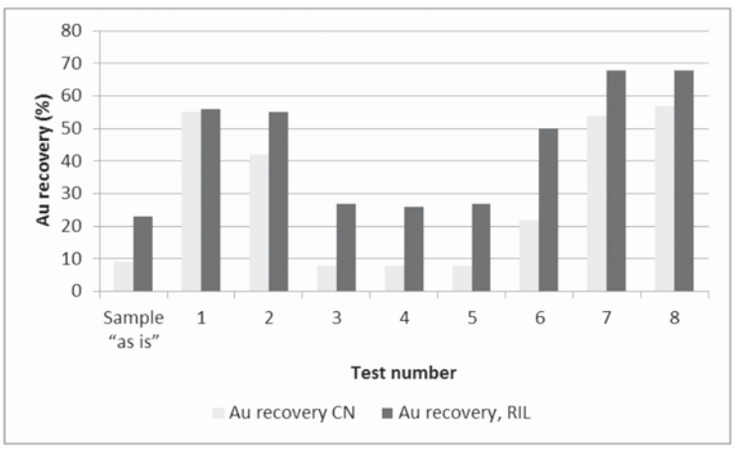

Figure 7—Effect of pre-treatment on recovery of gold

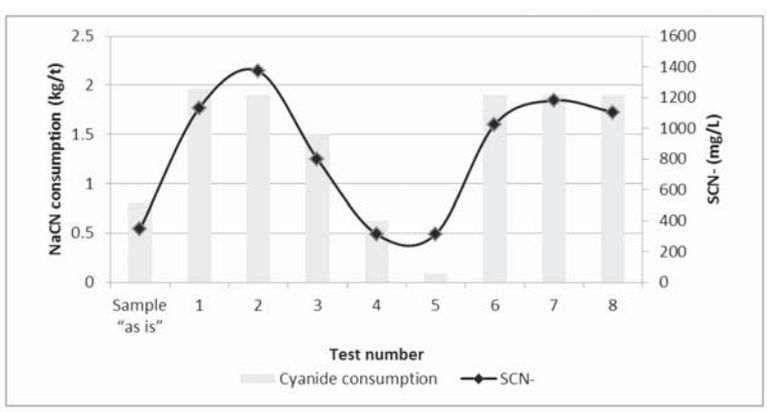

Figure 8—Cyanide consumption and thiocyanate formation during cyanidation

to evaluate the effect of ozonation on subsequent gold recovery. Figure 7 shows the results of these tests.

Pre-oxidation with ozone at pH 1 and 2 improved gold recoveries via cyanidation significantly, from 9% to 42–55%. Moreover, after pre-treatment at pH 1 subsequent cyanidation and RIL tests resulted in similar gold recovery values, indicating that ozonation destroyed the preg-robbing component in the ore. Pre-oxidation at pH 3 and above did not result in improved gold extraction, probably due to the formation of a passivating layer of ferric hydroxide on the surface of the sulphide minerals, which prevented further oxidation of sulphides and liberation of gold.

Pre-acidification to pH 2 (test 6) prior to cyanidation resulted in increased Au recovery via cyanidation as well as RIL (22% and 50% respectively) compared to the sample 'as is'. However, the improvement in gold recovery was lower than for test 2 (ozone was added at pH 2). An extended ozonation time improved Au extraction even further (tests 7 and 8).

Reagent consumptions and thiocyanate formation after ozonation

Cyanide added to the slurries could be consumed by sulphur species (reactive sulphide minerals and some possible intermediate products of sulphide oxidation such as elemental sulphur and thiosulphate) with the formation of thiocyanate as per the equations below (Gok, 2010):

$$Fe_7S_8 + CN^- \rightarrow 7FeS + SCN^- \quad [6]$$

$$FeS_2 + 4CN^- + 3O_2 + 6H_2O \rightarrow 4Fe(OH)_3 + 4SCN^- \quad [7]$$

$$S^\circ + CN^- \rightarrow SCN^- \quad [8]$$

$$S_2O_3^{2-} + CN^- \rightarrow SCN^- + SO_3^{2-} \quad [9]$$

$$S_4O_6^{2-} + CN^- \rightarrow 2SCN^- + 2SO_3^{2-} \quad [10]$$

Figure 8 shows the thiocyanate concentrations formed in the leach liquors and corresponding cyanide consumption during the various tests.

During direct cyanidation of the 'as is' sample, a cyanide consumption of 0.8 kg/t was reported, which is probably attributable to reaction with highly reactive sulphides. Pre-treatment conducted at low pH values (≤3) resulted in increased cyanide consumptions, presumably due to additional liberation of pyrite particles after carbonates and pyrrhotite were dissolved and/or intermediate products of sulphide oxidation were formed during ozonation.

It was expected that an extended oxidation time or increased temperature would improve the extent of oxidation of sulphur species to sulphate and minimize cyanide consumption downstream. Nevertheless, additional tests conducted (tests 7 and 8) for prolonged oxidation times did not decrease the subsequent cyanide consumption.

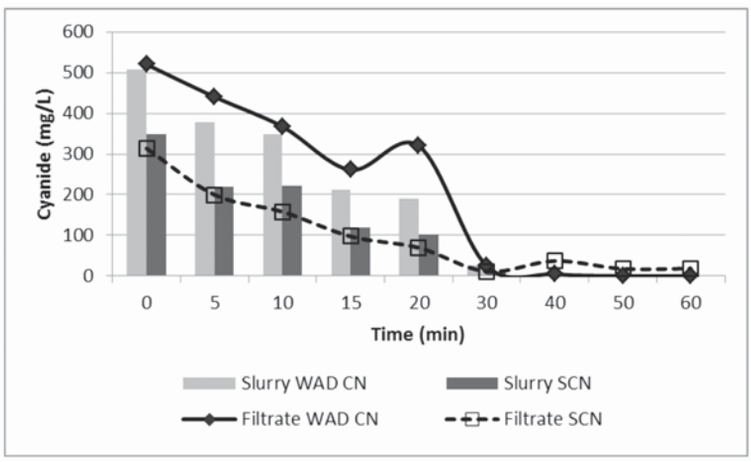

Figure 9—Kinetics of cyanide detoxification

However, a decrease in subsequent cyanide consumption was observed after pre-oxidation within the higher pH range (between 6 and 8). A similar trend was observed by Carrillo-Pedroza and Salinas-Rodríguez (2012). The decrease in cyanide consumption and SCN^- formation was attributed to the formation of ferric hydroxide on the surface of the sulphides during oxidation, which inhibited further dissolution of the sulphide minerals.

Cyanide detoxification

The tailings from the cyanidation tests were subjected to cyanide detoxification tests. The filtrate contained 500 mg/L WAD CN and 350 mg/L SCN^-. No SAD CN was detected in the samples. Detoxification was done at pH of 10.5. At a high pH and excessive ozone addition, the following reactions would be expected to take place (Parga, Shukla, and Carrillo-Pedroza, 2003):

$$O_3 + CN^- \rightarrow OCN^- + O_2 \quad [11]$$

$$SCN + 2\,O_3 + H_2O \rightarrow SO_4^{2-} + CNO^- + O_2 + 2H^+ \quad [12]$$

$$2CNO^- + 3O_3 + H_2O \rightarrow 2HCO_3^- + N_2 + 3O_2 \quad [13]$$

The thiocyanate and WAD cyanide concentration profiles in the slurry and filtrate samples achieved during the tests are presented in Figure 9.

Similar rates of CN^- and SCN^- detoxification were observed in both the slurry and filtrate samples. After 30 minutes of ozonation, more than 90% of CN^- and SCN^- anions were destroyed. Complete destruction of cyanide down to < 1 mg/L was achieved within 50 minutes of ozonation. The residual thiocyanate concentrations in the slurry and filtrate samples were 2 and 15 mg/L, respectively.

Cyanide regeneration

In an acidic medium cyanide exists mainly as hydrocyanic acid, which is less amenable to oxidation, while thiocyanate oxidation occurs at various pH values (Nava, Uribe, and Pérez, 2003). Cyanide can be regenerated from thiocyanate via ozonation at low pH according to the following reaction:

$$SCN^- + O_3 + H_2O \rightarrow SO_4^{2-} + HCN + H^+ \quad [14]$$

In order to identify the optimum conditions for thiocyanate conversion to HCN with minimal subsequent cyanide oxidation, three tests were conducted on the filtrate obtained from cyanidation of the residue generated after pre-oxidization of the sample at pH 2. The cyanide leach liquor, containing 1500 mg/L SCN^-, was acidified to pH values of 2, 3, and 4 prior to further ozonation.

Figure 10 illustrates the efficiency of thiocyanate oxidation (in terms of fractional oxidation: $\frac{C_0-C}{C_0}$,%) and the cyanide yield *vs* time.

It was found that cyanide regeneration from thiocyanate was most efficient at pH 2. After 40 minutes of ozonation, approximately 85% of the thiocyanate was oxidized to cyanide with a yield of 60%. Although oxidation of thiocyanate continued further to <10 mg/L SCN^- in solution, the cyanide concentration actually started to decrease. This could be attributed to either oxidation of cyanide by ozone or (most probably) liberation as HCN gas at this pH value.

At pH>3 oxidation/conversion of thiocyanate was slower and thus after 90 minutes of ozonation the residual SCN^- concentration in the solution was 174 mg/L. The maximal efficiency of cyanide production was about 48%. At pH 4, oxidation of thiocyanate was rapid. However, only a 16% cyanide yield was achieved after 5 minutes of ozonation. Any cyanide formed further was oxidized quickly.

Potential for implementation of ozonation at different stages of gold processing

As shown in Figure 11, in the case of the sample studied, ozonation technology has a good potential for application at different stages of gold processing. It improved the overall gold recovery and showed a high potential for the minimization of environmental impact associated with cyanidation. Moreover, regeneration of cyanide consumed by sulphur species could provide additional benefits with regard to OPEX.

There is a need to evaluate alternative options for the processing of this specific sample and provide direct OPEX and CAPEX comparisons in order to account fully for all the benefits of ozonation technology.

Conclusions

The evaluation of ozonation technology for treatment of a

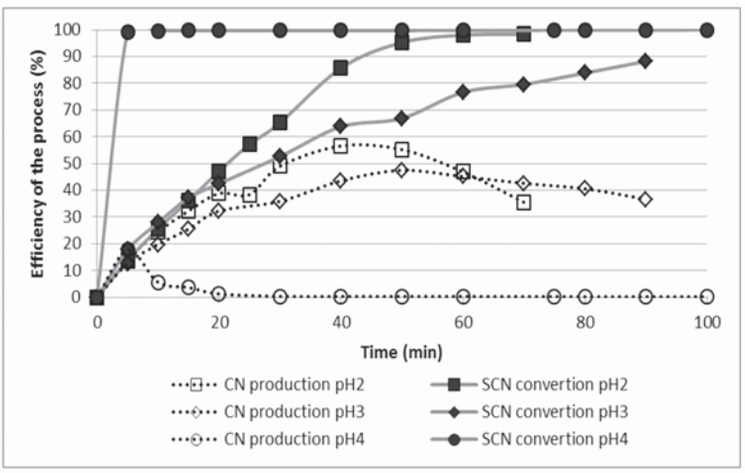

Figure 10—Cyanide regeneration from thiocyanate

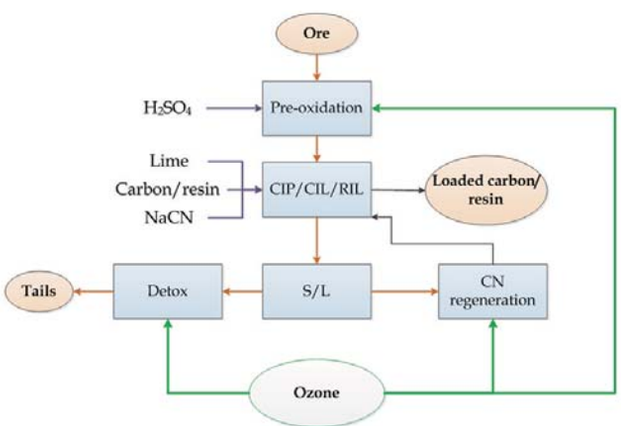

Figure 11—Flow sheet for treatment of refractory ore with ozonation implemented

double refractory ore sample indicated that it could be successfully applied for different stages of the gold recovery process.

Pre-treatment of the material after acidification to pH 1–2 via ozonation resulted in significantly improved gold recoveries during subsequent cyanidation, from 25% to 60–70%. Treatment of the sample with ozone in the pH range of 1 to 4 resulted in increased cyanide consumptions (from 0.8 kg/t to 1.9 kg/t) due to the formation of thiocyanates. Ozonation of the sample at pH 1 and 2 caused partial destruction of preg-robbing component. Ozonation at pH 6–8 did not improve gold recovery, but did result in reduced cyanide consumptions compared to the 'as is' sample.

Tests on detoxification of the cyanide/thiocyanate-containing gold leach slurry and filtrate (pH 10.5) via ozonation confirmed that ozone was an efficient oxidant for both the cyanide and thiocyanate species. More than 99% of CN^- and SCN^- were destroyed after 30 minutes of ozonation.

The regeneration of cyanide consumed by sulphur species with the formation of thiocyanate via ozonation at low pH values was found to be promising enough to warrant further investigations. At pH 2, 60% of thiocyanate was converted to cyanide after 40 minutes of ozonation.

References

Barlow, P. Not dated. Lifelineozone. http://www.lifelineozone.com/research/ozone%20basics/basic1.pdf [accessed 22 March 2016].

Bin, A.K. 2006. Ozone solubility in liquids. *Ozone: Science and Engineering*, vol. 28. pp. 67–75.

Botz, M.D. 2001. Technologies for the regeneration of cyanide. *Mineral and Metallurgical Processing*, vol. 18, no. 3. pp. 126–132.

Carrillo-Pedroza, F.R-A. and Salinas-Rodríguez, E.M-L-T-S. 2012. Oxidative hydrometallurgy of sulphide minerals. *Recent Researches in Metallurgical Engineering – From Extraction to Forming*. Nusheh, M. (ed.). InTech. pp. 25–42.

Ershov, B.M. 2009. The kinetics of ozone decomposition in water, the influence of pH and temperature. *Russian Journal of Physical Chemistry and Electrochemistry*. pp. 1295–1299.

Gok, O. 2010. Oxidative leaching of sulfide ores with the participation of nitrogen species - a review. *Journal of Ore Dressing*, vol. 12, no. 24. pp. 22–29.

González-Anaya, J., Nava-Alonso, F., and Pecina-Treviño, E. 2011. Use of ozone for gold extraction from highly refractory concentrate. *Ozone: Science and Engineering*, vol. 33, no. 1. pp. 42–49.

Grima, N. 2009. Kinetic and mass transfer studies of ozone. PhD thesis, School of Engineering Design & Technology, University of Bradford, UK. https://bradscholars.brad.ac.uk/bitstream/handle/10454/3351/Thesis%20-%20May%202009.pdf?sequence=2 [accessed 15 March 2016].

Khongkittikhoon, W., Lerdlattaporn, R., Nopharatana, M., and Songkasiri, W. 2011. Cyanide removal by ozone oxidation in tapioca starch industrial wastewater for recycling purposes: effects of pH and starch concentration. *Asian Journal of Food and Agro-Industry*, vol. 4, no. 5. pp. 286–296.

Kollmeier, J.A. 2002. In-situ MTBE remediation using air sparging augmented by ozone. National Ground Water Association, Westerville, Ohio.

Langlais, B. R. 1991. Ozone in Water Treatment: Application and Engineering. Lewis Publishers, Boca Raton, FL

Lenntech, B.V. 1998. Ozone generation. http://www.lenntech.com/library/ozone/transfer/ozone-transfer-mechanisms.htm [accessed 22 March 2016].

Loeb, B. 2011. Ozone: Science & Engineering: thirty-three years and growing. *Ozone Science & Engineering*, vol. 33, no. 4. pp. 329–342.

Lurje, J. 1971. Handbook of Analytical Chemistry. Science, Moscow.

Nava, F., Uribe, A., and Pérez, R. 2003. Use of ozone in the treatment of cyanide containing effluents. *European Journal of Mineral Processing and Environmental Protection*, vol. 3, no. 3. pp. 316–323.

OzoneLab™ Instruments. Not dated. What determines the final levels of ozone in water? http://www.ozoneservices.com/faq/faq024.htm [accessed 17 March 2016].

Parga, J., Shukla, S., and Carrillo-Pedroza, F. 2003. Destruction of cyanide waste solutions using chlorine dioxide, ozone and titania sol. *Waste Management*, vol. 23, no. 2. pp. 183–191.

Rodríguez-Rodríguez, C. N-A-S. 2014. Silver leaching from pyrargyrite oxidation by ozone in acid media. *Hydrometallurgy*, vol. 149. pp. 168–176. ◆

http://dx.doi.org/10.17159/2411-9717/2017/v117n8a5

Purification of a dilute platinum group metals process stream using waste yeast biomass immobilized on plaster of Paris

by D. Oke*, S. Ndlovu*, and V. Sibanda*

Synopsis

The removal of platinum group metals (PGMs) from a dilute industrial process stream using a packed bed column of ethanol-treated waste yeast biomass immobilized on plaster of Paris (POP) was investigated. The study also included the removal of base metals and other trace elements in dilute solution. The effects of feed flow rate and bed depth on the breakthrough characteristics of the adsorption system were determined. The results showed that removal was favoured by lower flow rates and higher bed depths. An increase in the bed depth with a decrease in flow rate increased the volume of effluent that could be treated effectively before breakthrough. The breakthrough curves for most of the elements do not resemble an ideal breakthrough curve, due to the complexity of the solution. The normalized concentration for most of the metals in solution remained high, even in the early stages of treatment when the sorbent material was most pristine. Generally, the affinity of the sorbent for the elements considered followed the order Pd^{2+}> SO_4^{2-} >Te^{2+}>Pt^{2+}>Ir^{3+}>Ni^{2+}>Cl->.Ru^{3+}>Se^{2+}> Na^{+}. The data from the column studies was fitted to Adam-Bohart and Thomas models. The Adam-Bohart model showed a superior prediction of the experimental data. COD analysis of the effluent was also carried out at different time intervals. The measured COD decreased from 200 mg/l to less than 68 mg/l after 30 minutes, which corresponds to the removal efficiency of about 66%.

Keywords

platinum group metals recovery, dilute process stream, biosorption, packed column, waste yeast biomass, immobilization.

Introduction

The recovery of metals from dilute platinum group metals (PGMs) process streams has a twofold advantage. Firstly, it minimizes contamination of the aquatic environment, and secondly, it recovers metals that have significant commercial value. Conventional methods for the removal of metals from wastewater have proven to be ineffective, especially in the case of very low metal concentrations. A satisfactory process would achieve the goal of metal recovery as well as wastewater purification at a relatively low cost, and without the generation of large amounts of residual solids. The search for new, effective and economical technologies for the removal of precious metals from waste streams has therefore shifted towards biosorption. Employing materials of biological origin allows existing knowledge to be applied to the development of technologies to treat metal- and organic-containing solutions. These biosorbents possess metal –sequestering properties capable of quickly and efficiently decreasing the concentration of metals ions in dilute complex solution from parts per billion to parts per trillion (Wang and Cheng, 2006). For economic reasons, researchers have paid much attention to various byproducts from the fermentation industries because these are available in large quantities. One such waste from the food and beverage industry is brewery waste biomass, *Saccharomyces cerevisiae*. During fermentation, the yeast biomass increases three- to six-fold. However, this brewery waste material is largely used only as swine and ruminant feeds (Soares and Soares, 2012). The biosorbents can be treated by various chemical or physical processes to improve the effectiveness of their functional groups, thereby increasing the metal binding capacities.

The technical viability and biosorption capacity of the *Saccharomyces cerevisiae* waste biomass for the removal of PGMs from synthetic solution in a batch system has been investigated previously (Oke, Ndlovu, and Sibanda, 2014). However, for practical and large-scale operation, a packed column is preferred since a batch system is usually limited to the treatment of small quantities of wastewater. Free biomass has low mechanical strength and is not suitable for use in column applications (Rose and Townsley, 1986). Furthermore, high hydrostatic pressures are required to generate suitable flow rates in packed columns, and these high pressures can disintegrate the free biomass. These problems can be avoided by the use of immobilized biomass systems. In the biosorption processes for metal removal from wastes and dilute process streams, different immobilization

* *University of the Witwatersrand, South Africa.*
 ISSN 2225-6253. This paper was first presented at the Hydrometallurgy Conference 2016 'Sustainable Hydrometallurgical Extraction of Metals', *1–3 August 2016, Belmont Mount Nelson Hotel, Cape Town.*

materials have been used. However, no published work is available on the treatment of dilute industrial PGM streams using *Saccharomyces cerevisiae* immobilized on plaster of Paris (POP). Therefore, the aim of this work was to use waste yeast immobilized on POP as a biosorbent for the purification of a dilute industrial PGM process stream. POP was chosen as a support material because of its cost-effectiveness compared to other support materials mentioned in the literature.

Materials and methods

Biosorbent

Spent waste yeast biomass was obtained from a fermenter at South African Breweries in Johannesburg. The yeast cells were initially washed with distilled water and the biosorbent separated by centrifugation. The biosorbent was air-dried and stored for further use.

Chemical treatment of yeast cells

Ethanol-treated yeast cells were prepared by suspending 30 g of cells in 100 ml of 700 g/l ethanol solution for 20 minutes (Goksungur, Uren, and Guvenc, 2002). After treatment, the yeast cells were collected by centrifugation, washed several times with distilled water, and air-dried.

Dilute process solution

The industrial dilute process solution used was collected at the process outlet stream of a South African PGM refinery.

Plaster of Paris (POP)

The POP used in biomass immobilization was purchased at a local hardware shop.

Yeast immobilization on plaster of Paris

Immobilization of the yeast biomass was carried out with POP as support material using the method reported by Ghosh, (1988). The ethanol-treated yeast was suspended in water and plaster was added to form a thick dough. The final concentration of yeast was 20% (w/v). Beads (4.5–5.5 mm) were cast from the plaster dough and kept overnight at 26–28°C. The beads were then washed under running tap water to remove any loosely adherent yeast and again kept overnight at 26–28°C. The immobilization procedure as reported by Ghosh (1988) was slightly modified: radiation killing of the yeast cells was avoided (radiation killing is a form of heat treatment using ultraviolet light), and the yeast cells were used as-is after immobilization for purification of the PGMs effluent.

Characterization the dilute industrial process stream

The dilute industrial solution was characterized for total solids (TS), total dissolved solids (TDS), total suspended solids (TSS), pH, chloride, ammonia, sulphate, and salinity (conductivity). The PGM and base metals contents were analysed by inductively coupled plasma–mass spectrometry (ICP-MS) (Perkin Elmer Nexlon 300D). Table I gives the chemical composition of the PGM stream as received.

Chemical oxygen demand (COD) was determined with a Spectroquant Pharo 300 in accordance with the instructions of the manufacturer.

Column experiments

Column experiments were conducted in an acrylic glass tube of 25 cm inner diameter and 45 cm height packed with yeast immobilized on plaster of Paris. Glass beads were introduced at the top and the bottom of the packed column to prevent the adsorbent from floating. The dilute PGM process solution was conditioned to pH 3 (the optimum pH for adsorption obtained in the batch experiments (Oke, Ndlovu, and Sibanda, 2014) using 0.1 M NaOH and HCl solutions. The solution, with known concentration of solutes, was pumped through the column in an upflow direction using a peristaltic pump (Watson Marlow 5045) with variable speed adjustment. The upflow movement was chosen because it minimizes clogging and unintentional filtration. Samples were collected from the column at regular intervals and analysed by ICP-MS (Perkin Elmer Nexlon 300D). Figure 1 is a schematic of the experimental set-up for the column study.

The experimental conditions chosen for investigating the sorption performance of POP yeast in a fixed- bed column were as follows: bed depth 6.5, 8.5, and 13 cm; flow rate 0.9, 1.3, and 2.1 ml/s. All experiments were carried out for 180

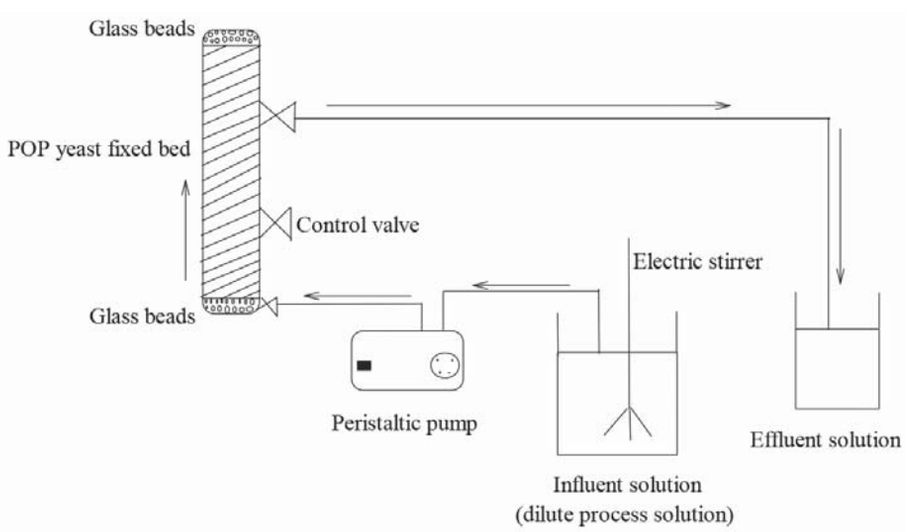

Figure 1—Experimental set-up for column study

minutes. The flow rates and bed depths were chosen based on information from the literature (Calero *et al.*, 2009; Danny, Porter, and McKay, 2000). The pH and the time used were based on the information gathered from the batch studies (Oke, Ndlovu, and Sibanda, 2014).

Control experiments

Control experiments were performed with only the POP beads without yeast to ascertain the adsorption characteristics of POP itself (if any).

Results and discussion

Characterization of dilute PGM solution

Table I gives a summary of the physico-chemical characteristics of the PGMS effluent stream. Most of the values are above the permissible limit set by the US Environmental Protection Agency (USEPA, 2010) as well as the Department of Water Affairs and Forestry, South Africa (DWAF, 1996).

The high concentration of sulphate, sodium, and chloride ions causes the solution to have a very high ionic strength. The ionic strength and the pH strongly influence metal speciation and the type of metal ion complexes in industrial wastewater. The solubility of most metals decreases as the ionic strength of the medium increases. According to the DWAF guidelines (shown alongside the dilute process stream characteristics in the table), the wastewater is not suitable for re-use in industrial processes. The pH, chloride, and sulphate levels are likely to lead to problems such as corrosion and scaling of process equipment.

Table I

Physico-chemical characterization of the dilute PGMs solution

Characteristic	Measured value	USEPA limits	DWAF guideline for industrial disposal
pH	1.8	n/a	5-10
Total conductivity (mS/m)	12,644	n/a	n/a
Colour	Brown	n/a	n/a
COD (mg/l)	200	5	0-75
TSS (mg/l)	1080	4	0-25
TDS (mg/l)	220	50	n/a
TS (mg/l)	1300	n/a	0-1600
Chloride (mg/l)	3497	n/a	0-500
Sulphate (SO_4) (mg/l)	10,947	5	0-500
t (NH_3) (total ammonia) (mg/l)	79.1	0.01	n/a
Ag (mg/l)	0.004	n/a	n/a
Au (mg/l)	0.015	0.005	n/a
Pd (mg/l)	0.248	0.02	n/a
Pt (mg/l)	1.88	0.1	n/a
Rh (mg/l)	0.065	0.02	n/a
Ir (mg/l)	8.25	0.02	n/a
Ru (mg/l)	0.937	0.1	n/a
Co (mg/l)	0.026	0.005	n/a
Cu (mg/l)	0.275	0.005	0.006
Zn (mg/l)	0.077	0.0002	0.05
Te (mg/l)	1.24	0.02	n/a
Se (mg/l)	416	0.01	0.05
Fe (mg/l)	1.17	0.005	0.0–10.0
Na (mg/l)	45100	0.1	n/a
Ni (mg/l)	2.08	0.005	n/a

Chemical oxygen demand (COD)

The chemical oxygen demand (COD) test is commonly used to indirectly measure the amount of organic compounds in water. During the adsorption process, the COD of the effluent was measured at different time intervals. The COD decreased from 200 mg/l to less than 68 mg/l after 30 minutes, which corresponds to a removal efficiency of about 66%. Beyond this time, there was no significant change in the COD level.

Column experiments

Continuous-mode sorption studies play an important role in evaluating the technical feasibility of a treatment process for industrial application (Akar and Divriklioglu, 2010). This work focused on the removal of metal species with high concentrations or those species found to be above their discharge limit (in the case of base metals and the anions) or with concentrations above 0.1 mg/l in the case of PGMs. The species of interest include sulphates, chlorides, Na, Ni, Se, Ru, Pd, Pt, and Ir. For the test work, the dilute process stream was conditioned to pH 3 (the optimum pH for PGM adsorption in the batch studies (Oke, Ndlovu, and Sibanda, 2014).

Control experiments

The results from the control experiments showed that the adsorption of the species of interest was due to the functional groups on the biomass, as reported by Oke, Ndlovu, and Sibanda, (2014), and not affected in any way by the POP.

Effect of flow rate

The effect of flow rate on the biosorption of the metals of interest was studied by varying the flow rate from 0.9 to 2.1 ml/s while the bed height was held constant at 13 cm. The breakthrough curves were constructed as C/C_0 (where C is the effluent concentration at time t, and C_0 is the initial concentration of the influent stream) *versus* time, as presented in Figures 2–4. Breakthrough is considered to have occurred when there is a sharp increase in the outlet concentration. The breakthrough time is arbitrarily inferred to occur at $C/C_0 = 0.05$ according to Oliviera *et al.* (2011). However, the breakthrough in this study is based on the allowable discharge limits of various metal of interest as outlined by USEPA (2010), as well as by DWAF (1996), as given in Table II. In addition, saturation was assumed to have occurred when the effluent concentration was generally at 90–95% of the influent concentration (Oliviera *et al.*, 2011). However, from examination of Figures 2–4, it can be concluded that saturation of the bed, by the above definition, was not reached. In addition, the steepness of most of the graphs shows that frequent and accurate monitoring of the effluent quality is needed to ensure that a high concentration of the contaminant is not allowed to exit the column before the run is terminated (Benjamin and Lawler, 2013). The steepness of the breakthrough curve determines the extent to which the capacity of an adsorbent bed can be utilized.

Figures 2–4 show the breakthrough curves of some of the elements studied at different flow rates. The choice of

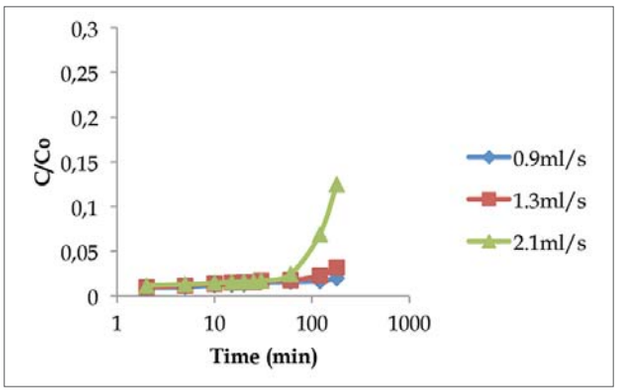

Figure 2—Breakthrough curves for palladium adsorption at different flow rates (C_o = 0.248 mg/l, bed height = 13 cm, T = 25°C)

elements was not based on any criteria, but is intended as a representation of the whole study, as due to space limitations the breakthrough curves for all the elements studied cannot be included in this manuscript. Figure 2 shows the effect of flow rate on the adsorption of palladium at an inlet metal concentration of 0.248 mg/l. The results show that if the maximum allowable limit for palladium is 0.02 mg/l (Table III), then the breakthrough time occurred at 180 minutes for a flow rate of 0.9 ml/s, 120 minutes for 1.3 ml/s, and 60 minutes for 2.1 ml/s. For a sharp breakthrough to occur at the lower flow rates, and for the bed to be saturated with palladium ions, the adsorption time must be prolonged beyond 180 minutes. Since a longer breakthrough time implies better adsorption capacity, when operating at lower flow rates it would take much longer for the adsorbent to be completely saturated with the adsorbate. It can be inferred from Figure 2 that despite the very low concentration of palladium in the influent, the sorbent has high affinity for palladium.

Figure 3 shows the effect of solution flow rate on the adsorption of sulphate ions at an inlet concentration of 10 947 mg/l .The figure shows that as the flow rate increased, the breakthrough time decreased from 30 minutes to 10 minutes. In addition, despite the high concentration of sulphate ions in solution, saturation of the column could not be achieved, unlike other ions with high concentrations in solution such as Se^{2+}, and Na^{+} (data not shown). This may be explained by using the point of zero charge (pHzc) of the yeast. The pHzc of the yeast is 6.31; at pH values lower than this, the surface of the sorbent will be positively charged and will thus attract negatively charged ions. This may be the reason why sulphate ions and metals such as platinum and palladium, which form negative complexes such as chloroanionic complex in solution, were easily adsorbed from the solution regardless of their concentration.

Figure 4 shows the effect of solution flow rate on the adsorption of tellurium at an inlet concentration of 1.24 mg/l. The results show that the breakthrough time decreased from 30 minutes to 10 minutes as the flow rate increased from 0.9 to 2.1 ml/s. In addition, it can be seen that the allowable limit (0.02 mg/l) for tellurium was achievable only at a flow rate of 0.9 ml/s.

Table II summarizes the breakthrough times at different flow rates for the different metals. The overall results show that as the flow rate increased, the breakthrough time decreased.

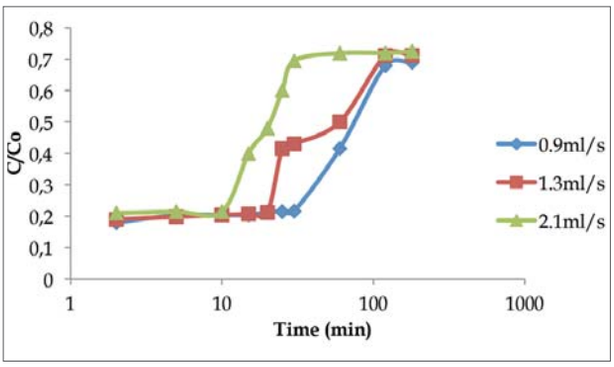

Figure 3—Breakthrough curve for sulphate adsorption at different flow rates (C_o = 10,947 mg/l, flow rate = 0.9 ml/s, T = 25°C)

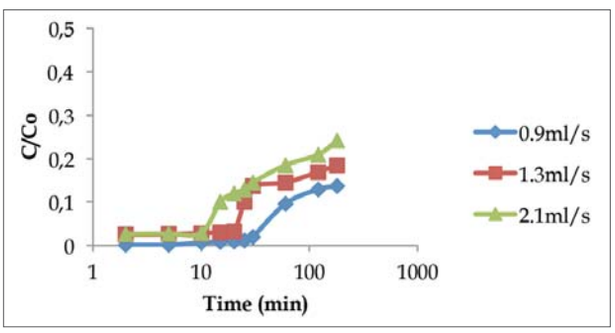

Figure 4—Breakthrough curve for tellurium adsorption at different flow rates (C_o = 1.24 mg/l, flow rate = 0.9 ml/s, T = 25°C)

With increased flow rate, the bed utilization, as well as the bed adsorption capacity, will be reduced. This is due to insufficient residence time of the solute in the column, leading to insufficient diffusion of the solute into the pores of the adsorbent. The solute therefore leaves the column before equilibrium is established. These results are in agreement with findings in the literature for systems of biosorption in columns for different metals using different sorbent materials (Calero *et al.*, 2009; Danny, Porter, and McKay, 2000; Khan, Bury, and Hogstrand, 2011). For most of the platinum group metals present in the solution under study, a prolonged residence time, typically more than 180 minutes, is required to reach column saturation, regardless of the flow rate used. The significant difference in breakthrough time for palladium compared with the other PGMs is due to the fact that the sorbent has high affinity for palladium, which is in agreement with the results obtained in the batch studies.

The experimental results indicate that a flow rate of 0.9 ml/s produces a classic breakthrough curve to work with compared to the higher flow rates tested, since a longer breakthrough time indicates higher efficiency of the

Table II

Breakthrough times (minutes) at different flow rates

Flow rate	Pt	Pd	Ir	Ru	Se	Te	Ni	Na	SO_4	Cl
0.9 ml/s	25	180	25	10	10	30	25	5	30	25
1.3 ml/s	10	120	10	5	2	20	15	2	20	15
2.1 ml/s	5	60	5	2	2	10	10	2	10	5

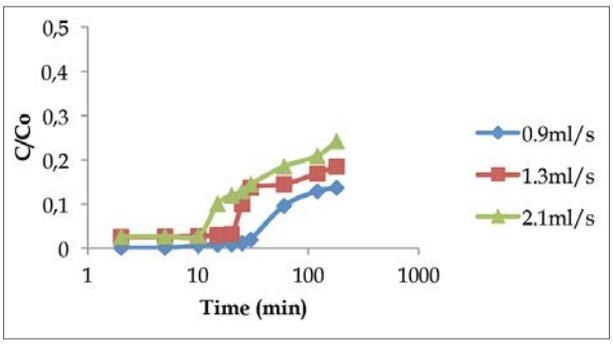

Figure 5—Breakthrough curve for palladium at different bed depth (C_o = 0.248 mg/l, flow rate = 0.9 ml/s, T = 25°C)

adsorbent. Therefore, the subsequent experiments were carried out at a flow rate of 0.9 ml/s.

Effect of bed depth

The retention of metal ions in a fixed-bed column depends, among other factors, on the quantity of solid sorbent used or on the bed depth of the column (Calero *et al.*, 2009). The sorption performance of plaster of Paris-immobilized yeast was assessed using bed depths of 6.5 cm, 8.5 cm, and 13 cm at flow rate of 0.9 ml/s. Figure 5 shows the effect of bed depth on the sorption of palladium. As the bed height decreased from 13 cm to 6.5 cm, the breakthrough time decreased from 180 minutes to 30 minutes. This is because at lower bed depth there are fewer binding sites, which are quickly taken up by the adsorbing ions.

Figure 6 shows the effect of bed depth on the sorption of sulphate ions. The results similarly show that the breakthrough time increased from 10 minutes to 30 minutes when the bed depth increased from 65 mm to 130 mm.

Figure 7 shows the effect of bed depth on the sorption of tellurium. The breakthrough time increased from 10 minutes to 30 minutes as the bed depth increased from 6.5 cm to 13 cm. The results demonstrate that the adsorbent has a high affinity for tellurium compared to platinum, ruthenium, and nickel, which were also present in lower concentration in the solution.

Table III summarizes the breakthrough times for different metals at different bed depths. Generally, the breakthrough time increased as the bed depth increased from 6.5 cm to 13 cm. Similarly, the time necessary for saturation of the column is higher as the bed depth is increased; in some cases a

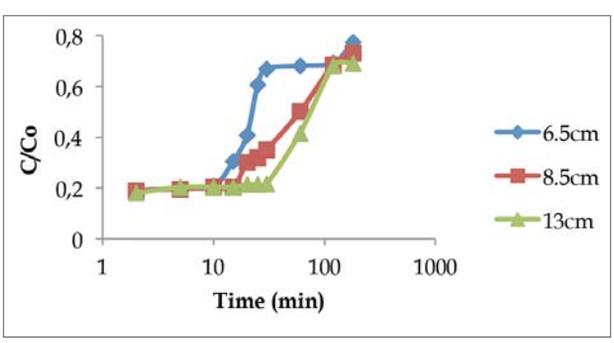

Figure 6—Breakthrough curve for sulphate adsorption at different bed depth (C_o = 10,947 mg/l, flow rate = 0.9 ml/s, T = 25°C)

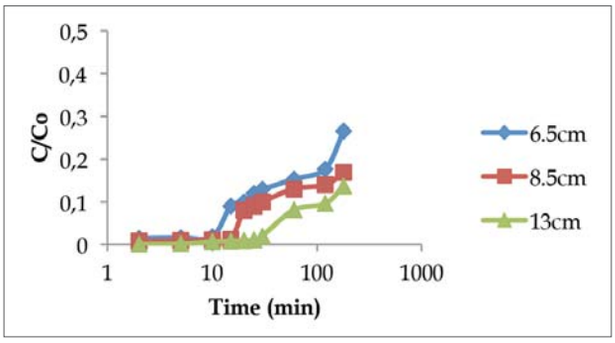

Figure 7—Breakthrough curves for tellurium adsorption at different bed depths (C_o = 1.24 mg/l, flow rate = 0.9 ml/s, T = 25°C)

contact time longer than 180 minutes was necessary. Although an increase in bed depth increased the breakthrough time, a very deep bed is not practical for a single column; instead, multiple columns should be designed (Netpradit, Thiravetyan, and Towprayoon, 2004). This is because when the bed height (the adsorbent dosage) increases to a certain level, the adsorption density (the amount adsorbed per unit mass) decreases.

Based on the information in Tables II and III, it is evident from the breakthrough times (t_b values at 0.9 ml/s and 13 cm) that the binding affinity for the PGMs in the solution under study on POP-immobilized yeast follows the order Pd^{2+}>Pt^{2+}>Ir^{3+}>Ru^{3+}, while the binding affinity for other elements in the solution follows the order Te^{2+}>SO_4^{2-}>Ni^{2+}>Se^{2+}>Cl->Na^+. Generally, the binding affinity for all the elements follows the order Pd2+> SO42->Te^{2+}>Pt^{2+}>Ir^{2+}>Ni^{2+}>Cl->Ru^{2+}>Se^{2+}> Na^+.

Table IV gives the allowable discharge limits of various elements (USEPA, 2010) and the metal concentration at breakthrough point (flow rate 0.9 ml/s and 13 cm bed depth). Most of the elements in the solution did not reach their allowable discharge limit even before breakthrough was achieved, except Pd and Te. Therefore a multiple column is recommended for practical purposes in treating effluents of this nature.

As the concentration of chloride was one of the highest among the contaminating anions, the chloride concentration was also monitored. The chloride concentration decreased in the early stage of treatment (at 0.9 ml/s and 13 cm bed depth), indicating that the column did adsorb chloride ions. Within 20 minutes, the chloride concentration had reached 2098 mg/l, equivalent to 40% removal. It is therefore expected that the use of more columns will inevitably continue to decrease the concentration of anions and other elements in solution, but a decision must be made regarding how many columns would be economically feasible.

Table III

Breakthrough times (minutes) at different bed depths

Flow rate	Pt	Pd	Ir	Ru	Se	Te	Ni	Na	SO_4	Cl
6.5 cm	10	30	10	2	2	10	10	2	10	10
8.5 cm	10	60	15	5	5	15	15	2	15	15
13 cm	25	180	25	10	10	30	25	5	30	25

Table IV

Discharge limits (USEPA, 2010) for tested elements in wastewater and breakthrough concentrations

Component	Pt	Pd	Se	Te	Ir	Ru	Na	SO_4	Ni	Cl
Limit (mg/l)	0.1	0.02	0.01	0.02	0.02	0.1	0.1	5	0.005	500
Concentration (C_b) at breakthrough(mg/l)	0.58	0.005	208	0.025	2.64	0.38	18 085	2 364	0.29	2 098

Once the breakthrough time had been determined, the breakthrough capacity Q_B (the column adsorption capacity at breakthrough point) of the adsorbent was calculated as (Goel *et al.*, 2005):

$$Q_B = \left(\frac{t_b Q_w C_O}{m} \right) \quad [1]$$

where t_b is the breakthrough time (minutes), Q_w is the flow rate of the influent wastewater (l/min), C_o is the inlet concentration (mg/l), and m is the mass (g) of the adsorbent. In addition, the volume of effluent treated (V_{ef}) at breakthrough was calculated as:

$$V_{ef} = Qt_B \quad [2]$$

The results presented in Tables V and VI show that, the bed adsorption capacity (Q_b) increases as the flow rate decreases and the bed height increases. However, a slightly different trend was observed for selenium and sodium with regard to the value of Q_b at different flow rates. The results indicated that the adsorption capacities (Q_b) for selenium and sodium at 2.1ml/s are higher than at 1.3ml/s. This may be a result of the low affinity of the adsorbent for these ions, which results in the same breakthrough value at the two flow rates.

Table V

Adsorption breakthrough data at different flow rates

Metal ion	Q (ml/s)	Q_b (mg/g)	V_{ef} (ml)
Platinum	0.9	0.058	1 350
	1.3	0.034	780
	2.1	0.027	630
Palladium	0.9	0.056	9 720
	1.3	0.053	9 360
	2.1	0.043	7 560
Iridium	0.9	0.258	1 350
	1.3	0.149	780
	2.1	0.12	630
Ruthenium	0.9	0.012	540
	1.3	0.008	390
	2.1	0.005	252
Nickel	0.9	0.065	1 350
	1.3	0.056	11 790
	2.1	0.060	1 260
Selenium	0.9	5.212	540
	1.3	1.500	156
	2.1	2.432	252
Tellurium	0.9	0.046	1 620
	1.3	0.044	1 560
	2.1	0.036	1 260
Sodium	0.9	282.500	270
	1.3	163.230	156
	2.1	263.690	252
Sulphate	0.9	411.460	1 620
	1.3	396.220	1 560
	2.1	320.020	1 260
Chloride	0.9	109.535	1 350
	1.3	94.930	1 170
	2.1	51.112	630

The increase in the bed adsorption capacity (Q_b) with increasing bed depth (Table VI) is due to the increase in the specific surface of the adsorbent, which supplies more fixation binding sites (Taty-Costodes *et al.*, 2005). Furthermore, the results show that an increase in the bed depth with a decrease in flow rate increased the volume of effluent that could be treated effectively before breakthrough. Since industrial effluents contain more than one metal ion in solution, calculating the volume of effluent treated at breakthrough point will give an indication of the volume of solution that can be treated in order for each metal to reach its allowable limit, *i.e.* if the breakthrough time for each metal in the effluent is known, then the volume of effluent that can be treated effectively can be determined. However, a slightly different trend was observed for sodium with regard to the value of Q_b at different bed depths. The adsorption capacity (Q_b) for sodium is higher at 6.5 cm bed depth than at 8.5 cm. This is a result of the close values of the breakthrough times at these bed depths.

Evaluation of kinetic models

The fundamental equations for a fixed-bed column depend on the mechanism responsible for the process (mass transfer from the liquid to the surface of the solid, diffusion and/or reaction on the surface of the solid), and include mass balances between the solid and the fluid and for the sorbed solute, rate of the process, *etc*. The equations derived to model the system with theoretical rigor are differential in nature and their solution usually requires complex numerical methods (Calero *et al.*, 2009; Danny, Porter, and McKay, 2000). Because of this, various simple mathematical models such as Adam-Bohart (Bohart and Adams, 1920), Thomas (Thomas, 1944), Thomas, and Yoon and Nelson (Yoon and Nelson, 1984) have been developed to predict the dynamic behaviour of a column and allow some kinetic coefficients to be estimated. The Adam-Bohart and Thomas models were used in this study to analyse the behavior of the packed column.

The column data fitted better with the Adam–Bohart model than with the Thomas model for all the conditions tested. The results from the model indicated that the greater the bed height, the higher the adsorption capacity, No, of the adsorbent and the lower the mass transfer coefficient, KAB.

Conclusions

The removal of PGMs, as well as base metals and other trace elements, from a dilute industrial PGM solution was

Table VI

Adsorption breakthrough data at different bed depths

Metal ion	Z (cm)	Q_b (mg/g)	V_{ef} (ml)
Platinum	6.5	0.037	540
	8.5	0.045	540
	13.0	0.058	1 350
Palladium	6.5	0.018	1 620
	8.5	0.029	3 240
	13.0	0.056	9 720
Iridium	6.5	0.198	540
	8.5	0.245	810
	13.0	0.258	1 350
Ruthenium	6.5	0.004	108
	8.5	0.009	270
	13.0	0.012	540
Nickel	6.5	0.050	540
	8.5	0.061	810
	13.0	0.065	1 350
Selenium	6.5	2.000	108
	8.5	4.120	270
	13.0	5.212	540
Tellurium	6.5	0.029	540
	8.5	0.037	810
	13.0	0.046	1 620
Sodium	6.5	217.350	108
	8.5	178.650	108
	13.0	282.530	270
Sulphate	6.5	263.780	540
	8.5	325.240	810
	13.0	411.460	1 620
Chloride	6.5	84.265	540
	8.5	103.898	810
	13.0	109.535	1 350

investigated using *Saccharomyces cerevisiae* waste yeast immobilized on plaster of Paris support material in a packed column. Dynamic adsorption conditions such as bed height (Z), and solution flow rate (Q) were tested to establish their influence on the purification process. The packed bed column was found to perform better with lower influent rate and greater bed depth. In addition, it was found that for the bed to reach saturation for most of the metals, an adsorption time greater than 180 minutes was necessary. Successful selective binding and recovery of metal from the mixed metal solutions depended on the binding affinity of the metals, which followed the order $Pd^{2+}>SO_4^{2-}>Te^{2+}>Pt^{2+}>Ir^{2+}>Ni^{2+}>Cl^-$ $>Ru^{3+}>Se^{2+}> Na^+$.

The study showed that if multiple fixed-bed columns are used, all the valuable metals can be recovered, and the concentration of other contaminants like sulphate, chloride, and sodium reduced to meet the Department of Water Affairs and Forestry (1996) guidelines for industrial water re-use. The purified stream could be used for dust suppression, firefighting, ash quenching, and irrigation *etc*. In light of continued population growth, ongoing contamination of both ground and surface waters, uneven distribution of water resources, and periodic droughts, consideration must be given to purifying industrial water. The recycling of the purified waste stream within the refinery would constitute a considerable saving in terms of water required from surrounding municipalities, which are already struggling to provide enough water.

Acknowledgements

The authors thank South African Breweries for the supply of the waste yeast used in this study, and the PGM refinery (which cannot be identified for confidentiality reasons) that provided the dilute process stream sample.

References

Akar, T. and Divriklioglu, M. 2010. Biosorption application of modified fungal biomass for decolorization of reactive red 2 contaminated solutions: batch and dynamics flow mode studies. *Bioresource Technology*, vol. 101. pp. 7271–7277.

Benjamin, M.M. and Lawler, D.F. 2013. Water Quality Engineering: Physical/Chemical Treatment Processes. Wiley, Hoboken, New Jersey.

Bohart, G.S. and Adams, E.Q. 1920. Behavior of charcoal towards chlorine. *Journal of Chemical Society*, vol. 42. pp. 523–529.

Calero, M., Hernainz, F., Blazquez, G., Tenorio, G., and Martin-lara, M.A. 2009. Study of Cr (III) biosorption in a fixed bed column. *Journal of Hazardous Materials*, vol. 171. pp. 886–893.

Danny, C.K., Porter, J.F., and McKay, G. 2000. Optimized correlations for the fixed-bed adsorption of metal ions on bone char. *Chemical Engineering Science*, vol. 55. pp. 5819–5829.

Department of Water Affairs and Forestry. 1996. South African Water Quality Guidelines. 2nd edn. Volume 3: Industrial Use. Pretoria.

Ghosh, G. 1988. Immobilization of baker's yeast using Plaster of Paris. *Biotechnology Techniques*, vol. 2, no. 3. pp. 217–219.

Goel, J., Krishna, K., Chira, R., and Vinod, K. 2005. Removal of lead (II) by adsorption using treated granular activated carbon and column studies. *Journal of Hazardous Materials*, vol. 125. pp. 211–220.

Goksungur, Y., Uren, S., and Guvenc, U. 2002. Biosorption of copper ions by caustic treated waste baker's yeast biomass, *Turkey Journal of Biology*, vol. 27. pp. 23–29.

Khan, F.R., Bury, N.R., and Hogstrand, C. 2011. Copper and zinc detoxification in Gammarux pulex. *Journal of Experimental Biology*, vol. 215. pp. 822–832.

Mack, C.L. 2005. Screening of technologies for the recovery of rhodium (III) metal ions from a precious metal refinery wastewater. MSc thesis. Rhodes University, South Africa.

Mack, C., Wilhelmi, B., Duncan, J.R., and Burgess, J.E. 2007. Biosorption of precious metals. *Biotechnology Advances*, vol. 25, no. 3. pp. 264–271.

Mack, C., Wilhelmi, B., Duncan, J.R., and Burgess, J.E. 2008. A kinetic study of the recovery of platinum ions from an artificial aqueous solution by immobilized saccharomyces cerevisiae biomass. *Minerals Engineering*, vol. 21. pp. 31–37.

Netpradit, S., Thiravetyan, P., and Towprayoon, S. 2004. Evaluation of metal hydroxide sludge for reactive dye adsorption in a fixed-bed column system. *Water Research*, vol. 38. pp. 71–78.

Oke, D., Ndlovu, S., and Sibanda, V. 2014. Removal of platinum group metals from dilute process streams: Identification of influential factors using DOE approach. *Journal of Environmental Chemical Engineering*, vol. 2. pp. 1061–1069.

Oliveira, R.C., Jouannin, C., Guibal, E., and Garcia Jr, O. (2011). Samarium (III) and praseodymium(III) biosorption on Sargassum sp: Batch study. *Process Biochemistry*, vol. 46, no. 3. pp. 736–744.

Ross, I. S. and Townsley, C. C. 1986. The uptake of heavy metals by filamentous fungi. *Immobilization of Ions by Biosorption*. Eccles, H. and Hunt, S. (eds). IRL Press, Chichester, UK.

Soares, E.V. and Soares, H.M.V.M. 2012. Bioremediation of industrial effluents containing heavy metals using brewing cells of Saccharomyces cerevisiae as a green technology; a review, *Environmental Science and Pollution Research*, vol. 19. pp. 1066–1083.

Taty-Costodes, V.C., Faudet, H., Porte, C., and Ho, Y.S. 2005. .Removal of lead (II) ions from synthetic and real effluents using immobilized Pinus sylvestris sawdust: adsorption on a fixed-bed column. *Journal of Hazardous Materials*, vol. 123. pp. 135–144.

Thomas, H.C. 1944. Heterogeneous ion exchange in a flowing system. *Journal of American Chemical Society*, vol. 66. pp. 1466–1664

United States Environmental Protection Agency. 2010. Permit Guidance. Research Triangle Park, North Carolina.

Wang, J. and Chen, C. 2006. Biosorption of heavy metals by *Saccharomyces cerevisiae:* A review. *Biotechnology Advances*, vol. 24. pp. 427–421.

Yoon, Y.H. and Nelson, J.H. 1984. Application of gas adsorption kinetics. Part 1. A theoretical model for respirator cartridge service time. *Journal of American Industrial Hygiene Association*, vol. 45. pp. 509–516..

AfriRock 2017

ISRM International Symposium
'Rock Mechanics for Africa'

30 September–6 October 2017

Cape Town Convention Centre, Cape Town

Keynote Speakers
Nick Barton
Sergio Fontoura
Luís Lamas
Dick Stacey
Nielen van der Merwe
Paul Buddery

BACKGROUND

The 2017 ISRM International Rock Mechanics Symposium is to be held in Cape Town. The conference theme is 'Rock Mechanics for Africa'.
Mining has traditionally been a mainstay of African economies, while Oil and Gas industries are rapidly growing throughout Africa. Infrastructure is being developed to support these industries. Rock engineering design is and therefore will continue to be essential for the growth of the continent. Prior to the conference, the ISRM Board, Council and Commission meetings will take place. Technical visits are being arranged for after the conference.

WHO SHOULD ATTEND

- Rock engineering practitioners
- Researchers
- Academics
- Mining engineers
- Civil engineers
- Petroleum engineers
- Engineering geologists.

TECHNICAL VISITS

The following technical visits are confirmed for the conference:

- Palabora Mine
- Tau Tona Mine
- Chapman's Peak
- SANIRE Presidential Tour

Sponsors

GEOBRUGG Safety is our nature
IDS GeoRadar
GROUNDWORK ROCK AND SUPPORT MONITORING
MACCAFERRI AFRICA
MINOVA
M and J MINING WE SUPPORT YOUR MINE
New Concept Mining Support for the World's Deepest Mines
REUTECH MINING
srk consulting
TRE ALTAMIRA A CLS Group Company
OPTRON
ROCBOLT TECHNOLOGIES

PROGRAMME

Saturday 30/09/2017	Sunday 1/10/2017	Monday 2/10/2017	Tuesday 3/10/2017	Wednesday 4/10/2017	Thursday 5/10/2017	Friday 6/10/2017
ISRM Board Meeting	ISRM Board Meeting	Workshop: ISRM Commission Meetings; ISRM Council Meetings	Technical Session; Morning Refreshments; Technical Session; Lunch; Technical Session; Afternoon Refreshments; Technical Session			Workshop; Technical Visits
	Board Dinner	Network Function		Conference Dinner		• Palabora Mine • Tau Tona Mine • Chapman's Peak

EXHIBITION/SPONSORSHIP

Sponsorship opportunities are available. Companies wishing to sponsor or exhibit should contact the Head of Conferencing.

For further information contact:
Camielah Jardine, Head of Conferencing
SAIMM, P O Box 61127, Marshalltown 2107
Tel: +27 (0) 11 834-1273/7 · E-mail: camielah@saimm.co.za
Website: http://www.saimm.co.za

Supported by

ISRM
SANIRE SOUTH AFRICAN NATIONAL INSTITUTE OF ROCK ENGINEERING
SAIMM THE SOUTHERN AFRICAN INSTITUTE OF MINING AND METALLURGY
South African National Committee on Tunnelling

Conference Announcement

http://dx.doi.org/10.17159/2411-9717/2017/v117n8a6

The process chemistry and mineralogy of brannerite leaching

by R. Gilligan*, and A.N. Nikoloski*

Synopsis

Brannerite (UTi_2O_6) is the most important uranium mineral after uraninite and coffinite, and the most common refractory uranium mineral. As the more easily leachable uranium ores are becoming exhausted, it is necessary to process the complex and refractory ores in order to meet the growing demand for uranium as an energy source. This typically requires either more intense leaching conditions or a better-designed process based on sound understanding of feed mineralogy and reaction chemistry. The present study was carried out to provide information that will enable the development of a more effective processing strategy for the extraction of uranium from ores containing brannerite. The leaching behaviour of brannerite in sulphate media under moderate temperature conditions was investigated and compared with its relative leachability in alternative acid and alkaline systems. The feed and the leached residues were characterized by XRD and SEM-EDX techniques. Brannerite dissolutions of up to 95% after 5 hours of leaching in ferric sulphate media, up to 89% in ferric chloride media under similar conditions, and up to 82% in 24 hours in sodium carbonate media were obtained. Since alkaline leaching was considered promising for acid-consuming ores, leaching was repeated with a high-carbonate brannerite-bearing ore, with comparable extractions. Mineralogical characterization showed that altered and amorphous regions are a regular feature of brannerite, and that pitting is typically observed on the surface of the leached grains. The leaching results, coupled with mineralogical data, showed that the uranium and titanium in brannerite generally dissolve congruently, with faster dissolution of the altered and amorphous regions in the brannerite grains than of the crystalline regions. We conclude that the extent of brannerite alteration is a key factor in process selection, along with the grade, liberation size, and gangue mineralogy.

Keywords
uranium, brannerite, leaching, acidic, alkaline, kinetics.

Introduction

Brannerite (UTi_2O_6) is present as a major uranium mineral phase in many uranium and rare earth element (REE) deposits around the world. It is the most important uranium mineral after uraninite and coffinite (Finch and Murakami, 1999). Brannerite is a refractory uranium mineral and dissolves slowly compared to other uranium minerals under typical processing conditions (Gilligan and Nikoloski, 2015a; Lottering *et al.*, 2008).

Brannerite is typically metamict, rendered amorphous by self-irradiation. A study of brannerite specimens from different locations and of varying ages showed that this process takes less than 10 million years (Lumpkin, Leung, and Ferenczy, 2012), much less than the age of most uranium ores. Altered and metamict brannerite is more reactive than crystalline brannerite. Recrystallizing brannerite by heating it in a furnace greatly reduces the rate of uranium extraction during leaching (Charalambous *et al.*, 2014).

Brannerite dissolves under oxidizing conditions in the conventional acidic ferric sulphate system, releasing uranium into solution as uranyl sulphate complexes such as $UO_2(SO_4)_2^{2-}$ (Equation [1]) and forming secondary titanium oxide through the reversible hydrolysis of titanyl ions and complexes (Equation [2]) (Gilligan and Nikoloski, 2015b; Gogoleva, 2012; Smits, 1984). This process is driven by the presence of ferric ions in solution which oxidize uranium to the hexavalent state, sulphate ions which complex uranium, and acid which attacks the titanium oxide.

$$UTi_2O_6 + 2FeSO_4^+ \rightarrow 2TiO_2 + UO_2(SO_4)_2^{2-} + 2Fe^{2+} \quad [1]$$
$$E_a = 36 \text{ kJ/mol}$$

$$TiO_2 + 2H^+ + 2SO_4^{2-} \leftrightarrow TiO\,SO_4^0 + H_2O \quad [2]$$
$$E_a = 48 \text{ kJ/mol}$$

The activation energy (E_a) values were derived from initial extraction rates measured by Gilligan and Nikoloski (2015b). At higher temperatures and under more strongly acidic conditions, the uranium and titanium in brannerite dissolve congruently through Equation [3] (Gilligan and Nikoloski, 2015b).

* *School of Engineering and Information Technology, Murdoch University, Perth, Western Australia.*

 This paper was first presented at the Hydrometallurgy Conference 2016 'Sustainable Hydrometallurgical Extraction of Metals', *1–3 August 2016, Belmont Mount Nelson Hotel, Cape Town.*

$$UTi_2O_6 + 2FeSO_4^+ + 2H^+ + 2SO_4^{2-} \rightarrow 2TiOSO_4^0 + UO_2(SO_4)_2^{2-} + 2Fe^{2+} + 2H_2O \quad E_a = 23 \text{ kJ/mol} \quad [3]$$

The resulting Fe^{2+} ions are re-oxidized to Fe^{3+} with an oxidant, which is usually pyrolusite (MnO_2), sodium chlorate ($NaClO_3$), or oxygen gas, depending on availability and process economics.

The majority of the work on brannerite leaching published to date has studied only the conventional ferric sulphate system. There is little information available on alternatives such as ferric chloride or sodium carbonate media. In this study, these alternatives were investigated as well as the ferric sulphate system.

The effects of deleterious ions such as phosphate on uranium extraction processes are well documented, though little if any information exists on the effects of these ions specific to brannerite. It is important to understand these interactions, as brannerite is often associated with apatite. Therefore selected acid leaching experiments were repeated with the addition of fluorapatite and fluorite.

Materials and methods

Bulk chemical analyses of the feed brannerite were performed by a local commercial mineral laboratory. The feed and residue solids were characterized by X-ray diffraction (XRD) and scanning electron microscopy using energy dispersive X-ray analysis (SEM-EDX) techniques following the procedures described in Gilligan, Deditius, and Nikoloski (2016).

We performed all ferric sulphate leaching experiments using the procedure described by Gilligan and Nikoloski (2015b). Similar procedures were used for the leach tests with alternative lixiviants, with some minor changes, such as the substitution of $FeCl_3$/HCl for $Fe_2(SO_4)_3/H_2SO_4$ in the chloride leaching experiments, or the addition of 10 g/L CaF_2 or $Ca_5(PO_4)_3F$ in the gangue interaction tests.

Alkaline leaching tests were run for 24 hours. The total carbonate concentration was kept constant at 1.00 mol/L, usually as 0.66 mol/L $NaHCO_3$ and 0.34 mol/L Na_2CO_3.

Characterization of the brannerite sample

We used a specimen of brannerite from the Dieresis deposit, in the Sierra Albarrana area of Spain. Bulk chemical analysis showed that the brannerite was within the typical range of compositions for brannerite (Gilligan, Deditius, and Nikoloski, 2016).

EDX analyses and element maps showed brannerite as the dominant phase, with lesser amounts of titanium oxide. Titanium oxide often formed linear zones through the brannerite surrounded on either side by silicon-enriched zones (Figure 1), consistent with published descriptions of altered brannerite (Lumpkin, Leung, and Ferenczy, 2012).

Despite the large amounts of brannerite identified by EDX, no crystalline brannerite was detected in the XRD analyses. These results indicate that the brannerite phase is metamict, as is typical for brannerite. Two broad peaks were present on the X-ray diffraction pattern, similar to brannerite from other localities (Charalambous *et al.*, 2012; Lumpkin *et al.*, 2012). The first broad peak ran from 20 to 35° 2θ, the second from 40 to 65° 2θ (Figure 6).

Some anatase (TiO_2) was detected in XRD analyses, as was crystalline thorutite ($(Th,U,Ca)Ti_2O_6$) (Figure 6). Fine-grained anatase is a common alteration product of brannerite from several localities (Charalambous *et al.*, 2012; Lumpkin, Leung, and Ferenczy, 2012; Smits, 1984). The specific alteration products vary between deposits, and are affected by the geochemistry of the area (Gilligan, Deditius, and Nikoloski, 2016; Lumpkin, Leung, and Ferenczy, 2012). Calculations using the Scherrer formula (Equation [4]) indicate that the anatase crystallites are 10–20 nm in size.

$$t = \frac{0.9\,\lambda}{B\cos\theta_B} \quad [4]$$

where t is the crystallite size, λ is the X-ray wavelength, B is the peak width in radians at half the maximum height, and θ_B is the diffraction angle, also in radians.

Leaching results

The extent of uranium extraction in the leaching experiments

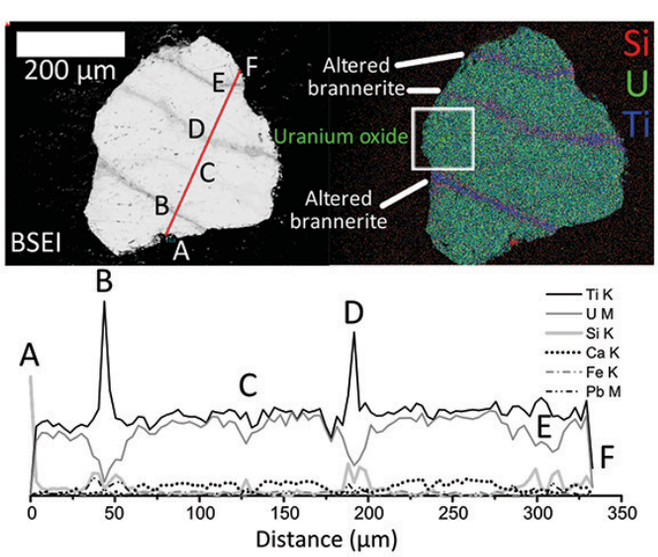

Figure 1—Backscattered electron image (top left), element map (top right), and EDX line analysis (bottom) of an unleached brannerite particle. The position of the line analysis is shown on the BSE image. Letters on the line analysis correspond to points on the BSE image

always exceeded titanium extraction. This is due partly to the presence of insoluble anatase, which is much more resistant to leaching than brannerite. Secondary titanium oxide formed in many experiments. This side-reaction was typically observed at higher temperatures and/or lower acid concentrations. Titanium leaching curves have been omitted from this paper for brevity.

Leaching in different media

Sulphate media were more effective than chloride media at the same temperature and acid concentration, with the exception of 2.00 M acid at 52°C (Figures 2 to 4). Leaching studies on synthetic brannerite suggest that the dissolution of brannerite is promoted by the formation of uranium (VI) complexes at the surface (Thomas and Zhang, 2003). Sulphate and carbonate ions form stable complexes with uranyl ions, while chloride ions do not.

Alkaline carbonate leaching is slow compared to acid leaching, with much longer leaching times required. Alkaline carbonate leaching is typically reported as difficult or unfeasible for refractory uranium ores containing brannerite, yet our results show that it is possible. Calculations indicate that the reaction between carbonates and brannerite is thermodynamically favourable, while experiments (Figure 2) show that it is kinetically slow. Alkaline carbonate media do not attack gangue, leading to reduced reagent consumption and fewer problematic species such as phosphate entering solution. Brannerite has been identified as associated with alkaline gangue in uranium deposits in Queensland, Australia (Wilde *et al.*, 2013) and in the Central Ukrainian Uranium Province (Cuney *et al.* 2012). Many of these deposits also contain apatite, which dissolves rapidly in acidic solutions and suppresses uranium dissolution (Figure 5). For this reason, alkaline carbonate leaching may be the only viable option for processing alkaline refractory uranium ores.

Effect of acid concentration

Variations in acid concentration had only a slight effect on the rate of leaching in sulphate media, but a much larger effect on the rate of leaching in chloride media (Figure 3). The most likely explanation for this lies in the nature of the aqueous uranium species formed. Uranyl chloride complexes are weak compared to uranyl sulphate complexes. Acid has a more active role in attacking brannerite in chloride leaching. Based on the extractions after 15 minutes, the rate of uranium dissolution is approximately first-order with respect to acid in chloride media. In sulphate media, the order of reaction with respect to acid concentration is approximately 0.5. Higher concentrations of acid are required for effective uranium extraction in chloride media compared with sulphate media.

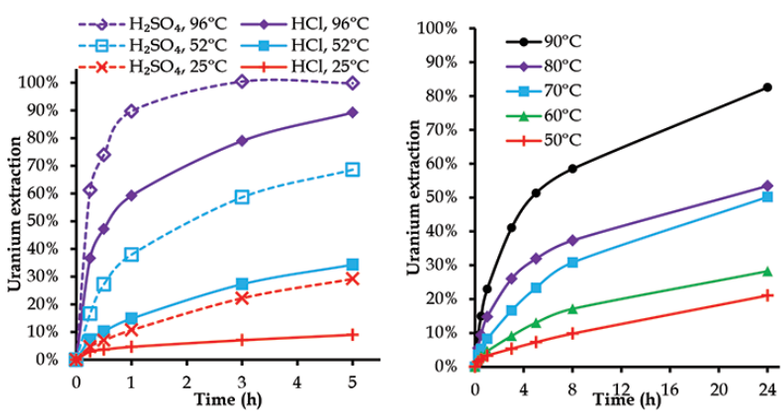

Figure 2—Uranium leaching curves for different temperatures. Left: acid media, 0.25 mol/L H_2SO_4/HCl with 0.05 mol/L Fe^{3+}. Right: alkaline media, 0.66 mol/L $NaHCO_3$, 0.34 mol/L Na_2CO_3 with 0.025 mol/L $K_3Fe(CN)_6$

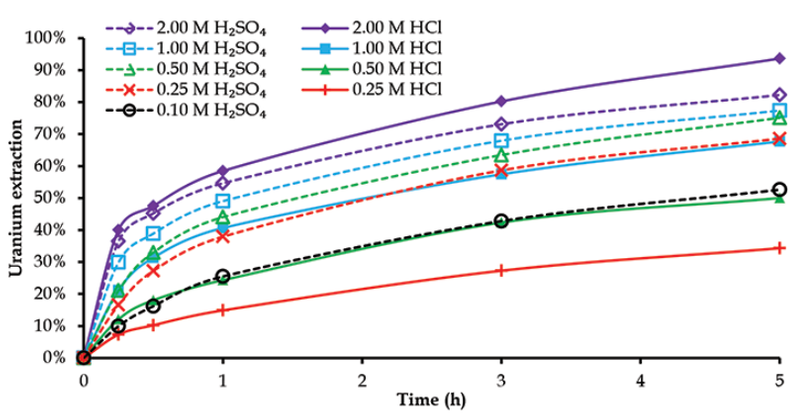

Figure 3—Uranium extraction curves at varied acid concentration at 52°C. Dashed lines: sulphate media; solid lines: chloride media

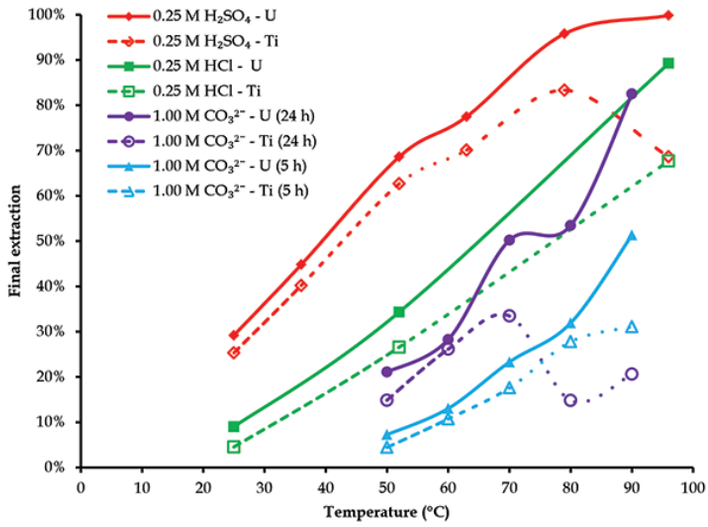

Figure 4—Final extractions of uranium (solid lines) and titanium (dashed lines) *vs* temperature in different leaching systems. 5-hour leaching points from the alkaline tests are shown to simplify comparison between acidic and alkaline media

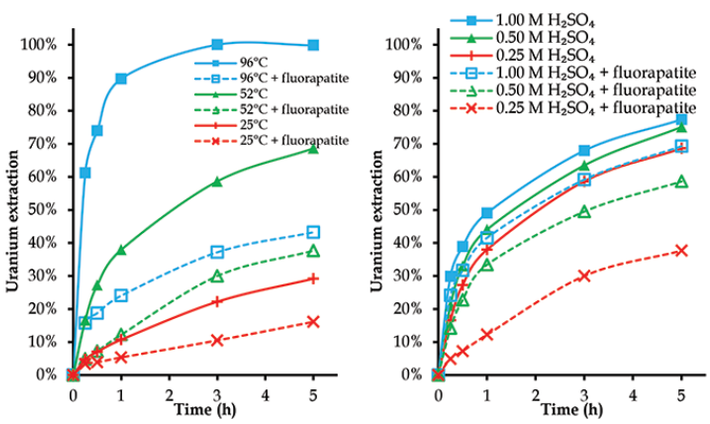

Figure 5—Uranium leaching curves in ferric sulphate media with and without phosphate. Left: varied temperature, 0.25 mol/L H_2SO_4. Right: varied acid concentration, 52°C

Chloride leaching offers no clear advantages over sulphate leaching. However, some preliminary results (based on data to be published in future) suggest that chloride leaching may be a promising alternative for high-phosphate uranium ores.

Effect of temperature

The rate of uranium leaching is strongly dependent on temperature, as has been commonly reported. In sulphate media, a 10°C increase in temperature has a similar effect on the rate of uranium extraction as a four-fold increase in acid concentration. Leaching at higher temperatures enables effective extraction at lower acid concentrations. The optimum temperature and acid concentration will vary with the nature of the gangue. Higher temperatures will also increase the rate at which acid-soluble gangue dissolves, increasing the amount of acid that must be added to control the pH (Ring, 1979).

Temperature has an even stronger effect on the rate of leaching in alkaline carbonate media. Increasing the leaching temperature from 50 to 90°C increased the uranium extraction over 24 hours in alkaline carbonate media from 21 to 83% (Figure 4). High temperatures, ideally over 100°C, appear to be required for alkaline leaching of refractory uranium ores to be effective.

Effect of gangue minerals

Phosphates are known to inhibit uranium leaching by binding to ferric ions, reducing the rate at which ferric ions oxidize uranium (IV) (Nicol, Needes, and Finkelstein, 1975). When leaching brannerite in ferric sulphate media, phosphate released by dissolving apatite suppresses uranium and titanium dissolution. In our experiments, this effect was decreased at higher acid concentrations (Figure 5). Higher sulphate concentrations favour the formation of ferric sulphate complexes over ferric phosphate complexes. Ferric sulphate complexes are more effective oxidants for uranium (IV) than ferric phosphate complexes (Nicol, Needes, and Finkelstein, 1975).

EDX analysis of brannerite particles leached in sulphate media along with apatite shows that many particles were coated with titanium oxide. This coating was enriched in

phosphorus. Phosphate appears to initiate the formation of the titanium oxide coating. The exact mechanism for this is not clear, though the speciation of titanium is known to influence the solid products formed through the hydrolysis of titanium (IV) ions. For example, the presence of sulphate ions favours the formation of anatase over rutile during hydrolysis and precipitation of titanium dioxide (Dambournet, Belharouak, and Amine, 2010). This coating was not observed on brannerite leached in the absence of phosphates. Typically, secondary titanium oxide only formed in sulphate media at less than 0.50 mol/L H_2SO and above 75°C.

Phosphates did not adversely affect uranium extraction in chloride media – instead, phosphates actually improved extraction. Chloride leaching may be an effective alternative for high-phosphate uranium ores, based on data to be published in future

Characterization of residues

Structural characterization (XRD)

The broad peaks, associated with metamict brannerite, in the X-ray diffraction pattern for the original brannerite are absent in the patterns for the residues from leaching with all lixiviants (Figure 6). These changes were most apparent for the leaches at higher temperature.

Metamict brannerite is known to be much more soluble than crystalline brannerite (Charalambous *et al.*, 2014). This explains the disappearance of the broad peaks on the XRD patterns of the leached residues. Brannerite feed samples that have undergone more alteration are less refractory.

Crystalline thorutite and microcrystalline anatase were also present in the leach residues. Anatase and thorutite are resistant to leaching over the range of conditions studied. Some of the anatase in the residues was from the original material, while other anatase formed during leaching. The difference between these phases is described in detail in Gilligan, Deditius, and Nikoloski (2016). In brief, anatase in the unleached material contained uranium, while anatase formed during leaching typically contained iron.

Microscopy and EDX analysis

After leaching at 25°C, much of the surface of the brannerite particles remained intact, with some pitted areas. When the leaching temperature was increased to 52°C, these pits covered the entire surface. Under the most intense acid-leaching conditions (0.50–2.00 mol/L H_2SO_4, 96°C), brannerite was entirely absent from the leached residues. Based on the observation of a large number of particles leached over the full range of conditions, the depth of the leach pits was around 10–20 μm after 5 hours of leaching. Some examples are shown in Figure 7.

The linear inclusions of titanium oxide in the feed particles (shown in Figure 1) are resistant to leaching, as is evident from the way they protrude from the surfaces of leached brannerite particles (Figure 7). The silicon-enriched altered brannerite surrounding these titanium oxide inclusions is more readily leached than the associated brannerite, as is evident from the depth of corrosion around the titanium oxide inclusions.

The reaction front at the base of the leach pits was cracked. EDX line analysis shows that the ratio of uranium to titanium is constant across the reaction front (Gilligan, Deditius, and Nikoloski, 2016). Although titanium dioxide is often reported to form a coating on the surface of leached brannerite particles (Gogoleva, 2012; Smits, 1984), there was no evidence for this happening in sulphate media.

In acidic media, a titanium oxide coating formed only in the presence of phosphates. The titanium oxide layer was enriched in phosphorus. This coincided with unusually low titanium to uranium extraction ratios. Phosphates released through the dissolution of gangue minerals such as apatite stabilize secondary titanium oxide on the surface of the brannerite, further inhibiting leaching (Gilligan and Nikoloski, 2016).

Brannerite leached in alkaline media at higher temperatures (80–90°C) was coated with titanium oxide. According to the leaching kinetics results, the titanium concentration began to decrease after 5–8 hours of leaching. Secondary titanium oxide formed faster at higher leaching temperatures. Line EDX analysis showed a sharp transition between the brannerite core and the secondary titanium oxide. The pitted and cracked brannerite underneath the titanium oxide coating resembled brannerite leached in acidic media around 60°C.

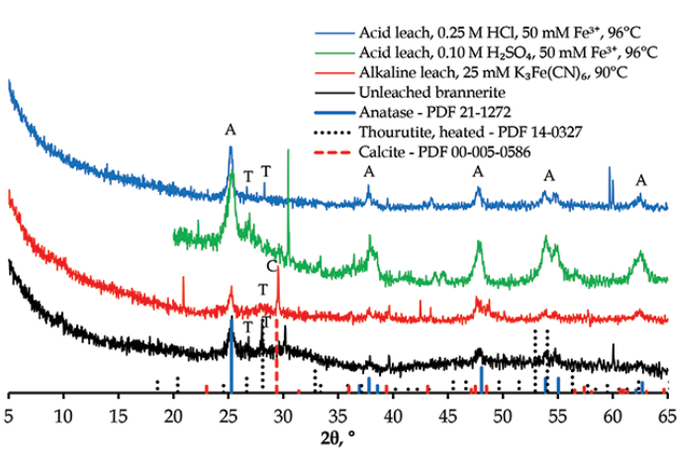

Figure 6—XRD patterns of selected leach residues compared with the unleached material. A: anatase, T: thorutite, C: calcite

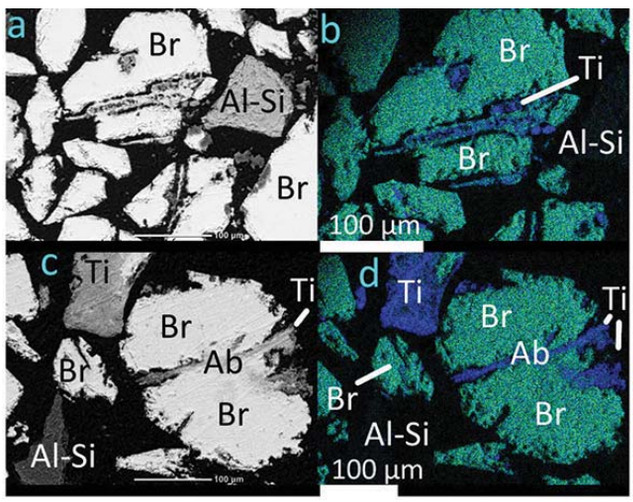

Figure 7—BSEI images (a, c) and element maps (b, d) of leached brannerite particles. Uranium is shown in green, titanium in blue. a and b: 0.50 mol/L H_2SO_4, 25°C; c and d: 0.10 mol/L H_2SO_4, 52°C. Phases: Ab: altered brannerite, Al–Si: aluminium silicate gangue, Br: brannerite, Ti: titanium oxide

Conclusions

Leaching experiments in several different lixiviants showed that the rate of uranium leaching from brannerite is strongly dependent on temperature, less so on acid concentration. Acidic ferric sulphate is an effective lixiviant for brannerite, though ferric chloride may be a better option when the ore contains soluble phosphates. While alkaline leaching is often assumed to be ineffective for the leaching of refractory uranium ores, our results show that it is possible and effective with sufficient time and/or temperature.

Altered zones of the brannerite were more heavily corroded compared to less-altered zones of the brannerite. These findings suggest that more heavily altered brannerite is less refractory than unaltered brannerite. The extent of alteration and the texture of brannerite grains vary between deposits. In light of these findings, it is proposed that the texture of the uranium minerals is an important consideration, along with grade, liberation size, and gangue mineralogy, in predicting the leaching behaviour of refractory uranium ores.

References

Charalambous, F.A., Ram, R., Pownceby, M.I., Tardio, J., and Bhargava, S.K. 2012. Chemical and microstructural characterisation studies on natural and heat treated brannerite samples. *Minerals Engineering*, vol. 39. pp. 276–288.

Charalambous, F.A., Ram, R., McMaster, S., Pownceby, M.I., Tardio, J., and Bhargava, S.K. 2014. Leaching behaviour of natural and heat treated brannerite-containing uranium ores in sulphate solutions with iron (III). *Minerals Engineering*, vol. 57. pp. 25–35.

Cuney, M., Emetz, A., Maercadier, J., Mykchaylov, V., Shunko, V., and Yuslenko, A. 2012. Uranium deposits associated with Na-metasomatism from central Ukraine: a review of some of the major deposits and genetic constraints. *Ore Geology Reviews*, vol. 44. pp. 82–106.

Dambournet, D., Belharouak, I., and Amine, K. 2010. Tailored precipitation methods of TiO_2. Anatase, rutile, brookite: mechanism of formation and electrochemical properties. *Chemistry of Materials*, vol. 22. pp. 1173–1179.

Finch, R. and Murakami, T. 1999. Systematics and paragenesis of uranium minerals. Uranium: mineralogy, geochemistry and the environment. *Reviews in Mineralogy*, vol. 38. pp. 91–179.

Gilligan, R., Deditius, A.P., and Nikoloski, A.N. 2016. The leaching of brannerite in the ferric sulphate system. Part 2: Mineralogical transformations during leaching. *Hydrometallurgy*, vol. 159. pp. 95–106.

Gilligan, R. and Nikoloski, A.N. 2016 The leaching of brannerite in the ferric sulphate system. Part 3: The influence of reactive gangue minerals. *Hydrometallurgy*, vol. 164. pp. 343–254.

Gilligan, R. and Nikoloski, A.N. 2015a. The extraction of uranium from brannerite — A literature review. *Minerals Engineering*, vol. 71. pp. 34–48.

Gilligan, R. and Nikoloski, A.N. 2015b. Leaching of brannerite in the ferric sulphate system. Part 1: kinetics and reaction mechanism. *Hydrometallurgy*, vol. 156. pp. 71–80.

Gogoleva, E.M. 2012. The leaching kinetics of brannerite ore in sulfate solutions with iron (III). *Journal of Radioanalytical and Nuclear Chemistry*, vol. 293. pp. 185–191.

Lottering, M.J., Lorenzen. L., Phala, N.S., Smit, J.T., and Schalkwyk, G.A.C. 2008. Mineralogy and uranium leaching response of low grade South African ores. *Minerals Engineering*, vol. 21, no. 1. pp. 16–22.

Lumpkin, G.R., Leung, S.H.F., and Ferenczy, J. 2012. Chemistry, microstructure and alpha decay damage of natural brannerite. *Chemical Geology*, vol. 291. pp. 55–68.

Nicol, M.J., Needes, C.R.S., and Finkelstein, N.P. 1975. Electrochemical model for the leaching of uranium dioxide: 1 – acid media. *Leaching and Reduction in Hydrometallurgy*. Burkin, A.R. (ed.). Institution of Mining and Metallurgy, London. pp. 1–11

Ring, R.J. 1979. Leaching characteristics of Australian uranium ores. *Proceedings of the Australian Institute of Mining and Metallurgy*, vol. 272. pp. 13–24.

Smits, G. 1984. Behaviour of minerals in Witwatersrand ores during the leaching stage of the uranium extraction process. *Applied Mineralogy*. pp. 599–616.

Thomas, B.S. and Zhang, Y. 2003. A kinetic model of the oxidative dissolution of brannerite, UTi_2O_6. *Radiochimica Acta*, vol. 91, no. 8. pp. 463–472.

Wilde, A., Otto, A., Jory, J., Macrae, C., Pownceby, M., Wilson, N., and Torpy, A. 2013. Geology and mineralogy of uranium deposits from Mount Isa, Australia: implications for albitite uranium deposit models. *Minerals*, vol. 3, no. 3. pp. 258–283. ◆

http://dx.doi.org/10.17159/2411-9717/2017/v117n8a7

Characterization of precipitate formed during the removal of iron and precious metals from sulphate leach solutions

by R. Coetzee*, C. Dorfling*, and S.M. Bradshaw*

Synopsis

Nickel sulphate leach solutions produced in the first leaching stage of base metal refineries contain impurities such as iron as well as precious metals (Rh, Ru, and Ir). Iron precipitation results in sludge formation, which needs to be controlled for efficient operation of downstream nickel recovery processes. Recovery of precious metals from the leach solution is also desired. This study aimed to evaluate the characteristics of the precipitate produced from a nickel sulphate leach solution containing 62.5–89.3 g/L Ni, 2.5 – 3.57 g/L Fe, and 10 mg/L of each of Rh, Ru, and Ir.

Seeded precipitation from ferric-containing solutions resulted in precipitates with a d_{50} particle size of 100.6 µm, which was two orders of magnitude larger than the reference goethite seed d_{50} particle size of 1.3 µm. The particle size distributions of the precipitates formed from ferrous solutions were similar to that of the reference goethite seed. The precipitates formed from ferrous-containing solutions at pH 2.5 and at pH 4 had increased micropore areas (72.8 m^2/g and 87.1 m^2/g, respectively) and decreased external specific surface areas (53.4 m^2/g and 49.0 m^2/g, respectively) compared to the goethite reference material (micropore surface area of 66.2 m^2/g and external surface area of 64.8 m^2/g). For ferric-containing solutions at pH 2.5, a decline in specific surface area from 131.0 m^2/g to between 82.0 m^2/g and 100.6 m^2/g was caused by aggregation and molecular growth inside micropores. Instantaneous iron precipitation from ferric solutions at pH 4 resulted in an increased Brunauer-Emmett-Teller (BET) surface area of 156.5 m^2/g due to poor ordering of crystal structure and a more amorphous surface structure.

Iron oxide phases present in the precipitates had elemental compositions similar to ferrihydrite and schwertmannite. Sulphate inclusion was more prominent during the rapid precipitation from ferric solutions than during precipitation from ferrous solutions. The precipitate formed at pH 2.5 was overall more crystalline than the precipitate formed at pH 4.0; nickel entrainment also increased with an increase in pH. Rhodium- and ruthenium-containing species were finely dispersed throughout the iron phases in the precipitates. Iridium precipitated primarily without the inclusion of iron or other precious metals; particles consisting of iridium (50–80 wt%), chloride, and oxygen were formed.

Keywords
base metals refining, nickel sulphate leach solution, iron precipitation, surface area, porosity, platinum group metals.

Introduction

The nickel sulphate solution produced in the first leaching stage in base metal refineries in the platinum industry can be treated by evaporation and crystallization to produce nickel sulphate hexahydrate crystals. At a specific base metal refinery, sludge formation within the heat exchangers and the holding tanks has been observed; this is believed to be due to precipitation of metal impurities in the stream. Iron is the most abundant impurity in the leach solution and in the sludge, while 'other precious metals' (OPMs, namely Ru, Rh, and Ir) are also present.

Sludge formation needs to be controlled to allow more efficient operation of the nickel crystallization section, while it can also serve as a mechanism for recovery of other precious metals that are present in the leach solution. The objective of this study was to investigate the precipitation behaviour of iron and other precious metals from the nickel sulphate leach solution at different pH values, temperatures, iron oxidation states, seeding conditions, and metal concentrations. The investigation focused specifically on the characteristics of the precipitate formed under different precipitation conditions. Solids characterization techniques that were used include X-ray diffraction (XRD), particle size distribution (PSD), Brunauer-Emmett-Teller (BET) surface area analysis, and scanning electron microscopy (SEM) with energy dispersive X-ray spectroscopy (EDS). Knowledge about the characteristics, structure, and composition of the precipitate formed at different conditions can assist in optimal management of sludge formation on site.

Iron precipitation

The precipitation of iron from acidic solutions proceeds primarily by hydrolysis of ferric, which leads to the formation of complexed iron hydroxides and, subsequently, solid precipitates. For precipitation of iron from ferrous-containing solutions, the first step would entail oxidation of ferrous to ferric. This oxidation step, presented in Equation [1], is typically rate-limiting when precipitation is performed below 150°C (Singer and Stumm, 1970). At higher temperatures, oxygen solubility may become rate-limiting, depending on solution chemistry (Lowson, 1982). Subsequent hydrolysis proceeds according to Equation [2] or, if the iron concentration

* *Department of Process Engineering, Stellenbosch University, South Africa.*

This paper was first presented at the Hydrometallurgy Conference 2016 'Sustainable Hydrometallurgical Extraction of Metals', *1–3 August 2016, Belmont Mount Nelson Hotel, Cape Town.*

exceeds 10^{-3} M, by means of dimerization shown in Equation [3] (Dutrizac, 1980).

$$4Fe^{2+} + O_{2(aq)} + 4H^+ \rightarrow 4Fe^{3+} + 2H_2O \quad [1]$$

$$Fe(OH_2)_6^{3+} \rightarrow Fe(OH)\ n(OH_2)_{6-n}^{3-n} + nH^+ \quad [2]$$

$$2Fe^{3+} + 2H_2O \rightarrow Fe_2(OH)_2^{4+} + 2H^+ \quad [3]$$

The hydroxyl complexes formed according to Equation [3] undergo polymerization to form longer iron hydroxyl compounds, which could incorporate other ligands and which serve as precursor for iron oxide and iron hydroxide precipitates. Jiang and Lawson (2006), for example, reported that substitution of hydroxide with sulphate ligands at low pH values and high sulphate concentrations results in the formation of sulphur-containing iron precipitates. Bigham *et al.* (1996) reported that some of the sulphur in ferrihydrite compounds may not be structurally incorporated, but rather adsorbed onto the surface of the iron species. In these cases, sulphur is considered an anionic impurity. The direct formation of iron sulphate complexes, which could serve as intermediate in the formation of iron sulphate precipitates, is also possible via Equations [4] and [5] (Cornell and Schwertmann, 2003).

$$Fe^{3+} + SO_4^{2-} \rightarrow Fe(SO_4)^+ \quad [4]$$

$$Fe(SO_4)^+ + SO_4^{3-} \rightarrow Fe(SO_4)_2^- \quad [5]$$

The type of precipitate that forms depends on the leach solution conditions. According to Cornell and Schwertmann (2003), rapid hydrolysis results in the formation of ferrihydrite, while slow hydrolysis at elevated temperatures will lead to the formation of akaganéite or its sulphate derivative, schwertmannite ($Fe_8O_8(OH)_x(SO_4)_y$). Commercial iron precipitation processes are designed to form one of the thermodynamically most stable species. Goethite (α-FeOOH) and haematite (α-Fe_2O_3) are the thermodynamically most stable iron hydroxide and iron oxide precipitates, respectively. In terms of iron sulphate precipitates, jarosite is the thermodynamically most stable precipitation product.

Seeding of growth medium is an important design parameter as it aims to provide a growth surface for targeted growth of certain iron phases without the requirement for nucleation. The mechanism by which precipitation then proceeds involves transport of the dissolved species to the surface, adsorption on the surface, and incorporation into the crystal. Incorporation in the crystal structure can be a result of reactions such as dehydration or dehydroxylation (Cornell and Schwertmann, 2003). Cation substitution is also possible, whereby foreign cations replace iron in the crystal structure; the likelihood of cation substitution occurring is determined by how closely the valence and ionic radius of the foreign cation resembles that of the ferric ion (Goldschmidt, 1937). Other mechanisms for co-precipitation include direct precipitation (by, for example, hydrolysis) and entrainment.

Experimental

Materials

The precipitation experiments were performed using three different synthetic nickel sulphate leach solutions. The compositions of the 'low' and 'high' solutions reported in Table I were based on the typical range of metal concentrations in the industrial leach solutions; some precipitation tests were also performed on synthetic solutions containing only iron and precious metals (labelled OPM in Table I) in order to develop a better understanding of the precious metals' precipitation behaviour. The synthetic solutions were prepared using the reagents listed in Table II. Goethite seed material (α-FeOOH, 30–63% Fe) was supplied by Sigma Aldrich.

Equipment

The precipitation tests were performed in closed 1.6 L glass vessels. The solution was stirred using magnetic stirrers set to a constant stirring speed of 600 r/min, and vortex formation was minimized by means of four epoxy-coated baffles inserted in the vessel. Agitation speeds between 300 r/min and 700 r/min were assessed; it was found that agitation at a rate of 600 r/min was sufficient to agitate solids, mix reagents with the solution, and ensure an evenly distributed temperature profile. A Pt-100 thermocouple connected to a hotplate with feedback control was used to control the temperature to within 2°C of the temperature set-point. The solution pH was controlled using a Eutech Alpha pH 560 controller with the output connected to a solenoid valve in the outlet of a burette filled with a sodium hydroxide solution, which was gravity-fed to the reaction vessel as required. A Liebig condenser connected to the vessel lid was used to minimize evaporation losses. The temperature and

Table II

Reagents used for preparation of the synthetic leach solutions

Metal	Source	Grade	Purity
Ni	$NiSO_4 \cdot 6H_2O$	Analytical Reagent	99%
Cu	$CuSO_4 \cdot 5H_2O$	Analytical Reagent	98.5%
Fe^{2+}	$FeSO_4 \cdot 7H_2O$	Analytical Reagent	98%
Fe^{3+}	$Fe_2(SO_4)_3 \cdot xH_2O$	Technical	97%
Co	$CoSO_4 \cdot 7H_2O$	Analytical Reagent	99%
Rh	$RhCl_3 \cdot xH_2O$	Not specified	38–40% Rh
Ru	$RuCl_3 \cdot xH_2O$	Reagent	38–42% Ru
Ir	$IrCl_3 \cdot xH_2O$	Reagent	Not given
As	As_2O_3	Analytical Reagent	> 99.8%
Na	NaOH	Analytical Reagent	> 99%
-	H_2SO_4	Analytical Reagent	> 99%

Table I

Metal concentrations in the respective synthetic leach solutions

Total metals	Ni (g/L)	Co (mg/L)	Fe (mg/L)	Cu (mg/L)	As (mg/L)	Rh (mg/L)	Ru (mg/L)	Ir (mg/L)
Low	62.5	650	2500	50	65	10	10	10
High	89.3	930	3570	70	93	14	14	14
OPM	–	–	2500	–	–	10	10	10

pH set-points for the respective tests are listed in Table III; the ranges of temperatures, pH values and metal concentrations were selected to correspond with the typical plant operating conditions.

Procedure

A working volume of 500 mL was used for all experiments. The solution was prepared by adding NaOH to 300 mL demineralized water. The amount of As_2O_3 required to achieve the As concentrations specified in Table I was dissolved in the alkaline solution before H_2SO_4 was added to lower the pH to 3. At this pH, the Ni, Co, Cu, and precious metal salts were added. The solution was then diluted to close to 500 mL and acidified to pH 1.7 before iron salts were added. Once all the metal salts had dissolved, the solution volume was made up to 500 mL. The solution was added to the glass vessel, agitation was started, and temperature control initiated. Once the set-point temperature had been reached, the initial sample was taken and the seed material and neutralizing agent added immediately afterwards. The solution was then left for a period of 6 hours, during which 4.5 mL liquid samples were taken intermittently (at 2, 15, 30, 60, 90, 120, 180, 240, and 360 minutes) to monitor metal precipitation over time. The solution that remained after six hours was filtered, and the solids residue washed with water and dried for analysis.

The precipitation tests were performed at different pH values, iron oxidation states, total metal concentrations, temperatures, and seeding conditions. A summary of the conditions investigated and the corresponding analyses is presented in Table III.

Analytical techniques

X-ray diffraction

The precipitates, already in a finely powdered form, were analysed using a Bruker AXS D8 Advance diffractometer; Cu-K radiation with a position sensitive Vantec-1 detector was utilized. The detected peaks were normalized and matched to the International Centre for Diffraction Data (ICDD) powder detection file database of 1998. Data evaluation was done with Bruker's EVA software. The step time, step size, and counting times were varied in order to yield good statistics. A tube voltage of 40 kV and current of 40 mA were applied.

Particle size distribution

Particle size distribution analysis was done by screening agglomerate samples with a pass size of 106 µm; the particle size distribution of the passing sample was determined using a Saturn DigiSizer 5200. The screening step was done to improve the repeatability of PSD analyses. With unscreened samples, the larger particle fraction gradually decreased in size and the smaller size fractions gradually increased with sequential tests. Water submersion and ultrasonic treatment alone did not adequately separate the solids into unit particles. A refraction index of 2.268 for goethite and 1.715 for jarosite were used. A flow rate of 12 L/min with 1 minute circulation time and 1 minute ultrasonic treatment time at 60% intensity was employed. The laser strength was 1.88 eV. Samples were pulped prior to analysis, and analysis was conducted with and without ultrasonic treatment.

BET surface area

Brunauer-Emmett-Teller (BET) theory surface area analysis with nitrogen gas was performed with a Micromeritics 3Flex 1.02. Subsequently, Harkins and Jura adsorption isotherm t-plots were calculated to determine the external surface area and the micropore area. Cornell and Schwertmann (2003) reported that crystal lattice level transformation might occur during BET surface area work at elevated outgassing temperatures. Dehydroxylation of ferric oxyhydroxides may also occur, causing slit-shaped micropores to be formed.

In this study, outgassing was initially performed at low temperatures to prevent crystal lattice transformation. Outgassing was performed overnight at a temperature of 90°C followed by outgassing overnight at 50°C. At low outgassing temperatures uncharacteristically low surface area (< 10 m^2/g) precipitates were reported, which indicated that outgassing at low temperature might not have removed all adsorbed gas. Thereafter, the standard outgassing temperature of 250°C was utilized. With reference goethite used for seeding, a BET surface area of 131.01 m^2/g was reported after 6 hours' outgassing at 250°C. The same sample was then outgassed for a further 17 hours at 250°C, which resulted in a BET surface area of 131.07 m^2/g. This confirmed the accuracy and reproducibility of the values. The remaining samples were outgassed at 250°C for 17 hours.

Scanning electron microscopy

Precipitates were analysed by scanning electron microscopy (SEM) with quantitative energy-dispersive X-ray spectroscopy (EDS) using a Zeiss MERLIN Field Emission Gun (FEG) instrument. The nickel, cobalt, iron, copper,

Table III

Experimental conditions and associated analytical techniques

pH	Fe oxidation	Composition	Temperature (°C)	Seeding	BET	PSD	XRD	SEM
4.0	2+	Low	70	Goethite	x	x		
2.5	2+	Low	70	Goethite	x	x		
2.5	3+	Low	70	Goethite	x	x		
4.0	3+	Low	90	Goethite	x	x		
2.5	3+	High	90	Goethite	x	x	x	
4.0	3+	High	90	Goethite			x	x
4.0	2+	Low	70	None				x
4.0	2+	High	90	None			x	
4.0	3+	High	90	None			x	
4.0	3+	OPM	90	None	x	x	x	x
2.5	2+	OPM	90	None				x
4.0	2+	OPM	90	None				x
2.5	3+	OPM	90	None			x	

sulphur, oxygen, chloride, ruthenium, rhodium, iridium, and arsenic contents of precipitates were determined by EDS using an Oxford Instruments® XMax 20 mm² detector and Oxford INCA software. Beam conditions during the quantitative analyses on the MERLIN FEG SEM were 20 kV and 16 nA, with a working distance of 9 mm. The mineral counting time was 15 seconds live-time for EDS. A cobalt standard was used for standardization and verification of the analyses. The system is designed to perform high-resolution imaging concurrently with quantitative analysis, with errors ranging from ± 0.1 wt% to 0.6 wt% on the major elements using EDS. Compositional data reported are averaged from at least three corresponding data points.

Backscattered electron (BSE) detector images were utilized to qualitatively define different precipitate phases. Secondary electron (SE) detector images provided surface morphology analysis, and visual observation of the precipitates. Composition maps were drawn, but were largely ineffective due to the predominance of iron and the little deviations seen in samples.

Results and discussion

Particle size distribution

The average particle size distributions (PSDs) for three samples precipitated at each of the respective sets of conditions are shown in Figure 1. The reference goethite sample had a d_{50} particle size of 1.3 μm; the peak at 12.7 μm was due to agglomeration. From Figure 1a, it is evident that particle growth occurred during precipitation from ferric solutions: the particles had a negative skew distribution with a d_{50} of 100.6 μm. The precipitation on goethite seed led to growth and agglomeration that did not disperse during pulping or ultrasonic treatment. Comparison of the results obtained for the low and high metal concentration solutions in Figure 1a reveals an increased volume fraction between 2 μm and 8 μm for the high metal concentration experiment. This could be ascribed to the fact that the high degree of supersaturation associated with this experiment resulted in precipitation by spontaneous primary nucleation and particle growth (2–8 μm) in addition to precipitation by growth of seed material (peak around 100 μm), which was the main precipitation mechanism for the low-concentration experiments.

The percentage iron precipitation achieved for the solutions containing ferrous were generally low. This was expected, given the fact that ferrous hydrolysis generally occurs to a noticeable extent only at pH values of 6 or higher, depending on the ferrous concentration. In the two tests for which solid residues were collected and analysed, the iron precipitation was 8.7% and 1.3% at pH 4 and pH 2.5, respectively. It was thus expected that there would be limited particle growth. The PSDs shown in Figure 1b indicate that there was no particle growth in these experiments. The agreement between the PSD of the reference goethite and that of the residue from these experiments is evident. The consistency of goethite seed in ferrous experiments therefore acts as a control, supporting the growth observed in ferric precipitation reactions.

The PSD for the iron precipitated without goethite seed is presented in Figure 2. This sample was not sieved to 106 μm prior to analysis with the Saturn DigiSizer 5200. Approximately 48% of the particles in the sample were larger than 106 μm, although this could to some extent be attributed to agglomerate formation. Even though the particles were larger than in the seeded experiments, the filterability of the precipitate was significantly worse than that from seeded experiments.

BET surface area

The BET surface areas obtained for the respective precipitates are listed in Table IV. Micropores are molecular-size pores sized less than 20 Å, mesopores range between 20 Å and 500 Å, and macropores are larger than 500 Å (Rouquerol *et al.*, 1994). The micropore surface area and external surface area can be considered to be two different active sites available for particle growth and adsorption. A decline in micropore surface area suggests molecular growth occurring on the corresponding active sites, while a decrease in external surface area can be ascribed to agglomeration.

The precipitate produced without seeding from the ferric-containing OPM solution had a BET surface area of

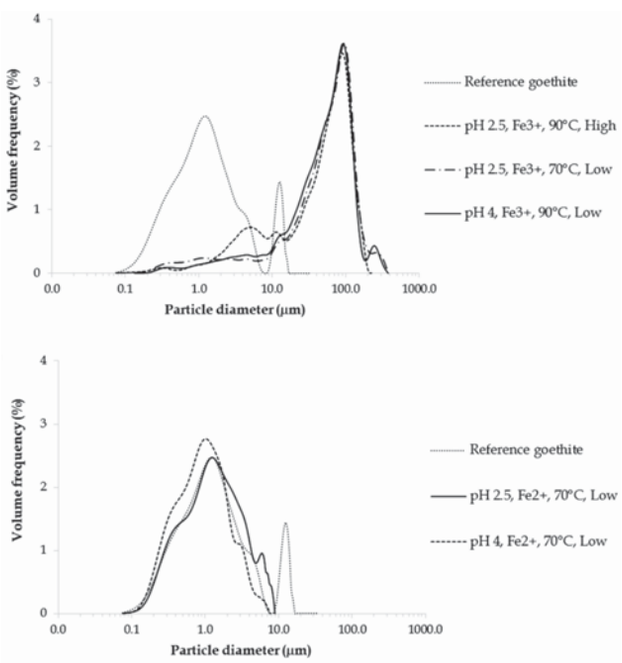

Figure 1—Particle size distributions for precipitates formed during seeded precipitation from (a) ferric solutions, and (b) ferrous solutions. 'High' and 'Low' in the legends refer to the metal concentrations defined in Table I

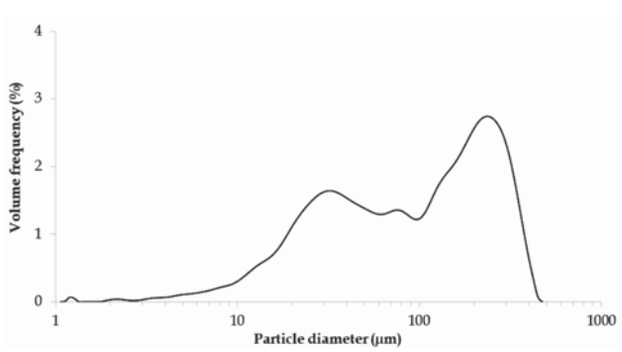

Figure 2—Particle size distribution for precipitate formed during unseeded precipitation from a ferric-containing OPM solution at pH 4 and 90°C

Table IV

BET surface areas measured for the precipitates formed at the respective conditions

pH	Fe oxidation	T (°C)	Composition	Fe precipitation (%)	BET surface area (m^2/g)	Micropore surface area (m^2/g)	External surface area (m^2/g)
4.0	3+	90	OPM	100%	215.8 ± 1.9	0.0	216.6
		Reference goethite		n/a	131.0±2.0	66.2	64.8
2.5	3+	90	High	75%	100.6 ± 0.5	44.3	56.3
2.5	3+	70	Low	69%	82.0 ± 0.2	43.9	38.1
4.0	3+	90	Low	100%	156.5 ± 0.8	64.0	92.6
2.5	2+	70	Low	1%	126.2 ± 1.5	72.8	53.4
4.0	2+	70	Low	9%	136.1 ± 1.2	87.1	49.0

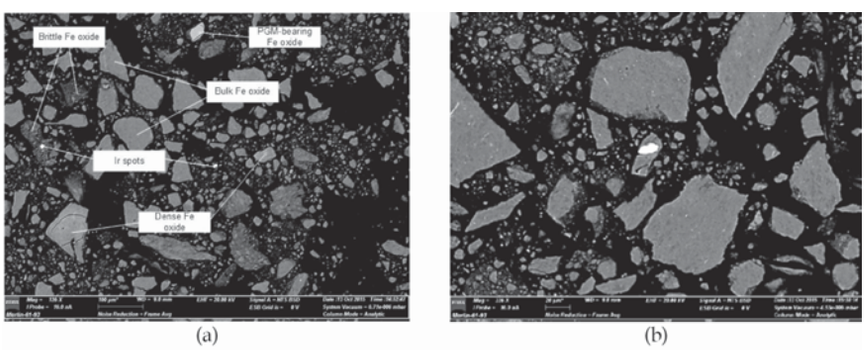

Figure 3—SEM (a) bulk and (b) magnified image of the precipitate produced from ferrous-containing OPM solution at pH 2.5 and 90°C

215.8 m^2/g. This precipitate was characterized as predominantly ferrihydrite, as discussed in the following section on SEM results. The expected surface areas of ferrihydrite compounds vary between 100 m^2/g and 700 m^2/g (Cornell and Schwertmann, 2003). The precipitation was generally rapid, and the resulting poorly ordered crystal structure contributed to the relatively high surface area compared to the reference goethite. As was observed from the PSD for this precipitate (Figure 2), the ferrihydrite formed agglomerated particles. The fact that no micropore surface area was measured for the precipitate suggested that the pores in the agglomerates were sufficiently large to be classified as external surface area rather than micropores.

The reference goethite sample had a BET surface area of 131.0 m^2/g. Goethite surface area is considered high in the range of 80 m^2/g to 150 m^2/g (Cornell and Schwertmann, 2003). The surface area was equally distributed between micropores and the external surface. The total BET surface areas of the precipitates produced from ferrous solutions were comparable with that of the reference goethite. The distribution did, however, indicate increased micropore surface area and decreased external surface area. The external surface area decrease implies that agglomeration occurred. The increased micropore surface area could be ascribed to a combination of chemical weathering of the goethite particles and formation of micropores due to growth on the external surface.

The total BET surface areas of the precipitate produced from solutions containing ferric decreased in the case of pH 2.5, due to a decrease in the micropore surface area as well as the external surface area of the particles. The solution with the higher total metal concentration was seeded with relatively more seed to maintain a 2:1 seed to Fe in solution ratio. The decrease in the total surface area could be ascribed to aggregation at pH 2.5. The micropore surface area declined by a third, but not to the extent of unseeded precipitated iron, where no micropore surface area was recorded.

The precipitate produced from the ferric-containing solution at pH 4 had a higher BET surface area than the reference goethite, with an increase in the external surface area being responsible for the increase in the total surface area. This could be ascribed to the rapid iron precipitation observed at pH 4, which resulted in poor ordering of crystal structure.

SEM and XRD

Precipitates formed from 'OPM' solutions

Figure 3 presents the backscattered SEM image of the precipitate formed from a ferrous-containing OPM solution during unseeded precipitation at pH 2.5 and 90°C. Three distinct iron oxide phases were observed, namely the bulk, brittle, and dense phases. Individual iridium phases also occurred. These iridium phases were very dense and could be readily observed, defined as 'Ir spots' in Figure 3a. In Figure 3b, the iridium phase in the centre possibly acted as growth surface for the bulk iron oxide phase. This observation was consistent for iridium in all other samples: iridium was either present as independent particles, or was enveloped within the bulk iron oxide phase. Ruthenium and rhodium were only observed in varying low quantities as part of iron oxide phases.

The elemental compositions of the phases identified in Figure 3 are summarized in Table V, with the bulk and brittle iron oxide phases having similar compositions. The dense phase had the highest iron content and incorporated the least anionic impurities (sulphate and chloride). The three iron phases corresponded stoichiometrically with the structural formulae of schwertmannite and ferrihydrite. The iridium

Table V

Elemental compositions of phases identified in Figure 3

	Fe (wt%)	O (wt%)	S (wt%)	Cl (wt%)	Ru (wt%)	Rh (wt%)	Ir (wt%)
Bulk Fe oxide	54.9 ± 0.4	40.4 ± 0.1	3.7 ± 0.1	0.5 ± 0.1			
Brittle Fe oxide	53.4 ± 0.7	40.7 ± 0	4.1 ± 0.1	1 ± 0.2			
Dense Fe oxide	58.1 ± 0.2	39.3 ± 0.1	2.5 ± 0.2				
Ir phase	2 ± 0.5	13.1 ± 0.1		23.3 ± 1.8			60.5 ± 2.9
OPM-bearing Fe oxide	44.6 ± 1	48.7 ± 0.4	3.1 ± 0.7	0.5 ± 0.3	0.7 ± 0.2	2.4 ± 0.2	

phases were approximately 5 μm in size; the most abundant iridium phase consisted of 60.5% iridium, 23.3% chloride, and 13.1% oxygen.

Increasing the pH from 2.5 to 4 resulted in the formation of a heterogeneous iron precipitate from ferrous-containing OPM solution, as shown in Figure 4. Three distinctly different phases were observed, namely dense, medium-dense, and bulk iron oxide. With the higher addition of a strong neutralizing agent, local regions with high pH were more likely to form, which could have resulted in the formation of the dense phases; this, in turn, acted as growth medium for the medium-dense and bulk iron oxide phases.

The elemental compositions of defined phases are reported in Table VI. Dense iron oxide phases, of 5 μm particle size on average, did not contain any sulphate or chloride ions. The medium-dense and bulk iron oxide phases contained the same quantities of sulphate and chloride ions. The presence of sulphate and chloride ions in the medium-dense and bulk phases suggested that anionic impurities were included in the crystal lattices of these phases, which might have been caused by poorly ordered crystal lattices. The bulk iron oxide phase indicated the consistent presence of OPMs. All three phases were most likely variants of ferrihydrite.

The lowest density phase was an unusual location for OPMs considering their high molecular weights. Its dispersed nature in the bulk iron phase indicated that initial iron precipitation was faster and aggregation could have captured the OPM solids during precipitation.

In the case of the precipitate formed from OPM solutions containing ferric, several phases were identified on the SEM images (Figure 5). Two homogeneous phases were observed, one of medium density (bulk iron oxide) and the other of low density. A heterogeneous medium-density iron oxide phase, which contained small interlocked high density phases, was also present.

The elemental compositions of phases defined in Figure 5 are summarized in Table VII. In contrast to the precipitate produced from the ferrous solutions, appreciably more sulphate was incorporated in the denser phases, with declining iron content as the density increased. The greater amount of sulphate suggests schwertmannite formation. Small amounts of sodium were also structurally incorporated, which might imply the presence of minor amounts of jarosite.

XRD analyses of the precipitates produced from ferric-containing OPM solutions could not characterize the iron oxide using conventional peak-matching. The diffractogram was compared to published results (Yu, Park, and Kim, 2002; Cornell and Schwertmann, 2003; Schwertmann and Carlson, 2005; Das, Hendry, and Essilfie-Dughan, 2011; Bazilevskaya, Archibald, and Martínez, 2012). It was deduced that the precipitate was a hybrid between poorly crystalline goethite and schwertmannite, but might also have contained ferrihydrite.

Unseeded precipitates

SEM images of the precipitate formed by unseeded

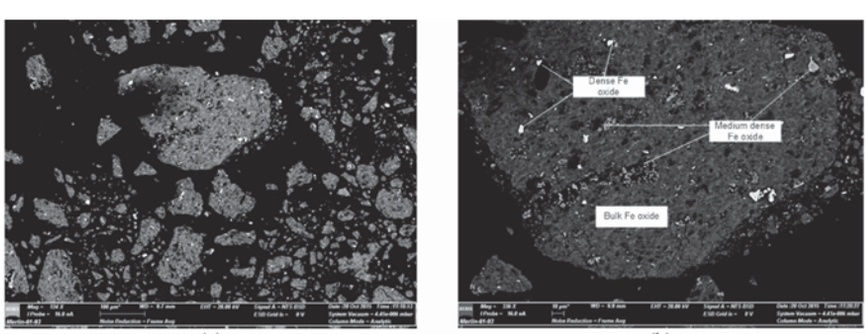

Figure 4—SEM (a) bulk and (b) magnified image of the precipitate produced from ferrous-containing OPM solution at pH 4 and 90°C

Table VI

Elemental compositions of phases identified in Figure 4

	Fe (wt%)	O (wt%)	S (wt%)	Cl (wt%)	Ru (wt%)	Rh (wt%)	Ir (wt%)
Dense Fe oxide	55.3 ± 0.4	44.7 ± 0.2					
Medium dense Fe oxide	56.2 ± 0	38.2 ± 0	1.9 ± 0.1	0.3 ± 0			
Bulk Fe oxide	55.1 ± 0.4	37.8 ± 0.2	1.9 ± 0.1	0.3 ± 0.1	1.5 ± 0.2	1.4 ± 0.2	1.2 ± 0

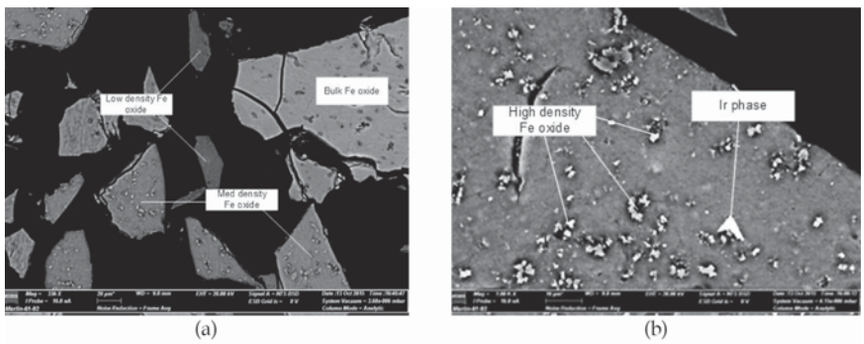

Figure 5—SEM (a) bulk and (b) magnified image of the precipitate produced from ferric-containing OPM solution at pH 4 and 90°C

Table VII

Elemental compositions of phases identified in Figure 5

	Fe (wt%)	O (wt%)	S (wt%)	Cl (wt%)	Ir (wt%)	As (wt%)	Na (wt%)
Bulk Fe oxide	53.6 ± 2.1	38.7 ± 0.9	3 ± 1			3.7 ± 0.2	
Low density Fe oxide	51.3 ± 1	40.5 ± 0.5	4.5 ± 0.6			3.1 ± 0.2	0.3 ± 0.2
Med density Fe oxide	47.5 ± 0.5	43.1 ± 0.3	6.3 ± 0.3			3.1 ± 0.1	
High density Fe oxide	37 ± 2.5	47.6 ± 1.3	9.2 ± 1.4			2.6 ± 0.3	1.8 ± 0.2
Ir phase	4.5 ± 0.4	2.5 ± 0.4		12.2 ± 2.3	80.7 ± 2.3		

precipitation from ferrous-containing nickel sulphate solution at pH 4 and 70°C are shown in Figure 6. The bulk phase consisted of two intergrown grain-like phases. Iridium phases were observed, and other homogeneous iron oxides also formed. The grain-like particles were brittle and readily broke under the electron beam.

Table VIII presents the elemental compositions of the identified phases. When other elements are excluded, the Fe:O ratio is 71:29; thus, if the stoichiometric ratio is considered in isolation, the predominant phases were predicted to be goethite/haematite-based. Relatively high and consistent OPM levels were observed for all the iron oxide phases; this could possibly be ascribed to the relatively small amount of iron precipitate formed. The lighter grains contained slightly less OPMs but more arsenic and nickel than the darker grains. Arsenic inclusion did not lead to varying Fe:O ratios and thus it did not necessarily affect the phase mineralogy, apart from co-precipitation.

Seeded precipitates

XRD analysis of the precipitates produced during seeded precipitation from ferric-containing nickel sulphate solutions showed that no iron phases other than goethite were formed. In the case of the high total metal concentration (89.3 g/L Ni) solution, nickel sulphate was detected in the precipitate, suggesting that scavenging of nickel occurred. The same was not evident for the precipitate produced from the low total metal concentration (62.5 g/L Ni) solution.

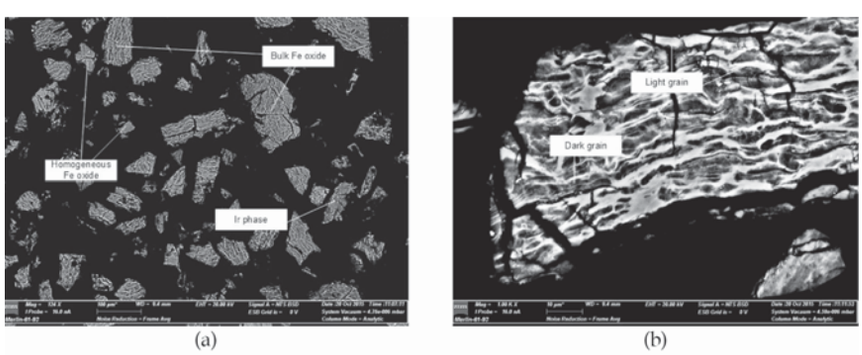

Figure 6—SEM (a) bulk and (b) magnified image of the precipitate produced from ferrous-containing solution without seeding at pH 4 and 70°C

Table VIII

Elemental compositions of phases identified in Figure 6

	Fe (wt%)	O (wt%)	S (wt%)	Cl (wt%)	Ru (wt%)	Rh (wt%)	Ir (wt%)	Ni (wt%)	As (wt%)
Darker grain	59.2 ± 0.3	23.6 ± 0.1	1.1 ± 0.1		2 ± 0.1	1.7 ± 0		2.3 ± 0.2	9.6 ± 0.1
Lighter grain	58.6 ±0 .4	24.1 ± 0.2	1.4 ± 0.1		1.4 ± 0.4	0.4 ± 0.4		2.6 ± 0.1	10.8 ± 0.2
Homo. Fe-oxide	59.1 ± 6.1	24.1 ± 0.8	1.2 ± 1		1.1 ± 0.4	0.6 ± 0.4		3.6 ± 6.2	9.5 ± 0.4
Ir phase	3.5 ± 0.5	14 ± 0.1		4.4 ± 1.8			78±2.9		

The SEM images of the precipitate formed by seeded precipitation from the ferric-containing solution (Figure 7) suggested that growth occurred on the seeding material. This was evident from the denser phase observable on the particle surface boundary, the relatively similar appearance of all particles in Figure 7a (there are no particles with clearly noticeable differences in densities or phases), as well as the shape of the crystals. The elemental composition of the seed phase reported in Table IX is in agreement with the composition of goethite. The elemental composition of the higher density inclusions (bright inclusions in Figure 7) indicates a higher oxygen to iron ratio than in the goethite seed material. These inclusions were attached to the bulk goethite particle, but might have been independently precipitated prior to agglomeration.

Conclusions

The effect of process conditions on the characteristics of iron precipitates formed from ferric and ferrous sulphate solutions was investigated, with specific attention to 'other precious metal' (OPM: Ru, Rh, and Ir) behaviour. While no changes in the PSD were observed during seeded precipitation from ferrous solutions, seeded precipitation from ferric solutions resulted in particle growth and, therefore, particles significantly larger than the goethite seed material. Increasing the pH from 2.5 to 4 during precipitation from ferric solutions resulted in an increase in the total BET surface area of the precipitate. This was ascribed to a more amorphous surface area which formed as a result of more rapid iron precipitation and poor ordering of crystal structure.

A wide variety of iron precipitation products were observed in the study, which were all best described under the ferrihydrite and schwertmannite umbrella. Iron oxide phases of varying iron, oxygen, and sulphate content were predominant. Increasing the pH from 2.5 to 4 generally resulted in more homogenous iron oxide phases in the precipitate. Goethite seeding induced targeted precipitation, resulting in goethite forming as the only iron species and limited OPM precipitation. Ruthenium and rhodium were only observed in low quantities within iron oxide compounds. These iron compounds were distinguishable yet variable. Iridium tended to precipitate without the inclusion of iron or other OPMs. The iridium precipitation product was complexed with chloride and oxygen in variable amounts. The iridium compound then served as a site for heterogeneous nucleation and growth of the bulk iron oxides.

Table IX

Elemental compositions of phases identified in Figure 7

	Fe (wt%)	O (wt%)	S (wt%)
Denser Fe oxide	51.4 ± 2.7	46.7 ± 2.7	1.2 ± 0.2
Goethite seed	64.7 ± 0.5	35.1 ± 0.1	0.2 ± 0.1

References

Bazilevskaya, E., Archibald, D.D., and Martínez, C.E. 2012. Rate constants and mechanisms for the crystallization of Al nano-goethite under environmentally relevant conditions. *Geochimica et Cosmochimica Acta*, vol. 88. pp. 167–182. http://doi.org/10.1016/j.gca.2012.04.026

Bigham, J.M., Schwertmann, U., Traina, S.J., Winland, R.L., and Wolf, M. 1996. Schwertmannite and the chemical modeling of iron in acid sulfate waters. *Geochimica et Cosmochimica Acta*, vol. 60, no. 12. pp. 2111–2121. http://doi.org/10.1016/0016-7037(96)00091-9

Cornell, R.M. and Schwertmann, U. 2003. The Iron Oxides: Structure, Properties, Reactions, Occurences and Uses. 2nd edn. Wiley.

Das, S., Hendry, M.J., and Essilfie-Dughan, J. 2011. Transformation of two-line ferrihydrite to goethite and hematite as a function of pH and temperature. *Environmental Science and Technology*, vol. 45, no. 1. pp. 268–275. http://doi.org/10.1021/es101903y

Dutrizac, J.E. 1980. The physical chemistry of iron precipitation in the zinc industry. *Proceedings of Lead-Zinc-Tin '80. The TMS-AIME World Symposium on Metallurgy and Environmental Control*, Las Vegas, Nevada. Cigan, J.M., Mackey, T.S., and O'Keefe, T.J. (eds). The Metallurgical Society of AIME, New York. pp. 532–564.

Goldschmidt, V.M. 1937. The principles of distribution of chemical elements in minerals and rocks. *Journal of the Chemical Society*, pp. 655–673. http://doi.org/10.1039/JR9370000655

Jiang, H. and Lawson, F. 2006. Reaction mechanism for the formation of ammonium jarosite. *Hydrometallurgy*, vol. 82, no. 3-4. pp. 195–198. http://doi.org/10.1016/j.hydromet.2006.03.013

Lowson, R.T. 1982. Aqueous oxidation of pyrite by molecular oxygen. *Chemical Reviews*, vol. 82, no. 5. pp. 461-493. http://doi.org/10.1021/cr00051a001

Rouquerol, J., Avnir, D., Fairbridge, C.W., Everett, D.H., Haynes, J.H., Pernicone, N., Ramsay, J.D.F., Sing, K.S.W., and Unger, K.K. 1994. Recommendations for the characterization of porous solids. *Pure and Appl. Chemistry*, vol. 66, no. 8. pp. 1739–1758. http://doi.org/doi:10.1351/pac199466081739

Schwertmann, U. and Carlson, L. 2005. The pH-dependent transformation of schwertmannite to goethite at 25°C. *Clay Minerals*, vol. 40, no. 1. pp. 63–66. http://doi.org/10.1180/0009855054010155

Singer, P.C. and Stumm, W. 1970. Acidic mine drainage: the rate determining step. *Science*, vol. 167, no. 3921. pp. 1121–1123.

Yu, J.Y., Park, M., and Kim, J. 2002. Solubilities of synthetic schwertmannite and ferrihydrite. *Geochemical Journal*, vol. 36, no. 2. pp. 119–132. http://doi.org/10.2343/geochemj.36.119 ◆

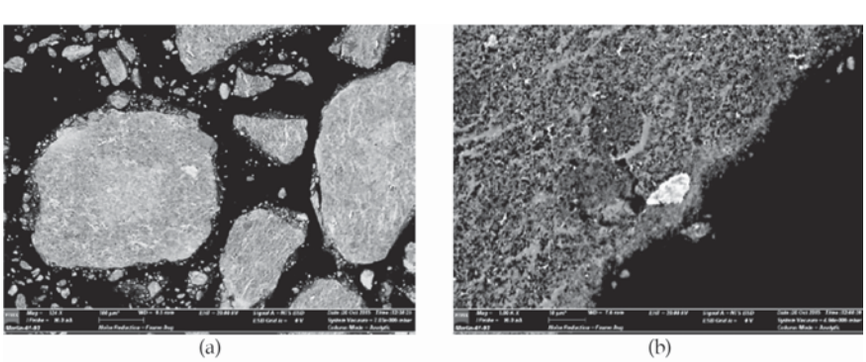

Figure 7—SEM (a) bulk and (b) magnified image of the precipitate produced from ferric-containing solution with seeding at pH 4 and 90°C

http://dx.doi.org/10.17159/2411-9717/2017/v117n8a8

Copper sulphate crystallization plants at remote locations

by D. Megaw*, J. Moolman*, P. Muzadi*, and T. Marcus*

Synopsis

The Central African Copperbelt is well known for its high-grade copper-cobalt deposits. Many hydrometallurgical copper refineries have been established in northern Zambia and in the Haut-Katanga and Lualaba provinces in the Democratic Republic of Congo to treat such orebodies. As the high-grade deposits at primary refinery sites become depleted, new ore deposits are exploited. These new deposits are often situated some distance from the refineries, thus necessitating upstream mineral processing in order to produce a concentrate that is then transported to the refinery, usually by road. In this paper a processing route that produces a copper sulphate product at the remote ore location is presented as a possible alternative to the production of a concentrate by dense media separation (DMS). The alternative process comprises crushing and screening of the ore, heap leaching, solvent extraction, and copper sulphate crystallization. Similar technology has been successfully implemented in South America; however, these plants have targeted copper sulphate as a final product, primarily for the animal feed additive market. Although the production of feed-grade copper sulphate offers producers a premium on the final product, the market demand is limited. The demand for LME-grade copper metal is orders of magnitude higher than that for feed-grade copper sulphate. An advantage of satellite copper sulphate production is that copper units supplied to the refinery for cathode production require less secondary processing than a DMS concentrate. The end product is attractive for copper cathode producers that have un-utilized solvent extraction (SX) and electrowinning (EW) capacity. When added to SX, the sulphate associated with the copper sulphate is recovered as sulphuric acid in the raffinate, supplementing the fresh acid requirements for leaching. The copper sulphate purity is such that it can also be added intermittently to the EW strong/advance electrolyte circuit, although care must be taken to maintain the sulphate balance in the EW circuit. The advantages and disadvantages of the two processing routes are compared.

Keywords
copper, copperbelt, solvent extraction, mineral processing, crystallization.

Introduction

The run-of-mine (ROM) ore extracted during mining operations usually undergoes primary mineral processing in the vicinity of the mine, as is the case for many copper processing plants established in the Central African Copperbelt region. In mineral processing, the valuable minerals are liberated from the ROM ore and separated from the gangue minerals, hence producing a higher quality product (concentrate) that is further refined to extract the metals of interest.

There are various mineral processing methods, such as ore sorting, heavy media separation, dense media separation (DMS), froth flotation, and magnetic separation. Selection of the mineral processing route generally depends on the characteristics of the ore and economic factors. While all the above-mentioned methods are well-proven, innovative mineral processing methods can be very advantageous for copper processing plants.

In this paper, an alternative to DMS aimed at producing a copper sulphate concentrate at satellite mining operations is presented. Similar technology has been successfully implemented in South American operations, and although the final product has been primarily targeted for livestock feed additives, it is equally attractive for LME-grade copper cathode producers that have un-utilized capacity at their existing metal production facilities. This process alternative is compared with the production of a concentrate via the more conventional DMS processing route.

Background

Dense media separation

The Central African Copperbelt is one of the world's largest and most mineralized copper-bearing geological settings. It stretches a distance of approximately 450 km from the northern Copperbelt Province of Zambia to the southeastern Haut-Katanga and Lualaba provinces of the Democratic Republic of Congo (DRC).

* *ProProcess Engineering (Pty) Ltd., South Africa.*
 ISSN 2225-6253. This paper was first presented at the Hydrometallurgy Conference 2016 'Sustainable Hydrometallurgical Extraction of Metals', *1–3 August 2016, Belmont Mount Nelson Hotel, Cape Town.*

Copper sulphate crystallization plants at remote locations

During the last upswing in the commodity cycle (2004–2008), this vast copper-rich region saw a growing influx of capital investment from multinational corporations to exploit its rich copper and cobalt deposits. Primary extraction and refining plants were constructed in the immediate vicinity of mining operations that offered the most lucrative returns.

Owing to the increased demand for copper and cobalt during this period, as well as the rapid depletion of the high-grade deposits, additional secondary resources needed to be considered by many of the established operations. These secondary resources are often situated some distance from existing refineries, and on-site upgrading of the ROM material is necessary to reduce the cost of transport to the refinery, particularly in view of the poor transportation infrastructure in the region. These satellite deposits are often of limited size and do not justify building additional refining capacity. It is common practice to treat copper ores, especially low-grade ores, at mineral processing plants situated at the satellite sites to produce an upgraded copper concentrate. This is frequently accomplished via the DMS process, and the concentrate produced is transported by road to a primary refinery for further beneficiation. The poor recovery of copper minerals via the DMS route results in large volumes of waste (floats) being generated, which often contain notable copper resources that remain unutilized.

A balance between metal recovery and concentrate upgrade via DMS often results in high transportation costs, and high overall production costs per ton of contained copper. The degree of beneficiation attained in the mineral processing plant plays a significant role, as transportation costs can rapidly escalate and reduce profitability. This, coupled with cyclical fluctuations in commodity prices, may drive away existing and potential investors, ultimately leading to the inefficient utilization or rejection of satellite copper resources.

Copper sulphate crystallization

An alternative processing route that provides a competitive advantage compared with other conventional mineral processing technologies is proposed, in which copper sulphate pentahydrate crystals are produced via the following unit operations:

- Crushing and screening of the ROM ore
- Heap leaching of the screened material
- Solvent extraction (SX) for the selective extraction of copper from the pregnant leach solution (PLS)
- Crystallization of copper as copper sulphate pentahydrate.

This process route can offer a total copper recovery from ROM of 65–70% (depending primarily on heap leach efficiency). Other advantages include:

- Lower transport costs due to the high grade (approx. 24% copper) of the intermediate product, compared with 10–15% for DMS
- Lower processing costs at the refinery. This is due to the supply of a higher grade copper intermediate that is easily converted into a form that favours good copper mass transfer in SX circuits with minimum co-transfer of soluble impurities
- Maximum utilization of existing refinery assets
- Supply of additional copper units to cathode producers. The copper sulphate pentahydrate produced is attractive for cathode producers that have unutilized SX and EW capacity. In SX, the sulphate associated with the copper sulphate is recovered as sulphuric acid in the raffinate and recycled to the leach circuit, thus reducing fresh acid requirements. In addition, the copper sulphate concentrate produced can be added intermittently to the EW strong/advance electrolyte circuit (in this case, the sulphate balance needs to be considered as the limiting rate). This will improve/maintain product cathode quality by maintaining favourable copper plating conditions during periods of reduced front-end minerals processing and leaching throughputs (less depletion of copper concentration in the spent and advance electrolyte)
- The modular approach adopted for the construction of copper sulphate crystallization plants (Figure 1) allows for retrofitting of the system for phased capacity expansions. The system components are built on movable skids, which can be positioned in a number of process configurations. The skid-mounted approach also means that the units are easily transported
- Other advantages of modular construction are:
  - Cost savings in terms of civil works – the plant is designed so that minimum site preparation is required
  - Low operational energy cost requirements, allows for off-grid power independence
  - Optimum utilization of space (reduced plant footprint)
  - Assembly and off-site testing of the various plant modules prior to transport to site, resulting in shorter installation times and minimum site disruption
  - Lower labour costs during construction (reduced site preparation and infrastructure requirements).

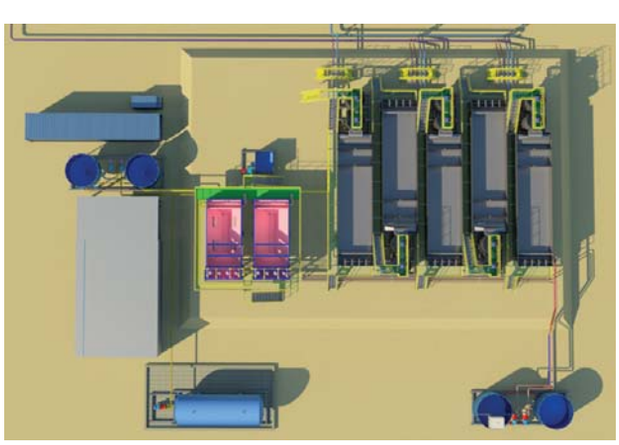

Figure 1—Modular copper sulphate crystallization plant concept

Copper sulphate crystallization plants at remote locations

Copper sulphate crystallization has been successfully implemented in South America with the establishment of two plants by Despromin.

Study methodology

The purpose of the study was to assess the technical and economic feasibility of implementing a satellite modular copper sulphate crystallization plant with an output of 8 kt/a contained copper. This nameplate capacity was chosen as it fits the copper sulphate module plant size. The process is compared to a typical DMS processing route for the same contained copper output. A further comparison is conducted to compare copper sulphate plant and DMS throughputs required to achieve the same final cathode output from the refinery. Simplified flow sheets of the copper sulphate crystallization processing route and DMS processing route are illustrated in Figure 2 and Figure 3, respectively.

Basis of cost estimates

For the purpose of this study, only major equipment items were costed as part of the capital cost (CAPEX) estimates. The estimate is within an accuracy range of -30% to +50%, in accordance with methodologies of the American Association of Cost Engineers (AACE) International Recommended Practice No. 18R-97.

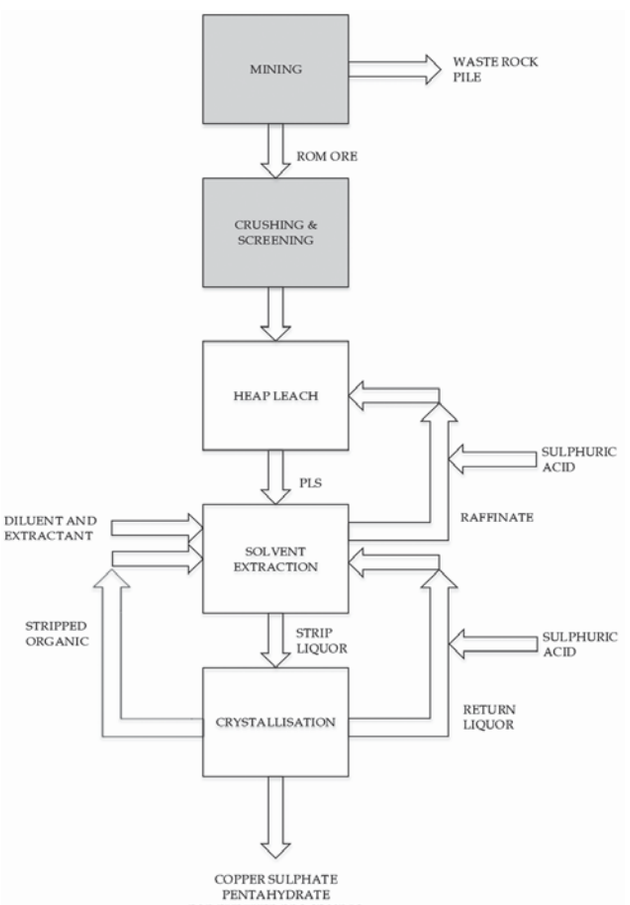

Figure 2—Simplified flow sheet of the copper sulphate crystallization process

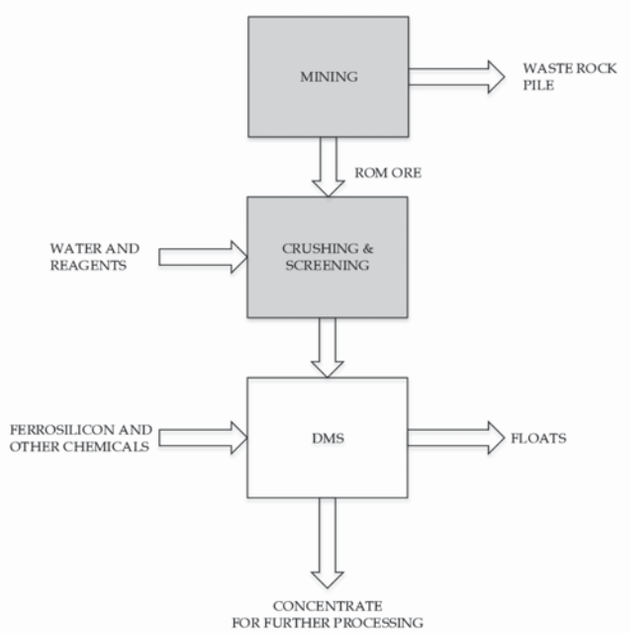

Figure 3—Simplified flow sheet of the DMS process

The estimated costs associated with major plant equipment required for the DMS plant were compared to the equipment costs for the copper sulphate crystallization plant. These costs were developed using an in-house cost database and quotations from equipment suppliers and vendors. Other items that form part of the capital costs, *i.e.* structural and civil work, electrical, instrumentation, and others, were excluded from the estimates.

The operating cost (OPEX) estimates were calculated at the order-of-magnitude accuracy level. In-house cost information and reagent consumptions were used as a basis for the estimates. The operating costs excluded costs associated with maintenance and repairs. Labour costs were excluded from the comparison as they were assumed to be similar for both process options. A contingency of 20% was applied. The currency used for the capital and operating cost estimates is US dollars.

Battery limits

The scope of the estimate is concerned with the pre-treatment of the ROM ore for the production of copper sulphate crystals via crushing and screening, heap leaching, solvent extraction, and crystallization, and the production of a concentrate via crushing, screening, and dense media separation. The estimates include costs related to the transport of the intermediary products, and exclude the additional downstream processing of the copper sulphate crystals or the DMS concentrate.

Cost estimates

A summary of the costs of major equipment for the copper sulphate crystallisation processing route and the DMS processing route is shown in Table I.

Table I

Summary of major equipment costs (8 kt/a contained copper output)1

Item	Copper sulphate crystallization (US$)	DMS (US$)
Crushing and screening	3 571 428.57	3 571 428.57
DMS plant	-	6 071 428.57
DMS with ancillaries (incl. product handling and sizing)	-	*285 714.29*
-1 mm beneficiation (spirals or other)	-	*1 785 714.29*
Heap leach	213 618.52	-
PLS pond construction	*91 452.12*	-
Raffinate pond construction	*91 452.12*	-
Heap pad construction	*30 714.29*	-
SX-crystallisation plant	2 282 858.14	-
SUBTOTAL	**6 067 905.23**	**9 642 857.14**
Contingency (20%)	1 213 581.05	1 1928 571.43
TOTAL	**7 281 486.28**	**11 571 428.57**

Note 1:

Inclusions	Exclusions
First fill of extractant	Slimes thickening and disposal
First fill of diluent	Process water distribution
Handling of final product	Mobile mining equipment

Table II

Summary of OME OPEX (8 kt/a contained copper output)

Item	Copper sulphate crystallization (US$)	DMS (US$)
Mining	6 096 526.23	7 717 193.06
Crushing	1 110 134.81	1 405 246.91
DMS	-	1 430 566.67
Heap leach	5 963 224.14	-
SX-crystallization	2 157 602.00	-
Acid transport	809 598.71	-
Transport of product	570 846.92	1 320 780.18
SUBTOTAL	**16 707 932.80**	**11 873 786.82**
Contingency (20%)	3 341 586.56	2 374 757.36
TOTAL	**20 049 519.36**	**14 248 544.19**

It can be seen that for a plant with a nameplate capacity of 8 kt/a contained copper, the estimated equipment cost for the copper sulphate crystallization route is significantly lower than that for the DMS processing route.

The operating costs of the two processes are presented in Table II. The power requirement is 500 kW for each processing route. Similar production outputs of 8 kt/a contained copper were targeted for comparison purposes. Region-specific information was used to estimate the costs tabled.

As can be seen from Table II, the operating costs associated with the copper sulphate crystallization processing route are significantly higher than those for the DMS process. However, the improvement in copper recovery to the final product, which results in an intermediate product with a copper content of approximately 24%, compared to only 10–15% for DMS, adds to the financial attractiveness of this processing route. A typical copper recovery of 50–55% is obtained in a DMS plant, compared to 65–70% for the copper sulphate crystallization route; which is equivalent to an increase in copper recovery of 25–30%.

Furthermore, the DMS concentrate needs to be introduced at the leach stage of the refining process, while the copper sulphate intermediary product can be introduced directly into the SX-EW circuit.

Table III compares the operating costs of the two processes based on the throughputs required to achieve the same final refined copper output. On this basis, the operating costs for the DMS processing route have almost doubled.

Table III

Summary of OPEX based on throughput for the same final cathode output from refinery

ITEM	Copper sulphate crystallization (US$)	DMS (US$)
Mining	6 096 526.23	11 289 874.67
Crushing	1 110 134.81	2 055 807.26
DMS	-	2 092 848.83
Heap leach	5 963 224.14	757 418.70
SX	-	987 649.90
SX-crystallixation	2 157 602.00	-
Acid transport	809 598.71	534 255.80
Transport of product	570 846.92	1 932 236.57
SUBTOTAL	**16 707 932.80**	**19 650 091.72**
Contingency (20%)	3 341 586.56	3 930 018.34
TOTAL	**20 049 519.36**	**23 580 110.06**

Comparing the capital and operating cost estimates, it can be concluded that the copper sulphate crystallization route is economically attractive for copper cathode producers. The copper sulphate route offers higher copper recoveries, has lower transport costs (per ton of contained copper) for the intermediary product, requires fewer process steps for copper metal production, produces copper units (as copper sulphate) that are readily available for copper mass transfer to the refinery SX-EW circuit under favourable extraction conditions, and lastly, the sulphate content of the copper sulphate product is recovered as sulphuric acid in the raffinate from SX, thus reducing the requirements for fresh acid addition to the refinery leach circuit.

Additional considerations

Proven technology

Two copper sulphate processing projects have been successfully implemented in South America for the production of copper sulphate pentahydrate crystals. One of them, at the Chapi copper mine in southeastern Peru, produces 28.8 kt/a of copper sulphate pentahydrate crystals (equivalent to 7.2 kt/a contained copper). Plant views are shown in Figures 4 and 5.

During the first year of operation, all copper sulphate produced was introduced into the SX-EW circuit of the Chapi copper cathode producer, which had spare EW capacity. This was done easily by dissolving the crystals in the feed liquor. Thereafter, copper sulphate crystals produced at the plant were used mainly as micronutrients in animal feeds. The plant operations have since been suspended due to depletion of feedstocks.

Cost competitiveness

Offtake of copper sulphate has economic benefits over copper concentrate:

- Higher value copper product based on contained copper per ton
- Reduction in transportation costs and overall production costs per ton of contained copper processed
- Lower costs of major equipment items.

Figure 4—SX area of the Chapi plant , Peru

Figure 5—Crystallization area of the Chapi plant, Peru

Environmental impact

The potential environmental impacts of the copper sulphate crystallization processing route are similar to a conventional copper heap leach and SX facility which primarily poses a risk of accidental release of process solutions from the heap leach facility to the environment, and elevated fire and explosion risk in the SX plant. These impacts are mitigated through adhering to environmental legislation put in place to reduce or minimize environmental consequences.

The copper sulphate crystallization process may seem to have an elevated environmental risk when compared directly with DMS. However, it should be kept in mind that many DMS concentrates are processed via a similar downstream hydrometallurgy route as that for producing copper sulphate.

Energy requirement

The rate of copper sulphate crystallization increases with increasing sulphuric acid and copper concentrations in the crystallization solution and with decreasing solution temperature. In order to increase the rate of crystallization a heat exchanger could be incorporated in the circuit. However, in the crystallization route considered here, the targeted rate of copper sulphate production is based on the acid concentration needed to maintain a specific rate of crystallization at an operating temperature that requires little or no additional forced cooling. The target lower crystallization temperature is achieved by having dual-duty acid make-up and dosing tanks in the circuit. This offers sufficient residence time to cool acid-addition electrolyte prior to dosing into the pregnant advance SX electrolyte for an effective crystallization rate.

Labour requirement

The staffing requirements for a DMS processing plant and a copper sulphate crystallization plant are similar, as shown in Table IV. However, personnel at the copper sulphate plant are required to have strong technical skills due to the higher level of plant automation and control employed.

Table IV

Staffing requirements per shift

Item[1]	Copper sulphate crystallization	DMS
Plant operators	4	5
Plant superintendent	1	1
Plant manager	1	1
TOTAL	6	7

[1]Includes operations, water services, and product handling. Excludes front end loader driver, forklift driver, and ROM loading operators.

Conclusions

Conventional methods of mineral processing are used to provide a more concentrated intermediate product that is suitable for treatment in hydrometallurgical facilities. Although techniques such as dense media separation are well established, the copper sulphate crystallization processing route offers a competitive alternative with potential improvement in 'first-pass ore processing' copper recovery.

Compared to the DMS process, for the same final cathode output at the refinery, the copper sulphate crystallization processing route offers an estimated 37% reduction in capital requirement. Based on typical OPEX rates for the specific operating region, the copper sulphate route offers an approximate 15% reduction in operating costs compared with DMS.

References

Despromin Ltd., Chile. 2016. Private communications. March 2016.

Moyer, H.R., III. 1979. Copper sulphate via solvent extraction and crystallisation. *Proceedings of the AIME Annual Meeting*, New Orleans, Louisiana, 18–22 February. ◆

http://dx.doi.org/10.17159/2411-9717/2017/v117n8a9

Recovery of uranium from nuclear conversion plant waste

by M. Potgieter*†, J.C. Barry*, D.J. van der Westhuizen†, and H.M. Krieg†

Synopsis

The ammonium diuranate (ADU) conversion process that was operated at the Nuclear Energy Corporation of South Africa (Necsa) in the past generated a significant amount of waste containing high concentrations of uranium, which can be re-used if the uranium can be recovered in a useful form. To attain this objective, the composition of the waste material and the amounts of impurities present were determined, followed by an investigation into various methods of uranium dissolution. For dissolution, water as well as different acid types and concentrations were investigated, and the efficiency of each method determined in terms of the uranium recovery as well as the extent of impurities extraction. It was found that the waste material was soluble in HNO_3, H_2SO_4, and HCl as well as water, with a maximum uranium extraction of 98% achieved in 3 M HNO_3 in 1 hour at a temperature of 80°C without the addition of an oxidizing agent. The thorium impurity content in relation to uranium was reduced from 8.4% to less than 1% with all acids investigated, as well as water. The most significant reduction in the total impurity content, from 24.3% to 10.8 %, was observed when using water, although this did not result in the highest uranium extraction.

Keywords

uranium, nuclear waste, conversion process, dissolution, purification, hydrogen peroxide.

Introduction

The ammonium diuranate (ADU) conversion process operated in South Africa from the 1970s was based on the direct conversion of ADU obtained from different mines (Ponelis, Slabber, and Zimmer, 1986; Ponelis, 1989). This approach differed from those of other countries operating conversion processes at that time in that the feed was not of nuclear grade. Since the ADU was sourced from various South African mines, the composition of the feed to the conversion plant at the Atomic Energy Corporation (AEC) varied. In addition, tail-end distillation of the uranium hexafluoride (UF_6) product was used, and as a result of the variability in the ADU a considerable proportion of unwanted elements or impurities, such as sodium (Na), potassium (K), and calcium (Ca), was present during the conversion process (Ponelis, Slabber, and Zimmer, 1986; Ponelis, 1989).

Basically, the ADU conversion process entailed the conversion of ADU to uranium tetrafluoride (UF_4), which was then converted to uranium hexafluoride (UF_6) in a fluorine flame reactor (Ponelis, 1989). The final product, thermally stable UF_6 gas, was then filtered to remove any foreign particles. Thereafter, the UF_6 was frozen out and distilled before being fed to the enrichment plant. Due to the incomplete conversion of UF_4 to UF_6 in the fluorine flame reactor, a significant amount of solid waste rich in uranium was formed, which accumulated at the bottom of the reactor. The incomplete conversion could have been caused by various factors, including sintering due to the low melting point of UF_4, inhomogeneous feed compositions, and the presence of various impurities. A study to determine the effect of alkali metal impurities on the conversion of UF_4 to UF_6 showed that the presence of these impurities had a significant effect on the sintering of UF_4 (Ponelis, 1989).

Owing to the high uranium content, the unreacted material is a nuclear liability and needs to be processed to recover a product that can be re-used in possible future conversion activities while reducing the amount of waste that is currently stored in drums. A search of the literature was undertaken to determine whether similar waste exists elsewhere, and how it is handled. Sasahira *et al.* (2007) mention an 'ash' that was formed during fluorination of UO_2 to UF_6, while Ohashi,

* *Uranium Chemistry Group, Plasma Technology, Applied Chemistry, Nuclear Energy Corporation of South Africa (Necsa), South Africa.*

† *Membrane Technology Group, Chemical Resource Beneficiation (CRB), North-West University (NWU), South Africa.*

 This paper was first presented at the Hydrometallurgy Conference 2016 'Sustainable Hydrometallurgical Extraction of Metals', *1–3 August 2016, Belmont Mount Nelson Hotel, Cape Town.*

Murashita, and Nomura (2014) extracted uranium from UF_4 residue and NaF adsorbents originating from conversion activities. It thus became clear that this waste material is unique, in terms of its intrinsic variety in composition as well as the amounts and types of impurities present.

In view of the solvent extraction (SX) process that is used to purify uranium (Kumar *et al.*, 2011), the waste material in its current solid form will have to be dissolved to obtain an aqueous solution containing the desired uranium. Furthermore, in order to extract uranium successfully using SX, the fluoride content should be low since fluoride is co-extracted by tributyl phosphate (TBP) (Volk, Vakhrushin, and Mamaev, 2000; Coleman, 1966).

It can be assumed that a significant amount of the contained uranium is in the UF_4 form, since the waste material was generated in the UF_4 to UF_6 conversion step in the process, and unreacted material would therefore consist of UF_4. For the envisioned SX process, provision should be made for the oxidation of insoluble U(IV) to soluble U(VI) during dissolution, possibly by means of the addition of an oxidizing agent. UF_4 can be completely solubilized by direct treatment with concentrated nitric acid (HNO_3) (Floreancig, 1983, Ohashi, Murashita, and Nomura, 2014). Luk'yanchev and Nikolaev (1963) studied the dissolution of UF_4 in sulphuric (H_2SO_4) and hydrochloric (HCl) acid, and found that the solubility of UF_4 increases with increasing HCl concentration, and reaches a maximum in H_2SO_4 at approximately 3 M. Ohashi, Murashita, and Nomura (2014) used an oxidizing agent (H_2O_2) during dissolution of UF_4 in H_2SO_4 and HCl as part of a study on the extraction of uranium from fluorine-containing waste. They found that UF_4 could be completely dissolved in 1.25 M HCl or 0.3 M H_2SO_4.

The aim of this investigation was, therefore, to dissolve the current waste material and to obtain the highest possible recovery of uranium in solution. Since no reference to similar waste material could be found, and a low solubility was expected due to its sintered nature, the waste material was milled prior to dissolution. The dissolution efficiency was investigated using water as well as different acids (HNO_3, H_2SO_4, and HCl) with and without the addition of H_2O_2 as an oxidizing agent. Water was included as a washing step prior to dissolution to determine its suitability for removing any water-soluble impurities. Since the waste material is known to contain high levels of fluoride (approx. 20%), different methods will be investigated for removing fluoride subsequent to dissolution but prior to SX, but this falls beyond the scope of the current study. In this paper the focus is mainly on cations in the waste material with concentrations above 0.5 mass%.

Experimental

Composition of waste material

The composition of the waste material was determined, focusing on the uranium (U) content and other major constituents that may ultimately influence the SX-based uranium recovery process. A sample of the waste material was dissolved in nitric acid (65 wt% HNO_3) in a 1:1 water to acid ratio. The solution was evaporated to dryness and the residue was re-dissolved in HNO_3 at the same concentration to achieve complete dissolution, followed by analysis using inductively coupled plasma-optical emission spectrometry (ICP-OES).

Dissolution tests

Nitric acid (HNO_3, 65 wt%), sulphuric acid (H_2SO_4, 98 wt%), and hydrochloric acid (HCl, 32 wt%) were obtained from Merck. The dissolution tests were conducted using HNO_3 at concentrations of 3 M and 1 M, H_2SO_4 at 2.5 M and 1.25 M, and HCl at 3 M and 1 M, as well as ultrapure water. Experiments were conducted in the absence and presence of 0.4 mL H_2O_2 (30 wt%, from Merck) as an oxidizing agent to aid the oxidation of insoluble U(IV) to soluble U(VI). For the solubility measurements, a 1 g sample of the waste material was added to a 100 mL acid solution and heated to 80°C on a hot plate. The temperature was chosen to be high enough to ensure fast reaction kinetics, but low enough to ensure that the solution did not boil, which would cause unwanted loss of solution as well as the evolution of noxious fumes. Each dissolution experiment was continued for 1 hour with continuous stirring using a stirrer bar, to ensure sufficient time for the reaction to proceed, after which the mixture was left to cool to room temperature. The mixture was then centrifuged and decanted to separate the solution from the residue. The residue was washed with distilled water, dried in an oven at 100°C, and weighed. A sample of each solution and residue was analysed using ICP-OES.

Using the acid with which the highest uranium recovery was attained, a more comprehensive study was subsequently undertaken in which additional acid concentrations were investigated under identical experimental conditions to the screening investigation described above.

Results and discussion

Composition of waste material

A rough estimate of the composition of the waste material was determined (data not shown) by X-ray fluorescence (XRF). Based on this data, the cations present at concentrations greater than 0.5% by mass were determined using ICP-OES. The results are shown in Table I.

Since uranium will be recovered by means of SX, lowering the amount of impurities that may have an influence on the SX process would be an added benefit. From Table I it is clear that Fe (28.0 mg/g), Th (44.5 mg/g), and Ca (50.0 mg/g) are the main impurity elements in the waste material. Currently, there are no clear specifications for the final product material that would result from recovery of uranium. However, it is envisaged that the product would be re-used in a nuclear conversion plant. Therefore, the ASTM standard for uranium ore concentrate (UOC) can be used to specify the maximum allowed levels of impurities of the final product. These are 1% for both calcium and iron and 2.5% for thorium (ASTM, 2013). The focus of the current study was to dissolve the waste material as a preparatory step for future purification by SX, and lowering the levels of these impurities would be a benefit if it can be achieved during this

Table I

Elements with concentrations > 0.5% by mass in the waste material

Element	Concentration (mg/g)	Standard deviation	Element	Concentration (mg/g)	Standard deviation
Al	11.0	0.14	Ca	50.0	0.57
Fe	28.0	0.14	K	7.5	0.07
Si	8.0	0.00	Na	8.0	0.00
Th	44.5	0.35	U	487.0	5.80

step. To facilitate the discussion on impurities, the content of each impurity was expressed as a percentage of the uranium according to the relationship:

$$\text{Impurity (i) \%} = \frac{[i]}{[i] + [U]} \times 100 \quad [1]$$

where i and U refer to the impurity and uranium respectively. The values are presented in Table II.

As mentioned previously, it can be assumed that most of the impurities originate from the feed material to the conversion process. Accordingly, the high thorium content resulted from the non-volatility of the formed ThF_4, which caused it to settle at to the bottom of the flame reactor together with the rest of the waste material not converted to UF_6. Since the residue was re-fed to the flame reactor to reduce the amount of waste, thorium as well as other impurities were further concentrated in relation to uranium.

Table II

Impurity contents relative to uranium

Element	Impurity %
Ca	9.3
Fe	5.4
Th	8.4
Other (Al, K, Na, Si)	1.2

Dissolution

Screening of lixiviants

To identify the most promising lixiviant for the extraction of uranium from the waste material, a series of screening experiments was conducted using nitric, sulphuric, and hydrochloric acids at two concentrations, with and without addition of H_2O_2. Another objective was to determine whether the more water-soluble impurities could be removed during this step, even if uranium dissolution was not achieved. The results for the screening experiments in the absence of H_2O_2 are presented in Figure 1. The percentage dissolution of each element was calculated using the following relationship:

$$E\ \% = \frac{E_{solution}}{E_{(solution + residue)}} \times 100 \quad [2]$$

where E represents the specific element investigated.

It can be seen that the uranium dissolution was above 78% for all the acids, and 82% for water, with the highest

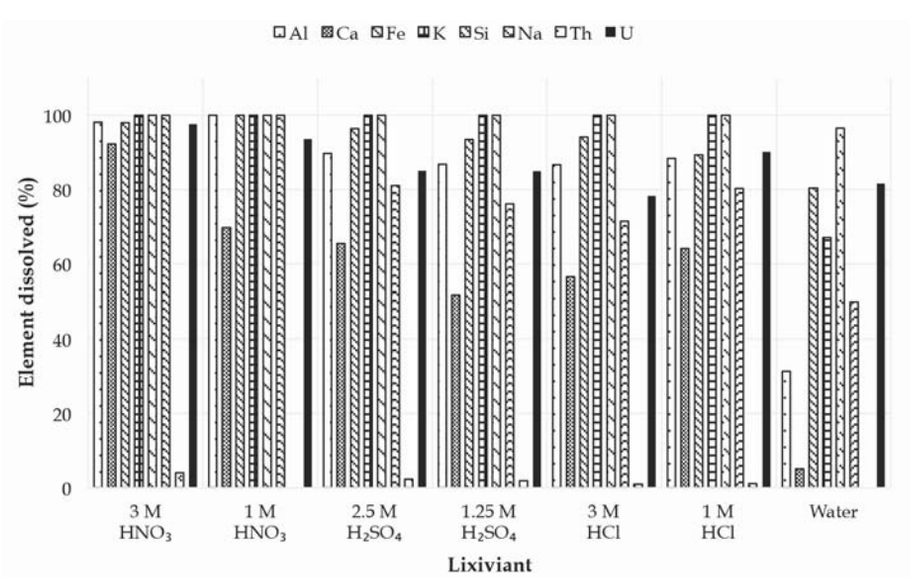

Figure 1—Effect of different lixiviants on the dissolution of various elements, in the absence of H_2O_2

uranium recovery (98%) observed in 3 M HNO_3. It is noteworthy that the thorium concentration in solution remained below 5% in all instances. The solubility of calcium, however, was significantly different in in different acids, and very limited in water. Although the calcium content in the waste material could be due to a mixture of various compounds, the behaviour observed could be explained by the presence of calcium sulphate dihydrate ($CaSO_4.2H_2O$), the solubility of which is 0.222 g/100 mL in hot water and 0.241 g/ 100 mL in cold water (CRC, 1976). Other calcium compounds show either very high or very low solubilities in water.

The solubility of $CaSO_4.2H_2O$ increases with an increase in acid concentration up to a maximum value (3.5 to 4.5 M for HNO_3, 2.5 to 3 M for HCl, and 1.5 M for H_2SO_4), and then decreases if the acid concentration is increased further (Vershkova *et al.*, 2003; Cameron and Breazeale, 1903; Ling and Demopoulos, 2004; Li and Demopoulos, 2005). For H_2SO_4, the initial increase in solubility of $CaSO_4.2H_2O$ has been attributed to the influence of the second dissociation constant of H_2SO_4, due to the higher solubility in the presence of HSO_4^- as well as to the increase in ionic strength in the presence of more H_2SO_4 (Marshall and Jones, 1966). The decrease in solubility at higher concentrations is believed to be due to a combination of effects which include changes in activity coefficient as well as salting-out due to the common-ion effect (Ling and Demopoulos, 2004; Calmanovici *et al.*, 1993). The increasing and decreasing solubility in HNO_3 was not clearly explained by Vershkova *et al.* (2003); however, Zhang *et al.* (2011) observed a decrease in the solubility of $CaSO_4.2H_2O$ in the order $HNO_3 > H_3PO_4 > H_2SO_4 > Ca(NO_3)_2$, also without offering an explanation, but which agrees with the results we obtained. A possible explanation for the behaviour in HCl was given by Li and Demopoulos (2005), who ascribed the initial increase in solubility to the presence of HSO_4^- formed during dissolution of $CaSO_4.2H_2O$, and the decrease at higher HCl concentrations to the influence of ion activity coefficients.

While the values in Figure 1 cannot be compared directly with those from the literature, due to the complexity of this waste material, the above does explain the higher calcium extractions at higher HNO_3 and H_2SO_4 concentrations. The lower calcium extraction at higher HCl concentration may indicate that the maximum $CaSO_4.2H_2O$ solubility was at a HCl concentration below 3 M.

The purities of the final uranium materials (calculated using Equation [1]) with regard to the three most prevalent impurities (Ca, Fe, and Th) are given in Table III. It is clear that both calcium (in acid) as well as iron (all acids and water) are nearly completely extracted during dissolution (see Table II for original concentrations). Some concentrations are higher than the original concentrations since the change in the amount of uranium extracted (<100%) was used to calculate the percentage impurity.

As mentioned above, the calcium level was significantly lowered from 9.3 to 0.6% by dissolution in water. The amount of iron was higher in all instances, with smaller differences from the initial value in instances where uranium recovery was higher (*e.g.* 3 M HNO_3). The reason for this is that iron was dissolved more completely compared to the other impurities (thorium was very insoluble, and calcium solubility depended on acid type and concentration). Therefore, since the impurity values are calculated in terms of the total amount of uranium present, the values for iron as an impurity would also be higher, especially if the uranium recovery is lower. A more in-depth discussion on the behaviour of iron follows in the next section. The amount of thorium was lowered so significantly in all instances that all lixiviants are suitable for the separation of uranium and thorium during the dissolution step.

Influence of H_2O_2

The influence of H_2O_2 on the recovery of uranium in water and different acids at various concentrations, as well as on the purity of the final uranium solution, was determined. H_2O_2 acts as an oxidizing agent to facilitate the oxidation of the insoluble U(IV) to more soluble U(VI). The influence of H_2O_2 on the amount of impurities extracted, as well as the uranium recoveries for the different lixiviants, is presented in Figure 2.

The secondary y-axis gives the difference in uranium recoveries in the absence and presence of H_2O_2. Therefore, a large positive value indicates a large increase in uranium recovery when H_2O_2 is added and a value of zero, no difference. The influence of H_2O_2 on uranium recovery was greatest when using 3 M HCl. In contrast, the influence of H_2O_2 was negligible when using HNO_3 and 2.5 M H_2SO_4. This can be explained in terms of the oxidizing ability of these acids. The standard electrode potentials (Table IV) show that HNO_3 is the stronger oxidizing agent, whereas the oxidizing ability of H_2SO_4, increases at higher acid concentrations, hence the diminished influence of H_2O_2 in the more concentrated H_2SO_4 solution. However, the influence of H_2O_2, which was high with 3 M HCl, decreased again at the lower HCl concentration, and was low in water.

The bar chart (primary y-axis) in Figure 2 shows the effect of H_2O_2 on the impurity level of the final uranium solution, taking into account all elements and using Equation [1]. For the percentage impurity extraction in the absence of H_2O_2, the combined totals of the values presented in Table III were used. It is clear that the presence of H_2O_2 had little influence on extraction of impurities. The purity of the solution increased slightly for HNO_3, HCl, and water while decreasing slightly for H_2SO_4 in the presence of H_2O_2.

Table III

Impurities in solution in relation to the dissolved uranium

Method	Ca (%)	Fe (%)	Th (%)	Other (%)
Initial	9.3	5.3	8.3	1.3
3 M HNO_3	9.6	5.5	0.6	5.4
1 M HNO_3	6.6	5.7	0.1	4.2
2.5 M H_2SO_4	8.1	6.1	0.3	3.4
1.25 M H_2SO_4	5.8	5.3	0.2	3.6
3 M HCl	6.9	5.8	0.1	3.7
1 M HCl	8.5	6.7	0.1	3.5
Water	0.6	6.2	0.1	4.0

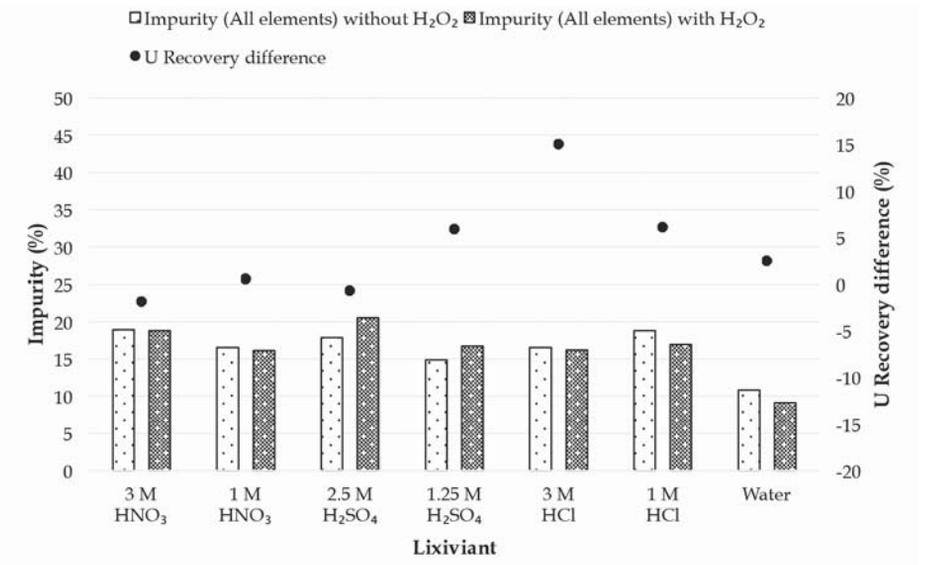

Figure 2—Influence of H_2O_2 on uranium recovery and purity of the solution

Table IV

Standard electrode potentials of acids and metals under investigation (CRC, 1976)

Medium/ metal	Equlibrium reaction	E^0 (V)
	More oxidizing	
H_2O_2	$H_2O_2 + 2H^+ + 2e^- \rightarrow 2H_2O$	+1.77
HCl	$Cl_{2(g)} + 2e^- \rightarrow 2Cl^-_{(aq)}$	+1.36
HNO_3	$NO^-_{3(aq)} + 4H^+_{(aq)} + 3e^- \rightarrow NO_{2(g)} + 2H_2O$	+0.96
	$NO^-_{3(aq)} + 3H^+_{(aq)} + 3e^- \rightarrow HNO_{2(aq)} + 2H_2O$	+0.94
Ferric	$Fe^{3+}_{(aq)} + e^- \rightarrow Fe^{2+}_{(aq)}$	+0.77
Uranium	$UO^{2+}_{2(aq)} + 4H^+ + e^- \rightarrow U^{4+} + 2H_2O$	+0.273
H_2SO_4	$SO_{4(aq)}{}^{2-} + 4H^+ \rightarrow SO_{2(g)} + 2H_2O$	+0.2
	$SO_{4(aq)}{}^{2-} + 4H^+ \rightarrow H_2SO_{3(g)} + H_2O$	+0.17
Hydrogen	$2H^+_{(aq)} + 2e^- \rightarrow H_{2(g)}$	0.00
Ferrous	$Fe^{2+}_{(aq)} + 2e^- \rightarrow Fe_{(s)}$	-0.44
Water	$2H_2O_{(l)} + 2e^- \rightarrow H_{2(g)} + 2OH^-_{(aq)}$	-0.8227
	More reducing	

As regards the three most abundant impurities (Ca, Fe, and Th), most of the thorium had already been removed in the absence of H_2O_2 (Table IV), and thorium removal was not further improved by adding H_2O_2. The effect of H_2O_2 on the dissolution of calcium and iron is shown in Figure 3.

The reason for the decrease in solution purity for H_2SO_4 in the presence of H_2O_2 (Figure 2) becomes clear from Figure 3, which shows higher amounts of calcium and, in certain instances, iron dissolved. The increase in calcium dissolution may be due to a reaction between calcium and H_2O_2 that results in the formation of a more acid-soluble calcium species such as calcium peroxide (CaO_2) (Tsentsiper and Vasil'eva, 1967). At present, it is not viewed as critical to the uranium recovery aspect of this study for this aspect to be investigated further. Furthermore, a decrease in the amount of iron dissolved in water was observed when H_2O_2 is added.

The influence of H_2O_2 on iron is unexpected since the purpose of H_2O_2 addition was to interact with U(IV). The influence of H_2O_2 on uranium recovery in water (Figure 2) was also surprisingly low, since water is not a particularly oxidizing environment (see Table IV) and it was expected that H_2O_2 would increase uranium recovery in water.

The observations thus far suggest that the oxidizing ability of each lixiviant, the presence of H_2O_2, and the iron present in the waste material influence each other, thereby influencing the recovery of both uranium and impurities. Fe^{3+} is known to oxidize insoluble U(IV) to soluble U(VI) (Ervanne, 2004; Venter and Boylett, 2009) while being reduced to Fe^{2+} according to the following simplified equation:

$$U(IV) + 2Fe^{3+} \rightarrow U(VI) + 2Fe^{2+} \quad [3]$$

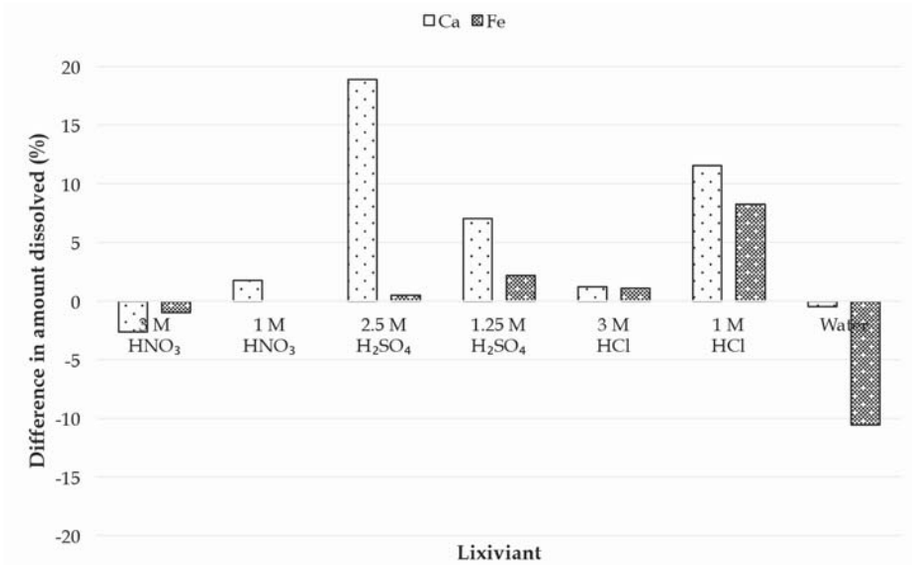

Figure 3—Influence of H_2O_2 on the amounts of Ca and Fe in solution

Since iron is present in the waste material in significant amounts, it may be possible that the oxidative dissolution of uranium is facilitated by Fe^{3+} and not directly by H_2O_2 as initially thought. In the presence of a strongly oxidizing acid such as HNO_3, which is a stronger oxidizer than Fe^{3+} (Table IV), the oxidation of U(IV) is facilitated mostly by the acid itself and the effect of iron is masked. The H_2O_2 then rather acts as an oxidizing agent to regenerate the formed Fe^{2+} back to Fe^{3+}, which is then again available to oxidize U(IV), as also described by Venter and Boylett (2009) for uranium leaching. The reaction of Fe^{2+} with H_2O_2 in the presence of acid can be represented by the following equation:

$$2Fe^{2+} + H_2O_2 + 2H^+ \rightarrow 2Fe^{3+} + 2H_2O \quad [4]$$

The higher uranium recovery in the presence of H_2O_2 with the lower concentration of H_2SO_4 can be explained by the lower oxidizing capability of H_2SO_4 at lower concentrations and its lower oxidizing capability compared with Fe^{3+}, as seen in Table IV. Therefore, the Fe^{2+} formed during oxidation of U(IV) can be re-oxidized by H_2O_2 to Fe^{3+}, which will in turn enhance the uranium recovery. A similar effect was observed in 3 M HCl and since this is the least oxidizing environment, the addition of H_2O_2 yielded the greatest enhancement of uranium recovery. The decrease in iron dissolution in water when H_2O_2 is added may indicate the formation of an insoluble iron species, the nature of which is unknown and which would have to be further investigated.

Influence of HNO_3 concentration

In the initial tests the highest uranium recovery was achieved in HNO_3. In addition, when using HNO_3 systems, the addition of H_2O_2 did not improve uranium recovery, while impurities such as iron had less of an influence on uranium recovery. To further optimize the dissolution, higher concentrations of HNO_3 were used to confirm the observations made during the screening, where only two values in the lower concentration range were included. For this purpose the effect of HNO_3 concentrations from 1 M to 12 M on the uranium recovery, as well as on the purity of the final solution, was investigated. The values for all elements dissolved in the different HNO_3 concentrations are presented in Figure 4, calculated similarly as in Figure 1.

The recovery of uranium in HNO_3 initially increased with increasing acid concentration, reaching a maximum of 98% at 3 M before declining to 78.75% in 12 M HNO_3. Currently, there is no explanation for this decrease in recovery at higher HNO_3 concentrations, and further investigation is needed.

Calcium dissolution increased with increasing HNO_3 concentration, from 69.83% at 1 M to 92.3% at 3 M, followed by a slight decrease to 88.05% at 6 M and then decreasing significantly to 63.03% at 12 M HNO_3. These observations again agree with results in the literature in terms of the solubility of $CaSO_4.2H_2O$ in HNO_3, where an increase is observed with increasing acid concentration up to a certain point, followed by a decrease at higher concentrations (Vershkova *et al.*, 2003). The amount of Ca, Fe, Th, and other impurities dissolved in relation to the amount of uranium dissolved was calculated using Equation [1], and the results are presented in Table V. Again, the thorium impurity was lowered from 8.4% to < 1% irrespective of the HNO_3 concentration. The amount of iron increased in all HNO_3 concentrations, with the lowest value at 3 M. For calcium, the lowest impurity levels were attained at 1 M and at 12 M, with the highest impurities at 6 M. The lowest total impurity level was obtained at 1 M HNO_3.

Influence of H_2O_2 in HNO_3

The results obtained when studying the influence of H_2O_2 in HNO_3 on uranium recovery and the purity of the final solution can be seen in Figure 5. The values of the bar chart (primary y-axis) represent the percentage impurity of the final solution calculated from all elements. The secondary y-axis shows the difference between the uranium recoveries in the absence and presence of H_2O_2.

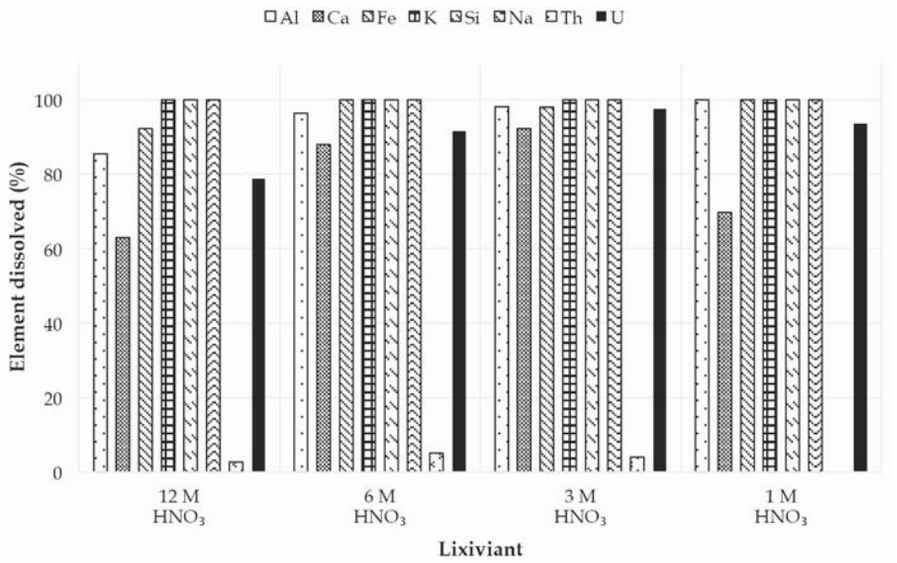

Figure 4—Dissolution of each element in different concentrations of HNO_3 in the absence of H_2O_2

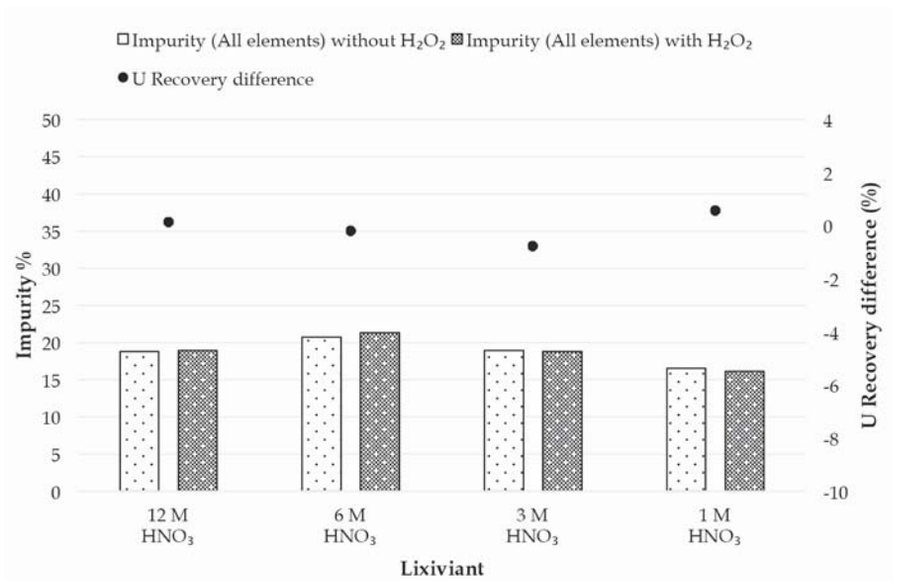

Figure 5—Impurity of the solution in relation to uranium (including all elements present) and difference in uranium recovery in the presence of H_2O_2

Table V

Impurities in solution in relation to uranium as a function of HNO_3 concentration

Method	Ca (%)	Fe (%)	Th (%)	Other (%)
Initial	9.3	5.3	8.4	1.3
12 M HNO_3	8.5	6.6	0.4	3.3
6 M HNO_3	10.6	6.2	0.5	3.0
3 M HNO_3	9.6	5.5	0.6	5.4
1 M HNO_3	6.6	5.7	0.1	4.1

These results confirm the observations from the screening tests, in that H_2O_2 has limited influence on uranium recovery in an HNO_3 environment and an insignificant influence on the purity of the final solution. Therefore, HNO_3 would be an ideal choice for dissolution of the waste material, after which further purification will be conducted.

Conclusions

The nuclear conversion plant waste material is soluble in different acids. Different uranium recoveries were obtained at different acid concentrations, with the highest recovery (98%) being obtained in 3 M HNO_3. Furthermore, for 3 M

HNO_3, it was not necessary to add an oxidizing agent to increase the uranium recovery or to decrease impurity levels. An advantage of all lixiviants studied is that thorium was largely removed from the waste material, decreasing from 8.4% to less than 1% in relation to the extracted uranium. The waste material was also leachable in water, with 82% uranium recovery combined with a significant reduction in the total amount of impurities in relation to uranium (from 24.3% to 10.8%).

The influence of H_2O_2 on uranium recovery was found to be greatest in less oxidizing environments, especially in 3 M HCl. This is probably due to the role of Fe^{3+} as an oxidizing agent for the oxidative dissolution of U(IV), Fe^{3+} being in turn reduced to Fe^{2+}. The H_2O_2 then acts to regenerate Fe^{2+} to Fe^{3+}, which is once again available for oxidation of U(IV). In view of the significant amounts of fluoride present in the waste material, future work to will investigate suitable methods for fluoride removal.

Due to the environmental liability around the conversion plant waste material, successful dissolution thereof opens up possibilities for re-use of the material once the uranium has been purified. Not only will the amount of waste in storage be reduced, but a valuable product will be obtained that may possibly be used as feed material to a conversion process.

Acknowledgements

We would like to thank the National Research Foundation (NRF), the Nuclear Energy Corporation of South Africa (Necsa), and the Chemical Resource Beneficiation (CRB) group for funding that made this work possible. We would also like to acknowledge Mr L. Nkadimeng for help with experimental work.

References

ASTM. 2013. Standard specification for uranium ore concentrate. 3. ASTM International, West Conshohocken, PA.

Calmanovici, C.E., Gabas, N., and Laguérie, C. 1993. Solubility measurements for calcium sulfate dihydrate in acid solutions at 20, 50 and 70°C. *Journal of Chemical Engineering and Data*, vol. 38. pp. 534–536.

Cameron, F.K. and Breazeale, J.F. 1903. Solubility of calcium sulphate in aqueous solutions of sulphuric acid. *Journal of Physical Chemistry*, vol. 7. pp. 271–577.

Coleman, C.F. 1966. Recovery of uranium and zirconium from aqueous fluoride solutions. US patent US3243257.

CRC. 1976. Handbook of Chemistry and Physics. CRC Press, Boca Raton, FL.

Ervanne, H. 2004. Detecting and minimizing interferences in uranium oxidation states during dissolution of solid phases. *Journal of Radioanalytical and Nuclear Chemistry*, vol. 260. pp. 249–253.

Floreancig, A. 1983. Method of dissolving impure uranium tetrafluoride. France patent application.

Kumar, J.R., Kim, J.-S., Lee, J.-Y., and Yoon, H.-S. 2011. A brief review on solvent extraction of uranium from acidic solutions. *Separation and Purification Reviews*, vol. 40. pp. 77–125.

Li, Z. and Demopoulos, G.P. 2005. Solubility of $CaSO_4$ phases in aqueous HCl + $CaCl_2$ solutions from 283 K to 353 K. *Journal of Chemical and Engineering Data*, vol. 50. pp. 1971–1982.

Ling, Y. and Demopoulos, G.P. 2004. Solubility of calcium sulfate hydrates in (0 to 3.5) mol.kg-1 sulfuric acid solutions at 100°C. *Journal of Chemical and Engineering Data*, vol. 49. pp. 1263–1268.

Luk'yanchev, Y. and Nikolaev, N.S. 1963. The solubility of uranium tetrafluoride in aqueous solutions of acids. *Atomic Energy*, vol. 15. pp. 1184–1187.

Marshall, W.L. and Jones, E.V. 1966. Second dissociation constant of sulfuric acid from 25 to 350° evaluated from solubilities of calcium sulfate in sulfuric acid solutions. *Journal of Physical Chemistry*, vol. 70. pp. 4028–4040.

Ohashi, Y., Murashita, S., and Nomura, M. 2014. Extraction of uranium from solid waste containing uranium and fluorine. *Minerals Engineering,* vol. 61. pp. 32–39.

Ponelis, A.A. 1989. Die invloed van alkali-metaalonsuiwerhede op die uraandioksiedhidrofluorineringsreaksie. PhD thesis, University of Pretoria.

Ponelis, A.A., Slabber, M.N., and Zimmer, C.H.E. 1986. Conversion of non-nuclear grade feedstock to UF_4. *Proceedings of Advances in Uranium Refining and Conversion*. International Atomic Energy Agency, Vienna. pp. 111–139.

Sasahira, A., Kani, Y., Iino, K., Hoshino, K., and Kawamura, F. 2007. Development of FLUOREX process as a progressive LWR reprocessing system. *Proceedings of the Global 2007 Conference on Advanced Nuclear Fuel Cycles and Systems*, Boise, Idaho, 9-13 September 2007. American Nuclear Society, La Grange Park, IL

Tsentsiper, A.B. and Vasil'eva, R.P. 1967. The reaction of calcium hydroxide with hydrogen peroxide vapor. *Bulletin of the Academy of Sciences of the USSR*, Division of Chemical Science, vol. 16. pp. 2445–2447.

Venter, R. and Boylett, M. 2009. The evaluation of various oxidants used in acid leaching of uranium. *Proceedings of Hydrometallurgy 2009*. Southern African Institute of Mining and Metallurgy, Johannesburg. pp. 445–255.

Vershkova, Y.A., Tareeva, O.A., Ivlev, K.G.M., and Lokshin, E.P. 2003. Solubility of calcium sulfate dihydrate in nitric acid at 20°C. *Russian Journal of Applied Chemistry*, vol. 76. pp. 156–157.

Volk, V.I., Vakhrushin, A.Y., and Mamaev, S.L. 2000. Extraction of uranium and thorium with TBP from fluoride - nitric acid solutions. *Journal of Radioanalytical and Nuclear Chemistry*, vol. 246. pp. 697–702.

Zhang, Q.Y., Huang, X.H., Tang, H.B., and He, H. 2011. Electrochemical behavior of uranium(VI) in 1-butyl-3-methylimidazolium chloride. *He-Huaxue yu Fangshe Huaxue (Journal of Nuclear and Radiochemistry)*, vol. 33. pp. 101–105. ◆

http://dx.doi.org/10.17159/2411-9717/2017/v117n8a10

Status of the phasing out of the Chamber of Mines of South Africa Certificates of Competency

by H. Grobler* and J.A. Maritz†

Synopsis

The Chamber of Mines of South Africa (CoMSA) Certificates of Competency (CoCs) were introduced to standardize stand-alone in-house qualifications for persons working in the South African Mining and Minerals Industries (SAM&MS). When the Higher Education Qualification Framework (HEQF) Act was introduced in 2007, one of the unintended consequences was that it implied that CoMSA could no longer issue its OBET non-compliant CoCs. In response to these developments, the intention was to phase out CoMSA CoCs by establishing a deadline for the last entry for new candidates into the CoMSA CoC system at 31 August 2015, before it was finally recognized that these changes would have a wider impact in the SAM&MS involving mine environmental control (MEC), rock engineering (RE), mine surveying, and other disciplines. Three institutes, namely the Institute of Mine Surveyors of South Africa (IMSSA), the South African National Institute for Rock Engineers (SANIRE), and the Mine Ventilation Society of South Africa (MVSSA) made a combined representation, and it was agreed that the said deadline could be extended to 31 August 2018. This means that the complete suite of 'new' (Outcomes Based Education and Training [OBET])-compliant qualifications must be registered on the appropriate level of the National Qualifications Framework and sub-frameworks by the South African Qualifications Authority (SAQA), and implemented by approved education and training providers and accredited by the respective Quality Councils (QCs). In the case of the South African Mining and Mineral Sector (SAM&MS) the Mining Qualifications Authority (MQA), being the custodian of qualifications for the SAM&MS in terms of Section 41,(3) of the Mine Health and Safety Act 1995 (MHSA), Act 27 of 1995 and Regulations as amended, supported by the relevant professional associations (PAs) will apply to the relevant QC to be appointed as Development Quality Partner (QDP) and/or Quality Assessment Partner (AQP) to develop, implement and quality assure (QA) 'mining-technical related' qualifications. The application process to have an OBET-compliant qualification developed and registered on the NQF is tenuous at best, and it is anticipated that a minimum of two years will be required to achieve this for one level of Quality Council for Trades and Occupations (QCTO)-compliant qualifications. The positive spin-off of this crisis is that 'learned societies' and PAs active in the SAM&Ms were drawn into the development and implementation of a range of recognized OBET-compliant occupational qualifications required to develop the knowledge and skills needed in the Industry. This paper outlines the requirements for such qualifications and outlines the progress made towards the development and implementation thereof.

Keywords

mining qualifications, curriculum development, accreditation, outcomes-based education and training.

Introduction

Chapter 4 of the Mine Health and Safety Act 1995 (MHSA), Act 27 of 1995 deals with tripartite institutions and in accordance of Section 41(3), a Mining Qualifications Authority (MQA) is established to advise the Minister on qualifications, standards, assessments, examinations, quality assurance, and accreditation of mining qualifications. In this role the MQA is to advise the Minister on the registration of qualifications on the National Qualification Framework (Department of Mineral Resources, 2011). In Schedule 7(g) (GNR 612 of 24 June 1998) it is determined that the Authority must '*assure the quality of education and training..., without itself being provider of education...'.* The functions of the MQA is defined in Chapter 4 46(1)(a-f) of the MHSA.

With the establishment of the NQF in 1995, three quality Quality Councils (QCs) were established for the setting of and quality assurance of competency standards. These Quality Councils are the Council for Higher Education (CHE), which deals with formal tertiary education on NQF levels 5 through 10; the Further Education and Training Quality Council (FETQC) (Umalusi), which deals with qualifications on NQF levels 1 through 4; and the Quality Council for Trades and Occupations (QCTO), which deals with qualifications on NQF Levels 1 through 8. The Occupational Qualifications Framework (OQF) was developed to address labour market needs in respect of occupations and was designed to provide occupational qualifications as well as the minimum access requirements for these qualifications. The OQF intends to provide clear articulation with qualifications in the general and further education framework and

* *University of Johannesburg, South Africa.*

‡ *University of Pretoria, South Africa.*

 ISSN 2225-6253. Paper received Apr. 2016; revised paper received Mar. 2017.

seamless progression to the Higher Education and Training (HET) Framework. Occupational qualifications contain three distinctive components, namely; a knowledge component, a skills component, and a work experience component. (Mining Qualification Authority, 2016). The role of SAQA is to protect the integrity of the NQF and facilitate harmonization between the said sub-frameworks in order to promote 'seamless horizontal and vertical articulation and progression' through the different levels of the NQF. The QCTO system requires that a Community of Expert Practice (CEP), made up of practitioners active within a specific occupation, will be involved in standard setting (DQPs) and quality assurance (AQPs) of QCTO-compliant qualifications. This role was previously fulfilled by the Standard Generating Bodies (SGBs) under the original Skills Development Act. In the new context, the various PAs inclusive of the Institute of Mine Surveyors of South Africa (IMSSA, the Mine Ventilation Society of South Africa (MVSSA), and the South African National Institute for Rock Engineers (SANIRE) should be involved as the relevant CEPs for the qualification required for their respective occupations.

The ideal AQP should operate in close collaboration with the recognized industry-specific 'Learned Society' or PA in an attempt to complete the development, implementation and QA of occupational qualifications. The role of the appointed AQP is to:

- Set the national standard for the occupational competence described in the qualification
- Develop, maintain, and apply external assessment tools to ensure a standardized national process for achieving the qualification. This would include tools such as an item bank test. The positive legacy of the CoMSA CoC is that an excellent record of past assessment tools and question banks are available to develop into a new 'test bank' for external assessment. In this process, assessments for each qualification on the relevant level of the NQF, using Blooms taxonomy as the point of departure, must be developed. The AQP must determine policies and procedures for assessments. A schedule of assessment dates, criteria for assessment sites, and the accreditation of these sites must be compiled. The AQP can then register assessors and moderators (specified qualifications and experience and courses required)
- Evaluate results of the assessment and in collaboration with the QCTO, and deal with quality assurance issues for Providers.
- Research and evaluate the impact of the qualification and recommend actions to improve the impact in order to achieve the National Skills Strategy and contribute towards achieving the National Development Strategy.

The role of PAs is to ensure that their qualifications meets the competency and legislative requirements, ensure that the qualification will contribute to the maintenance of professionalism, and to advise on any changes that may be required to meet future occupational needs. The purpose of the National Skills Development Strategy (NSDS) is to create a national framework of learning that will facilitate access, mobility and progression in education and training. (Mining Qualifications Authority, 2016).

Using the abovementioned principle as the point of departure, the PAs stated, at a recent industry presentation, that *'Industry training was isolated and did not lead to nationally accredited qualifications.'* CoMSA has been issuing CoCs since the 1970s. Although these CoCs have always had an excellent reputation and enjoyed recognition within the SAM&MS, they do not comply with the requirements of the NQF system, *i.e.* they are not OBET-compliant qualifications registered on the appropriate level of the 10-level NQF.

As a result of the developments within the NQF and recent legislation, the CoMSA CoCs have to be phased out and replaced with OBET-compliant qualifications registered on the appropriate level of the NQF. The original intent of the phasing-out period was that the last enrolment of new candidates into the CoMSA system would take place on 31 August 2015. However, because the assessment system of the QCTO was not ready, this date was postponed until 31 March 2016 for the May 2016 examination, and then postponed again to August 2016 (Anderson, 2016). Following a representation to the Executive of CoMSA, it was agreed to extend the deadline to the 31 December 2020. This agreement will see the last enrolment for new candidates into the system on 31 August 2018 (Mabena, 2016). At this point the QCTO-compliant qualifications must be in place for all the said mining-technical disciplines.

The mine surveying, mine environmental, and rock engineering disciplines are extremely reliant on the CoMSA certificates in order for persons in these fields to progress to the CoC as defined in the MHSA (Anderson, 2016). A significant percentage of persons working in these three fields are working full-time in industry and are by necessity forced to make use of 'distance learning' options in order to obtain a recognized industry qualification. A summary of the average number of persons sitting examinations for the various CoMSA certificates for the period 2009–2015 is given in Table I.

Table I

Candidates per CoMSA Certificates of Competency (Source: CoMSA)

Certificate	Average 2009–2015
Elementary Mine Survey	159
Advanced Mine Survey	119
Advanced Mine Valuation	97
Mine Survey Draughting	15
Mine Environmental Control Intermediate	112
Mine Environmental Control	71
Strata Control Hard Rock	149
Strata Control Coal	14
Rock Engineering: Theory	98
Rock Engineering: Application	86
Rock Engineering: Hard Rock	47
Rock Engineering: Coal	7
Rock Engineering: Massive	3
Rock Engineering: Surface	4

A mine surveyor who has obtained the CoMSA Advanced CoC may, upon application, be accepted as a candidate for the Government Certificate of Competency (GCC) examinations. For mine environmental control (MEC)/mine ventilation and rock engineering practitioners, the advanced CoMSA CoCs are by regulation recognized as proof of competency required in accordance with the MHSA. The throughputs for these qualification have not been ideal.

Unintended consequences – the HEQF and the COMSA CoC

When the HEQF Act was introduced in 2007, it meant by implication that the CoMSA could no longer issue CoCs at Levels 5 through 8 as it would have to become recognized as an accredited HET provider. In response to these changes Grobler suggested that the COMSA CoC be modified in order to ensure articulation from the replacement OBET-compliant qualifications into the formal HE system. With the advent of the HEQF, the option of replacing the CoMSA CoCs with HEQF-compliant qualifications seemed plausible but would have to comply with the requirements of the new Skills Development Act 2008.

Using the mine surveying discipline as an example, the intention was to replace the CoMSA Elementary Certificate with a QCTO-compliant Higher Certificate (NQF Level 5) and the CoMSA Advanced Certificate with a QCTO-compliant Advanced Certificate (NQF Level 6). The provision of Level 2 through Level 4 qualifications would be addressed through the QCTO process. The said Levels 2 through 4 QCTO-compliant qualifications have been developed using the existing basic surveying and sampling curriculum and portions of the CoMSA Elementary CoC. These two certificates were intended to replace the CoMSA CoC and offer an alternative to the current National Diploma which, in terms of the original HEQF Act, was considered to be a 240-credit, 2-year full-time qualification, which did not seem feasible at the time. The University of South Africa (UNISA) planned to offer the said two qualifications. However, during the 2013 accreditation visit of the South African Council for Professional and Technical Surveyors (PLATO) to UNISA, the accreditation panel advised against these proposed certificates and proposed that the 2-year National Diploma be considered the preferred qualification. This suggestion had the unintended, serious repercussion in that no person would be able to complete a CoMSA CoC in less than two years through a distance learning mechanism. Although the intention of this recommendation seemed acceptable for the uninformed, it has left a large percentage of mining technical practitioners with low Grade 12 examination results without a route to obtain qualifications that could ultimately lead to acceptance for the GCC examinations. Although these changes were well publicized at the time, the original 2016 deadline set by CoMSA was not in any way adjusted to accommodate the said changes. This CoMSA decision affected not only the mine survey and sampling disciplines, but also the EMC and SC/RE disciplines. It should be noted that the survey draughting discipline was not considered at all in any of these arrangements.

Deadlines

The challenge remains to meet the required deadlines for the phasing out/replacing of the CoMSA CoC as a result of the requirements placed on the development of QCTO-compliant qualifications. These challenges include, *inter alia:* the registration of existing training providers; the development of an NQF Level 5 QCTO-compliant qualification for mine surveyors and mineral valuation practitioners; the development of an NQF Level 7 qualification to address the requirements for an appropriate Level 7 qualification and work experience required for acceptance as candidate for the GCC examinations for mine surveyors; and, most importantly, addressing the perceived gap in education, training, and development between the new suite of QCTO-compliant qualifications and the CoMSA CoC. It is argued that the deadline for the replacement of the CoMSA CoC should be extended to address this 12–18 month approval period for the registration of a QCTO-compliant qualification and to deal with learners who are still in the competency development process. The IMSSA is committed to supporting and/or facilitating this process as far as possible, but lacks the resources to effectively deal with the requirements since it relies on voluntary contributions from its members. As a result of the delays in the processes, the IMSSA approached CoMSA and requested that the deadline for the termination of the CoMSA CoC be extended in order to address any resultant time lag caused by the transition from the current CoMSA CoC to the 'new qualifications'.

The recognition of the CoMSA CoC by tertiary Institutions

The CoMSA CoC was introduced to standardize stand-alone in-house qualifications for persons working in the SAM&MS. For this reason, most surveyors refer to this approach as the 'practical route' as studies are completed while employed in the SAM&MS. Most mining houses in the 1970s and 1980s developed their own 'suites' of 'qualifications' in order to ensure quality in training and development for their employees. Unfortunately the CoMSA CoC was never evaluated for equivalency with OBET-compliant qualifications registered on the NQF and therefore does not enjoy recognition when a learner want to enter the mainstream academic route at a traditional university, university of technology, or combined university. With the introduction of the HEQF Act the Chamber could no longer offer these qualifications.

Regulating the Mine Surveying occupation

In order to ensure a commonality between the various mine-specific competency requirements, CoMSA developed three CoCs that accommodated the three stages of competency required by a mine surveyor to progress to a point where he or she could be promoted to a senior position and become eligible to enrol as a candidate to the examinations for the GCC: Certificated Mine Surveyor. This 'suite' of CoMSA CoCs continues to enjoy strong support from the SAM&MS. From figures obtained from CoMSA it appears that for the period

2009–2015, an average 159 candidates attempted the Elementary Certificate: Mine Surveying and 119 candidates attempted the Advanced Certificate: Mine Surveying. Chapter 17(1)(b) of the MHSA defines a Competent Person:

- *'in the case of a surface mine where blasting does not take place, a person in possession of a mine surveyor's certificate of competency issued by the department;*

or

- *'…a person who has passed the examination for mining legislation as is required for the mine surveyor's certificate of competency issued by the Department and who is in possession of either:*
  - *(i) an Advanced Certificate in mine surveying issued by the Chamber of Mines of South Africa and who has at least three (3) years practical experience in mine surveying; or…*
  - *(ii) an Advanced Certificate in mine surveying issued by the Chamber of Mines of South Africa and who has at least three(3) years practical experience in mine surveying; or…*
  - *(iii) a person who has been assessed competent against a qualification recognized by the Mining Qualification Authority for this purpose. (DMR, 2011)*

The CoMSA CoCs availale to mine surveyors and samplers are:

- *Basic Certificate*—Mine Survey and Sampling (NQF level 4)
- *Elementary Certificate*—Survey- and Sampling (NQF level 2)
- *Advanced Certificate*—Survey- and Mineral Valuation
- *Certificate*—Mine Survey Draughting, which has not been addressed at this point and is a matter that requires urgent remedial action to be taken to ensure that an equivalent OBET-compliant qualification will be provided for this occupation.

Statistics for five years of examinations, held twice a year, provided the throughput percentages shown in Table II.

A review of credits obtained by these four CoC, when compared with the curriculum of the current National Diploma reveals the following:

- CoMSA CoC: Elementary Mine Survey provides 21.25 credits at level 5 on the NQF
- CoMSA CoC: Elementary Sampling provides 21.25 credits at level 5 on the NQF
- CoMSA CoC: Advanced Mine Survey provides 21.625 credits at level 6 on the NQF (made up of 2.5 credits at level 5 and 19.125 credits at level 6 of the NQF respectively)
- CoMSA CoC: Advanced Mine Survey provides 24.5 credits at level 6 of the NQF (made up of 7.5 credits at level 5 and 17.0 credits at level 6 of the NQF respectively).

The total credit for the entire CoMSA CoC in mine surveying (including sampling/valuation) is therefore 93.625, which is short of the minimum of 120 credits for an NQF Level 5 'Higher Certificate'. It may be possible to reach the required 120 credits if notional hours of learning can be awarded to the trial survey component of the Advanced Certificate.

What will replace the CoMSA CoC?

It was originally intended that the CoC in mine surveying be replaced by the HEQF-compliant Higher and Advanced Certificates. The Level 5 Higher Certificate (Mine Surveying) would replace the CoMSA Elementary Certificate and the Level 6 Advanced Certificate (Mine Surveying) was intended to replace the CoMSA Advanced Certificate. This process reached an advanced state of preparation before a seemingly unrelated decision relating to the reintroduction of the Blasting Certificate caused it to be abruptly terminated. Fortunately, while the HEQF-compliant qualifications were developed, two NQF Level 4 QCTO-compliant qualifications were developed in a parallel process. Since occupational qualifications are linked to occupations that are coded in accordance with the classification of the Organizing Framework Occupations (OFO) code for occupations, the qualification descriptors are mining technician with specialization (surveyor, mining). The QCTO-compliant qualifications consist of three distinct components, namely: theoretical, skills, and practical (portfolio). The two qualifications are:

1. NQF Level 4: SAQA 94870 Occupational Certificate: Mining Technician (Mining Sampler: Hardrock)
2. NQF Level 4: SAQA 94876 Occupational Certificate: Mining Technician (Mining Surveyor).

The foundational learning competency for these qualifications, articulation and Recognition of Prior Learning (RPL) based on an appropriate assessment either for entry or progression to other qualifications, must still be completed. The IMSSA intends partnering with the MQA in order to complete the required processes. This will require a team of

Table II

Throughput rate for Mine Surveying examinations (source: CoMSA)

	Elementary		Survey	Advanced	Advanced Survey	
	Sampling	Surveying	Draughting	Valuation	Theory	Legislation
Average 2009–2015	36%	26%	54%	50%	31%	38%

Table III

Credit equivalence between a National Diploma and the CoMSA CoC (Grobler, 2016)

Codes and Credits comparison for Chamber of Mines Elementary and Advanced

Course	Code	Semester	Code	Module Name	NQF Credits	NQF Level	Element Survey	Element Valuation	Advanced Survey	Advanced Valuation	GCC
N.Dip	440-1	S1	BQT1112	Quantitive Techniques 1	10	5				5.0	5.0
N.Dip	440-1	S1	CSA121	Communication Skills 1	10	5					
N.Dip	440-1	S1	EIR1111	Computer Skills 1	5	5					
N.Dip	440-1	S1	MOT1111	Mineral Exploitation	17	5	4.25	4.25			17
N.Dip	440-1	S1	MTH121	Mathematics 1	13	5					13.0
N.Dip	440-1	S1	MWT1111	Science Mining 1	15	5					
				TOTAL	70		4.25	4.25	0	5	35
N.Dip	440-1	S2	CAD1111	Computer Aided Draughting 1	10	5					
N.Dip	440-1	S2	EDM1111	Mechanical Engineering Drawing 1	10	5			2.5		5.0
N.Dip	440-1	S2	ENM31-1	Environmental Management III	10	5					
N.Dip	440-1	S2	MAS11-1	Accounting Skills 1	10	5				2.5	5.0
N.Dip	440-1	S2	MSY1111	Minerals Survey 1	17	5	17.0				17.0
N.Dip	440-1	S2	MTH231	Mathematics 2	10	5					
				TOTAL	67		17	0	2.5	2.5	27
N.Dip	440-1	S3	MGN21-1	Engineering Management II	13	6					
N.Dip	440-1	S3	MNM31-1	Numerical Methods	13	6					
N.Dip	440-1	S3	MSY2111	Minerals Survey II	17	6			17.0		17.0
N.Dip	440-1	S3	MVN1111	Mineral Valuation 1	17	5		17.0			17.0
N.Dip	440-1	S3	MWG2111	Mining Geology II	10	5					10.0
				TOTAL	70		0	17	17	0	44
N.Dip	440-1	S4	MSG3121	Structural Geology III	10	6					10.0
N.Dip	440-1	S4	MSS21-1	Statistics - Mining II	13	6					13.0
N.Dip	440-1	S4	MSY3111	Minerals Survey III	17	6			2.125		4.25
N.Dip	440-1	S4	MVN2111	Mineral Valuation II	13	6				17.0	17.0
N.Dip	**440-1**	**S4**	**MGN32-1**	**Engineering Management III**	**15**	6					
				TOTAL	68		0	0	2.125	17	44.25
B.Tech	728-1	S5	ACS41-1	Applied Computer Skills IV	10	7					
B.Tech	728-1	S5	GEO411	Geostatistics IV	10	7					2.5
B.Tech	728-1	S5	MIN21-1	Mining II	15	7					
B.Tech	728-1	S5	MSL41-1	Mineral Survey Legislation IV	10	7			5		10.0
				TOTAL	45		0	0	5	0	12.5
B.Tech	728-1	S6	GEOP411	Geostatistics Project IV	13	7					13.0
B.Tech	728-1	S6	MES41-1	Mining Economics IV	10	7					10.0
B.Tech	728-1	S6	MTL3211	Mining Technical Services III	13	7					
B.Tech	728-1	S6	PDS41-1	Precise Deformation Surveys IV	13	7					
				TOTAL	49	28	0	0	0	0	23
							21.25	21.25	26.625	24.5	185.75

Table IV

Survey qualification models (source: Grobler)

Level	Chamber of Mines *approximate*	Old Qualifications	New Qualifications		
NQF Level 10					Philosophiae Doctor
NQF Level 9					Masters Degree
NQF Level 8		Bachelor of Technology			Honours Degree
NQF Level 7	Govt. Cert. of Competency	National Diploma			Bachelor of Mine Surveying or Bachelor of Engineering Technology
NQF Level 6	COM Advanced		SAQA Mine Survey 6	National Diploma	
NQF Level 5	COM Elementary		SAQA Mine Survey 5		
NQF Level 4	COM Basic	Grade 12	SAQA Mine Survey 4	Grade 12	Grade 12

subject and technical experts or CEPs to develop the necessary learning materials and assessment guides. These two registered Level 4 qualifications will still require:

1. Training providers that have been accredited by the approved AQP
2. An item-bank test and external assessments must be developed
3. The split between the content in the learnership (per cent theory and per cent practical) must be registered with the Department of Labour (DOL)
4. The AQPs must prepare examination papers, model answers, and assessment tools.

The need to develop a Level 7, second-stage qualification for graduates prior to their acceptance as candidates to the GCC examination has been identified in this process. This crucial issue still needs to be finalized.

CoC in Mine Environmental Control (MEC)

The MEC occupation/practice has been regulated by legislation since 1917, when the first regulations under the Mines and Works Act that required the appointment of dust inspectors were promulgated. Soon, other occupational environmental issues such as noise, illumination, thermal environment, airborne pollutants, radiation, and flammable gases were added to the responsibilities of the MEC practitioner. The MEC practitioner is also tasked with the design and management of fire prevention, detection, and firefighting strategies. Currently these responsibilities are set out in Section 12 of the MHSA and regulations (Beukes, 2016). The CoMSA CoCs in MEC are referred to in the regulations of the MHSA, thereby defining the CoMSA CoC as proof of competency. For this discipline there are two such CoCs, namely;

- Intermediate Certificate in MEC (considered equivalent to Level 4 on the NQF), which consists of a practical and two written examinations (paper 1 and paper 2)
- Certificate in MEC (considered equivalent to Level 6 or 7 on the NQF), which consists of six papers.

The CoC in MEC is required by the MHSA for persons who are responsible for environmental control at a mine. Regulation 22.15(5)(a) that the Competent Person referred to in regulations 5.1(1), 9.2(3), and 16.1(1), depending on the nature of the mine, should be in possession one of the following :

i) A valid CoMSA CoC in MEC
ii) A valid CoMSA Intermediate CoC in MEC.

The examination for the Intermediate CoC is a prerequisite for entry into the examinations for the CoMSA Certificate in MEC. Statistics for five years of these examinations, held twice a year, are shown in Table V.

These figures indicate an average pass rate of 36% for the Intermediate Certificate and 28% for the Certificate in MEC.

What will replace these CoMSA CoCs?

The CoCs in MEC are unique to the SAM&MS and the number of candidates is consequently limited. As a result, there is not enough critical mass for universities to register a standalone qualification in this discipline and therefore most of the feed into the profession is sourced from on-the-job distance learning candidates. Work is currently in progress to expedite the completion and implementation of the NQF Levels 3 and 4 QCTO-compliant qualifications. An NQF Level 6 qualification has been developed in collaboration with the University of the Witwatersrand (Wits), which will consist of seven one-week modules offered at the University. The curriculum of the qualification will consist of a written examination two weeks after the conclusion of lectures and the submission of an assignment report two weeks after examination. The curriculum will consist of seven modules:

- Module 1—Fluid flow dynamics
- Module 2—Thermal engineering
- Module 3—Planning, applied economics, technical literature, and information management
- Module 4—Risk management, fire and explosions, gases, statistics
- Module 5—Occupational hygiene – (Wits to help enhance the level of this module)
- Module 6—Legislation
- Module 7—Mathematics.

The final step will be the development and registration of an QCTO-compliant NQF Level 7 qualification and an appropriate plan and schedule for the development thereof (Beukes, 2016)

CoC in Rock Mechanics/Engineering

The CoMSA CoC in Rock Mechanics (RMC) was introduced in the 1970s to standardize and regulate the various competency models used by South African mining houses. The weakness of the independent 'mining house systems' was that it limited the movement and reciprocal recognition of rock engineering practitioners within the SAM&MS. Based on this shortcoming, the Group Rock Engineering Committee (one of CoMSA's sub-committees) decided to initiate a CoC in Rock Mechanics for tabular mining in 1977. By 2002 the

Table V

Throughput rate for Mine Environment Control examinations

	Interm. P1	Interm. P2	Paper 1	Paper 2	Paper 3	Paper 4	Paper 5	Paper 6
Average 2009–2015	47%	26%	16%	23%	20%	35%	35%	37%

CoMSA RMC was incorporated into the regulations of the MHSA. Post-2002, the original RMC made provision limited to the practice areas of underground tabular and coal mines. The provisions of the RMC were subsequently expanded in October 2007 to include CoCs for massive underground and surface mining (Lucas, 2016). The inclusion of the CoC in the definition of a Competent Person in Section 22.14.1(8) of the MHSA implies that the RMC is the prescribed competency requirement for a RM/RE practitioner in the SAM&MS. The following CoMSA CoCs, subdivided into appropriate specialization areas, are provided for the RM/RE discipline:

- CoC in Strata Control:
  i. Hard rock
  ii. Coal
- CoC in Rock Mechanics:
  i. Metalliferous mines
  ii. Coal mines
  iii. Massive underground mines
  iv. Surface mines.

Section 22.14.1(8) of the MHSA requires competent RM/RE practitioners to be in possession of a valid, appropriate RMC to be eligible to perform the following work:

'At every underground mine where a risk of rock bursts, rock falls or roof falls exists, and at every other mine where a significant risk of rock bursts, rock falls or roof falls exists, the employer must ensure that the input of a competent person is properly and timeously considered and integrated into mine design, planning and operations.'

The said Competent Person is defined as follows in Section 22.14.1(8) of the regulations:

'a person who is at least in possession of either the Chamber of Mines Certificate in Rock Mechanics [Metalliferous Mines], or the Chamber of Mines Certificate in Rock Mechanics [Coal Mines], whichever is appropriate for the type of mine concerned.'

The relevant Strata Control Certificate for hard rock or coal mining is a prerequisite for obtaining the RMC. Following on the RMC written exams (papers 1 and 2), a candidate can complete the CoC examinations in either hard rock, coal, massive, or surface mining by submitting a portfolio of evidence proving competence and completing a practical examination. Statistics for five years of these examinations, held twice a year, indicate the pass rates in Table VI.

The implicit reference in the regulations of the MHSA to the CoMSA CoC underlines the crucial importance of these qualifications within the SAM&MS and the implication that this needs to remain so for the foreseeable future. It should, however, be noted that a process is currently underway to update and revise the legislation to cater for a 'new' (OBET-compliant) qualification registered on the NQF when the current CoMSA CoC is discontinued. The proposed 'new competency model' also needs to make provision that a RE/RM practitioner registered in the appropriate category with a statutory body such as the Engineering Council of South Africa (ECSA) or the South African Council for Natural Scientists SACNASP) be eligible to practice as a Rock Mechanic/Engineer on an operation in the SAM&MS.

Replacement of the CoMSA RMC

Indications are that the current CoMSA RMC will in time be replaced by appropriate QCTO-compliant NQF Level 3, 4, and 6 qualifications. At the entry level for the hard rock sector, a Level 3 occupational qualification will be required for an Observer (SAQA ID: 96464). This qualification carries a credit loading of 108 (*i.e.* equivalent to 1080 notional hours of learning). The RMC will be replaced with an appropriate Level 4 occupational qualification, similar to the Level 3 occupational qualification, which has also already been registered by the QCTO. The said Level 4 occupational qualification will provide for the Hardrock (SAQA ID: 94038)

Table VI

Throughput rate for Rock Engineering examinations (source: CoMSA)

	S/C Met.	S/C Coal	Paper 1 Theory	Paper 2 Application	Paper 3.1 Hard Rock	Paper 3.2 Coal	Paper 3.3 Massive mining	Paper 3.4 Surface
Average 2009–2015	30%	12%	12%	25%	25%	33%	28%	32%

Table VII

Occupational qualifications in Strata Control registered on the NQF (source: Maritz, 2016)

SAQA ID	Qualification	NQF Level	Credits
96464	Occupational Certificate: Mining Technician (Strata Control Observer: Underground Hardrock)	3	108
94038	Occupational Certificate: Mining Technician: (Strata Control Practitioner: Underground Hardrock)	4	198
94878	Occupational Certificate: Mining Technician: Strata Control Practitioner (Coal)	4	264

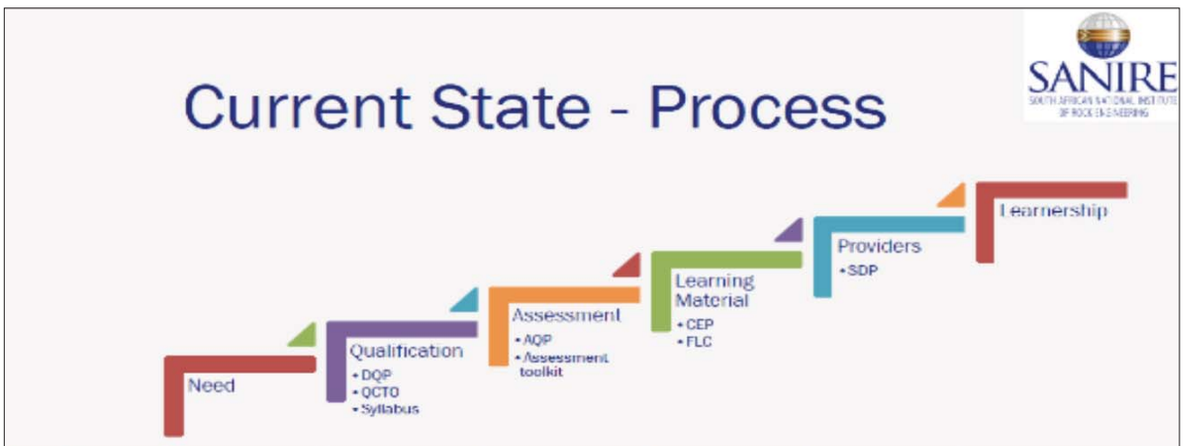

Lvl	Type	Need	Qual	Assess	LM	Prov	LS
3	HR	X	X				
4	HR	X	X	/			
	Coal	X	X	/			
	Massive	X	X	/			
	Surface	X		/			
6	All	X		/	X		

Figure 1—SANIRE current state and progress (source: Maritz, 2016)

or Coal (SAQA ID: 94878) practice areas, as is the case with the current RMC. The credits for the said two Level 4 occupational qualifications are 198 for hard rock and 264 for coal. The reason for more credits being associated with the coal qualification is that some of the Hardrock observer material, which may already have been acquired by hard rock practitioners during their Level 3 learning, provides them with Recognition of Prior Learning (RPL) in relation to the requirements of the Level 4 occupational qualification. The registered occupational qualifications are summarized in Table VII.

The RMC will be replaced by a Level 6 qualification, the application for development of which has been submitted to the QCTO jointly by the MQA and SANIRE. The development of the said occupational qualification has been approved by QCTO as a prioritized occupation and development is currently in progress (Figure 1). The said qualification will be registered under the OFO code 311701 as a specialization (*i.e.* Rock Engineering Officer) under the Mining Technician occupation.

The abovementioned qualifications need to be in place by 2020 when the current CoMSA CoC will be discontinued.

Four essential processes to be completed

In order for RE/RM practitioners in the three practice areas to complete the transition to the 'new qualifications' and be registered on the appropriate level of the 10-level NQF, the QCTO, in collaboration with the MQA as DQP and AQP, CoMSA, and the relevant PAs, needs to complete the following four essential processes.

1. Approved DQP develops qualification

a) An occupational profile describing the occupation (occupational descriptor) and the tasks, practical skills, and work experience must be developed. Qualifications must be 'fit for purpose' and reflect the requirements of the SAM&MS. Occupational qualifications must reflect three forms of learning, including a minimum of 20% of the credits for knowledge and theory, a minimum of 20% for practical skills, and the balance allocated to the *'appropriate needs of the particular occupation'* (Mining Qualification Authority, 2016)

b) A planned curriculum that includes the specifications for the knowledge, practical skills, and work experience modules, and the work experience record must be developed. An external assessment specification must be developed for the respective curriculum

c) The learning curriculum, which includes the sequence of learning, the learning processes and methods, and the formative assessment criteria must be developed

d) The development of learning material comprising facilitator guides, learning resources, learning tools, presentation material, lesson plans, and assessment tools must be completed.

2. Establish Assessment Quality Partner (AQP)

Coupled with the relevant MHSA regulations and the specific reference in Chapter 17 to the provisions in respect of the role, functions, and responsibilities. the MQA is ideally positioned to be appointed as the AQP for the proposed new

occupational qualifications. Training providers are required to be accredited through an AQP and registered with the QCTO. The QCTO is to perform a 'light touch' accreditation of training providers, assessing on key points in the learning process but not the entire process (Mining Qualification Authority, 2016). The assessment process will address four areas: namely the written assessment, evaluation of practical skills, evaluation of projects or assignments, and evaluation of job performance. Such assessments will address the knowledge, skills, and work experience components of a qualification.

3. Enabling delivery

a) It is intended that the delivery strategy for the new occupational qualifications be discussed in a workshop with the providers in order to map the proposed curriculum to the content of the current CoMSA CoCs to ensure that the curriculum is relevant and updated

b) Guidelines for the development of the new learning material must be developed in this forum

c) The accreditation of registered providers will require cooperation between the MQA and the relevant PAs, subject to the guidance of the QCTO, to ensure that this process does not delay the phasing in of the new occupational qualifications. Progress with the registration of providers is currently unsatisfactory.

4. Registration of learnerships

Learners will be able to register for the new occupational qualifated that this process may take in excess of two years to complete successfully, based on the experience of one of the PAs.

The action plan for the short to mid-term

A meeting was scheduled with the Executive of CoMSA to request the extension of the phasing out date by one year in order to facilitate the introduction of the new occupational qualifications. Concerns were raised in respect of the expeditious conclusion of the process to register qualifications and achieve all the goals set by the QCTO. Since CoMSA was sympathetic to the request, a one-year extension was granted (Mabena, 2016). This extension will provide sufficient time to develop the qualifications in a systematic, effective, and efficient manner that will meet the requirements of the SAM&MS, the MQA, the QCTO, and the relevant PAs.

The deliverables that must be met for the new suite of qualifications include the following:

1. Finalize the blueprints for the qualifications for each Exit Level Outcome (ELO):
    a. The blueprints for the MEC, Sampling, and Mine Surveying qualifications have been completed. The blueprint for the RE/RM practice area was expected to be completed by 25 May 2016 , following which it would be ready for approval and implementation (Anderson, 2016)
    b. The NQF Levels 4, 5, and 6 occupational qualifications for the Mine Survey, Mine MEC, and RE/RM qualifications must be completed and replace the current CoMSA CoCs before the 2020 deadline
    c. The envisaged NQF Level 7 occupational qualifications for the Mine Surveying practice area, leading towards eligibility to enrol for the GCC examinations must be developed and put in place with the support of the stakeholders in the SAM&MS and the DMR Commission of Examiners (Grobler, 2016)
2. Discuss these blueprints with the QCTO and obtain approval
3. Develop five sets of assessment tools, including questions and memoranda for these questions.
    a. The assessment tools, including the question papers, for the occupational qualifications in MEC, Sampling, and Mine Surveying have been completed. The assessment tools for the RE/RM qualifications were completed on 23–25 May 2016 (Anderson, 2016). This is now ready for approval and implementation
    b. A study of six models of competency evaluation identified a number of common aspects that can be developed into a comprehensive model that should be more effective than the written examination process currently favoured by some countries (Grobler, 2016). The portfolio of evidence and examination procedures for this proposed NQF Level 7 'second-stage' occupational qualification for mine surveyors must be agreed upon by the relevant stakeholders and completed
4. Moderate the assessment tools through a work session
5. Finally, agree on the assessment tools and publish an exemplar of these assessments.

Conclusions

The implication of not addressing the transformation of the current qualifications framework for mining-technical occupations in the SAM&MS would be a shortage of competent practitioners in the Mine Environmental Control (MEC), Rock Engineering (RE), and Mine Surveying disciplines (occupations) as well as other related occupations. A delay in the development of the new OBET-compliant qualifications could result in an inappropriate and unacceptable lag period between the phasing out of the CoMSA CoCs and the introduction of the new suite of OBET-compliant occupational qualifications. Such a situation may impact on individuals starting their careers now, since there would be no process available for them to obtain suitable and recognized qualifications that will underpin progression to the different occupations. This would introduce a risk at a time where vocational skills and qualifications may not be seen as a priority in the current economic downturn, but will certainly have a significant impact on the availability of competent persons who can fill the different mining-related occupations in the SAM&MS in the future.

Competency is considered to be the culmination of education, skills, knowledge, and experience that enables practitioners in the SAM&MS to interpret situations in a manner that would reduce occupational health and safety-related risks and to avoid any significant OH&S risks in the execution of their duties. The process of replacing recognized CoMSA CoCs has provided the affected occupations/practitioners with an ideal opportunity to reflect upon and rectify any issues with the current CoCs through the development of new OBET-compliant occupational qualifications. Persons entering their respective occupations/professions should henceforth be enabled through the best methods of competency development that will be recognized not only in the SAM&MS, but also by tertiary education institutions in South Africa. The concern that a gap will be created during period between the introduction of the new suite of OBET-compliant qualifications and the phasing out/replacement of the CoMSA CoCs is, fortunately, being addressed. The positive spin-off of this crisis is that the relevant 'Learned Societies' and PAs involved in the SAM&MS were forced to get involved with the development and implementation of the necessary portfolio of recognized vocational qualifications to enable, educate, and train practitioners within the SAM&MS. Despite the current economic downturn, the new envisaged range of occupational qualifications will have a positive impact on the sustainability of the various occupations and professions and ensure the continued availability of competent practitioners in these scarce skills to sustain the future of the Industry.

The extension of the deadline for the phasing out of the CoMSA CoCs has provided an essential respite for all those that make use of Competent Persons who are in possession of these well-respected and recognized industry CoCs. It is essential that the momentum gained over the past 18 months be maintained and exploited in order to establish new OBET-compliant qualifications and education providers well in advance of the new deadline. The further advantage of replacing the CoMSA CoCs with OBET-compliant qualifications registered with SAQA at the appropriate level on the NQF, in that persons may eventually be absorbed into 'mainstream' tertiary education, must not be underestimated. The new occupational qualifications will enable a system that will enhance mobility and recognition not only nationally, but also internationally. The study completed on behalf of the MQA by the University of Johannesburg on the throughput rates of the CoCs and the report by Cheadle, Thompson, and Haysom should be considered and implemented.

The new competency and regulatory model for the SAM&MS

The implementation of a New/Futures, Competency, and Regulatory Model for the SAM&MS is paramount for the sustained provision of competent practitioners for the relevant occupations and professions as proposed by the 2004 international benchmarking in respect of Regulatory Practice in other relevant countries, emulated by the Cheadle, Thompson, and Haysom report and the University of Johannesburg report on the throughput rates of certain CoCs.

The 'New Model' proposes the following transformatory interventions:

- Replacement of the relevant CoMSA CoCs as well as the relevant CoCs currently issued by the DMR with appropriate OBET-compliant qualifications registered by the relevant QC at the appropriate level of the 10-level NQF

Supported, where necessary, by an appropriate DMR-driven regulatory (Licence-to-Practice (LtP)) system

or

- Replacement of selected CoMSA CoCs as well as relevant CoCs ('the big five') issued by the DMR with registration in the appropriate category with a Statutorily Established Body inclusive of the ECSA, SACNASP, and the SAGC as the preferred competency determination mechanism (the 'New Competency and Regulatory Model for the SAM&MS'),

Supported, where necessary, by an appropriate DMR-driven regulatory (Licence-to-Practice (LtP)) System.

References

Anderson, C. 2016a. Chamber of Mines Certificates Notification No. 1, January 2016. Johannesburg.

Anderson, C. 2016b Paper for comment. (H. Grobler, interviewer). 29 April.

Beukes, M. 2016. Qualifications in relation to the Mine Environmental Control certificate and the development there of aligned to the NQF. Mine Ventilation Society of South Africa, Johannesburg.

Cheadle, Thompson, and Haysom

Department of Mineral Resources (DMR). 2011. Mine Health and Safety Act No 29 of 1996. i ,27 May 2011. Pretoria.

Grobler, H. 2013. 117 years of education for mine surveyors. Institute of Mine Surveyors of South Africa.

Grobler, H. 2016. Can an examination guarantee competency? A critical review of international second stage qualification models leading to a sum-mative competency assessment. *Proceedings of the International Society of Mine Surveyors Conference 2016*, Brisbane. International Society of Mine Surveyors.

Lucas, J. 2016. Concerns regarding the definition of a competent person in terms of Regulation 22.14.1(8) of the Mine Health and Safety Act, Act 29 of 1996. South African National Institute of Rock Engineering. https://www.sanire.co.za/component/docman/cat_view/106-key-documents?Itemid=230

Mabena, V. 2016. Phasing out period of the Chamber of Mines certificates. Chamber of Mines of South Africa, Johannesburg.

Mining Qualifications Authority. 2016. The Occupational Qualification Framework. From curriculum to implementation. *Presentation at a work session with the Department of Mineral Resources*. ◆

http://dx.doi.org/10.17159/2411-9717/2017/v117n8a11

The role of pulp potential and the sulphidization technique in the recovery of sulphide and oxide copper minerals from a complex ore

by M. Kalichini*‡, K.C. Corin*, C.T. O'Connor*, and S. Simukanga†

Synopsis

Kansanshi copper mine is situated in the northwestern province of Zambia. Weathering has given rise to a vertically zoned profile comprising leached, refractory, oxide, mixed, and hypogene sulphide mineralization. As a result of the mineral variations, the processing plant treats three distinct ore types, *viz.* oxide, sulphide, and mixed. The objective of this study was to investigate the floatability of a complex Kansanshi mixed copper ore comprising sulphide and oxide minerals, with a view to achieving an optimal flotation performance in the treatment of the Kansanshi orebody, with a special focus on the sulphidization process. This required an in-depth analysis of the mineralogy of the feed as well as tailings samples after different flotation processes involving a range of reagent types and dosage procedures. Controlled potential sulphidization (CPS) has been adopted over slug sulphidization as the industry standard for the recovery of oxide copper minerals through flotation. Two potential ranges were investigated in this study; –300 to –400 mV and –400 to –500 mV. Optimum flotation performance was observed in the potential range of –300 to –400 mV and a NaHS:SIBX ratio of 7:1 during CPS. CPS was also found to be economically superior to slug addition.

Keywords
sulphidization, copper oxide minerals, flotation.

Introduction

Kansanshi copper mine is situated in the northwestern province of Zambia. Unlike the stratiform deposits common to the Zambian Copperbelt, mineralization in the Kansanshi deposit occurs in quartz-carbonate veins, with the lowest exposed rock unit being the basal limestone comprising albite ($NaAlSi_3O_8$), dolomite ($CaMg(CO_3)_2$), minor muscovite ($KAl_2(Si_3Al)O_{10}(OH,F)_2$), chlorite, and dispersed sulphides (Speiser, Hein, and Porada, 1995; Broughton, Hitzman, and Stephens, 2002). While the Copperbelt ores are enriched in cobalt (Selley *et al.*, 2005), the Kansanshi deposit contains miniscule amounts of cobalt – less than 50 ppm (Broughton, Hitzman, and Stephens, 2002).

Copper oxide minerals form as a result of supergene processes that occur when copper sulphide minerals are exposed to the effects of weathering (Reich *et al.*, 2009) and encompass a series of defined assemblages that reflect a variable pH, oxidizing geochemical environment, known as the oxide zone, in which the source rock, host rock mineralogy, and iron-copper sulphide mineral abundance, among other factors, determined which oxide mineral formed (Chavez, 2000). Broughton, Hitzman, and Stephens (2002) surmised that in the Kansanshi deposit, weathering has given rise to a vertically zoned profile comprising leached, refractory, oxide, mixed, and hypogene sulphide mineralization, with the thickness of the various mineraliation facies being dependent on vein abundance, the quantity of acid-forming sulphides, and the stratigraphic level in relation to carbonate-bearing lithologies. The ore deposit contains both primary and secondary copper minerals and is therefore classed into three distinct types, *viz.* sulphide, oxide, and mixed. The mixed ore contains oxide, supergene oxide, and hypogene sulphide copper species, with the greater part of the deposit being made up of sulphide and mixed ores. The oxide ore has a much higher copper grade than the mixed and sulphide ores but contributes less to the resource (Broughton Hitzman, and Stephens, 2002).

In the last couple of decades, research in this area has focused on the need for a better understanding of the mineralogy of oxide ores being treated (O'Meara, 1961; Lee, Nagaraj, and Coe, 1998; Lee *et al.*, 2009), as this gives an indication of mineral associations, inclusions, liberation, as well as gangue mineralogy, all of which have profound effects on flotation. When oxide copper minerals are hosted in a matrix of acid-consuming gangue such as calcite, acid leaching becomes an uneconomic processing option and froth flotation is the preferred process. Where the oxides are chemically well defined, as in the case of malachite, flotation is relatively easy (Phetla and Muzenda, 2010; Lee, Nagaraj, and

* *University of Cape Town, South Africa.*

† *University of Zambia, Lusaka, Zambia.*

‡ *First Quantum Minerals Ltd, Kansanshi Mine, Solwezi, Zambia.*

 ISSN 2225-6253. Paper received Dec. 2016; revised paper received Feb. 2017.

Coe, 1998; Lee *et al.*, 2009; Hope, Woods, and Parker, 2010; Hope *et al.*, 2012). This is not the case with chrysocolla, however, because of its amorphous nature (McKeown, 1994; Hope *et al.*, 2012).

Sulphidization as a method of promoting the recovery of oxidized ores was patented in 1905 (Schwarz, 1905) and has since been developed and adapted as the preferred pretreatment method prior to the flotation of oxide and mixed copper ores containing both oxides and sulphides. The reagents used in this technique of activating base metal oxides are alkali sulphides (Soto and Laskowski, 1973) such as sodium sulphide (Na_2S) and sodium hydrosulphide (NaHS). Slug sulphidization, in which the sulphidizing agent is added to the pulp in a single slug dose, has been investigated (Jones and Woodcock, 1979; Quast *et al.*, 2005) but is generally not preferred because of the difficulty in controlling the pulp potential, thus leading to poor mineral recoveries due either to under-sulphidizing or depression of minerals due to over-sulphidizing. Controlled potential sulphidiation (CPS) has been applied in numerous operations around the world, including Zambia (Chabuka and Witika, 2001; Wills and Napier-Munn, 2006), the Democratic Republic of Congo (Ferron and Manu, 1994) and China (Wenbin, 1993).

Generally, CPS gives better results than slug sulphidization in laboratory studies. These results are, however, difficult to reproduce at plant scale. *'...The main drawback of CPS is that the optimum dose of the sulphidising agent is highly dependent on the time of conditioning, procedures of mixing and other variables, leading usually to poor reproducibility in a plant situation.'* (Lee *et al.*, 2009). The change in the nature of the feed also has an effect on CPS (Jones and Woodcock, 1979). Nagaraj and Gorken (1991) suggested that the use of an on-stream analyser could eliminate the uncertainty in dosing NaHS and possibly minimize the necessity of changing the collector dosage. A wide range of potentials have been proposed as 'optimum' in the CPS of malachite-rich ores, *viz.* –300 to –380 (E_S) mV (Feron and Manu, 1994), –500 (E_S) mV (Quast *et al.*, 2005), and +50 (E_h) mV or +250 (E_h) mV, depending on the concentration of the sulphidizing agent (Soto and Laskowski, 1973), where E_h is the oxidation-reduction potential as measured by a platinum electrode, while E_S is the potential value of an ion-selective electrode such as Ag/AgCl. The potential has also been shown to be dependent on the concentration of the sulphidizer (Soto and Laskowski, 1973), the nature of the sulphidizing agent used (Quast *et al.*, 2005), and the overall pulp chemical conditions (Feron and Manu, 1994).

The objective of this study was to investigate the floatability of a complex Kansanshi mixed copper ore comprising sulphide and oxide minerals with a view to achieving an optimal flotation performance in the treatment of the Kansanshi orebody. This required an in-depth analysis of the mineralogy of the feed, as well as tailings samples after different flotation processes using a range of reagent types and dosage procedures. The focus on the mineralogical study of tailings rather than concentrate was to identify those minerals that did not respond favourably to the various flotation procedures used. This also addressed the question regarding the relative roles of the sulphidizer in contributing either to the flotation of possibly tarnished chalcopyrite particles or to the flotation of oxides such as chrysocolla which are associated with chalcopyrite.

Experimental methods

A high-grade sample of mixed ore was obtained by belt-cut at Kansanshi. The sample assayed 1.17% Cu. Mineralogical analysis was performed using a LEO SEM-based QEMSCAN QS18 platform equipped with two Bruker 4010 SDD detectors for all analyses.

A 1% (w/v) sodium isobutyl xanthate, SIBX, collector stock solution was made up to be dosed as required for each test. The frother, DOW200, was used as provided. A 10% (w/v) stock solution of sulphidizing agent, NaHS, was made up to be dosed as required for each test.

An Eriez Magnetics® MASCLAB belt-driven stainless steel laboratory-scale rod mill was used for all milling in the test work. The mill had an internal diameter of 200 mm and a length of 297 mm, and was charged with 20 mild steel rods of three diameters, *viz.* six 16 mm, eight 20 mm, and six

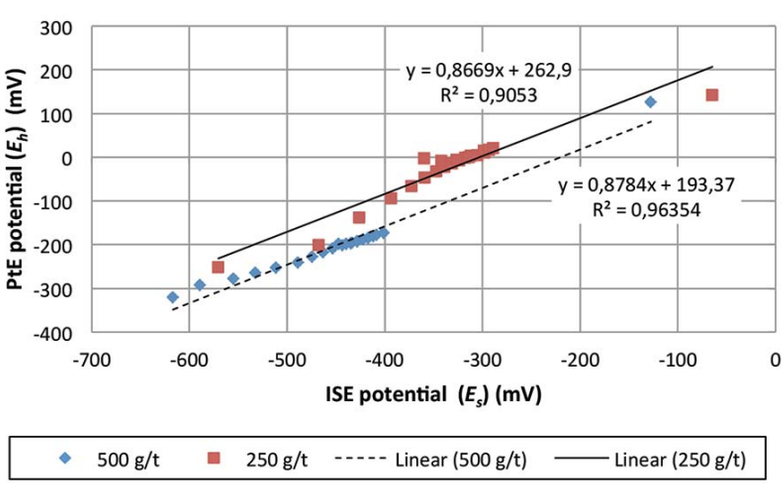

Figure 1—Relationship between E_h and E_s

25 mm rods. All flotation tests were carried out in triplicate in a 3 L Barker flotation cell. The cell is made of clear Perspex to enable visual control of froth depth and is fitted with a top-driven variable speed impeller. Flotation was carried out at an impeller speed of 1500 r/min and air flow rate of 7 L/s. Various electrode systems were used to monitor the pulp chemistry during sulphidization. A YSI 556 MPS multi-probe system was used to measure and log the temperature, pH, dissolved oxygen (DO), and redox potential (*vs* SHE) (E_h) of the system, and the sulphidization potential, E_S, was measured using a HANNA silver/silver-chloride ion-selective electrode (ISE) and HANNA HI 8424 meter. The main difference between the two meters is that the YSI (Pt) is capable of data logging, whereas the HANNA (Ag/AgCl) system is not. The use of the two pulp potential probes was aimed at determining the relationship, if any, between E_h and E_S. E_h and E_S potentials of continuously stirred LQ ore were monitored after slug addition of 250 g/t and 500 g/t of NaHS. Figure 1 shows the linear relationship between the two expressions within defined potential ranges; –300 to –400 mV and –400 to –500 mV. Since the YSI (Pt) electrode showed more consistent readings as well as the ability to measure more than one parameter, this electrode was used throughout the test work.

A grind size of 80% passing 150 µm was chosen to replicate site conditions. Bearing in mind that this ore contained both sulphide and oxide copper minerals, the flotation procedures developed focused on optimizing firstly the sulphide mineral recovery and then the oxide mineral recovery by investigating CPS. A schematic of the flotation procedures is given in Figure 2. Sulphide mineral recovery tests were conducted over 10 minutes, during which four concentrates were collected. After determining the dosage and time required for optimum sulphide mineral recovery, two different sulphidization techniques were investigated. The first set of sulphidization tests used slug sulphidization. In the case of CPS, the same initial procedure was followed. However, at the point of NaHS addition, three sulphidization stages were added to the flotation procedure and two potential ranges were investigated. The NaHS dosage was determined by the potential range that was targeted namely –300 to –400 mV or –400 to –500 mV. The total NaHS dosages required throughout the tests were 219 g/t and 397 g/t respectively. The conditioning time for each NaHS addition was 3 minutes. Three NaHS:SIBX ratios were investigated within each sulphidization stage, *viz.* 20:1, 10:1, and 7:1. The conditioning time after each SIBX addition was 2 minutes. The third, fourth, and fifth concentrates were collected for 3 minutes each, during which time the potential may have increased, requiring further NaHS addition in the second and third sulphidization stages.

Results

Mineralogy of the ore

The bulk mineralogy of the ore as determined by QEMSCAN is given in Table I. The ore contained both sulphide and oxide copper minerals. The two most abundant copper minerals were chrysocolla (3.8 wt%) and chalcopyrite (1.0 wt%). The major gangue minerals in the ore were calcite (29.1 wt%), plagioclase feldspar (23.8 wt%), and quartz (16.4 wt%).

Table II shows the copper deportment in the ore. 63.1% of the copper reported as chrysocolla, 22.2% as chalcopyrite, 1.5% as cuprite, and 2.9 % as malachite/azurite. The focus of the study was therefore on chalcopyrite and chrysocolla because they were the two most abundant copper minerals.

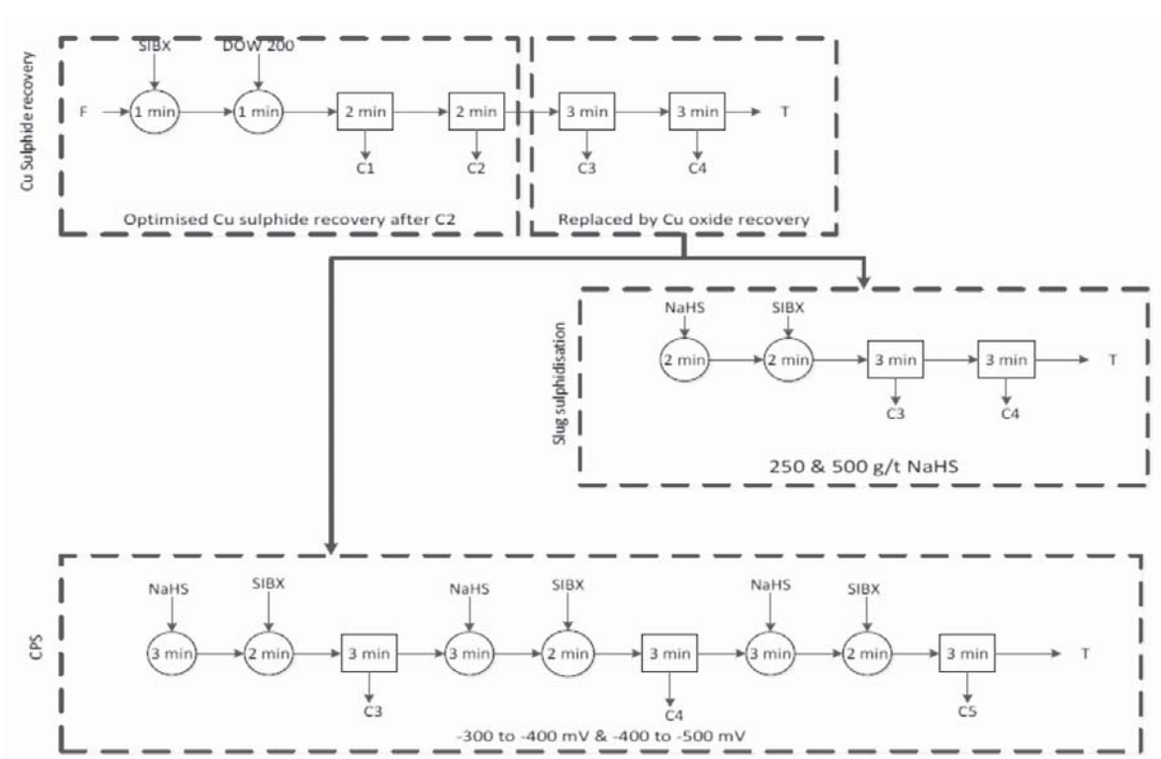

Figure 2—Schematic of flotation procedures

Table I

Bulk mineralogy of the mixed ore

Mineral	Average content (wt%)
Pyrite	1.0
Pyrrhotite	0.7
Chalcopyrite	1.0
Bornite	>0.1
Covellite	>0.1
Other sulphides	0.1
Cuprite	>0.1
Malachite/azurite	0.1
Chrysocolla	3.8
Amphibole	3.8
Mica	9.2
Kaolinite	1.7
Plagioclase feldspar	23.8
Quartz	16.4
Calcite	29.1
Fe-Ti minerals	1.1
Limonite	6.7
Others	1.7

Table II

Copper deportment

Mineral	Cu deportment (%)
Chalcopyrite	22.2
Bornite	0.6
Chalcocite/digenite	0.2
Covellite	0.4
Cuprite	1.5
Malachite/azurite	2.9
Chrysocolla	63.1
Mica	0.1
Kaolinite	5.6
Plagioclase feldspar	0.1
Quartz	0.4
Limonite	3.2

Table III

Liberation criteria used in mineralogical analysis

Criterion	Area percentage mineral exposed
Liberated	≥ 90%
Middlings	90–30%
Locked	≤ 30%

The liberations of chalcopyrite and chrysocolla were determined using QEMSCAN. Table III shows the definitions of liberation used.

Figure 3 shows the extent of liberation of chalcopyrite and chrysocolla. About 29.8% of the chrysocolla (1.1% of the 3.8% in the ore) and 51.5% of the chalcopyrite (0.5% out of the 1.0% in the ore) were fully liberated. Association data indicated that the chalcopyrite was mostly associated with chrysocolla, *viz.* 42.9% of the chalcopyrite was associated with chrysocolla and 3.9% with malachite. Most of the chrysocolla was associated with limonite, *viz.* 39.4%. 1.26% of the chrysocolla was associated with malachite and 4.0% with chalcopyrite.

Batch flotation

Tests using SIBX

Initial tests were conducted to optimize chalcopyrite and secondary copper sulphide mineral recovery using SIBX. Collector dosages of 20 g/t, 30 g/t, and 50 g/t were investigated. Figure 4 shows the grade-recovery results for these tests. Both Cu recovery and grade increased with an increase in collector dosage from 20 g/t to 30 g/t, but decreased when the dosage was increased to 50 g/t. 30 g/t SIBX gave the highest Cu recovery (24.7%) at a grade of 14.5% and was thus selected as the best dosage from the three values tested for sulphide mineral recovery. The tailings from the 30 g/t SIBX test were subjected to mineralogical analysis using QEMSCAN. Table IV shows that 5.8% of the copper that was not recovered was chalcopyrite and 1.2% was malachite, but the bulk of the copper in the tailings was hosted in chrysocolla, *viz.* 78.8%.

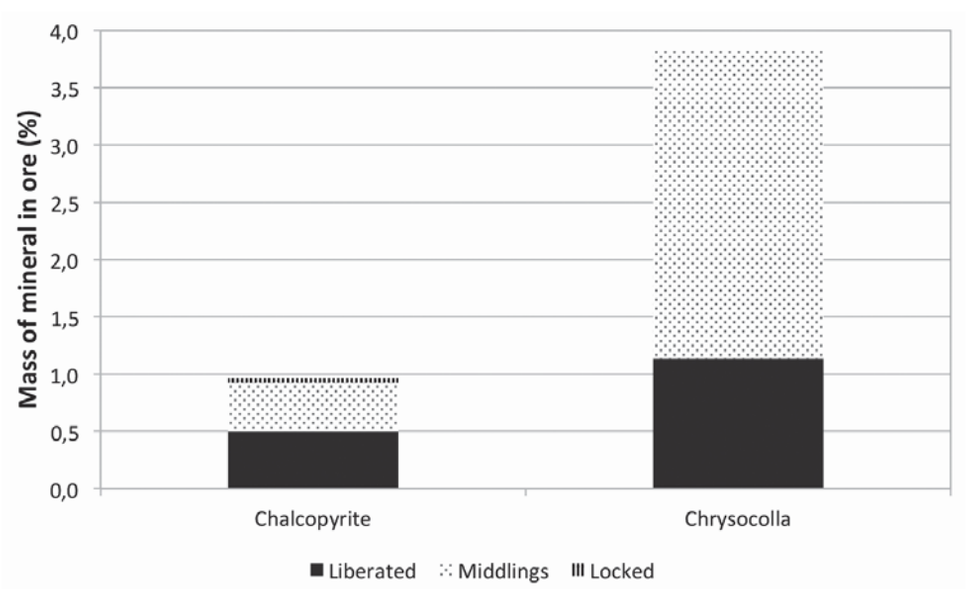

Figure 3—Chalcopyrite and chrysocolla liberation

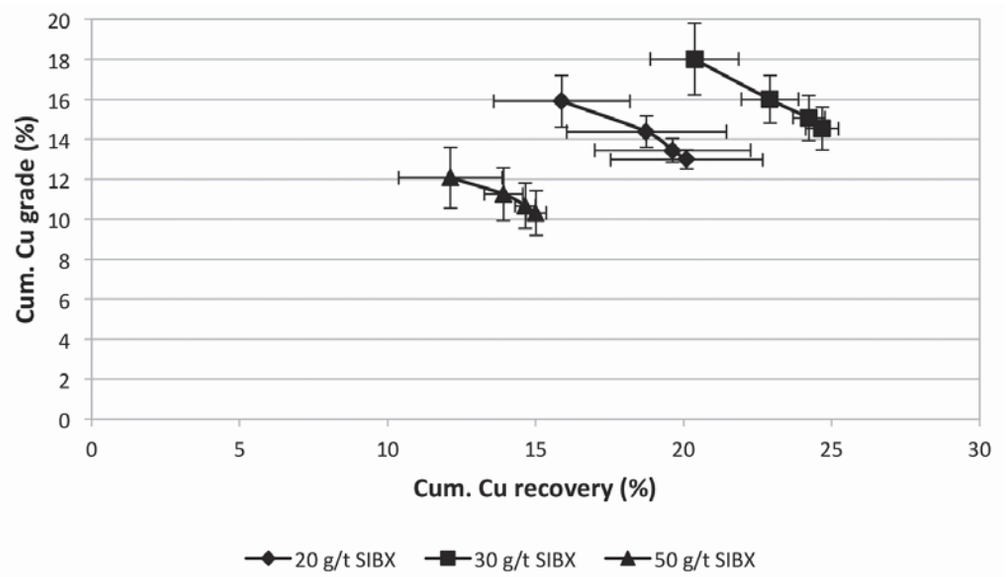

Figure 4—Cu grade *versus* recovery for flotation of mixed ore with 20 g/t, 30 g/t, and 50 g/t SIBX

Table IV

Copper deportment of tailings after flotation with 30 g/t SIBX

Mineral	Cu deportment (%)
Chalcopyrite	5.8
Bornite	0.3
Chalcocite/digenite	>0.1
Covellite	0.2
Cuprite	1.1
Malachite/azurite	1.3
Chrysocolla	78.8
Mica	0.1
Kaolinite	8.6
Plagioclase feldspar	>0.1
Quartz	>0.1
Limonite	3.8

Effect of adding NaHS

It can be seen from Figure 5 that introducing NaHS into the pulp, regardless of whether the reagent was added using the slug or CPS addition technique, led to increased solids and water recovery. This phenomenon was also observed by Becker *et al.* (2014), who noted that the addition of NaHS in the absence of a hydroxamate collector increased water recovery when compared to a test in which only SIBX was added. This appears to indicate that the NaHS also plays a froth stabilizing role. For the slug sulphidization procedure in particular, increasing the NaHS dosage from 250 g/t to 500 g/t resulted in a 41% increase in water recovery from 237 g to 333 g with a negligible increase in solids recovery (31.13 g to 31.52 g). Using the CPS procedure resulted in an even greater increase in water recovery compared to tests without NaHS or using slug addition. The solids recoveries were almost twice those with only SIBX, and greater than those in

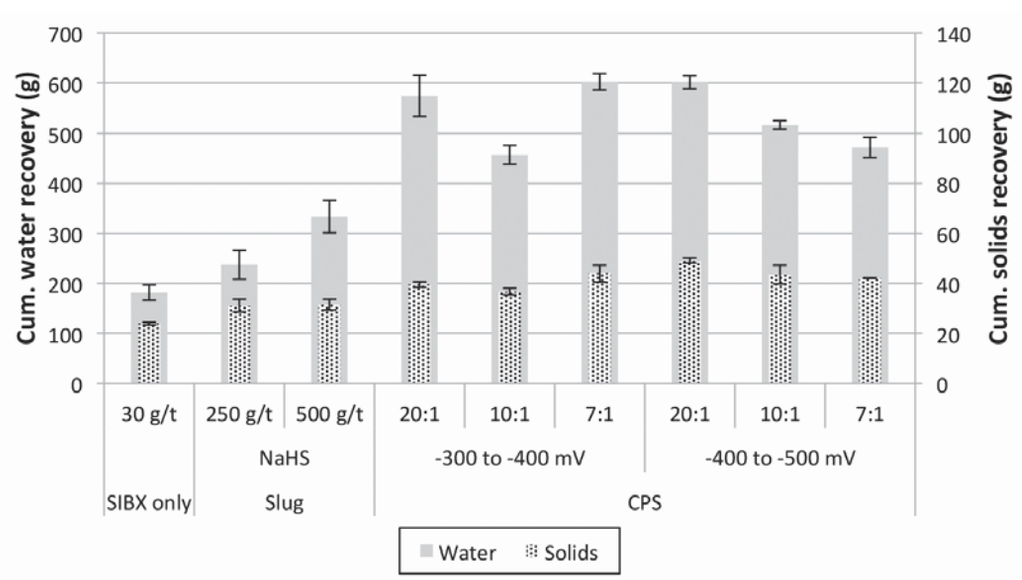

Figure 5—Cumulative solids and water recoveries for the flotation of mixed ore with 30 g/t SIBX, followed by slug sulphidization with 250 g/t and 500 g/t NaHS and CPS at –300 to –400 mV and –400 to –500 mV using NaHS:SIBX ratios of 20:1, 10:1, and 7:1

the case of slug addition. It is important to note that in the case of CPS when adding NaHS to control the potential in the range of –300 to –400mV, the total NaHS addition was 219 g/t, but in the case of the higher potential range of –400 to –500mV it was 397 g/t. It should be noted that a fifth concentrate was included in these tests, which may induce higher solids and water recoveries.

The increase in solids recovery after the introduction of NaHS, whether by slug addition or CPS, can be attributed partly to the recovery of oxide minerals that were not recovered during flotation with SIBX only. It is noteworthy that the increase was greater in the case of CPS than for slug addition. The grade-recovery trends are summarized in Figure 6. In the case of slug addition, Cu recovery increased with increasing NaHS addition. The same observation has been made in the case of slug sulphidization of oxidized lead-zinc-silver material with Na_2S (Jones and Woodcock, 1979) and malachite with calcium polysulphide (Quast *et al.*, 2005). CPS addition of NaHS also increased Cu recovery when compared to the base case (30 g/t SIBX), although the grades were lower, thus illustrating that NaHS addition using the CPS method increased the mass pull. Clearly, NaHS plays a role in enhancing the recovery of the oxides of copper. In fact, the average Cu recovery when NaHS was added did not vary significantly when comparing slug and CPS addition procedures. In both cases the average recovery was in the region of 30%.

In the case of CPS, the highest solids recoveries were paired with the highest water recoveries for both potential ranges. CPS addition of NaHS also resulted in a significant increase in Cu recovery from the 22.9% observed for the base case (30 g/t SIBX) to an average of about 30%. However, CPS treatment resulted in a general decrease in grade, from approximately 15% to 10%, compared to slug sulphidization. This indicates a greater but unselective mass pull of solids into the concentrate, thus reducing the copper grade. This is an interesting result, since the highest water recoveries were also observed in CPS. This relationship between solids and water recovery is typical of a greater degree of entrainment of non-floatable minerals. Clearly, the CPS method results in greater true flotation of oxide minerals, but there is also an increased recovery of gangue minerals due to the higher water recovery, which is indicative of a greater froth stability.

The tailings after slug sulphidization treatment with 500 g/t NaHS were subjected to mineralogical analysis, and the copper deportment is illustrated in Table V. Two important observations arise. Firstly, comparison of the above results to those shown in Table V indicates that all of the chalcopyrite that had not been recovered in the pre-sulphidization stage was recovered after sulphidization. This is consistent with the recoveries of 22.9% without sulphidization (loss of 5.8% to the tailings) and 30% recovery after sulphidization with essentially no chalcopyrite reporting to the tailings. Since the chalcopyrite in the feed to sulphidiation had been shown to be mostly liberated, it is possible that some of it had become tarnished due to *in situ* weathering or during storage and

Table V

Copper deportment in tailings after slug sulphidization with 500 g/t NaHS

Mineral	Cu deportment (%)
Chalcopyrite	0.80
Bornite	0.06
Chalcocite/digenite	>0.1
Covellite	0.10
Cuprite	0.09
Malachite/dzurite	0.63
Chrysocolla	84.79
Mica	0.14
Kaolinite	9.15
Plagioclase feldspar	>0.1
Quartz	>0.1
Limonite	4.18

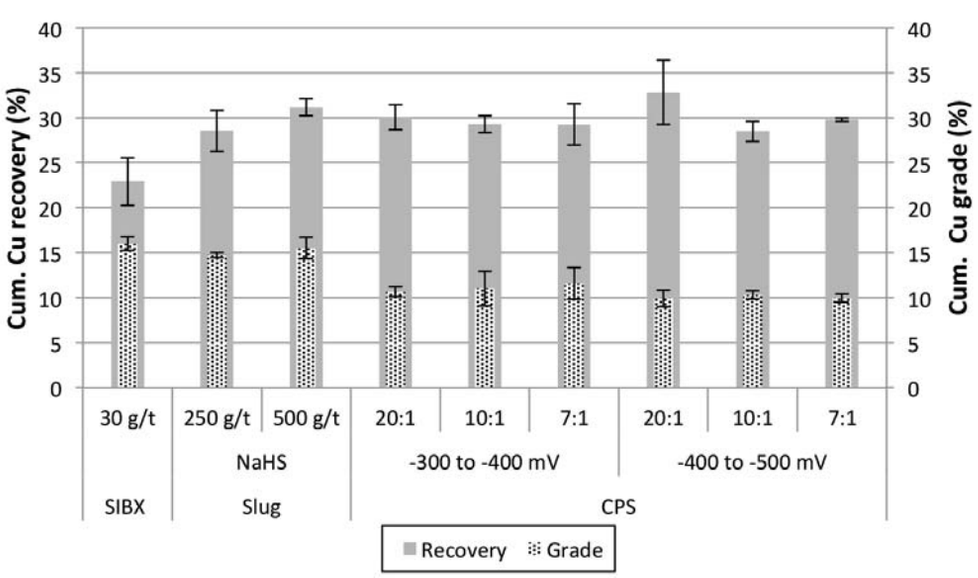

Figure 6—Cumulative grade-recovery trends for the sulphidization-flotation of mixed ore with 30 g/t SIBX, followed by slug sulphidization with 250 g/t and 500 g/t NaHS and CPS at potential ranges of –300 to –400 mV and –400 to –500 mV using NaHS:SIBX ratios of 20:1, 10:1, and 7:1

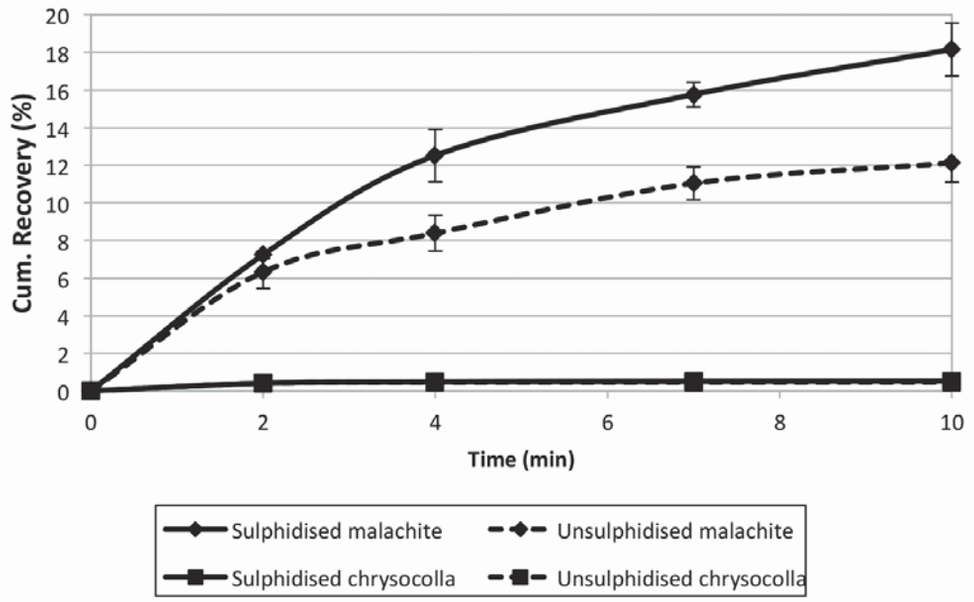

Figure 7—Recovery-time plots for the microflotation of pure malachite and chrysocolla

therefore required sulphidization. Sulphidization followed by xanthate flotation has been shown to recover tarnished chalcopyrite (Clark *et al.*, 2000) and other sulphide minerals such as pentlandite (Newell and Bradshaw, 2007). Secondly, all the other oxide copper minerals except chrysocolla responded positively to the NaHS/xanthate flotation treatment. These findings are consistent with observations made by Kottgen and Bastin (2009). In this context, the floatability of a relatively pure sample of a typical copper oxide mineral before and after sulphidization is clearly of interest. Microflotation tests with NaHS and SIBX (Figure 7) showed clearly that malachite, which is a typical example of such a mineral, was recovered after NaHS/xanthate (sulphidized) treatment but that chrysocolla did not respond positively to such treatment. Unsulphidized refers to tests done with only xanthate addition. Clearly, any chrysocolla that reported to the concentrate after sulphidization would do so due to its association with chalcopyrite, and not due to true flotation.

Conclusion

The objective of this study was to investigate the floatability of a complex Kansanshi mixed copper ore comprising sulphide and oxide minerals with a view to achieving maximum copper recoveries and grades. The major focus of the study was on the use of two different methods of sulphidization, *viz.* slug addition and controlled potential sulphidization (CPS). In all cases the addition of NaHS, irrespective of the addition procedure used, resulted in higher recoveries of Cu. Slug addition at 500 g/t resulted in a slightly higher Cu recoveries than at 250 g/t, but in both cases the grades were similar to that with only SIBX as collector. The CPS method resulted in an increase in Cu recovery but a decrease in grade compared to slug sulphidization. Mineralogical analysis of the tailings samples obtained after sulphidization showed no residual chalcopyrite, and that a significant amount of oxide minerals had been collected. Microflotation studies showed that sulphidization favoured the recovery of malachite but not of chrysocolla. This suggests that the increase in copper recovery after sulphidization was a result of the flotation of chalcopyrite that had not responded to xanthate treatment, due possibly to some degree of tarnishing.

Acknowledgements

The assistance of the Julian Baring Scholarship Fund (JBSF) and First Quantum Minerals Ltd. (FQML) is acknowledged with thanks.

References

Becker, M., Harris, Wiese, J., and Ramonotsi, M. 2014. Investigation into the mineralogy and flotation performance of oxidised PGM ore. *Minerals Engineering*, vol. 65. pp. 24–32.

Broughton, D.W., Hitzman, M.A., and Stephens, A.J. 2002. Exploration history and geology of the Kansanshi Cu (-Au) deposit, Zambia. *Integrated Methods for Disccovery: Global Exploration in the Twenty First Century*. 1st edn. Goldfarb, R. and Nielsen, R. (eds). *Special Publication* 9. Society of Economic Geologists, Boulder, CO. pp. 141–153.

Buswell, A.M., Bradshaw, D.J., Harris, P.J., and Ekmekci, Z. 2002. The use of electrochemical measurements in the flotation of a platinum group minerals (PGM) bearing ore. *Minerals Engineering*, vol. 15. pp. 395–404.

Chabuka, C. and Witika, L.K. 2001. Optimisation of the Baluba East ore treatment. *African Journal of Science and Technology*, vol. 1, no. 4. pp. 36–42.

Chavez Jr, W.X. 2000. Supergene oxidation of copper deposits: zoning and distribution of copper oxide minerals. *Society of Economic Geologists Newsletter*, vol. 41, no. 1. pp. 10–21.

Clark, D.W., Newell, A.J.H., Chilman, G.F., and Capps, P.G. 2000. Improving flotation recovery of copper sulphides by nitrogen gas and sulphidisation conditioning. *Minerals Engineering*, vol. 13, no. 12. pp. 1197–1206.

Ferron, C.J. and Manu, N.N. 1994. Recovery of copper oxide minerals by sulphidisation flotation. *Reagents for Better Metallurgy*. Mulukutla, P.S. (ed.). Society for Mining, Metallurgy & Exploration, Littleton, CO. pp. 156–164.

Hope, G.A., Woods, R., and Parker, G.K. 2010. Interaction of hydroxamates with malachite. *ECS Transactions*, vol. 28, no. 6. pp. 27–37.

Hope, G.A., Buckley, A.N., Parker, G.K., Numprasanthai, A., Woods, R., and McLean, J. 2012. The interaction of n-octanohydroxamate with chrysocolla and oxide copper surfaces. *Minerals Engineering*, vol. 36-38. pp. 2–11

Jones, M.H. and Woodcock, J.T. 1979. Control of laboratory sulphidization with a sulphide ion-selective electrode before flotation of oxidised lead-zinc-silver dump material. *International Journal of Mineral Processing*, vol. 6. pp. 17–30.

Kottgen, A. and Bastin, D. 2009. Mineralogical analysis of the "Red Ore" flotation circuit - Kansanshi. University of Liege. http://hdl.handle.net/2268/155492

Lee, J.S., Nagaraj, D.R., and Coe, J.E. 1998. Practical aspects of oxide copper recovery with alkyl hydroxamates. *Minerals Engineering*, vol. 11, no. 10. pp. 929–939.

Lee, K., Archibald, D., McLean, J., and Reuter, M.A. 2009. Flotation of mixed copper oxide and sulphide minerals with xanthate and hydroxamate collectors. *Minerals Engineering*, vol. 22, no. 4. pp. 395–401.

McKeown, D.A. X-ray absorption spectroscopic study of copper in an amorphous coppe rsilicate: chrysocolla. *Journal of Non-Crystalline Solids*, vol. 180, no. 1. pp. 1–10.

Nagaraj, D.R. and Gorken, A. 1991. Potential-controlled flotation of and depression of copper sulphides and oxides using hydrosulphide in non-xanthate systems. *Canadian Metallurgical Quarterly*, vol. 30, no. 2. pp. 79–86.

Newell, A.J.H. and Bradshaw, D.J. 2007. The development of a sulfidisation technique to restore the flotation of oxidised pentlandite. *Minerals Engineering*, vol. 20. pp. 1039–1046. DOI:10.1016/j.mineng.2007.04.012

O'Meara, A. 1961. A mineralogical approach to Copperbelt metallurgical problems. *Proceedings of the 7th Commonwealth Mining and Metallurgical Congress*, Kitwe, Zambia. Watts, W. (ed.), Institution of Mining and Metallurgy, London. pp. 333–383.

Phetla, T.P. and Muzenda, E. 2010. A multistage sulphidisation flotation procedure for a low grade malachite copper ore. *International Journal of Chemical, Molecular, Nuclear, Materials and Metallurgical Engineering*, vol. 4, no. 9. pp. 580–586.

Quast, K.B., Tsatouhas, G., Wong, K.Y., and Newell, R. 2005. The use of polysulfide as an alternative sulfidising reagent for the CPS flotation of oxide copper ores. *Proceedings of the Centenary of Flotation Symposium*, Brisbane, Australia, 6-9 June 2005. Johnson, G.J. (ed.). Australasian Institute of Mining and Metallurgy, Carlton, Victoria. pp. 1027–1032.

Reich, M., Palacios, C., Vargas, G., Luo, S., Cameron, E.M., Leybourne, M.I., and You, C. 2009. Supergene enrichment of copper deposits since the onset of modern hyperaridity in the Atacama Desert, Chile. *Mineralium Deposita*, vol. 44. pp. 497–504.

Schwarz, A. 1905. Process of concentrating ores. US Patent US807506.

Selley, D., Broughton, D., Scott, R., Hitzman, M., Bull, S., Large, R., and Barra, F. 2005. A new look at the geology of the Zambian Copperbelt. *Society of Economic Geologists, 100th Anniversary Volume*. Hedenquist, J.W., Thompson, J.F.H., Goldfarb, R.J., and Richards, J.P. (eds). pp. 965–1000.

Soto, H. and Laskowski, J.S. 1973. Redox conditions in the flotation of malachite with sulphidizing agent. *Transactions of the Institution of Mining and Metallurgy Section C- Mineral Processing and Extractive Metallurgy*, vol. 82. pp. C153–C157.

Speiser, A., Hein, U.E., and Porada, H. 1995. The Kansanshi Copper Mine (Solwezi area, northwestern Zambia): Geology, wall-rock alteration and fluid inclusions. Mineral Deposits; from their Origin to their Environmental Impacts. *Proceedings of the 3rd, Biennial Meeting: Society for Geology Applied to Mineral Deposits*. Pasava, J., Kribek, B., and Zak, K. (eds), Society for Geology Applied to Mineral Deposits (SGA), Prague. pp. 389–392.

Wenbin, Z. 1993. Thirty-year plant practice of sulphidisation - flotation of copper oxidised ores. *Proceedings of the XVIII International Mineral Processing Congress*, Sydney, Australia. Australasian Institute of Mining and Metallurgy, Melbourne. pp. 23–28.

Wills, B.A. and Napier-Munn, T. 2006. Wills' Mineral Processing Technology. 7th edn. Elsevier, Oxford. ◆

http://dx.doi.org/10.17159/2411-9717/2017/v117n8a12

Mining redesigned - innovation and technology needs for the future—a South African perspective

by M. Hermanus*

Synopsis

This paper outlines global and local developments in minerals extraction of relevance to mining companies, equipment manufacturers, and state institutions, and describes a new attempt to revitalize mining in South Africa. This initiative, Operation Mining Phakisa, arises from a multi-stakeholder process and has the potential to provide a coherent and comprehensive response to the wide range of issues impacting the sector. The South African mining sector is in a predicament as contradictions rooted in its apartheid past have come home to roost, mineral prices remain stubbornly low, and another industrial revolution affecting all industries, including mining, gets underway.

Keywords

mining, structural change, innovation, transformative technology, multi-stakeholder process.

Economic setting

In early 2016, when many commodity prices and profits were at historically low levels and there was no expectation of imminent change, mining companies began rethinking their business models at the same time as mineral-rich countries began revisiting their plans on how to better extract social value from mining. These developments followed on the heels of record returns to mining companies and massive expansion of the sector consequent to growth in Asia, especially China and other developing economies. Since mining companies appeared to have secured more than their fair share of returns, demands increased for mining to support infrastructure and industrial development. But by then the commodity cycle was well past its 2011 peak, when a decade of growth in the east and elsewhere came to an abrupt end (Schussler, 2016).

In 2016 The World Bank lowered price expectations for 37 out of the 46 commodities that it monitors. Among the important mineral commodities included in the index are oil and iron ore. According to the World Bank, compared to prices in 2014, the price of energy minerals fell by 45% in 2015 and of that metals fell by 8% on the back of slow demand in China starting in 2010 (World Bank Group, 2016). Structural changes in the Chinese economy appear to be the main reason for these falling prices, with investments in commodity-intensive sectors such as public infrastructure and heavy industry giving way to 'commodity-light' investments in services and consumption. In addition, China was turning its attention to investment outside of the country to rebuild ancient trade routes across Eastern Europe and Asia, over land and sea – the so-called 'Silk Routes'. This is an ambitious plan with interrelated objectives, such as increasing the country's trade options, enabling Chinese companies to work outside of China (since demand is slow at home), and acquiring assets along the routes in exchange for infrastructure. Of themselves, the new Silk Routes are not expected to affect commodity prices, either positively or negatively (Bloomberg, 2016).

Falling demand for minerals has led to lower levels of return and reduced interest from investors and lenders, and has brought many longstanding uncertainties and externalities associated with the business of mining into the foreground and into the public eye. These include uncertainties around energy supply, the future of fossil fuels, and the availability of water; the costing of environmental and health impacts, access to mining land and land use, and the magnitude and severity of environmental and social impacts (Bardi, 2014; Thorndahl, 2011; Marinovich, 2016; Momberg and Rich, 2015; Ernest and Young, 2015).

Exploration activity has also been affected by dwindling investor interest, with greenfield exploration dropping to 29% of total exploration globally and exploration finance dropping to 9% of 2007 levels on Canadian exchanges (PDAC, 2016). While at a global level lower energy costs staved off the closure of high-cost mines, mining companies continued to experience difficulties centred on

* *Natural Resources and Environment Unit of the CSIR (Council for Scientific and Industrial Research), South Africa.*

 ISSN 2225-6253. Paper received July 2016; revised paper received Apr. 2017.

the viability of current mining methods and the (high) full costs of mining operations. While 'lean and low-cost' is the desired state for many operators, there are limits to the adjustments that can be made by mining companies. In most countries minerals are national assets and mining companies are expected to contribute to economic and social development, over and above the usual benefits associated with extraction and the payment of royalties. In developing countries this includes the contribution which mining can make to industrial and social development.

Against the backdrop of global developments and trends, this paper reflects on how these issues and the attendant tensions are playing out in South Africa. A recent report by the Prospectors and Developers Association of Canada (PDAC *et al.*, 2015, p. 1) was forthright about the future of mining, stating bluntly that 'innovation is the key to mining survival'. This is a theme that features strongly in the deliberations which are underway in South Africa about the shape and future of gold and platinum mining in particular.

Why is innovation considered a necessity for mining?

Mining companies typically adjust to lower demand and prices by delaying expenditure, cutting operational costs, and reducing output. In an environment of structural change, mining companies are at the same time challenged to assess and adjust their operations in fundamental ways.

The necessity of innovation in mining has become a refrain across the globe. Deloitte and Ernst and Young (Deloitte Touche Tohmatsu Ltd., 2015, pp. 1-3; Ernst and Young, 2015, pp. 2-3) argued in recent reports that innovation by mining companies would be an appropriate response to low commodity prices, and would better position them to weather the prolonged downturn that is expected to follow the supercycle. Both the Prospectors and Developers Association of Canada (PDAC) and Deloitte observed that while most mining companies agreed on the need to innovate, and while many were engaged in some form of innovation, innovation programmes were generally neither strategic, consistent, nor systematic. While some programmes took in novel ways to raise productivity, for example through automation, enhanced drilling or rock-breaking systems, integrated real-time data, and savings on energy costs, most were focused on optimizing existing systems.

Surprisingly, major mining companies were found on the whole to be less competent innovators than junior miners or service and supply companies (PDAC *et al.*, 2015, pp. 2, 10-11; Deloitte *et al.*, 2016, pp. 8-13). In overview, innovation efforts were largely directed towards 'better, cheaper extraction' with smaller investments going towards innovations which are new and which bring either incremental or transformational change (PDAC *et al.*, p. 8). Yet mining companies also acknowledged that step change was required for growth and efficiency, and that more sustainable methods of generating value were required (PDAC *et al.*, 2015, p. 10).

Nonetheless, even under normal conditions levels of mining are not easily lowered as companies are inclined to continue to mine in order to maintain cash flow or employment levels (particularly when required to do so), to avoid penalties for reduced port or rail usage such as in Australia, and to stave off mine closure costs. To improve their prospects, mining companies have been advised to stay close to investment initiatives in China to benefit from potential infrastructure rollouts, to develop new strategies to reduce debt and raise finance, and to anticipate that for prices to recover, the supply of minerals would have to shrink.

Parallel developments transforming industry in general

Increasing costs and pressures on the mining sector have arisen at a particularly inauspicious time, as a fourth industrial revolution gets underway. The first industrial revolution, which started in the 19th century, entailed the use fossil fuels to power machines, which stimulated steam-powered mechanical production. The second, which got underway from the late 19th century onwards, was grounded in breakthroughs in electricity distribution, communication systems, and power generation, which accelerated mass production and trade. The third industrial revolution, which is still unfolding, started in the 1950s and involved the development of electronics, digital systems, computing power, and communication technology. This greatly enhanced the generation, processing, and sharing of information (World Economic Forum, 2016; UBS, 2016).

It is already apparent that next industrial era will be characterized by extreme automation and connectivity, involving cyber-physical systems that create wholly new capabilities for people and machines. Of relevance to the mining sector are the transformative technologies associated with this fourth industrial revolution and its potential to deepen inequality and reduce job security. Higher levels of unemployment and lower levels of job creation are anticipated, with many of the resulting jobs expected to require high levels of education and specialized study. In contrast, mining is expected to provide more employment and secure work, as it has done historically.

The main challenge of the fourth industrial revolution is whether it can contribute substantively to broad-based growth and income security (World Economic Forum, 2016). Developed countries with high levels of skills, established and flexible education systems, solid infrastructure, and well established legal systems stand to benefit. Developing countries in which low-skill labour is most abundant and in which the economy is dominated by agriculture, low-skill services, and small informal manufacturing businesses, are most at risk (UBS, 2016). This does not bode well for the prospects of developing countries in which unemployment and poverty is high. Globally, 1% of the population increasingly commands the greatest share of wealth (½ of all household wealth in 2015), and many countries, mostly developing, are already more unequal than others (World Economic Forum, 2016). Studies show that unequal societies tend to be more violent and less trustful (Wilkinson and Pickett, 2010), and mining is increasingly undertaken in these localities, with 90% of the world's major mining countries described as developing (World Bank and International Finance Corporation, 2002).

To whom and by what means the benefits of mining accrue is already a source of discontent as new-generation technological solutions become available to mining companies, and tensions between job creation and industrial

development intensify. Thus, mining countries are in need of comprehensive, well-thought-out strategies for optimizing mining and the mining value chain for development. Mining companies obviously have a strong interest in business sustainability, and given that orebodies are geographically fixed, company-level plans and priorities are likely to correspond with country-level priorities. However, the two sets of interests are not necessarily convergent or interchangeable. This is especially so as many companies are transnationals, and investor and shareholder expectations are not ultimately subordinate to national considerations.

Examples of innovation in mining

Rio Tinto offers an example of strategic and transformational innovation amongst the major mining companies with a programmes aimed at achieving 'massive' efficiency in surface bulk mining through autonomous mining, increasing efficiency in recovery by sorting waste before it arrives at processing plants, and tunnelling to access deep orebodies faster (Rio Tinto plc and Rio Tinto Ltd., n.d., 2014). The 'Mine of the Future' and other new mining systems incorporate technologies such as driverless haul trucks, autonomous rail systems, robotic mining, and autonomous drilling systems. Mining equipment manufacturers are already employing sensors that capture data from fixed and mobile equipment to avoid downtime, optimize equipment operation (including navigation), and improve safety. Systems and technologies for managing mine tailings and treating water are also in demand, while the need for energy savings and access to power has created demand for installed power generation facilities at mines (Deloitte Touche Tohmatsu, 2015., pp. 9-13, 25).

The Deloitte report of 2015 pointed out that mining companies could make, and to a certain extent are making, use of technologies that cut across sectors, and by so doing secure the future of mining. These technologies have the potential to change the face of mining, although the initial crossover gains may be difficult to achieve. They include:

- Networks. Mines share their operational data with suppliers through sensors and onboard computers on mining equipment, with the possibility of eliminating all unplanned maintenance
- Machine learning. As autonomous machines and automation takes off, the machines will be capable of improving their performance / learning. Ultimately, mines could be fully autonomous, and controlled from a central hub in which staff are located
- 3D printing of critical parts on mine sites
- Modular equipment which can be constructed closer to site
- Genomics. Advances in this field have the potential to lead to successful bio-extraction and bio-remediation technologies
- Wearables. Personal protective equipment (PPE) with embedded sensors has the potential to track fatigue, alert people to the presence of machines, and direct mine services such as water and ventilation to specific parts of a mine
- Hybrid airships. This innovation, pioneered by Lockheed Martin (Mining.com, n.d.) and companies outside of mining such as Solarship, is aimed at overcoming the problems associated with inhospitable terrain and remote sites. It could open up new ways of transporting mining equipment
- Energy alternatives and energy-aligned work cycles to both reduce costs and increase flexibility.

Cronimet Chrome Mining SA is an example of a company experimenting with a novel photovoltaic-diesel power system (Cronimet Mining, n.d.).

Beyond technology

Improving mining operations and businesses does not depend only on technological success. Capital efficiency, an expanded approach to the business of mining, leadership, and an ability to work with and accommodate stakeholders are also important. PDAC and Deloitte describe these success factors as the ability of mining companies to successfully adopt new technology, to be responsive to the changing business environment, and to be accepted as reliable social partners.

New approaches to capital efficiency are related to technological innovation, and are reflected in considerations about power generation, water treatment, the management of tailing dams, and alternative uses of mined-out land (Deloitte Touche Tohmatsu, 2015, p. 8). Also included are novel arrangements for making full or better use of the capital tied up in heavy equipment.

Different approaches to the overall mining business model have emerged. Eurasian Minerals is an example of an exploration and mining company which secures its margin through a variety of means, by combining royalties, investments in key properties, and exploration discovery (PDAC *et al.*, 2015, p. 5). As the mining business model evolves, regulators, which generally hold mining companies responsible for all the activities associated with the extraction cycle, are also challenged to revisit established approaches to regulating mines.

There is general recognition of the importance of the approach and outlook of the people leading or responsible for the key initiative of mining companies. They are required to respond to social and political complexities, growing concerns over inequality and marginalization, volatile business and operating environments, and to institutionalize innovation. Nonetheless it is apparent that although mining companies face many unique challenges, there are lessons to be learnt from other industries that have faced similar challenges to truly engage employees, and to realize gains available through networked assets and stakeholder engagement.

Also of strategic significance is the need to align company and stakeholder interests, and mining companies are advised to ensure that their social investments are consistent with their 'underlying and long-term needs'. Water, power, and technical training are cited as examples of needs that may be mutual and could lead to mutual benefits (Deloitte Touche Tohmatsu, 2015, pp. 16, 25, 28).

As the longer term outlook remains challenging, with exploration tailing off and traditional mining methods becoming less cost-efficient, mining companies will remain hard-pressed to ensure a pipeline of new projects, mine effectively, develop new ways of being profitable, and

support social objectives. The PDAC report recommends that mining companies come together in a structured way to discuss, promote, and foster innovation (PDAC *et al.*, 2015, p. 11).

Given the emphasis on transformational change for long-term success, it is possible that the mining sector will become more tiered than ever, with different needs for different classes of mining companies with different resources and capabilities.

South African mining is not immune to these trends and developments. In addition, its past and current disputes over land use, land ownership, and employment opportunities are indicative of entrenched problems. Setting worker and community engagement processes to rights and establishing respectful and mutually beneficial relationships continues to be especially challenging. These issues are explored in part in the next section of this paper.

Historical context of South African mining

The need for innovation in the mining sector present governments everywhere with significant challenges, and this is particularly evident in South Africa. While the country has a long history of mining and mining research, the sector is under pressure to adapt to new circumstances in which long-standing practices are no longer acceptable or economic.

Over the course of the 20th century, South African mining companies such as Anglo American, De Beers, Rand Mines, JCI, and Gold Fields grew to become global giants. Until well into the 1980s, these companies invested across and beyond the mining value chain. In the early years as mining grew, small engineering works and companies supplying support services were established around the gold mining industry, and local production of much of the equipment essential for deep-level mining got underway. These developments drove industrialization in South Africa (Turok, 2014; Innes, 1984). South African mining companies also supported the largest private research and development facility in the world, the Chamber of Mines Research Organisation (COMRO). COMRO was established in 1964 as the Mining Research Laboratory of the Transvaal, and was strongly supported by the gold mining sector until the mid-1980s. By 1989 COMRO's budget had shrunk considerably, and by the 1990s it was no longer associated with the Chamber of Mines. The internationalization of the South African economy and the globalization of South African mining companies undid the need for close cooperation in mining R&D in South Africa (Pogue, 2006).

COMRO's programmes built on the outcomes of *ad-hoc* research projects that were carried out from 1908 onwards into mine ventilation control, mining-induced earth tremors, and hydropower. Over time, rockburst-related research settled on three main themes: mine layouts, support units and systems, and rockburst control (Durrheim, 2010). A mechanization programme was formally initiated in 1974 and from the outset involved equipment manufacturers (Pogue and Rampa, 2006). The programme involved improving efficiencies in gold mining and focused on a suite of hydraulic technologies which included hydraulic drilling and hydraulic power systems. The ultimate aim was to establish a viable mining equipment industry that could serve South African mines. However, funding dried up before these technologies were proven.

In the final instance, the sector remained dependent on cheap labour, secured from migrant workers, and coal-based energy. But in post-apartheid South Africa, political conditions and economic conditions changed and these underpinnings have fallen away.

In the deracializing economy of today, labour is no longer as cheap as it was in the apartheid years, and the legal framework which made it possible to treat black workers as disposable no longer exists. The degrading conditions in which mineworkers laboured in South Africa and the general system which denied the humanity and dignity of black South Africans are well documented by historians, sociologists, and others (Wilson, 1972; Bundy, 1988; Innes, 1984; Platsky and Walker, 1985; Flynn, 1992; McCulloch, 2013).

In addition, energy costs are high and rising. The reasons for the relatively high cost of energy in South Africa are complex and the impacts on mining are related to the peculiarities of deep-level mining, which requires large power inputs. Coal-based power accounts for 90% of electricity supply, and the rising cost of power runs contrary to the decline in the price of coal in the global market. Rising electricity costs are due to Eskom's (the local state-owned power utility) requirements to fund new generation capacity as well as maintain its existing and ageing power stations. These costs were estimated at R340 billion in 2013, excluding borrowing costs (TIPS and Global Green Institute, 2014, p. 7). The decline of the South African currency also affected the cost of power through the cost of borrowing and the translation of coal prices into the local currency. All of these factors pointed to the likelihood of above-inflation increases for many years into the future. Based on 2009 average standard prices, the price of electricity was due to triple in 2017, affecting the operations of underground mines in particular. At this time electricity costs were expected to amount to 17% and 23% of the total costs for the extraction platinum group metals and gold respectively (Baxter, 2015). The refrigeration plants and ventilation systems required to enable work in deep mines account for a substantial portion of the power needs in these operations.

The South African mining sector has shrunk in size and value, in the face of decisions made by mining companies and developments in the local and global environment, (PWC, 2015, p. 9). During the 1990s, when the country opened up to the global economy, key mining companies listed outside of the country unbundled their investments in the mining and industrial sectors and spent less on research and development (R&D). Since then, many mining assets have not been managed with an eye to development. Policies to empower previously disadvantaged individuals and change the ownership structure of the sector took priority from 2000 onwards. Since many empowerment deals were highly leveraged, benefits to local communities or for community development were limited, and little impact has been made on the legacy of the apartheid labour market. To compound matters, the minerals and energy complex, which is the historical backbone of the South African economy and which enabled industrialization, was systematically dismantled in the period 1994 to 2015 as efforts shifted towards building a knowledge economy (Blankley and Booysens, 2010).

The minerals and energy complex of South Africa has been held up as an example of how mining escaped being an enclave activity (Kaplan, 2011). On the other hand, low levels of beneficiation of South Africa's primary mineral products such as gold, diamonds, chrome, platinum, and copper are considered, in contrast, as evidence of the enclave character of the mining sector (Turok, 2013). Notwithstanding these debates, the complex's development remains an artefact of its time, of mining conditions which needed unique technology and organisation, and of a system of racial exploitation which made such mining economically viable.

The developments and priorities of the last few decades resulted in local technology and industrialization taking a back seat in South Africa. Given the particular characteristics of the country's gold and platinum deposits, R&D was (and remains) essential to developing and maintaining viable means of extraction. In coal mining, in contrast to gold and platinum mining, the main R&D challenges centred on adapting coal mining equipment to the task of cutting hard and siliceous coal seams. This challenge was solved for existing coalfields, but as coal mining is expected to continue on a large scale in at least the medium term, extraction in the north-lying coalfields could present new R&D challenges. R&D is also required to ensure that mining breaks with the past and brings broad benefits to society.

Current context of South African mining

Given the importance of moving away from coercive labour practices that were the norm under apartheid, the absence of cheap labour, cheap energy, and easily accessed orebodies, as well as falling commodity prices, South African mining companies have been searching for a fresh approach. The initial response of gold and platinum miners was to reduce the costs of operations by lowering levels of production and employment. But even as mine shafts closed rather than opened, the idea that automation could revive the growth of the sector and secure its future gained currency. However, this idea, if pursued in isolation from other interventions in the wider economy, has the potential to fly in the face of needs for job creation and decent work.

Furthermore, the significance of the place of mining in the South African economy leaves little room for complacency about the sector's waning fortunes. In 2013 it was estimated that 60% of all export revenue stemmed from the export of minerals and metals. This figure belies the size of mining's contribution to the gross value added by all sectors in the South African economy, which has shrunk, from a high of 21% in 1980 when the gold price peaked (Kantor, 2013) to 8% in 2015 (Statistics South Africa, 2016). Mining remains an important employer in the country and accounts for significant investments in infrastructure. In the gold sector alone, in 2015, R23.4 billion was spent on the remuneration of approximately 120 000 employees, and R9.4 billion was spent on capital infrastructure. Yet over the preceding decade, the rate of gold production in South Africa declined more rapidly than that of other top 10 producers, at –7.7% per annum. Over the same period, employment declined by 4.4% per annum. Although wages increased on an average of 11% per annum, these increases have made no impact on the apartheid era wage gap. Rising electricity prices also contributed to the rapid downscaling of the gold sector. Without systemic changes in gold mining methods, the sector is expected to continue to shrink so that by 2025 production is expected to have halved relative to 2015 levels, and employment levels are expected to have declined to 43% of 2015 levels, or 68 000 employees (This is Gold, 2015, pp. 2-4).

Operation Mining Phakisa

The crisis in mining was recently addressed through a multi-stakeholder process, Operation Mining Phakisa. The Phakisa got underway in August 2015, under the leadership of the Department of Planning, Monitoring and Evaluation (DPME), which is situated in the Presidency. It was aimed at identifying and acting on key 'constraints to investment in and growth of the sector' (Brand South Africa, 2015). The Phakisa produced a strategy and concrete plans, all dependent on the collaborative input and efforts of the key stakeholders clustered around mining. The stakeholders involved included government departments such as the Department of Performance Monitoring and Evaluation (DPME), the Department of Mineral Resources (DMR), the Department of Trade and Industry (DTI), the Department of Science and Technology (DST) the Department of Water and Sanitation (DWS), the Department of Environmental Affairs (DEA), the Chamber of Mines (COM), the South African Mining Development Association (SAMDA), representatives of major mining companies, the National Union of Mineworkers (NUM), the Solidarity and UASA trade union, Bench Marks Foundation (an NGO), and universities such as the University of the Witwatersrand, and University of Pretoria. The Phakisa started with individual and group consultations with stakeholders, which laid the groundwork for a five-week 'laboratory' at which specific plans were developed. These consultations were conducted by staff of the DPME. Although efforts were made to create an inclusive process, the Association of Mineworkers and Construction Union (AMCU) was conspicuously absent from the Phakisa, the DMR played a notably low key role, and SAMDA representatives were dissatisfied with the level of priority (too low from their perspective) attached to the mine ownership aspects of transformation.

In overview, this DPME-led process set its sights on rebuilding the mining sector through technological excellence, social inclusion, and job creation. Stakeholders agreed that the problems in the mining sector were deep-rooted and structural, tending towards self-reinforcement. The outcomes of the process required cooperation and commitment from each of the major stakeholders, and had to be viable in both financial and practical terms. Plans were developed to support investment in mining and to build local expertise in mechanized mining methods, the manufacture of mining equipment, and provision of mining-related services. Solutions to the problems experienced by communities affected by mining and associated with degraded mining land were also discussed. This discussion could pave the way for R&D aimed at addressing social needs and linking industry and society. All plans at the Phakisa were developed and

priced collaboratively, and implementation was made conditional on securing sufficient commitment from each of the stakeholders. This included co-funding and other arrangements which lock the private and public sector into partnerships. If it was clear that these criteria could not be met, the initiative under consideration was abandoned.

The plans developed at the Phakisa, were not entirely new. They were informed in part by other developments and plans that preceded the Phakisa, such the papers and engagement that led to the promulgation of the Mineral Resources and Petroleum Development Act, the country's National Development Plan, the Mining Charter, and the work of the Mining Growth Development and Employment Task Team.

The outcomes of the Mining Phakisa ultimately took forward calls for a coherent and coordinated approach by government, with the support of the private sector, to build a 'joined-up economy'. This approach requires the extraction of (finite) mineral resources to be closely associated with concurrent initiatives to increase levels of industrialization and human capital development (Turok, 2014), and could provide the means for African countries to foster commodity-led industrialization (Lopes, 2015).

Many agreements were reached at the Phakisa. For example, it was agreed that the effects of the downturn on mineworkers and their dependents amounted to a crisis requiring immediate attention. To this end a national initiative led by the Commission for Conciliation, Mediation and Arbitration (CCMA) was proposed and accepted. Long- and short-term measures were devised to stimulate investment in mining and activate the mining and industrial value chain associated with mining. These included fostering inclusive participation in the mining sector by increasing the number of emerging miners, transforming the racial structure of the economy, developing new mining methods, addressing the energy crisis in mining, and targeting specific beneficiation opportunities. Plans were also developed to address the negative legacies of mining. Lastly, it was acknowledged that the dysfunctional relationships between the state and the mining sector, and between organized labour and the mining sector, needed to be set right. These relationships were to be reconfigured through the process of implementing plans conceived collaboratively.

'The broad aim … is to galvanise growth, transformation, investment and employment creation along the entire mining value chain, in relevant input sectors and in mining related communities.'

Mining equipment – implications and opportunities

In light of these developments, the South African mining industry is now challenged to adopt appropriate technologies while supporting the development of national manufacturing capabilities *i.e.* the sector must be 'properly industrialized'.

This work stream of the Phakisa builds on several current and earlier initiatives and programmes such as the Industrial Policy Action Plan (IPAP) of the DTI, which focuses on specific economic sectors and employment, the Mining Charter of the DMR, which focuses on issues of ownership and socio-economic development, as well as the R&D strategy developed by the DST, and a wide-ranging strategy on sustainable growth and meaningful transformation developed in a tripartite forum, the Mining Industry Growth and Development Task Team, which was established by the DMR in 2008.

The main aspects of IPAP that are relevant to mining are located in the mineral beneficiation section, which aims to increase local inputs in the mining value chain both upstream and downstream by focusing on capital goods, consumables, and services. Four key value chains were analysed by the DTI, namely ferrous metals, polymers, titanium, and platinum group metals (Department of Trade and Industry, 2014, pp. 82-83).

The current Mining Charter contains a number of provisions of relevance to development and industrialization. It sets ownership, economic interest, and management control of mining entities by 'black economic empowerment' (BEE) groups and individuals at 26%, the procurement of capital goods from BEE companies at 40%, and the contributions by multinational suppliers to socio-economic development of local mining communities at 0.05% of the annual income of local mining companies. The Charter has been under review for some time, and key issues in the recently released revised draft Charter include the retention of BEE ownership at 26% and 'equitable' distribution of these stakes among workers, black entrepreneurs, and communities; an offset of up to 11% of BEE requirements against beneficiation; an increased level (60%) for local procurement of capital goods from BEE companies; and increased levels (>60%) of procurement for consumable and services from local BEE companies (South Africa, 2016). The Charter review process is unfolding in parallel to developments arising from the Phakisa, and while there are opportunities for synergy, there are also points of difference that are still to be settled.

The following elements of the Phakisa process are central to reviving mining and pertinent to the interest of government, mining companies, and equipment suppliers.

- Advancing R&D pertaining to fuel cell development to reduce reliance on coal and diesel, and to leverage off the country's abundant platinum deposits
- Developing new systems of mining for narrow tabular seams. This involves mechanization and automation drawing on new developments in interconnectivity and autonomous processes
- Increasing emphasis on local manufacture of capital equipment and local ownership of manufacturing companies
- New technology for addressing the environment impacts of mining, and repurposing of mining land to new ends such as energy and clean water production, biomass production and agriculture, including new technology for the beneficiation of mining waste
- Targeted beneficiation of specific minerals such as iron ore (steel), platinum, manganese, and titanium
- Incubation of beneficiation industries
- Local skills and business development
- Self-generation of energy at mine sites
- Renewed commitments to supporting exploration.

As is evident from the above list, these initiatives are not unrelated to global developments in mining technology, but the emphasis is on localization. The Council for Industrial

and Scientific Research (CSIR) was tasked with hosting a hub or mining-related R&D in support of the technical R&D aspects of the outcomes of the Mining Phakisa. The roles of the CSIR include managing the hub facility, which it owns; facilitating and managing tenancy by stakeholders from government, industry, the science councils, universities, and professional bodies; facilitating the development of appropriate pilot facilities at the site under the guidance of a public-private sector steering committee; and participating in or contributing to R&D projects to the extent that relevant competencies are available in the organization. The other aspects of the mining value chain are already served by dedicated institutions such as the Council for Geoscience, which focuses on exploration and matters related to Earth science, and Mintek, which focuses on the beneficiation of mineral resources. The University of the Witwatersrand and the University of Pretoria, which are home to schools of mining engineering, are expected to play a direct role in the development of mining technology, while the activities of many other universities are central to solving problems in mineral beneficiation, treating minewater, addressing environmental impacts, and providing energy solutions. At present, funding available for geoscience and mineral beneficiation R&D far outstrips that available for the mining (extraction) process itself, hence the Phakisa focus of this aspect of the minerals value chain.

The CSIR's immediate R&D tasks are to:

- Identify and initiate mechanization solutions for South African mines which support local manufacture and solve problems related to cutting hard rock
- Install and test sensor systems for environmental monitoring in mines
- Investigate non-explosive rock-breaking methodology
- Contribute to the development of a framework and decision support system for real-time monitoring technology to support personnel-machine interactions, machine-rock interactions, and machine-to-machine communication
- Contribute to the development of mining layouts and support systems to provide for mechanized mining
- Understand the role of rock engineering in mechanized mining in South Africa.

These tasks are to be accomplished through collaboration with other research institutions, mining companies, and manufacturers in the country.

Since the conclusion of the Mining Phakisa, work has started on establishing the 'Mining Hub'. In essence, the need for a strong collaborative centre for mining-related research is in the process of being re-established, with government committed to partnering with industry. The DST committed seed money towards its establishment and further funds have been secured through interactions with Treasury. Plans to bring equipment suppliers and mining companies into the hub have already been successfully implemented. The DTI's substantial role in the hub is informed by its Resources Capital Goods Development Programme (Davies, 2015). These first steps to address the technology needs of South African mines, and the process envisaged, should ensure that the appropriate technologies are developed and that impetus is given to the development of local industry.

However, the hurdles inherent in developing mechanization and automation processes for the South African mining sector are still to be overcome. These are significant. Identifying and mechanizing those parts of the mining process which would immediately benefit from mechanization is the first challenge, and thereafter lies a meticulous phase of revisiting the extraction process in its entirety to properly understand the conditions, processes, equipment, and skills requirements for automation. This all before automation can be realized, and most likely not for all mines. Since this is a long and painstaking pathway it provides stakeholders, if they remain committed, with the time to build deep consensus on the way forward, and properly plan for the scale and impact of the changes to come.

Conclusions

The operational and business models of mining are being revisited across the world and in South Africa. The private sector (mining companies and investors) has to re-conceptualize how mining can be undertaken profitably and to the benefit of society, both locally and at large.

In South Africa, a coordinated technical innovation programme has been initiated as part of a larger plan which also addresses the social and environmental legacies of mining and spearheads reindustrialization. The ingredients for success, namely co-funding, public-private partnerships, linking R&D to industry, and social needs and co-planning are all present.

Building local expertise, manufacturing capability, and skills development are central to this endeavour, but the challenges that lie ahead are immense. Most significant are the difficulties of transferring tasks currently performed by mineworkers to machines while concurrently creating manufacturing and other jobs opportunities. Implicit is the need to revisit and redesign mining processes to support automation and to create development opportunities in the wider economy.

The mining Phakisa has opened up many opportunities for the private sector, especially for equipment manufacturers. Under enabling conditions the response of the private sector to the call to innovate will determine whether these opportunities can be realized. For many companies in the mining, industrial, and financial sectors, the emphasis on localization may present fundamental shifts in business strategy.

References

Bardi, H. 2014. Extracted. How the Quest for Mineral Wealth is Plundering the Planet. Chelse Green Publishing.

Baxter, R. 2015. The future of the South African Mining industry. Chamber of Mines of South Africa, Johannesburg.

Blankley, W.O. and Booysens, I. 2010. Building a knowledge economy in South Africa. *South African Journal of Science*, vol. 106, no. 11/12. pp. 1–6.

Bloomberg. 2016. Commodities crash boosts China's new Silk Road. http:// http://www.hellenicshippingnews.com/commodities-crash-boosts-chinas-new-silk-road/

Brand South Africa. 2015. Mining operation phakisa gets going. https://www.brandsouthafrica.com/investments-immigration/business/economy/development/phakisa-mining-150515

Bundy, C. 1988. The Rise and Fall of the South African Peasantry. 2nd edn. David Philip. Cape Town.

Cronimet Mining. Not dated. Cronimet mining energy. http://www.cronimet-mining.com/en/energy

Davies, R. 2015. Mining still a key pillar for SA economy. http://allafrica.com/stories/201502091736.html

Deloitte Touche Tohmatsu Ltd. 2015. Tracking the trends 2016. The 10 top issues mining companies will face in the coming year. https://www2.deloitte.com/content/dam/Deloitte/global/Documents/Energy-and-Resources/gx-er-tracking-the-trends-2016.pdf

Deloitte, Monitor, Doblin, Investing In African Mining Indaba, and Chamber of Mines. 2016. Innovation State of Play. Africa. Mining Edition 2016. http://www.polity.org.za/article/innovation-state-of-play-africa-mining-edition-2016-feb-2016-2016-02-09

Department of Trade and Industry. 2014. Industrial policy action plan 2016/17. Economic sectors and Employment Cluster. IPAP 2014/15-2016/7. Pretoria.

Durrheim, R.J. 2010. Mitigating the risk of rockbursts in the deep hard rock mines of South Africa: 100 years of research. *Extracting the Science: A Century of Mining Research*. Brune, J. (ed.). Society for Mining, Metallurgy and Exploration, Littleton, CO. pp. 156–171. http://africaarray.psu.edu/publications/pdfs/SME100_Durrheim_Rockburst%20research.pdf

Ernest and Young. 2015. Business risks facing mining and metals 2015-2016. http://www.ey.com/gl/en/industries/mining---metals/business-risks-in-mining-and-metals-old-2

Flynn, L. 1992. Studded with Diamonds and Paved with Gold. Miners, Mining Companies and Human Rights in Southern Africa. 1st edn. Bloomsbury, London.

Innes, D. 1984. Anglo. Anglo American and the Rise of Modern South Africa. Ravan Press, Johannesburg.

Kantor, B. 2013. How important is mining in the SA economy? It depends on how you measure it. http://www.zaeconomist.com/sa-economy/how-important-is-mining-to-the-sa-economy-it-depends-on-how-you-measure-it/

Kaplan, D. 2011. South African mining equipment and related services: growth constraints and policy. *MMCP Discussion Paper* no. 5. http://www.prism.uct.ac.za/papers/mmcp%20paper%205_0.pdf

Lopes, C. 2015. Is the commodities super cycle slowdown a shock for Africa?. https://www.uneca.org/es-blog/commodities-super-cycle-slowdown-shock-africa [Accessed 16 April 2016].

Marinovich, G. 2016. Murder at Small Koppie. The real story of the Marikana massacre. Penguin Random House South Africa, Cape Town.

McCulloch, J. 2013. South Africa's Gold Mines and the Politics of Silicosis. Jacana Press, Johannesburg.

Mining.com. Not dated. Breakthrough aircraft to tranform remote mining. http://www.mining.com/breakthrough-aircraft-to-transform-mining-economics

Momberg, J. and Rich, E. 2015. Beyond Governments: Making Collective Governance Work. Lessons from the Extractive Industries Initiative (ETI). Greenleaf Publishing.

PDAC, Monitor, Doblin, Deloitte. 2015. Innovation state of play. Mining edition 2015. https://www2.deloitte.com/content/dam/Deloitte/br/Documents/energy-resources/Innovation_State_of_Play.PDF

PDAC. 2016. PDAC briefing note. A capital opportunity: responding to the prolonged downturn in mineral exploration financing. http://www.pdac.ca/docs/default-source/public-affairs/budget-2016-pdac-recommendation---metc.pdf?sfvrsn=2

Platsky, L. and Walker, C. 1985. The Surplus People. Forced Removals in South Africa. 1st edn. Ravan Press, Johannesburg.

Pogue, E. 2006. Missed opportunities? A case study from South Africa's mining sector. *Resource Intensity, Knowledge and Development Insights from Africa and South America*. Lorentzen, J. (ed.). HSRC Press, Cape Town. Chapter 5, pages 179-213. http://www.ieri.org.za/sites/default/files/outputs/Resource_Intensity_Chapter_5_mining_sector.pdf

Pogue, E. and Rampa, M. 2006. Innovation in resource-based technology clusters. Investigating the lateral migration thesis. Human Sciences Research Council, Pretoria.

PWC. 2015. SA Mine, 7th edn. Highlighting trends in the South African mining industry. https://www.pwc.co.za/en/assets/pdf/sa-mine-2015.pdf

Rio Tinto plc and Rio Tinto Ltd. Not dated. Technology and innovation. http://www.riotinto.com/technology-and-innovation-160.aspx

Rio Tinto plc and Rio Tinto Ltd. 2014. Mine of the Future. Next generation mining: people and technology working together. https://www.youtube.com/watch?v=9l_EbGLItyY

This is Gold. 2015. SA gold, today and tomorrow fact sheet 2015. http://www.thisisgold.co.za/downloads/finish/4-fact-sheets/59-south-african-gold-today-and-tomorrow

Schussler, M. 2016. The depressive super cycle. https://www.moneyweb.co.za/moneyweb-opinion/the-depressive-super-cycle/ [Accessed 30 May 2016].

South Africa. 2016. Reviewed Broad Based Black Economic Empowerment Charter for the South African Mining and Minerals Industry, 2016. *Government Gazette*, vol. 610, no. 39933, 15 April 2016.

Statistics South Africa. 2016. Gross Domestic Product, 4th Quarter 2016. http://www.statssa.gov.za/publications/P0441/GDP_presentation-Q4_2016.pdf [Accessed 30 March 2017].

Thorndahl, M. 2011. International Development Policy: Energy and Development. Graduate Institute of International and Development Studies, Geneva.

TIPS and Global Green Institute. 2014. The impact of electricity price increases on the competitiveness of selected mining sector and smelting value chains in South Africa. https://www.tips.org.za/research-archive/sustainable-growth/green-economy-3/item/download/912_d664ce65069c5a9f0f699a4121604fa9

Turok, B. 2013. Problems in the mining industry in South Africa. http://ecdpm.org/great-insights/growth-to-transformation-role-extractive-sector/problems-mining-industry-south-africa/

Turok, B. 2014. The scope for domestic value addition in a mining economy: the South African case. *New Agenda.* https://ifaacapetown.files.wordpress.com/2015/02/prof-turok.pdf

UBS. 2016. Extreme automation and connectivity: the global, regional, and investment implications of the fourth industrial revolution. https://www.ubs.com/global/en/about_ubs/follow_ubs/highlights/davos-2016.html

Wilkinson, R. and Pickett, K. 2010. The Spirit Level: Why Equality is Better for Everyone. Penguin.

Wilson, F. 1972. Labour in the South African Gold Mines 1911-1969. Cambridge University Press, Cambridge, UK.

World Bank Group. 2016. Commodity Markets Outlook. Weak growth in emerging economies and commodity markets. January. https://openknowledge.worldbank.org/handle/10986/23680

World Bank and International Finance Corporation. 2002. Mining and Development. Treasure or trouble. Mining in developing countries. http://siteresources.worldbank.org/INTOGMC/Resources/treasureortrouble.pdf

World Economic Forum. 2016. What is the Fourth Industrial Revolution? https://www.weforum.org/agenda/2016/01/what-is-the-fourth-industrial-revolution/ ◆

http://dx.doi.org/10.17159/2411-9717/2017/v117n8a13

Gold CIP and CIL process optimization in a capital constraint environment

by C.A. Snyders*, G. Akdogan*, S.M. Bradshaw*, and A.P. van Wyk*

Synopsis

This article focuses on the use of a model in combination with economic analysis to extract maximum value out of current gold operations, without the need for additional capital. Two South African case studies (CIP and CIL) are presented to show that an optimum point of operation exists. This optimum point of operation, however, depends on several economic factors such as the gold price, exchange rate, and utility costs in combination with plant conditions such as the feed rate and Au grade. As these parameters fluctuate, the operating conditions will have to be adjusted to achieve the maximum value. Operating at a maximum will require regular decision-making and adjusting of operating conditions, especially in times of a constrained economy.

Keywords
gold recovery, optimization, CIP, RIP, economic, analysis, modelling.

Introduction

The well-known carbon-in-pulp (CIP) and carbon-in-leach (CIL) gold recovery processes are fairly robust. Considering the constantly changing characteristics of run-of-mine (ROM) ore, a robust process is in general a great advantage for a mineral processing plant. The disadvantage, however, is that because less input is required from operators and metallurgical personnel, the process may not always be running under optimized conditions.

Several tools have been developed over the years to assist in achieving maximum value from the gold recovery process, including several models that can predict the leaching and adsorption of Au in the CIP or CIL process. These models are predominantly used by design houses to design and size the plant, and in most cases this is where the usage of these models stops. The reason for this is not clear, as an accurate CIP model will also be of great assistance in the day-to-day operation of the plant, especially in times of constantly fluctuating gold prices and exchange rates, and rapidly increasing input costs. In the past, many research investigations have focused mainly on the specific model or one of the unit processes, and not on the plant as a whole. This study, therefore, aims to make use of the well-known Nicol-Fleming first-order kinetic adsorption model (Nicol, Fleming, and Cromberge, 1984a, 1984b, 1984c) which has been calibrated to plant data, in combination with an economic analysis in order to determine the operational conditions that will result in maximum revenue. This will also highlight the plant sensitivity to certain variables, ultimately allowing for greater plant understanding. Although this model is not the most accurate, it still predicts the gold in solution and gold on carbon profiles very well, and can be combined with economic models with relative ease to arrive at the optimum operating conditions. More accurate results will require more experimental data for the more complex and rigorous models to be used.

Model development

It is widely accepted that the performance of the adsorption circuit directly influences the elution and regeneration circuits. What is often neglected, however, is how the performance of the elution and regeneration circuit will influence the adsorption circuit. Fleming *et al.*, (2011) state that, in order to consistently achieve low barren losses in the adsorption section, it is important to maintain a low concentration of gold on the carbon in the last adsorption stage, which effectively means that the carbon must always be eluted efficiently. Fleming *et al.* (2011) showed that by increasing the amount of gold on the eluted carbon being recycled to the adsorption section from zero to 50 g/t, an increase in the soluble gold losses of 370% could occur. Elution, however, takes place at a cost and an economic trade-off study is required to determine the operating point for optimum value.

The Nicol-Fleming model is one of the first and simplest models. It assumes that all tanks can be modelled as perfectly mixed reactors and that a steady-state condition with a

* *Stellenbosch University, South Africa.*
 ISSN 2225-6253. Paper received Aug. 2016; revised paper received May. 2017.

countercurrent flow of both carbon and solution is achieved, such that the gold concentration in the solution and gold loading on the carbon can be assumed to be constant in each adsorption tank. It predicts the gold in solution and gold on carbon profiles very well, and can be combined with economic models with relative ease to arrive at the optimum operating conditions.

The rate of gold adsorption onto activated carbon is described by:

$$\frac{d[Au]_c}{dt} = k(K[Au]_s - [Au]_c) \quad [1]$$

This rate equation can be combined with a mass balance (Equation [2]) over the entire countercurrent CIP adsorption circuit to yield a model that can be used to describe the performance of the circuit.

$$V_S([Au]_s^0 - [Au]_s^N) = V_C([Au]_c^0 - [Au]_c^N) \quad [2]$$

where

V_S = Flow rate of the feed solution
$[Au]\ s$ = Gold concentration in the feed solution
$[Au]\ s^N$ = Gold concentration in solution leaving stage N
V_C = Flow rate of activated carbon
$[Au]\ c^N$ = Gold loading on carbon entering stage N
$[Au]\ c^0$ = Gold loading on carbon leaving the first stage
k = Kinetic constant
K = Equilibrium constant.

Since the plant variables such as solution flow rate and grades, tank size, carbon advance rate, and carbon concentration in each tank are known, the model can be calibrated against plant data to determine both k and K.

Nicol, Fleming, and Cromberge (1984b) also found that the method outlined above can be extended to a CIL operation by the inclusion of a leaching rate expression (Equation [3]) and assuming that the rate of leaching is independent of the activated carbon present.

$$-\frac{d[Au]_{L,t}}{dt} = k_L([Au]_{L,t} - [Au]_{L,e})^2 \quad [3]$$

where

$[Au]_{L,t}$ = Concentration of the gold in the ore
$[Au]_{L,e}$ = Minimum achievable residue grade
k_L = Leaching rate constant

Once both k and K are determined, the effect of changing an operating variable (such as the carbon advance rate) can now be determined by calculating the impact on the downstream processes, in terms of both frequency and cost. The revenue or loss incurred is calculated by Equation [4], where the variable costs are assumed to include all the costs that are affected by the changing variables. By equating the 'fixed costs' of the base case (condition where the plant normally operates) to a value that will result in zero revenue, a differential cost for each scenario can be calculated, which effectively will determine how much more revenue (or loss) can be realized by changing a certain operating variable.

Operational revenue = Value of Au produced – 'Fixed costs' – 'Variable costs' [4]

Case studies for both a CIP plant and a CIL plant are presented.

The CIP case study

A plant evaluation on a 180 000 t/month CIP plant was performed. The plant consists of six Kemix pump cells in a carousel flow arrangement, a hydrochloric acid pre-wash, high-pressure elution at 125°C, kiln regeneration, and electrowinning.

Parameter determination and calibration

The values for k and K were determined through empirical fitting by averaging plant data such as the head grade, feed flow rate, solid/liquid mass fraction and eluted carbon loadings over 3- to 5-day periods as input parameters to the model. Averages over these relative short periods were used to compensate for the leaching retention time (approx. 35 hours), the slurry retention time during adsorption, as well as the carbon retention time. Thirteen periods in total (Table I) were selected for calibration, which included periods of higher and lower feed rates and solid/liquid mass fractions. Estimated values for k and K were obtained from the literature (Fleming *et al.*, 2011) and were then adapted to obtain the best fit.

The plant operates a carousel CIP circuit with three 8-hour shifts and one elution per day. Carbon is transferred from the lead tank to elution at the end of the night shift or start of the morning shift, and the carbon loading is determined before elution. Carbon loadings are again determined later in the morning, afternoon, and night shifts. Since the carbon is modelled as a continuous flow (Equation [2]), the model predicts the carbon loading just prior to elution or a carbon transfer. With one elution per day, the carbon residence time for the model is therefore taken as 24 hours. An example of the plant carbon loadings in each tank for the period 1–5 December 2015 compared to the model-predicted values can be seen in Figure 1. For this particular example, the model-predicted loading (indicated by X) compares well for stage 1 (stage before elution), stage 5, and stage 6 while overpredicting the loading in stages 2, 3, and 4. Predictions for the other 12 periods were found to be similar. From the six stages, the loading prior to elution is rather important as this will ultimately determine the Au produced after elution and electrowinning. The dotted line in Figure 1 serves as an indication of the increases in measured gold loading on the carbon throughout the day.

Figure 2 compares the Au grade in solution for each stage to the model-predicted values for the sampling period.

The model-predicted solution tails are compared to actual plant data in Table I, while the product of the adsorption constants (kK) as a function of the solid/liquid mass fraction (%) of the pulp, determined in this study, is compared to literature data in Figure 3.

Considering Figures 1 to 3 as well as Table I, the model with determined kK values was deemed a reasonable theoretical representation of the specific operation that can be used to quantify the relative influence of a wide range of variables, allowing for better understanding of the plant and making it possible to optimize performance.

CIP base case

A base case representing the daily operation of the plant was chosen. The operating parameters for this base case are shown in Table II. The corresponding variable costs,

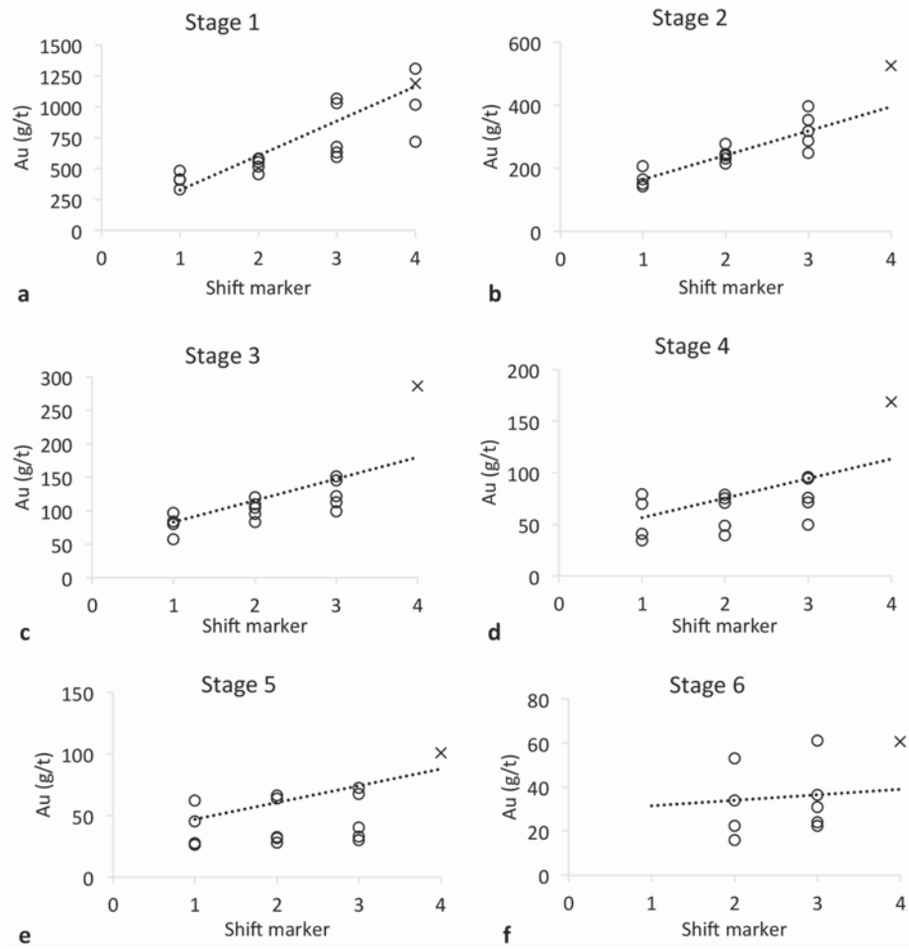

Figure 1—Predicted *vs* measured carbon loadings for each adsorption stage (a to f) and shift (x-axis) 1: morning shift, 2: afternoon shift, 3: night shift. 4: prior to elution, O: measured values, dotted line: measured value trend line, X: model prediction)

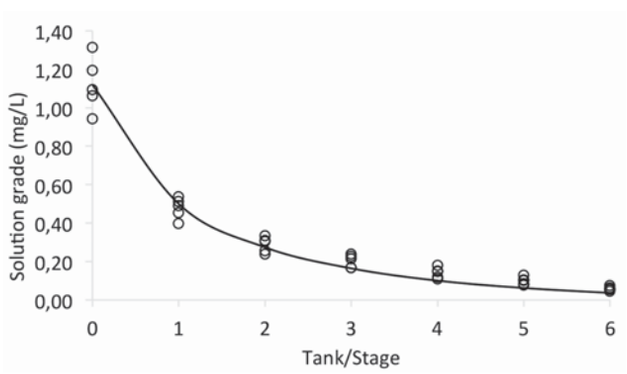

Figure 2—Predicted *vs* measured solution grade (1–5 December 2015) in each stage of the carbon adsorption circuit, with stage 0 being the Au feed grade to the first adsorption tank and stage 6 the tails. The model predictions are depicted by the line, and the plant measurements by the circles

determined from plant data, are shown in Table III. Unless otherwise stated, these conditions will be used in all cases.

With the base case set, and using the model representing plant conditions, the effect of changing operating parameters (carbon advance rate, elution efficiency, carbon concentration, gold grade, solid/liquid mass fraction and feed flow rate) was determined.

Table I

Predicted *vs* measured solution tails grade

Date	Au losses (mg/L)		
	Average of actual	St. dev of actual	Predicted
17–19 Mar 2015	0.07	±0.006	0.09
16–18 Jun 2015	0.05	±0.005	0.02
21–25 Jun 2015	0.08	±0.036	0.09
31 Oct–3 Nov 2015	0.05	±0.007	0.04
5–7 Nov 2015	0.07	±0.009	0.07
8–10 Nov 2015	0.06	±0.008	0.05
11–13 Nov 2015	0.05	±0.004	0.05
26–30 Nov 2015	0.04	±0.008	0.05
1–5 Dec 2015	0.06	±0.010	0.04
6–10 Dec 2015	0.06	±0.007	0.06
11–15 Dec 2015	0.05	±0.009	0.06
16–20 Dec 2015	0.06	±0.005	0.06
21–24 Dec 2015	0.06	±0.004	0.06

Carbon advance rate

The carbon advance rate or carbon residence time is one of the easiest parameters to change on the plant and will basically determine the amount of Au the carbon is loaded to before elution takes place (upgrade ratio). As per Table III,

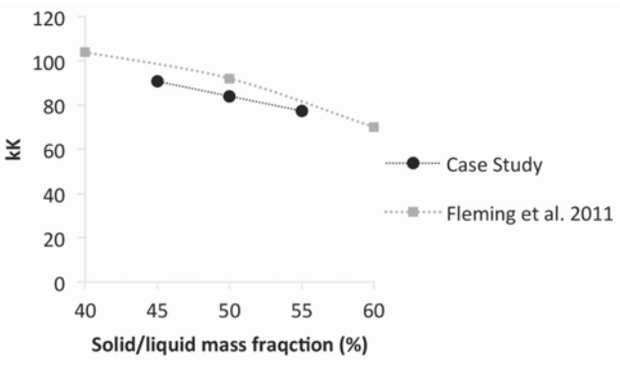

Figure 3—Plant-determined *kK* values compared to values from Fleming *et al.* (2011)

Table II

Base case conditions for the CIP case study

Feed flow rate	230	t/h
Solids percentage	50	%
Adsorption tank size	100	m^3
Stages	6	
Carbon retention time per stage	24	h
Carbon concentration	45	g/L
Carbon loading after elution	40	g/t
Au solution feed grade	1	mg/L
Au price	1250	US$/oz
Exchange rate	15.4	R/US$

Table III

Variable costs for the base case CIP operation

Variable costs	R/day	R/ton carbon
Acid washing	R186	R31
Elution	R41 926	R6 988
Regeneration	R4 455	R743
Electrowinning	R211	R35
Carbon breakage	R2 615	
Gold on carbon fines loss	R2 166	
Total variable cost	**R51 558**	

the costs of elution, acid washing and regeneration are major contributors to the variable cost. This cost can immediately be reduced by increasing the carbon residence time, which will increase the carbon loading and decrease the frequency of elution and regeneration. These costs are, however, offset by the adsorption capacity of the higher-loaded carbon, which will cause an increase in the gold losses to the tailings. Figures 4a and 4b show the effect of the carbon residence time on the differential revenue/loss as well as the change in variable cost and Au loss to the tailings.

Even though the plant is well designed and operating within the design parameters, by reducing the carbon residence time in each tank from 24 hours to 17 hours, an additional R10 000 per day may be realized, resulting in approximately R 3.3 million per annum for a 330-day operating year. The carbon loadings will reduce from approximately 1200 g/t for the base case to 880 g/t for a residence time of 17 hours, while the Au in solution to the tailings should decrease from 0.051 mg/L to 0.042 mg/L. This decrease in Au in the solution tails is the primary reason for the increased revenue. The revenue and optimum point of operation determined here are, however, associated with a specific Au price and rand/dollar exchange rate, both of which have been known to fluctuate quite dramatically. Figure 5a shows how the point of optimum performance in terms of carbon residence time shifts with a fluctuating Au rand value. For an Au price of $1100 per ounce with a rand/dollar exchange rate of 13.3 (early September 2015), the optimum carbon residence time would have been 19–20 hours. As the value of the Au increases in rand terms, the optimum carbon residence time will shift to more frequent elution and can make a difference of several thousand rand per day or several million rand per annum.

Figure 5b shows the effect of increasing electricity costs on the plant. An increase in the electricity cost of 6 cents per kWh will shift the optimum residence time from 17 hours to 18 hours. A change in actual operation here is probably not warranted, but it does demonstrate the sensitivity of the plant to certain parameters and therefore assists in decision-making. Both Figures 5a and 5b illustrate that operating the process at a constant set of conditions will not result in optimum revenue, but the conditions rather need to be

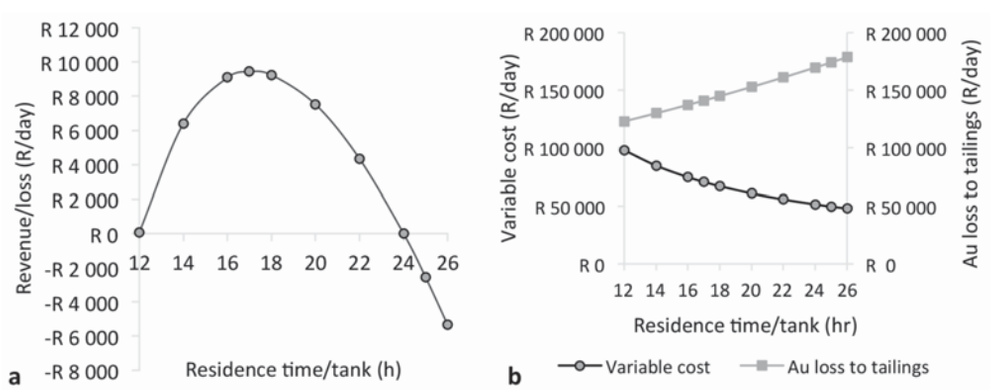

Figure 4—(a) The differential daily revenue/loss with varying carbon residence time compared to the current operation at 24 hours, and (b) the associated operational costs and Au value loss to the tailings

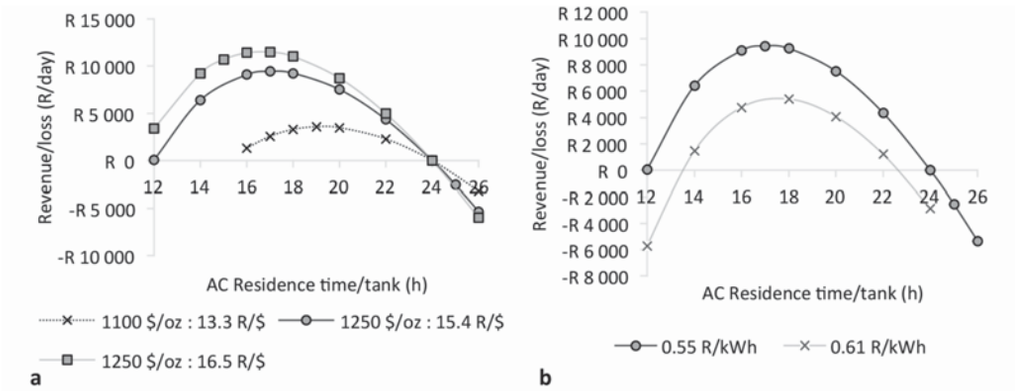

Figure 5—Determination of the optimum carbon residence time for (a) fluctuating rand/dollar exchange rate and Au price and (b) electricity costs

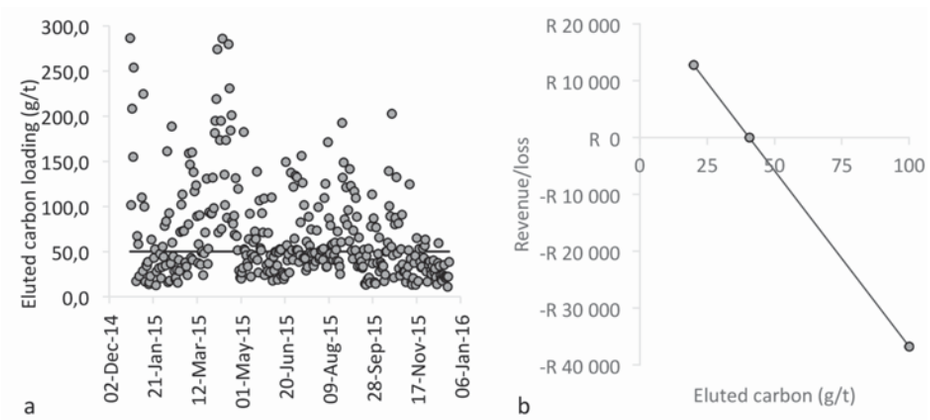

Figure 6—(a) Operational carbon loadings after elution, and (b) the impact on the differentail revenue/loss per day, assuming the base case at 40 g/t carbon loading after elution

adapted when any of the costs (including raw materials, utilities, and labour) changes.

Operational changes such as these, however, may often fall outside the bounds of practicality or plant limitations, and it may be argued that changing operational parameters on the plant is not that easy. Some of this operational problems may lie with the management of the plant and how quickly and easily decisions are communicated and then carried out. Other limitations may be a result of the installed process, such as the time it takes for effective elution to take place (Zadra or AARL). In such instances, the focus will first have to shift to reducing the elution time without sacrificing efficiency; or if the process is already at an optimum, determining whether it will be worthwhile to install another elution column, for example.

Elution efficiency

The importance of efficient elution and the impact on the adsorption section in terms of potential gold losses have already been stated. Figure 6a indicates the achieved elution efficiencies of the present case study in terms of the Au loading on the carbon being recycled to the adsorption section (straight line at 50 g/t as set target), while Figure 6b highlights the importance of efficient elution for the daily revenue of the plant (base case carbon loading of 40 g/t assumed after elution). No apparent reason for the less efficient elution (or highly efficient elution (< 25 g/t)) in Figure 6a could be determined from the plant data or operating practices, and as such no additional costs were included in the derivation of Figure 6b to achieve the more efficient elution. Determining how to achieve consistently low carbon loadings will, however, be crucial for improving the accuracy of the model and optimizing profitability. In addition, it is also important to realize that once poor elution has occurred, the high temperatures (approx. 750°C) in the regeneration kiln will convert some or all of the gold cyanide complexes on the activated carbon to Au particles (Oladele, Snyders, and Bradshaw, 2015), which will require more stringent conditions to elute.

Carbon concentration

The effect of carbon concentration is shown in Figure 7.

A disadvantage of increasing the carbon concentration is that more fines will be generated in the circuit, which leads to higher gold losses on these carbon fines. The amount of fines generated will be different for each plant, and due to the lack of data for this specific case study, values from literature (Baily, 1991) were used. It was also assumed that the Au loading on the carbon fines will be similar to the carbon loadings in the last stage of adsorption, due to equilibrium being reached between the carbon fines and larger size fractions when mixed (Nicol, Fleming, and

Cromberge, 1984c). This loss is depicted in Figure 7b, which shows the increasing variable cost that will result due to an increase in the carbon concentration in each tank. The increasing cost, however, does not outweigh the decrease in Au loss to the tailings due to improved adsorption, and the plant revenue will therefore increase with the higher carbon concentration. In this case the carbon concentration is limited by the size of the elution column (5 t) and is therefore the maximum concentration achievable without any additional capital requirements.

With the higher carbon concentration, the optimum carbon residence time now also shifts to the right, and was found to be 20 hours with a carbon loading of approximately 940 g/t and a tailings grade of 0.036 mg/L.

Gold grade

Except for a blending strategy and perhaps some influence in ore selection, plants usually have limited control over the feed Au grade and simply have to treat what is being fed to the plant. It is in this sense that the carbon process is fairly robust, since extraction efficiencies will remain high with variation in Au grade. Figure 8 shows the impact of carbon residence time on the optimum performance of the plant when the Au grade changes from 0.5 mg/L to 2.3 mg/L. The feed grades to the plant have varied within this range at certain periods within a timespan of a year. While the impact of operating with a sub-optimum carbon residence time with an Au feed grade of 0.5 mg/L is minimal, significant value can be realized by adapting the carbon advance rate for higher Au feed grades.

Eluting every 22 to 23 hours for a feed grade of 0.5 mg/L results in a gold loading of approximately 600 g/t with a tailings grade of 0.028 mg/L, while at 2.3 mg/L feed grade the carbon will be loaded to approximately 1380 g/t with a tailings grade of 0.073 mg/L. To reduce this tailings grade even further, the carbon concentration can be increased as indicated in the previous section.

Solid/liquid mass fraction

As regards the solid/liquid mass fraction of the feed pulp, two main scenarios can be considered. The first scenario assumes that the dry tons feed flow rate to the adsorption section remains constant while the effect of the solid-liquid mass fraction is being considered. With the dry tonnage feed flow rate to the plant remaining constant, a higher solids mass fraction will result in the slurry flow rate decreasing and the slurry residence time per tank increasing. The second scenario (usually the option that most plants would consider) takes advantage of the lower slurry flow rate and increases the dry tonnage feed rate to a point where the slurry residence time remains constant. Since the second scenario requires a much wider investigation, which needs to include the cost of crushing, milling, and leaching, which were not part of the initial investigation, this scenario was not considered further.

Figure 9 shows the results on the differential revenue/loss for scenario 1. Figure 9 is based on the assumption that leaching is not affected and that the same amount of Au is leached with less dilution, resulting in a higher solution feed grade to the adsorption section. Even

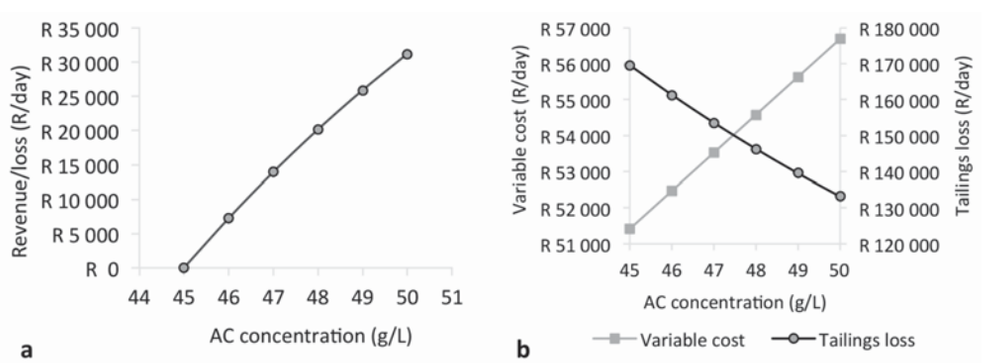

Figure 7—(a) The effect of carbon concentration on differential revenue/loss per day, and (b) the operating cost and Au loss to tailings

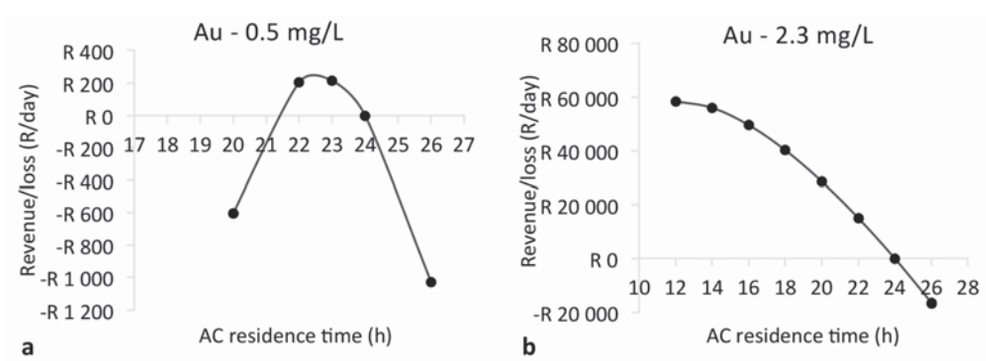

Figure 8—The effect of Au feed grade on the optimum carbon residence time

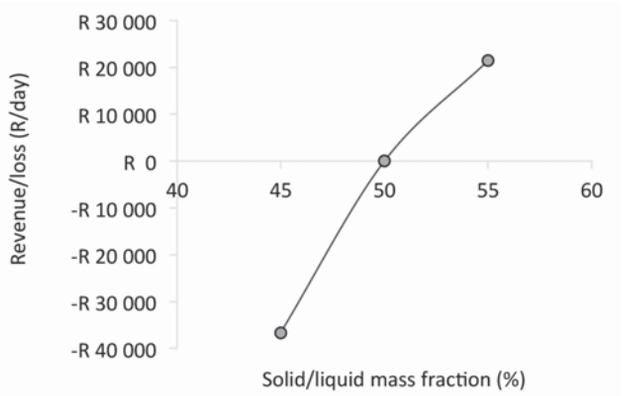

Figure 9—The effect of the solid/liquid mass fraction on the differential plant revenue/loss with a constant dry tonnage feed

though the adsorption constants for the higher solids concentration are lower (Figure 3), the combination of the higher solution grade and the lower solution flow rate will result in a higher adsorption driving force, with ultimately less Au loss to the tailings.

Feed flow rate

According to Figure 10a, feed flow rates to the adsorption section can vary quite significantly, between 200 and 300 t/h. The effect of the different flow rates is shown in Figure 10b. For each flow rate, the revenue/loss was set to zero at 24 hours carbon residence time and the flow rates cannot, therefore, be directly compared. The figure does, however, illustrate that the higher the feed rate, the more frequently elution needs to take place. The cost benefit also increases with flow rate, and it is shown that an additional R25 000 per day could have been realized if elution took place every 14 hours when the plant was operating at 250 t/h. During times of lower feed rate (start-up for example), less frequent elution is advised.

The high variability in the actual plant operating conditions, as indicated by Figure 6 as well as Figure 10, also offers an equal opportunity for revenue improvement if these variables can be stabilized. Making regular changes to the operating variables increases the risk of introducing further instability, which can lead to losses.

Optimized conditions

The impact of carbon residence time, carbon concentration, and solids-liquid ratio on the differential revenue for this case study is shown in Figure 11. Operating the plant at a carbon concentration of 50 g/L, at 55% solids, and eluting every 22 hours has the potential of adding R50 000 per day or R16.5 million per 330-day work year to the balance sheet without any capital requirements.

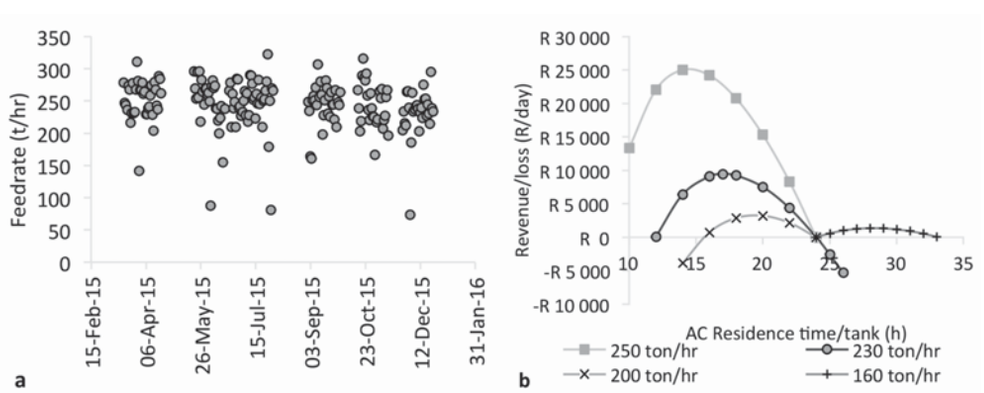

Figure 10—(a) Actual CIP plant feed rates, and (b) the optimum carbon residence times for these feed rates

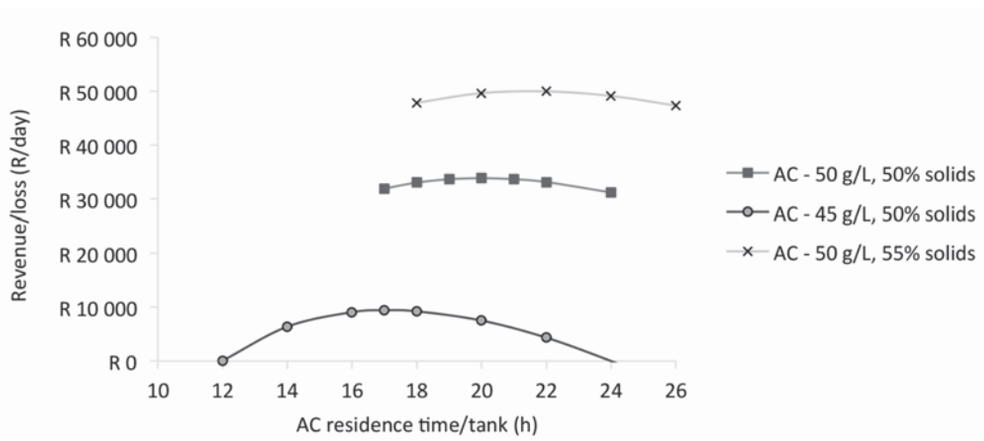

Figure 11—The impact of carbon residence time, carbon concentration, and the solids-liquid ratio on the differential revenue of the plant

CIL case study

The second case study focused on a much smaller CIL plant, which consists of six conventional cells, all containing carbon, a hydrochloric acid pre-wash, high-pressure elution at 110°C, kiln regeneration, and electrowinning.

Model calibration

The values for k, K, and k_L as per Equations [1], [2], and [3], were determined through empirical fitting by averaging plant data over 3 days as input parameters to the model. The data fitting is shown in Figures 12a to 12d.

The model-predicted solution tails losses are compared to actual plant data in Table IV, and the model-predicted gold produced compared to actual gold produced in Table V.

The predictions are less accurate than those in the CIP case study. This may be attributed to the consistently changing nature of the feed material for the CIL plant, which treats a combination of scrap material for other plants as well as re-treating old tailing dumps.

CIL base case

As per the previous case studies, the plant was evaluated by determining the differential revenue or loss that can be realized if some of the operating parameters are changed. The parameters for the base case of the operation (Table VI) and the corresponding variable costs (Table VII) were determined; unless otherwise stated, these conditions will be used in all cases.

Carbon advance rate and elution efficiency

Similar to the first case study, the optimum carbon advance rate was determined by calculating the differential revenue or loss to the plant if the carbon residence time is to change. Since a conventional flow arrangement (instead of the carousel arrangement) is employed, only a portion of the carbon can be pumped to elution, and therefore the carbon advance rate is controlled based on the amount of carbon sent to elution each day. The plant target is elution of 1000 kg of carbon per day, or one elution daily (1 t column). To remain consistent with plant practice, the carbon advance rate is reported in a similar format for this case study.

Figure 13 indicates that it will be beneficial to slow the carbon advance rate and elute less frequently. With a carbon advance rate of 1000 kg being eluted each day, the corresponding Au loading on the carbon is only

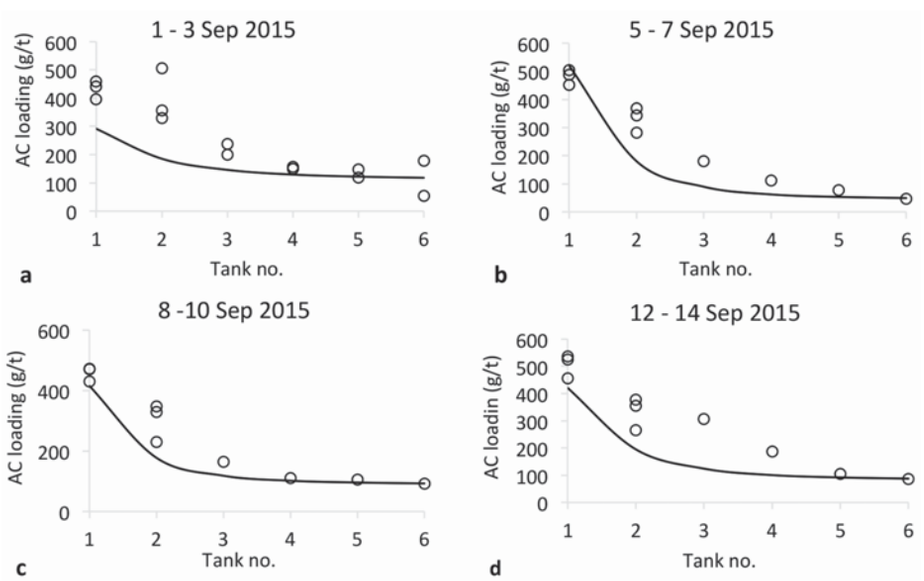

Figure 12—Predicted *vs* measured carbon loadings in each stage of the CIL circuit

Table IV

Predicted *vs* actual Au lost to tailings

	Tailings losses (mg/L)	Predicted tailings losses (mg/L)
1–3 Sep 2015	0.025	0.024
5–7 Sep 2015	0.015	0.011
8–10 Sep 2015	0.016	0.018
12–14 Sep 2015	0.029	0.019
15–17 Sep 2015	0.032	0.031
19–21 Sep 2015	0.048	0.023
22–24 Sep 2015	0.053	0.023
26–28 Sep 2015	0.054	0.025

Table V

Predicted *vs* actual Au produced per day

	Actual Au produced (g/day)	Predicted Au (g/day)
1–3 Sep 2015	162	149
5–7 Sep 2015	471	459
8–10 Sep 2015	234	269
12–14 Sep 2015	292	284
15–17 Sep 2015	278	267
19–21 Sep 2015	253	254
22–24 Sep 2015	372	365
26–27 Sep 2015	247	249

Table VI

Base case conditions for the CIL case study

Feed flow rate	10	t/h
Solid/liquid mass fraction	50	%
Adsorption tank size	95	m^3
Stages	6	
Carbon retention time per stage	48	h
Carbon concentration	20	g/L
Carbon loading after elution	45	g/t
Elution column	1	ton
Au price	1100	US$/oz
Exchange rate	16.5	R/US$

Table VII

Variable costs for the base case CIL operation

Operating costs	R/day
Acid washing	R680
Elution	R9 855
Regeneration	R1 494
Electrowinning	R201
Carbon breakage	R4
Total operating cost	**R 12 235**

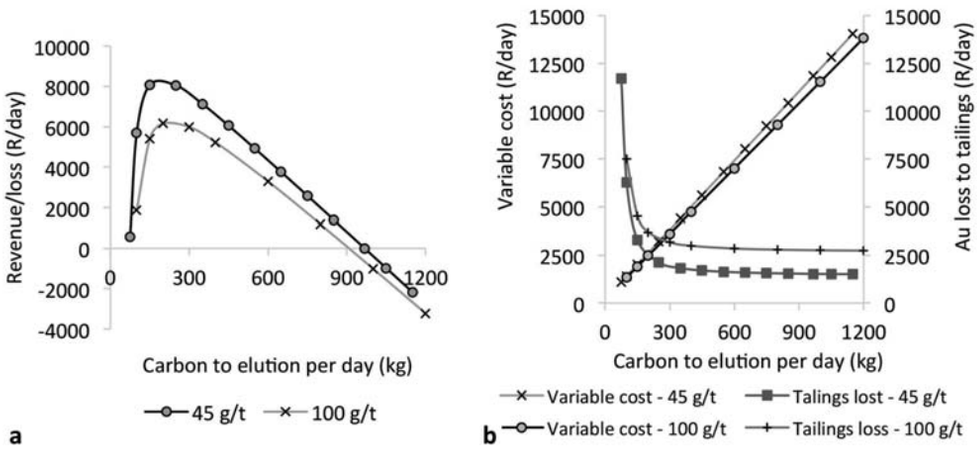

Figure 13—(a) The differential daily revenue/loss with varying carbon advance rates, and (b) the associated operational costs and Au value loss to the tailings for both a high-efficiency elution (45 g/t) and a lower efficiency elution (100 g/t)

approximately 520 g/t. Eluting every second day (500 kg to elution per day), will result in an increase of the carbon loading to approximately 960 g/t, and 1500 g/t for every third day (330 kg to elution per day). It is important, however, to realize that these values were calculated by assuming that the k and K values (indicating Au adsorption) will remain constant regardless of the time the carbon spent in the circuit, and do not take into account the potential for increased carbon poisoning with time. Since the effect of carbon poisoning on the adsorption constants is currently not known, but will require a separate dedicated study, a conservative approach is recommended when decreasing the carbon advance rate. The potential cost benefit of less frequent elution for this case study is clear, however.

Figure 13 also shows the effect of elution efficiency on the differential revenue to the plant. In this case, it was assumed that whenever a less efficient elution was performed, it was due to a shorter elution cycle that used less water and energy. Figure 13b shows the impact of a shorter elution cycle on the variable cost compared to the increased tailings loss as a result of the less efficient elution. Although the impact is less than in the CIP case study, due to the CIL plant being much smaller with much reduced feed flow rates, it still shows that a high elution efficiency will be beneficial to the cost balance sheet.

Carbon concentration

The effect of carbon concentration is shown in Figure 14a. In this case, it is beneficial to increase the carbon concentration from 20 g/L to 30 g/L, where revenue reaches a plateau and any additional increase in carbon concentration will not add further value. This plateau is due to leaching and adsorption taking place concurrently in the CIL circuit. Adding more carbon to enhance adsorption while the leaching remains slow, will therefore not increase value.

Carbon profile

The actual plant carbon profile for the six tanks was reviewed. The carbon concentration in the lead tank (tank 1) was found to be consistently higher than for tank 6. An example of this profile is shown in Figure 15a. The impact of the carbon profile was modelled and the results are shown in Table VIII. Figure 15a shows the carbon profile, while Figure 15b shows the change in solution concentration.

The benefit of equal amounts of carbon per tank, as well as the swopped carbon profile, lies in the higher amount of carbon in tank 6, which prevents Au losses to the tailings. For the equal and swopped carbon profiles, a higher Au solution concentration in the first two tanks (as per Figure 15b) occurs and the risk of preg-robbing by natural carbon fines increases (the primary reason for a CIL circuit).

Conclusion

Two case studies (CIP and CIL processes) were simulated to determine the sensitivity of the plant to certain changing variables. These were combined with an economic analysis to

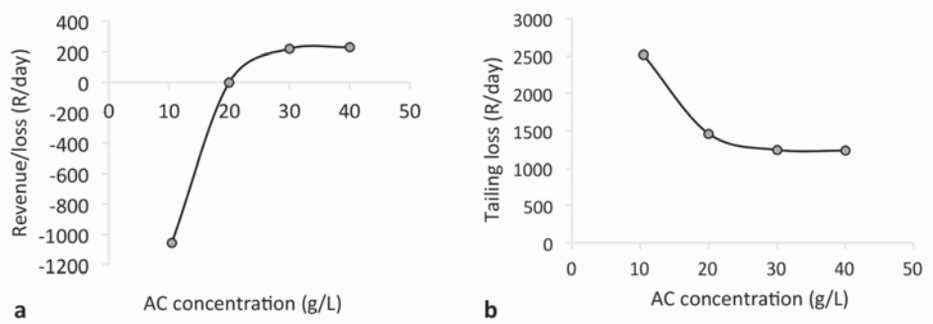

Figure 14—(a) The effect of carbon concentration on differential revenue/loss per day, and (b) Au loss to tailings

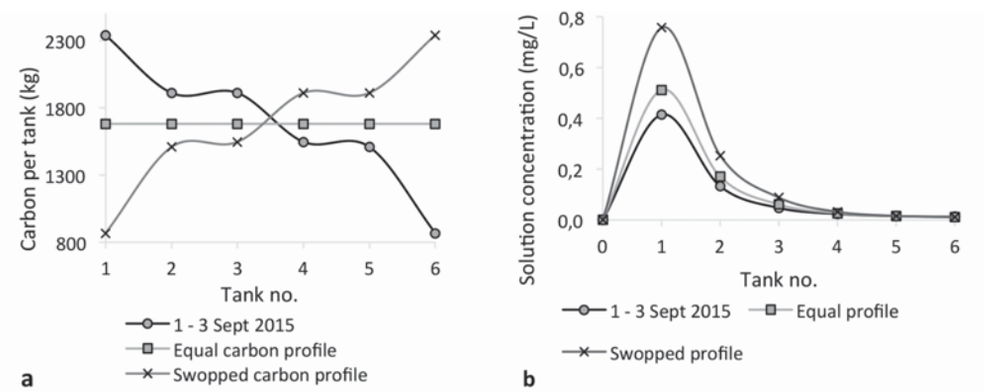

Figure 15—(a) Carbon profile for the six tanks, and (b) effect of the carbon profile on the Au solution concentration

Table VIII

Differential revenue with regard to changing the carbon profile through the six tanks

	Revenue/loss (R/day)	Revenue (R/year)
1–3 Sep 2015	R0	R0
Equal carbon profile	R228	R75 153
Swopped carbon profile	R303	R100 003

determine the operating parameters that yield the highest value. For both case studies, additional value could be realized without any additional capital requirements by adjusting the frequency of elution, carbon concentration, and the solid/liquid mass fraction of the feed. To achieve maximum value, the operating conditions need to be monitored and readjusted, if required, as they are strongly dependent on both extrinsic (commodity prices and inflation) and intrinsic factors (feed rate, gold grade, elution efficiency).

Acknowledgments

The authors would like to thank the respective plants for their assistance and provision of the plant data.

References

Baily, P.R. 1991. Adsorption plant design. *Proceedings of Recent Developments in In-Pulp Technology*, Randburg, South Africa, 7–8 October 1991. South African Institute of Mining and Metallurgy, Johannesburg.

Fleming, C.A., Mezei, A., Bourricaudy, E., Canizares, M., and Ashbury, M. 2011. Factors influencing the rate of gold cyanide leaching and adsorption, and their impact on the design of CIL and CIP circuits. *Minerals Engineering*, vol. 24, no. 6. pp. 484–494.

Nicol, M.J., Fleming, C.A., and Cromberge, G. 1984a. The adsorption of gold cyanide onto activated carbon. I. The kinetics of adsorption from pulps. *Journal of the South African Institute of Mining and Metallurgy*, vol. 84, no. 2. pp. 50–54.

Nicol, M.J., Fleming, C.A., and Cromberge, G. 1984b. The adsorption of gold cyanide onto activated carbon. II. The kinetics of adsorption from pulps. *Journal of the South African Institute of Mining and Metallurgy*, vol. 84, no. 3. pp. 70–78.

Nicol, M.J., Fleming, C.A., and Cromberge, G. 1984c. The adsorption of gold cyanide onto activated carbon. III. Factors influencing the rate of loading and the equilibrium capacity. *Journal of the South African Institute of Mining and Metallurgy*, vol. 84, no. 4. pp. 85–93.

Oladele, T.P., Snyders, C.A., and Bradshaw, S.M. 2015. The effect of temperature, contact time and agitation speed during pre-treatment on gold elution. *Proceedings of World Gold 2015*, Misty Hills, Muldersdrift, Gauteng, South Africa, 29 September – 1 October 2015. Southern African institute of Mining and Metallurgy, Johannesburg. ◆

http://dx.doi.org/10.17159/2411-9717/2017/v117n8a14

The benefits and knowledge gained in refractory testing with slag and nickel matte

by D. Gregurek*, V. Reiter*, A. Franzkowiak†, A. Spanring†, B. Drew†, C. Pichler‡, and D.R. Flynn§

Synopsis

Post-mortem studies of the lining refractories in the top-blown rotary converter (TBRC) at Stillwater Mining Company showed severe corrosion due to slag attack and high levels of sulphur. This led to a two-year collaborative project aimed at obtaining a better understanding of the wear phenomena and improving the refractory lining life in the TBRC. Initially, a complete phase chemical characterization was carried out. This was followed by FactSage™ calculations based on the slag and matte samples provided. The information from these sources fed into rotary kiln tests conducted at various process temperatures with several selected magnesia-chromite and alumina-chromia bricks in combination with a calcium ferritic slag. During the second year of the investigation a detailed test programme with nickel matte and preselected refractory brands was undertaken in the pilot TBRC at the University of Leoben, Austria. The detailed phase chemical investigation and the results and outcome of the tests are described in detail. A vital insight has been gained into the properties of a slag-matte system not previously studied. Additionally, the refractory wear trigger in the TBRC vessel has been identified, using time-lapse techniques, as the high-temperature spikes resulting from this highly exothermic desulphurization reaction. To limit refractory wear in service, the high-temperature spikes should be retarded by restricting the availability of fuel and the oxygen.

Keywords

refractories, magnesia-chromite bricks, post-mortem studies, calcium ferritic slag, nickel matte, rotary kiln, TBRC corrosion resistance test.

Introduction

In pyrometallurgy, owing to the challenges arising continuously from changing feed and the processing of more complex materials, metal producers are continuously adapting and optimizing their processes to new conditions (Davenport *et al.*, 2011; Crundwell *et al.*, 2011). In numerous cases the performance of pyrometallurgical processes is influenced by knowledge and control of the slag (Pawlek, 1983; Colclough, 1925; Sorokin *et al.*, 1994). The importance of good slag-making can be typically summed up by the old adage in smelting lore, 'look after your slag and the metal will look after itself' (Colclough, 1925). However, it is not only the plant operators who acknowledge the importance of the slag; it is also the furnace designers and refractory suppliers, who realize that knowledge of slag chemistry and the impact of the slag on the refractory are important for the optimization of refractory campaigns to improve equipment availability (Colclough, 1925; Sorokin *et al.*, 1994; Gregurek *et al.*, 2014). The detail in these ideas is discussed in this paper.

In the nonferrous metal industry, particularly in copper- and nickel-smelting furnaces, magnesia-chromite bricks are the refractory of choice because of their high corrosion resistance imparted by properties of the amphoteric species (Routschka and Wuthnow, 2012; Rigaud, 2011). Nevertheless, the refractory lining is exposed to complex wear caused by chemical, thermal, and mechanical stresses (Barthel, 1981; Gregurek and Majcenovic, 2003). Therefore an extensive understanding of the wear phenomena through post-mortem studies is an important requirement for the refractory producer, as it provides the basis for both customer recommendations and innovative product development.

RHI AG collaborates with many clients in order to achieve the optimum refractory solution for a given metal production process. The arrangement enables targeted refractory development, a better process understanding, and ultimately, lower operating costs. To achieve this goal the RHI Technology Center Leoben (TCL) in Austria combines practical corrosion-testing techniques and equipment such as an induction furnace, rotary kiln, cup tests, and drip-slag tests together with microscopic analyses followed by pilot-scale trials to arrive at a comprehensive understanding of brick wear (Gregurek *et al.*, 2013).

Throughout a two-year collaborative project between Stillwater Mining Company in the USA and RHI AG, practical tests were

* *RHI AG, Technology Center Leoben, Leoben, Austria.*

† *RHI AG, Vienna, Austria.*

‡ *CD Laboratory University of Leben, Leoben, Austria.*

§ *Stillwater Mining Company, Columbus, USA.*

 ISSN 2225-6253. Paper received Nov. 2015; revised paper received May. 2017.

carried out with different refractory types (selected magnesia-chromite and alumina-chromia bricks), utilizing 120 kg of calcium ferritic slag and 215 kg of nickel matte provided by Stillwater. The tests were conducted in a rotary kiln and in a pilot top-blown rotary converter (TBRC).

A detailed multi-stage programme was considered to be crucial to obtain a better understanding of refractory performance. The initial characterization of the slag and matte, with complete chemical and mineralogical analysis, was followed by a determination of melting points measured with a heating microscope and from thermochemical data in FactSage™. Finally, pilot-scale tests were carried out.

This paper provides an insight into the corrosion test work conducted at TCL and the value gained from post-mortem examinations.

Post-mortem investigation and analytical procedure

Generally, each post-mortem investigation starts with a visual inspection carried out on a section of the brick, followed by selection of samples for chemical analysis and phase chemical examination. The chemical analyses were carried out by X-ray fluorescence spectroscopy (XRF; Bruker S8 TIGER). The phase chemical investigation was conducted on polished sections with a reflected-light microscope and scanning electron microscopy (SEM; JEOL JSM-6460) combined with energy-dispersive and wavelength-dispersive X-ray spectrometry. Additionally slag and matte samples were investigated by X-ray diffractometry (XRD; Bruker D8 ADVANCE).

The post-mortem investigation was carried out on used refractory (magnesia-chromite brick of type 60:40) from the working lining of the TBRC at Stillwater Mining Company. The refractory life was 105 heats. The residual brick thickness was 170–180 mm. The immediate refractory hot face was slightly declined and covered with a thin coating of slag (Figure 1a). Cracks running parallel to the brick hot face could be observed.

Chemical analysis showed considerable enrichment of the refractory hot face with CaO, Fe_2O_3, NiO, and CuO (Table I). Some CoO and sulphur were also detected.

The mineralogical investigation revealed the following microstructural changes and areas (Figures 1b–1d):

- At the immediate hot face a 0–2 mm reaction layer consisting of Fe-Ni-Cr-(Mg-Co) oxide, Ni-Fe-Cu-Co-Mg oxide, and Ca-Fe oxide of the type dicalcium ferrite (C_2F) was observed (Deer, Howie, and Zussman, 1992)
- Behind this to a depth of approximately 15 mm from the hot face, the microstructure had degenerated completely and was brittle. The typical microstructure of the product containing coarse grains and fines was no longer visible, and the individual brick components could barely be distinguished. Owing to iron oxide enrichment of the magnesia component, an Mg-Fe oxide of magnesia-wüstite type had formed (Figure 1b). Chromite was heavily corroded by iron oxide (Figure 1c), a reaction resulting in the formation of Mg-Ni-Al-Cr-Fe oxide
- In the zone and area between 15–25 mm from the hot face the brick microstructure had been infiltrated by Ca-Al-Fe oxide. The oxide filled the pores. Owing to diffusion the chromite rims were enriched in iron oxide. These iron oxide-containing melts tend to equilibrate with chromite. Therefore the margins of chromite crystals already showed a higher iron content. Nevertheless, the chromite composition was not homogeneous with respect to iron content: the diffusivity of iron ions was not sufficient to achieve chemical equilibrium in the time available. Additionally, microscopic inspection showed that magnesia fines and calcium silicates acting as binder phases had been lost. Nevertheless, the reaction products were not present at the same location. Microscopic investigation of the cold end helps to explain this (see below)
- Below this, up to a depth of approximately 35 mm from the hot face, the brick microstructure was infiltrated with Cu-Fe sulphide and Ni-(Fe) sulphide
- At the refractory cold face the sulphur-based corrosion of the magnesia and the interstitial phase within the magnesia were visible. The main reaction products were Ca sulphate and Mg sulphate (Figure 1d). Obviously, sulphur attack caused the corrosion observed in the vicinity of the hot face. Melts containing Mg^{2+}, Ca^{2+}, and SO_4^{2-} percolated to the cold end, where the temperature remained above the respective invariant points. The separation of the reaction products from the reactants hindered chemical equilibrium close to the hot face. Therefore conditions for corrosion were maintained.

Figure 1e shows the virgin brick microstructure for comparison. The brick is based on fused magnesia-chromite and chromium ore.

Characterization of slag and matte

The first step prior to the experimental work was the characterization of the slag and matte samples from Stillwater Mining, which is described in the following sections.

Table I

Chemical analysis of the magnesia-chromite brick from the TBRC (wt%)

Sample	MgO	Al_2O_3	SiO_2	SO_3[1]	CaO	Cr_2O_3	Fe_2O_3[2]	NiO	CoO	CuO
Hot face (2–20 mm)	35	5	1	1	5	12	34	4	0.4	2
Unused brick	54.5	7.5	0.8		0.8	23.0	13.0			

[1]Total sulphur determined as SO_3
[2]Total iron determined as Fe_2O_3

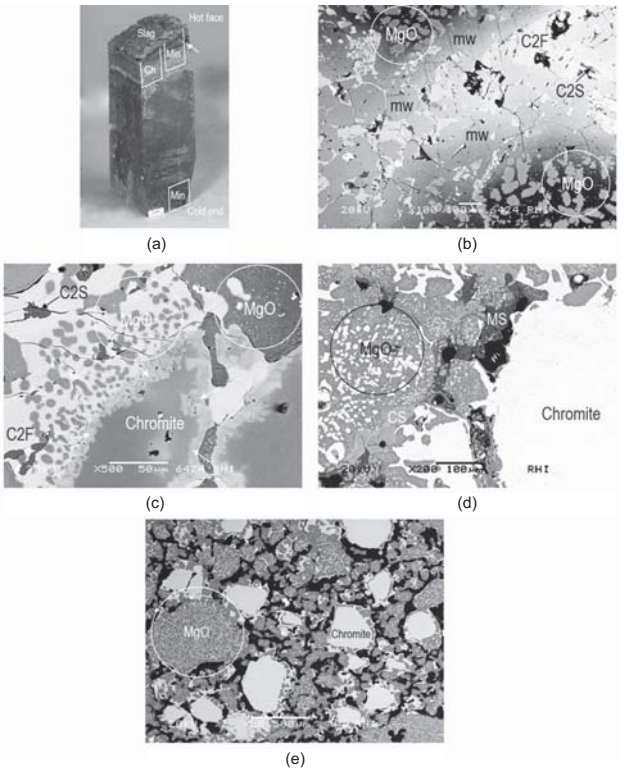

Figure 1—(a) Macroscopic view of used magnesia-chromite brick from the TBRC. Partly declined brick hot face covered with a thin coating of slag. A crack is parallel to the hot face (arrow). Samples for chemical analysis (Ch) and phase-chemical examination (Min) are indicated. (b) Microstructural detail approximately 5 mm from the hot face. Corroded magnesia-component (MgO) with the formation of magnesia-wüstite at rims (mw). Calcium ferrite (C_2F) enriched with Cr_2O_3. Dicalcium silicate (C_2S). (c) Microstructural detail approximately 10 mm from the hot face. Severe corrosion of chromite. At rims of chromite, formation of Ni-Ca-Mg-Fe-Al-Cr oxide (white arrows). (d) Microstructural detail of brick cold end. Sulphur attack of the magnesia component (MgO) and interstitial phase. Mg sulphate (MS) and Ca sulphate (CS) are the main reaction products. (e) Microstructural detail, with original brick microstructure for comparison. Magnesia component (Mg)

Slag characterization

The slag is a Ni-, Cu-, and S-rich Ca-Fe oxide (calcium ferritic-type slag – Table II). The main slag components include two different Ca-Fe oxides (one of type C_2F) and Ni-Mg-Fe-(Cr)-(Co) oxide of type magnesia-ferrite (Figures 2a and 2b).

Different Cu-(Fe)-Ni-(Pd) sulphide inclusions – predominantly Ni sulphide (Ni_3S_2, heazelwoodite), Cu sulphide (Cu_2S, chalcocite), and Pd-Pt-enriched Cu-Fe-Ni sulphide – were found in the slag. In addition to the phase chemical investigation, the melting point was determined with a heating microscope (Luidold, Schnideritsch, and Antrekowitsch, 2011). The melting temperature determined lay between 1350°C and 1410°C (measurements were carried out in air). Liquidus and solidus temperatures were estimated with the help of FactSage™ for the composition of slag and matte (Bale *et al.*, 2002). Under oxidizing conditions the calculated solidus and liquidus temperatures of slag were, respectively, 1057°C/1111°C and 1481°C/1424°C.

Matte characterization

The matte is a Ni-Cu-Fe-Co–bearing sulphide containing precious metals such as platinum and palladium (Table III). However, owing to a lack of standards and an overlap between palladium and rhodium spectra (rhodium-bearing XRF spectrometer), the exact palladium content could not be determined. Traces of Al_2O_3 and SiO_2 (<1 wt%) were also detected.

From phase chemical examination and X-ray diffractometry, we determined the main components of solid nickel matte to be Fe-Ni sulphide (pentlandite), Ni sulphide, and Cu-Fe sulphide (chalcopyrite) (Figures 2c and 2d). A Pt-

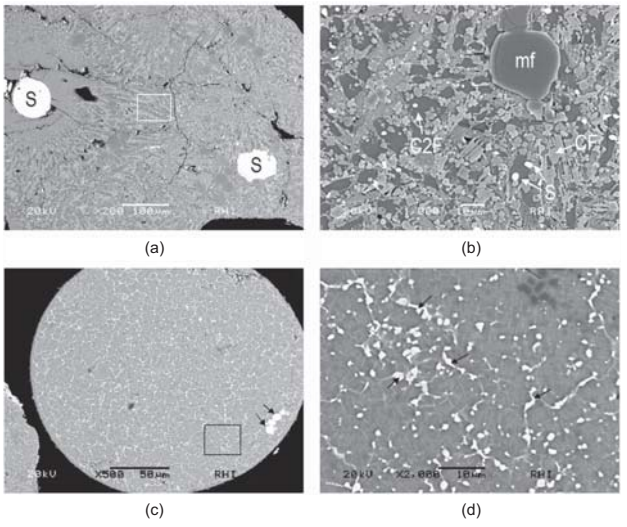

Figure 2—(a) Typical microstructural detail of granulated calcium ferritic slag with Cu-(Fe)-Ni-(Pd) sulphide inclusions (S). (b) Detail from Figure 2a. Ca-Fe oxides of type calcium ferrite (CF) and dicalcium ferrite (C2F). Ni-Mg-Fe-(Ca)-(Cr)-(Co) oxide of type magnesia-ferrite (mf). Sulphide inclusions (S). (c) Typical microstructural details of granulated matte. Pd, Pt-enriched Cu-Fe-Ni sulphide (arrows). (d) Detail from Figure 2c

Table II

Chemical analysis (by XRF) of the sample of slag from Stillwater Mining Company (wt%)

Na_2O	MgO	Al_2O_3	SiO_2	SO_3[1]	CaO	Cr_2O_3	Fe_2O_3[2]	NiO	CoO	CuO	PbO
0.3–0.8	1–2	0.5–0.6	1	5–9	15–19	0.7–0.9	48–58	8–15	0.5	4–7	0.1–0.3

[1]Total sulfur determined as SO_3
[2]Total iron determined as Fe_2O_3

Table III

Chemical analysis (by XRF) of the sample of matte from Stillwater Mining Company (wt%)

Pt	Pd*	S	Fe	Ni	Co	Cu	Zn	Pb	All_2Ol_3	CaO
0.3	–	21	30	34	0.6	13	0.1	0.3	0.6	0.6

*Could not be determined

and Pd-bearing Fe-Ni-Cu-Co-S phase was also detected. Some traces of calcium ferritc slag granules were also observed.

The phase constitution and the liquidus temperature of the matte were calculated with FactSage™ in the same way as for the slag. The FTmisc database was used for the calculations (the liquid sulphide solution was called FTmisc-MATTE). The stable solid phases were determined to be (Fe,Ni,Cu)S (pyrrhotite), $(Fe,Ni,Cu)_9S_8$ (pentlandite), (Co,Cu,Fe,Ni,Pb):Vacancy, and $(Fe,Ni_2,Cu_2)S$. These phases are solid solutions. The solidus and liquidus temperatures of the matte were calculated to be 667°C and 1132°C respectively.

Selected refractories and experimental work

Selection of refractories

Five magnesia-chromite brands (MCB1, MCB2, MCB3, MCB4, and newly developed MCB5), as well as one alumina-chromia brand (ACB1), were selected for both rotary kiln tests. The MCB1 (type MCr 50, ISO 10081-2) represents a standard direct-bonded magnesia-chromite brick consisting of fused magnesia and chrome ore. MCB2 is a high-quality, dense magnesia-chromite brick (type MCr 50, ISO 10081-2) based on magnesia-chromite co-clinker (OXICROM™ sinter) and chrome ore. MCB3 and MCB4 are also high-quality magnesia-chromite bricks (type MCr 60) based on fused magnesia-chromite and chrome ore. The newly developed MCB5 brick contains fused magnesia-chromite and has a higher Cr_2O_3 content (Type MCr 40) (Gregurek *et al.*, 2012). ACB1 is an alumina-chromia brick (type ACr 60/30, ISO 10081-4) based on chromia-corundum and chromium oxide.

Testing in the pilot TBRC was carried out with three magnesia-chromite brands (MCB4, MCB6, and MCB7). MCB6 and MCB7 (type MCr 50, ISO 10081-2) represent high-quality magnesia-chromite bricks consisting of fused magnesia-chromite and chrome ore. The MCB7 is a dense magnesia-chromite brick.

The chemical analyses of all the brick brands are listed in Table IV.

Rotary kiln tests

In the rotary kiln, with a diameter of 92 mm, up to six different brick brands were installed and tested simultaneously (Figure 3a). The furnace was heated with a propane-oxygen mixture. The first rotary kiln test with calcium ferritic slag was carried out between 1500°C and 1550°C. The second rotary kiln test was conducted at 1650°C. Temperatures higher than in the Stillwater process were chosen to simulate a process duration of several months. Both tests were carried out for 20 cycles. During testing, 1.5 kg of slag was charged to the kiln per cycle.

Pilot TBRC tests

Testing with nickel matte in the pilot TBRC, which was heated by a methane-oxygen burner, was carried out at a process temperature of approximately 1650°C (Figure 3b). This temperature was chosen because of the rotary kiln test results: it generated an identical post-mortem structure at this temperature. Oxygen was added to remove sulphur (Figure 3c). In total four trials were carried out under different sets of process parameters. The process parameters for all tests are summarized in Table V.

After reaching a process temperature of 1650°C, oxygen was introduced into the TBRC, which resulted in a significant increase in temperature (test 1). To mitigate this effect the energy was reduced by lowering the total gas flow rate to the burner. After a converting time of approximately two hours a liquid matte was tapped from the furnace.

A comparison of different refractory materials is generally based on differences in their corrosion behaviour under similar process conditions. For this purpose an additional test (test 2) was undertaken. It included the use of an off-gas analyser to provide information about desulphurization in the treated material during the oxidation step. The main variables are plotted in Figure 4. To provide oxygen for desulphurization the air ratio (λ) was varied. The value of λ defines an oxygen surplus ($\lambda > 1$) or an oxygen-deficient proportion ($\lambda < 1$) during the process.

At the starting point of the measurement ($t = 0$ minutes) all the material was charged into the furnace. After a few minutes, the first measurement with a type-S thermocouple was taken (1490°C). The temperature of the liquid bath was measured. Increasing λ resulted in a release of energy due to the reaction between sulphur and oxygen. A reduction in the

Table IV

Chemical analyses of several brands of RHI refractory used for testing (wt%)

Brand	MgO	Al_2O_3	SiO_2	CaO	Cr_2O_3	Fe_2O_3[1]	ZrO_2
MCB1	50.0	8.0	0.8	0.8	26.0	14.0	
MCB2	58.0	6.0	0.5	1.2	20.0	14.0	
MCB3	62.0	6.5	0.8	0.7	18.5	11.5	
MCB4	67.0	3.5	0.4	0.6	23.0	5.3	
MCB5	46.3	13.0	0.4	0.3	27.5	10.0	
MCB6	54.5	7.5	0.8	0.8	23.0	13.0	
MCB7	56.5	6.0	1.3	0.6	25.5	10.0	
ACB1		55.0	4.5		30.0	0.5	6.5

[1]Total iron determined as Fe_2O_3

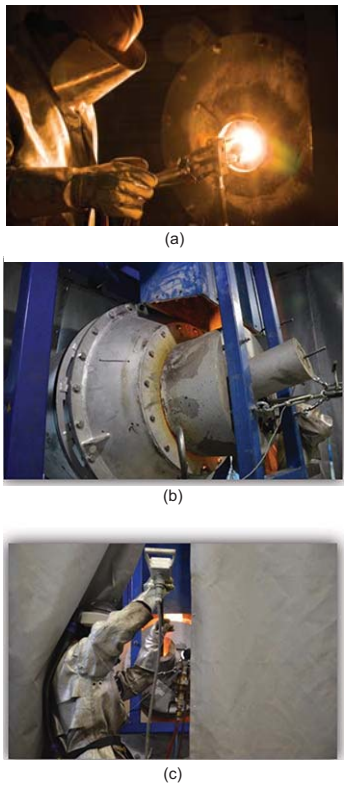

(a)

(b)

(c)

Figure 3—(a) Rotary kiln test at RHI Technology Center Leoben (TCL), during adjusting burner position after slag change. (b and c) Pilot TBRC testing at CD laboratory, University of Leoben, Austria. TBRC furnace during heating up (b) and during discontinuous temperature measurement for process control (c)

Table V

Process parameters for the pilot TBRC test

Test no.	1	2	3	4
Mass of charging matte [kg]	35	50	55	63
Temperature [°C]	1650	1650	1600	1600
λ	1–1.5	1–2	1–2.27	1.22

total gas flow rate (methane-oxygen) was used to mitigate this energy input through the exothermic oxidation of sulphur, by supplying small amounts of free oxygen.

The effect of increasing oxygen content (with constant oxygen flow though the burner) on temperature was determined after 60 minutes. This led to temperatures higher than the maximum of the thermocouple (for type-S limited to <1750°C, as shown in Figure 4). These two initial trials built the basis for the subsequent analysis of the pilot TBRC refractory lining. After trials 1 and 2, a new vessel was prepared for two additional trials with the same refractories.

The occurrence of exothermic reactions caused by the oxidizing treatment was evident in trials 3 and 4. Also evident was the stability of the refractory under process conditions. For a better comparison of different linings, the linings should be exposed to test conditions over several batches. These two trials, therefore, were consequently undertaken with the same brand of brick as used in the initial trial.

As mentioned, unlike tests 1 and 2, the subsequent trials 3 and 4 were carried out under constant temperature. In test 3, λ was varied under a constant gas flow rate, whereas in test 4 the burner capacity was varied under constant λ. With both variations the same result was achieved; nevertheless, the control of the furnace was much easier when maintaining the burner power at constant λ (Figure 5).

Results of the experimental work with slag

The macroscopic overviews of selected bricks after testing are shown in cross-section in Figure 6a–e. Two different measures are used to describe refractory performance in contact with slag, namely the area and depth for wear and infiltration respectively. The measure for wear describes the amount of refractory material that was removed during testing. The subsequent infiltration shows the area that was in contact with slag. The results from both trials, following determination of the wear area and wear depth across the final cross-sectional profile, are presented in Tables VI and VII. The main results of the phase chemical investigations are shown in Figures 7a–f.

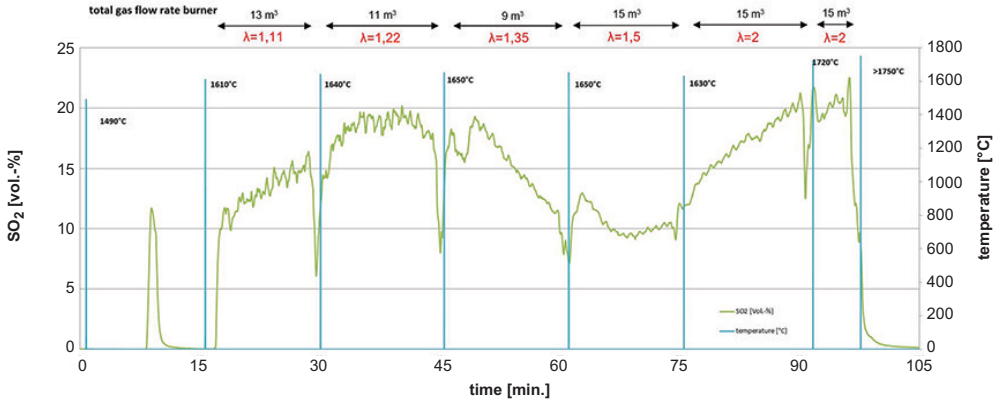

Figure 4—An example of temperature measurement during the first two TBRC tests. The temperature was continuously measured by a thermocouple in the TBRC gas room. For process control a discontinuous temperature measurement of the liquid matte was taken every 15 minutes, shown as spikes in the chart. Additionally, λ and the total gas flow rate were recorded

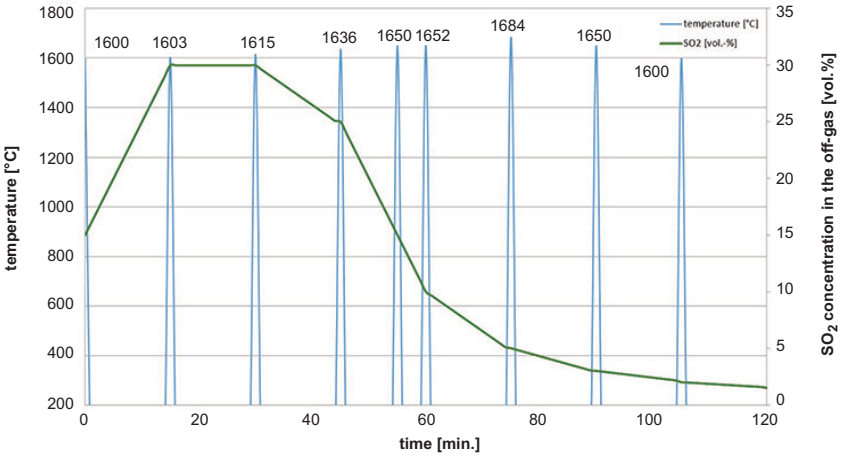

Figure 5—Example of the temperature and SO_2 content of the off-gas during tests 3 and 4. For process control the temperature of the liquid matte was measured (discontinuously) every 15 minutes, shown as spikes in the diagram

Table VI

Extent of wear and corrosion in the rotary kiln test (trial at 1500°–1550°C)

Brick brand	Wear area* (cm^2)	Wear depth* (mm)	Infiltration area* (cm^2)	Infiltration depth* (mm)
MCB1	2	4	54	28
MCB2	2	3	41	20
MCB3	0	0	43	21
MCB4	0	0	38	20
MCB5	0	0	46	24
ACB1	65(1)	5(1)	94	>20

*Based on macroscopic wear evaluation from the final cross-sectional profile
(1)Not representative due to high thermal shock

Table VII

Extent of wear and corrosion in the rotary kiln test (trial at 1650°C)

Brick brand	Wear area* (cm^2)	Wear depth* (mm)	Infiltration area* (cm^2)	Infiltration depth* (mm)
MCB1	25	22	104	50
MCB2	15	14	94	46
MCB3	20	18	94	47
MCB4	10	12	85	45
MCB5	24	21	105	56
MCB6	15	14	94	44

•Based on macroscopic wear evaluation from the final cross-sectional profile

Rotary kiln test at 1500–1550°C

All brick samples tested showed cracks caused by thermal shock during kiln operation. In the magnesia-chromite brick brands, either minimal or no wear was visible (Table VI). The greatest infiltration depth was identified in MCB1. The high wear observed for the alumina-chromia brick ACB1 can be explained by crack formation caused by thermal shock from the initial testing and subsequent loss of refractory

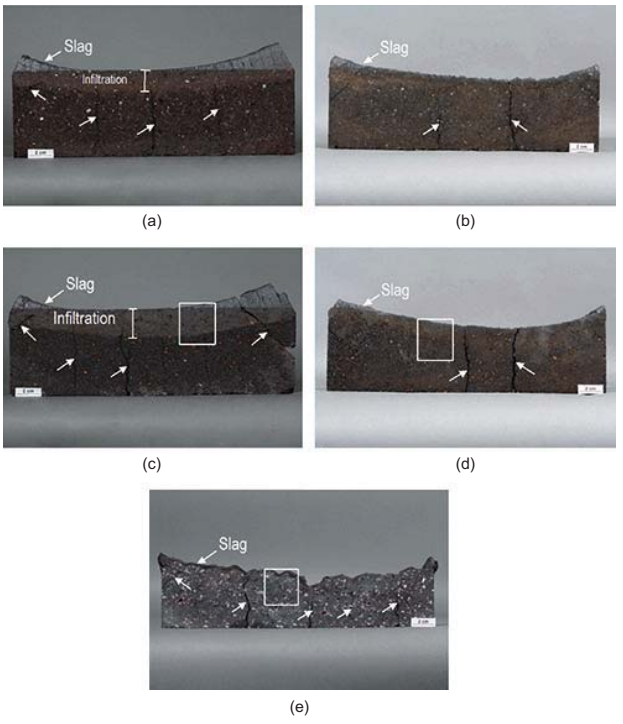

Figure 6—Cross-sectional view of selected magnesia-chromite MCB4 (a, b), MCB1 (c, d), and alumina-chromia ACB1 (e) bricks after the rotary kiln test at 1500–1550°C (left side: a, c, e) and 1650°C (right side: b, d). A slag coating covers the immediate brick hot face. Crack formations are indicated with white arrows. Polished sections were prepared from the portions indicated by white rectangles

The main microstructural changes to the magnesia-chromite bricks investigated, after the rotary kiln test, are summarized below (for example MCB1, see Figures 7a and 7b).

The immediate brick hot face was covered with a 1–2 mm thick reaction zone. Within this area the magnesia component was completely dissolved. Only some chromite relics were still visible. Below the reaction zone a deep-reaching infiltration by calcium ferrite and corrosion of the brick microstructure was observed.

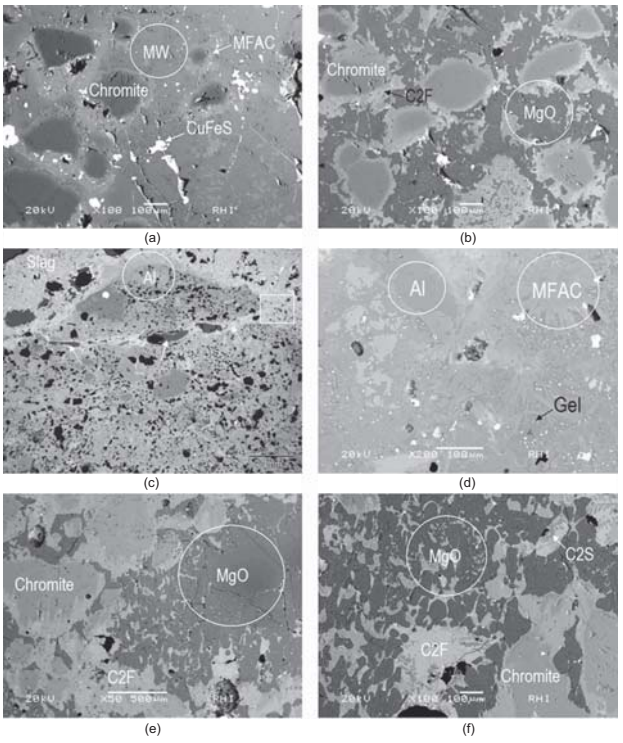

Figure 7a–b—Microstructural details in the magnesia-chromite brick MCB1 after the rotary kiln test at 1500–1550°C, approximately 2 mm (a) and 10 mm (b) from hot face. Severe corrosion and degeneration of the brick microstructure. Corroded magnesia (MgO) and chromite. Formation of Ni–rich magnesia-wüstite, (Ni)-Fe-Mg oxide (MW), Mg-Fe-Al-Cr oxide of spinel structure (MFAC), calcium ferrite (C_2F) enriched with Cr_2O_3, and CuFeS from matte infiltration. Figure 7c–d Microstructural details of the alumina-chromia brick ACB1 after the rotary kiln test at 1500–1550°C. (c) Immediate brick hot face. Below the slag coating, infiltrated and corroded brick microstructure was observed. The crack that formed parallel to the hot face is partly filled with slag (arrows). Corroded fused alumina (Al). (d) Detail from Figure 7c, showing degenerated, recrystallized, and infiltrated brick microstructure. Mg-Fe-Al-Cr oxide of spinel structure (MFAC). The Ca-Al silicate is gehlenite, $Ca_2Al_2SiO_7$ (Gel). Figure 7e–f Microstructural details of the magnesia-chromite brick MCB1 after rotary kiln test at 1650°C. Corrosion of the magnesia and chromite was significantly higher than in the first rotary kiln test at 1500–1550°C. Corroded MgO and chromite. Calcium ferrite (C_2F) enriched with Cr_2O_3. Dicalcium silicate (C_2S)

In the infiltrated and completely degenerated brick microstructure (0–5 mm from the hot face) the single brick components could no longer be distinguished. The high supply of Fe oxide resulted in the formation of a low-melting Ni-rich magnesia-wüstite ([Ni]-Fe-Mg oxide). The chromite and chromite precipitates (Routschka and Wuthnow, 2012) were corroded. Owing to the corrosion of chromite, (Ca)-Mg-Fe-Al-Cr oxide and (Ca)-Fe-Cr-Al oxide of spinel structure formed. In Figure 7a the brick is partly infiltrated by matte.

In the case of the alumina-chromia brick ACB1 (Figures 7c–d), infiltration of the microstructure can be traced over the entire polished section (0–20 mm from the hot face). Nevertheless, the greatest microstructural changes were observed in the area 0–2 mm from the hot face. In that area of the brick, pore-filling infiltration, recrystallization of a Cr-corundum–bearing matrix, corrosion of a Zr mullite, and the formation of Mg-Fe-Al-Cr oxide and (Na)-Ca-Al silicate of type gehlenite ($Ca_2Al_2SiO_7$) took place. The immediate hot face was covered with a 1–2 mm thick reaction zone. In the infiltrated brick microstructure, cracks formed parallel to, but also vertical to, the hot face. These cracks were partly filled with slag.

Rotary kiln test at 1650°C

Owing to the high wear observed during the test, the alumina-chromia brick ACB1 was replaced by magnesia-chromite brick MCB6. Compared with the first rotary kiln test, the refractory wear and the infiltration depth for all bricks were significantly higher (Table VII). In cross-section, the greatest wear was observed for MCB1/MCB5 and the lowest for MCB2.

Phase chemical investigation revealed the brick microstructure in MCB1 to be highly degenerated, especially between 0–20 mm from the hot face. Infiltration, corrosion of both brick components (magnesia and chromite), and the formation of a low-melting Cu-Ni-rich magnesia-wüstite were observed after the second rotary kiln test (Figures 7e and 7f). Nevertheless, the microstructural changes were much more distinctive than those in the first rotary kiln test at 1500–1550°C. The chromite rims were highly enriched in Fe oxide and Ni oxide (Figure 8). Additionally, owing to the decomposition and oxidation of Cu-Fe-Ni sulphide, sulphur attack and formation of sulphur-bearing phases could be observed at the end of infiltration.

Thermodynamic calculations

The interactions of different combinations of refractory materials with the calcium ferritic slag can be described thermodynamically in respect of the potential reaction products formed at the interface and the solubility of the refractory components in the slag.

The calculations were run in FactSage™ for temperatures of 1550°C and 1650°C under oxidizing conditions. The phase constitution of a system was calculated under the assumption that the defined elements or compounds of the system react entirely or partially to reach a state of chemical equilibrium. Reaction kinetics were not considered in the thermochemical calculations.

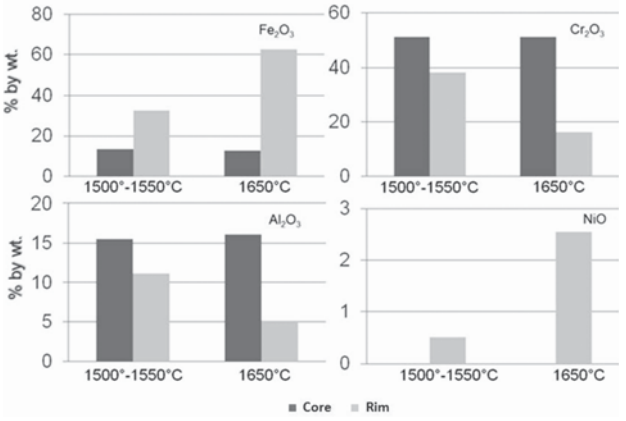

Figure 8—Magnesia-chromite brick MCB1. Significant differences in the chemical composition of chromite at the rim and core at two different test temperatures

The equilibrium phases and phase compositions were determined on the basis of the refractory-slag ratio. For this purpose a variable <*A*> was introduced, which is defined as the mass ratio of refractory material to the total mass of refractory plus slag. <*A*> = 0 describes the composition of a slag not in contact with refractory, and <*A*> = 100 describes the composition of a refractory that is not in contact with slag.

The slag amount as a function of <*A*> was compared for the different refractory bricks (see Figures 9a and 9b) at 1550°C and 1650°C. The alumina-chromia brick showed a considerably higher solubility than the magnesia-chromite brands. The refractories can be ranked according to solubility, which increases in the order:

MCB4 < MCB5 < MCB3 < MCB1 < MCB2

Of the magnesia-chromite bricks investigated, the MCB4 brick shows the lowest solubility. However, the difference in solubility between the various brands, with the exception of MCB2, is small.

Results of the experimental work with matte

During the first two tests in the pilot TBRC none of the tested magnesia-chromite brick brands showed wear. In cross-section, the deeply infiltrated brick microstructure over the whole cross-section (approx. 60 mm from the hot face) was visible (Table VIII). Only in the case of brick MCB6 was the infiltration depth 47 mm from the hot face (Figure 10a).

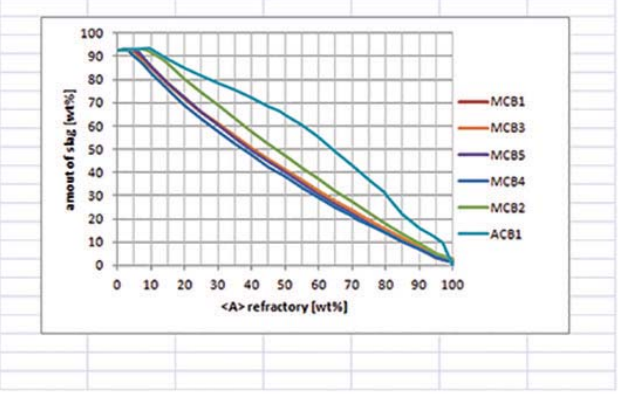

(a)

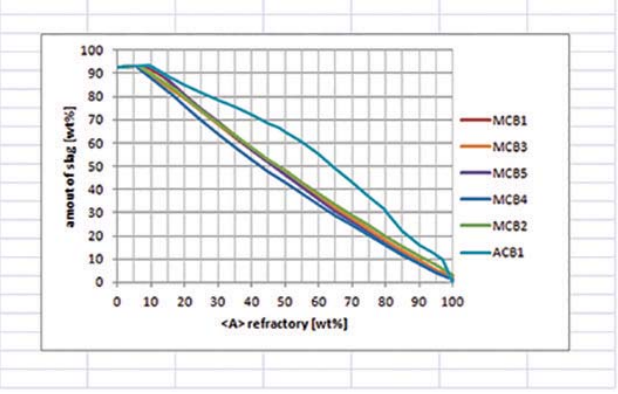

(b)

Figure 9—FactSage™ calculations of slag amounts at 1550°C (a) and 1650°C (b)

Table VIII

Results of the first two TBRC tests at 1650°C

Brick brand	Wear area* (cm^2)	Wear depth* (mm)	Infiltration area* (cm^2)	Infiltration depth* (mm)
MCB4	–	–	142–196	60
MCB6	–	–	128–172	47
MCB7	–	–	153–201	60

*Based on macroscopic wear evaluation from the final cross-sectional profile

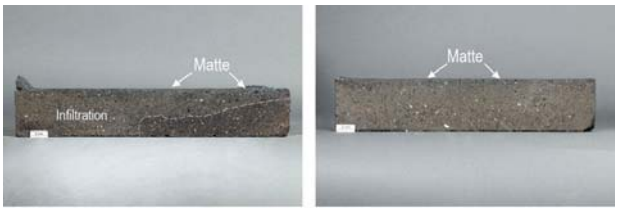

(a) (a)

Figure 10—Cross-sectional view of selected magnesia-chromite brick MCB6 after TBRC trials 1 and 2 (a), and 3 and 4 (b). Matte coating covering the immediate brick hot face

After tests 3 and 4, all tested magnesia-chromite bricks showed almost no wear, although a deep-reaching infiltration of the brick microstructure over the complete cross-section (Figure 10b) was observed.

Owing to similar wear behaviour in all trials, the main microstructural changes can be summarized as follows.

- All samples showed a thin reaction zone (0–2 mm from the hot face). Within this zone a strongly degenerated and recrystallized brick microstructure was visible. The coarse grains and the matrix fines in the brick could no longer be distinguished. The magnesia component was highly enriched in Fe oxide and Ni oxide. The chromite precipitates and the rims of chromite grains were also enriched in these oxides
- Below the reaction zone a deeply infiltrated brick microstructure could be observed. The main infiltrate was a (Cu)-Fe-Ni–bearing sulphide (Figure 11a)
- During the first two tests, the corrosion of magnesia by sulphur was minimal
- During the final two tests (3 and 4), the corrosion of magnesia fines and the coarse magnesia grains by sulphur was significant. Idiomorphic and newly precipitated MgO crystals and Ca sulphate were also observed (Figure 11b).

Summary and conclusions

The post-mortem studies carried out on refractories in the TBRC at Stillwater Mining Company showed the following features.

- Aggressive chemical attack due to calcium ferritic slag. The attack manifests as a deep-reaching infiltration of the brick microstructure and corrosion of brick components, virgin magnesia, and chromite

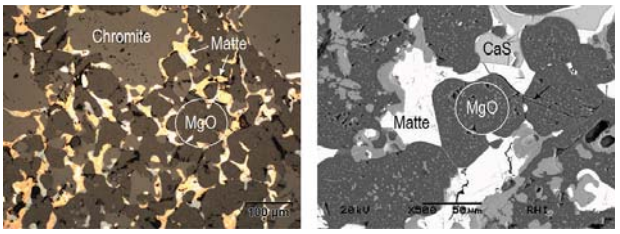

(a) (b)

Figure 11—Typical microstructural details of MCB6 after trials 3 and 4. Reflected-light microscopy (a) and scanning electron microscopy (b). Approximately 10 mm from the hot face. Infiltrated and corroded brick microstructure, showing corroded magnesia component (MgO), mickel matte,.and idiomorphic Ca sulphate (CS)

- Such a degenerated brick and brittle microstructure is highly susceptible to crack formation and spalling, especially in the case of frequent thermal shocks typical of TBRC operation.

These phenomena lead to decreased refractory performance and lifetime.

The chemical characterization of slag and matte, particularly the determination of the melting points, was important for experimental work.

The following observations can be summarized from the from both rotary kiln tests.

- There was significantly higher wear and infiltration of the brick microstructure at 1650°C for the same number of cycles. The lowest wear and infiltration, especially at 1650°C, was displayed by the MCB4 brick
- There was sulphur attack and the formation of sulphur-bearing phases at the limit of infiltration owing to the decomposition and oxidation of Cu-Fe-Ni sulphide
- As in the post-mortem study, there was severe degeneration of the brick microstructure due to chemical attack by the calcium ferritic slag. The microstructural changes were more distinctive than those in the first rotary kiln test at 1500–1550°C, which led to the chosen TBRC temperature
- Compared with the magnesia-chromite bricks, the alumina-chromia brick ACB1 showed significantly higher wear due to thermal shock
- FactSage™ showed that magnesia-chromite bricks withstand the calcium ferritic slag better than the alumina-chromia brick in respect of the solubility of refractory in the slag.

The main results of four pilot TBRC tests carried out with nickel matte can be summarized as follows.

- Unlike the refractory in the rotary kiln tests, there was no macroscopically visible wear due to hot erosion. Nevertheless, during tests 3 and 4 complete infiltration of the brick microstructure by matte occurred
- All tested magnesia-chromite bricks showed similar and deep-reaching infiltration of the brick microstructure over the whole cross-section (0–60 mm from the hot face). During the first two trials, only the MCB6 brick showed slightly lower infiltration depths
- In the first 2 mm beneath the hot face, the brick microstructure was strongly recrystallized. This resulted from the massive supply of Fe-Ni oxide caused by the oxidation of the nickel matte. This microstructural degeneration is similar to that seen in the rotary kiln test
- During the first two tests, the expected sulphur attack from the oxidation of nickel matte did not occur
- During tests 3 and 4, a significantly more aggressive sulphur attack in the infiltrated brick microstructure was observed
- The most important issue during the pilot TBRC test work was the exceptionally rapid rise in temperature due to the exothermic reaction caused by SO_2 formation.

To replicate accurately the refractory wear mechanisms in the multi-stage production process, a dual test programme utilizing both a rotary kiln and a TBRC was required. The evaluation of the simulated process samples in the multi-stage production showed identical features on the macro and micro scales to those seen in the initial post-mortem evaluation, thereby validating the original findings.

A vital insight has been gained into the properties of a slag-matte system not previously studied. Additionally, the refractory wear trigger has been identified in the TBRC vessel, using time-lapse techniques, as the high-temperature spikes resulting from this highly exothermic desulphurization reaction. To limit refractory wear in service, the high-temperature spikes should be retarded by restricting the availability of fuel and oxygen required to maintain this highly exothermic reaction.

The recommendations from this work have been implemented by the client, and the advantages are already apparent. The development of compatible refractory materials for this matte-slag system enabled client-oriented and tailor-made refractory solutions to be implemented that promoted smooth and efficient operations with increased campaign life.

References

Bale, C.W., Bélisle, E., Chartrand, P., Decterov, S.A., Eriksson, G., Hack, K., Jung, I.-H., Kang Y.-B., Melançon, J., Pelton, A.D., Robelin, C., and Petersen, S. 2002. FactSage thermochemical software and databases – recent developments. *Calphad*, vol. 33, no. 2. pp. 295–311.

Barthel, H. 1981. Wear of chrome magnesite bricks in copper smelting furnaces. *Interceram*, vol. 30. pp. 250–255.

Colclough, T.P. 1925. A study of the reactions of the basic open-hearth furnace. *Transactions of the Faraday Society*, vol. 21. pp. 202–223.

Crundwell, F.K., Moats, M.S., Ramachandran, V., Robinson, T.G., and Davenport, W.G. 2011. Extractive Metallurgy of Nickel, Cobalt and Platinum-Group Metals. Elsevier, Oxford. pp. 147–158.

Davenport, W.G., King, M., Schlesinger, M., and Biswas, A.K. 2011. Extractive Metallurgy of Copper. Elsevier, Oxford.

Deer, W.A., Howie, R.A., and Zussman, J. 1992. An Introduction to the Rock-Forming Minerals. 2nd edn. Pearson Education, Essex. 3–15 pp.

Gregurek, D. and Majcenovic, C. 2003. Wear mechanism of basic brick linings in the nonferrous metals industry – Case studies from copper smelting furnaces, *RHI Bulletin*, vol. 1. pp. 17–21.

Gregurek, D., Ressler, A., Reiter, V., Franzkowiak, A., Spanring, A., and Prietl, T. 2013. Refractory wear mechanisms in the nonferrous metal industry: Testing and modeling results. *Journal of Metals*, vol. 65, no. 11. pp. 1622–1630.

Gregurek, D., Spanring, A., Ressler, A., and Breyner S. 2012. High performance brands for the nonferrous metals industry. *Proceedings of the International Smelting Symposium*, Orlando, Florida, 11–15 March, The Minerals, Metals & Materials Society, Warrendale, PA. pp. 39–46.

Gregurek, D., Wenzl, C., Reiter, V., Studnicka, H.L., and Spanring, A. 2014. Slag characterization: A necessary tool for modelling and simulating refractory corrosion on a pilot scale. *Journal of Metals*, vol. 66, no. 9. pp. 1677–1686.

Luidold, S., Schnideritsch, H., and Antrekowitsch, H. 2011. Schmelzmetallurgische Beurteilung von nichteisen-metallhältigen Schlacken (Melt metallurgical assessment of non ferrous slag). *Berg- und Huettenmännische Monatshefte*, vol. 156, no. 1. pp. 1–5.

Pawlek, F. 1983. Metallhüttenkunde. Walter de Gruyter, Berlin.

Rigaud, M. 2011. Corrosion of refractories and ceramics. *Uhlig`s Corrosion Handbook*. 3rd edn. Revie, R.W. (ed.). Wiley, Hoboken, NJ. pp. 387–398.

Routschka, G. and Wuthnow, H. 2012. Handbook of Refractory Materials. 4th edn. Vulkan-Verlag, Essen.

Sorokin, M.L., Bystrov, V.P., Nikolaev, A.G., and Komkov, A.A. 1994. Thermodynamic of nickel matte converting. *Proceedings of a Symposium sponsored by the Extraction and Processing Divison Pyrometallurgical Committee*, San Francisco, California, 27 February–3 March. The Minerals, Metals & Materials Society, Warrendale, PA. pp. 59–69.

Conference Announcement

science & technology
Department:
Science and Technology
REPUBLIC OF SOUTH AFRICA

advanced metals initiative

SAIMM
THE SOUTHERN AFRICAN INSTITUTE OF MINING AND METALLURGY

AMI Precious Metals 2017

THE PRECIOUS METALS DEVELOPMENT NETWORK (PMDN)

3 ECSA CPD points will be allocated to all attending delegates

In Association with **Platinum 2017**

17–19 October 2017 —Conference
20 October 2017— Technical Visits

Protea Hotel Ranch Resort, Polokwane, South Africa

BACKGROUND

The Precious metals Development Network (PMDN) of the DST's advanced metals initiative (AMI) programme will host the AMI's annual conference in 2017.

The AMI Precious Metals 2017 Conference will be held in association with the Platinum 2017 Conference. The Platinum conference series has covered a range of themes since inception in 2004, and traditionally addresses the opportunities and challenges facing the platinum Industry.

This AMI Precious Metals 2017 Conference will present a forum where scientists and technologists can come together to learn and discuss the latest advances in precious metals (platinum group metals and gold) science and technology, under the broad themes of:

- Catalysis
- Materials
- Chemistry

OBJECTIVES

- To bring together researchers, industry and government stakeholders to share and debate the latest trends, research and innovtion in the precious metals field.
- To provide a forum for researchers and industry to present progress made over the past few years on precious metal R&D and applications.
- To promote the activities of the AMI's PMDN.
- To network and share information.

WHO SHOULD ATTEND

- Platinum group metals and gold mining houses
- Precious metal industrial players
- Government departments
- Science Councils
- Higher Educational Institutes
- Anyone involved or interested in precious metals' R&D

EXHIBITION/SPONSORSHIP

Sponsorship opportunities are available. Companies wishing to sponsor or exhibit should contact the Conference Co-ordinator.

For further information contact:
Head of Conferencing, Camielah Jardine
SAIMM, P O Box 61127, Marshalltown 2107
Tel: +27 11 834-1273/7 ·Fax: +27 11 833-8156 or +27 11 838-5923
E-mail: camielah@saimm.co.za · Website: http://www.saimm.co.za

MINTEK
Specialists in mineral and metallurgical technology

necsa
We're in your world

CSIR
our future through science

The Southern African Institute of Mining and Metallurgy are hosting the

7th International Platinum Conference

'Platinum— A Changing Industry'

In Association with AMI Precious Metals 2017

18–19 October 2017 — Conference • 20 October — Technical Tours

Protea Hotel Ranch Resort, Polokwane, South Africa

BACKGROUND

The 7th International Platinum Conference is to be held in Polokwane, Limpopo, South Africa in October 2017.

The Platinum conference series has covered a range of themes since inception in 2004, and traditionally addresses the opportunities and challenges facing the platinum Industry. This prestigious event attracts key role players and industry leaders through:

- High quality technical papers and presentations
- Facilitating industry networking
- Having large, knowledgeable audiences
- Global participation, and
- Comprehensive support from industry role players.

The Platinum 2017 Conference will be held in association with the Precious Metals Development Network (PMDN) of the DST's Advanced Metals initiative (AMI Conference 2017)

Thie AMI conference presents a forum where scientists and technologists can come together to learn and discuss the latest advances in precious metals (platinum group metals and gold) science and technology.

The 2017 event will, under the guidance of the organising committee, structure a programme which covers critical aspects of this continually evolving and exciting industry.

However the success and relevance of this event to the industry really depends on your participation and support. You can participate in this event as an organising committee member, author/presenter, delegate or sponsor.

We look forward to your support and engagement in the 7th International Platinum Conference.

Thank you.

Dr Gordon Smith
Chair—Organising Committee

ABOUT THE VENUE

The Protea Hotel Ranch Resort Polokwane, on the Eastern Limb of the Southern African Bushveld is the exciting new venue for the 2017 Platinum Conference. Polokwane is the capital city and urban heartbeat of Limpopo, known as the gateway city as it is a stepping stone to a diversity of natural attractions from mountains to wilderness areas. The city is in close proximity to a number of Platinum operations allowing for multiple technical visits.

WHO SHOULD ATTEND

- Academics
- Business development managers
- Concentrator managers
- Consultants
- Engineers
- Exploration managers
- Explosives engineers
- Fund managers
- Geologists
- Hydrogeologists
- Innovation managers
- Investment managers
- Market researchers and surveyors
- Marketing managers
- Mechanical engineers
- Metallurgical managers
- Metallurgical consultants
- Metallurgists
- Mine managers
- Mining engineers
- New business development managers
- Planning managers
- Process engineers
- Product developers
- Production managers
- Project managers
- Pyrometallurgists
- Researchers
- Rock engineers
- Scientists
- Strategy analysts
- Ventilation managers

Sponsor

bme · CiDRA Minerals Processing · ERIEZ · FLSmidth · Murray & Roberts · Murray & Roberts Cementation · RHI · SANDVIK

FOR FURTHER INFORMATION CONTACT:
Conference Co-ordinator: Gugulethu Charlie
E-mail: gugu@saimm.co.za • **Tel:** +27 11 834 1273/7 • **www.saimm.co.za**

SAIMM The Southern African Institute of Mining and Metallurgy

ami advanced metals initiative

NATIONAL & INTERNATIONAL ACTIVITIES

2017

15–16 August 2017 —**The SAMREC and SAMVAL Codes**
Advanced Workshop: Can you face your peers?
Emperors Palace, Hotel Casino Convention Resort, Johannesburg
Contact: Gugulethu Charlie
Tel: +27 11 834-1273/7, Fax: +27 11 838-5923/833-8156
E-mail: gugu@saimm.co.za, Website: http://www.saimm.co.za

22–24 August 2017 — **The biennial Southern African Coal Processing Society Conference and Exhibition**
'Coal Processing – the key to profitability'
Graceland Hotel, Casino and Country Club, Secunda
Contact: Gerda Craddock
Tel: +27 11 432-8918, E-mail: gerdac@mineralconcepts.co.za
Website: www.sacoalprep.co.za

30 August–1 September 2017 — **MINESafe Conference 2017**
Striving for Zero Harm—Driving Excellence through Compliance
Emperors Palace, Hotel Casino Convention Resort, Johannesburg
Contact: Camielah Jardine
Tel: +27 11 834-1273/7, Fax: +27 11 838-5923/833-8156
E-mail: camielah@saimm.co.za, Website: http://www.saimm.co.za

11–15 September 2017 — **Uranium 2017 International Conference**
Extraction and Applications of Uranium — Present and Future
Swakopmund Hotel, Swakopmund, Namibia
Contact: Camielah Jardine
Tel: +27 11 834-1273/7, Fax: +27 11 838-5923/833-8156
E-mail: camielah@saimm.co.za, Website: http://www.saimm.co.za

20–21 September 2017 — **Global Mining Standards and Guidelines Group (GMSG)**
Creating community to drive operational excellence
Emperors Palace, Hotel Casino Convention Resort, Johannesburg
Contact: Gugulethu Charlie
Tel: +27 11 834-1273/7, Fax: +27 11 838-5923/833-8156
E-mail: gugu@saimm.co.za, Website: http://www.saimm.co.za

30 September–6 October 2017 — **AfriRock 2017: ISRM International Symposium**—*Rock Mechanics for Africa*
Cape Town Convention Centre, Cape Town
Contact: Camielah Jardine
Tel: +27 11 834-1273/7, Fax: +27 11 838-5923/833-8156
E-mail: camielah@saimm.co.za, Website: http://www.saimm.co.za

2 October 2017 — **One-DayShort Course**
Empirical methods, rock mechanics, and structural geological methods useful for excavation in jointed/fractured media
Cape Town Convention Centre
Contact: Camielah Jardine
Tel: +27 11 834-1273/7, Fax: +27 11 838-5923/833-8156
E-mail: camielah@saimm.co.za, Website: http://www.saimm.co.za

17–20 October 2017 — **AMI Precious Metals 2017**
The Precious Metals Development Network (PMDN)
Protea Hotel Ranch Resort, Polokwane
Contact: Camielah Jardine
Tel: +27 11 834-1273/7, Fax: +27 11 838-5923/833-8156
E-mail: camielah@saimm.co.za, Website: http://www.saimm.co.za

18–20 October 2017 — **7th International Platinum Conference**
Platinum—A Changing Industry
Protea Hotel Ranch Resort, Polokwane
Contact: Gugulethu Charlie
Tel: +27 11 834-1273/7, Fax: +27 11 838-5923/833-8156
E-mail: gugu@saimm.co.za, Website: http://www.saimm.co.za

25 October 2017 — **14th Annual Student Colloquium**
Johannesburg
Contact: Gugulethu Charlie
Tel: +27 11 834-1273/7, Fax: +27 11 838-5923/833-8156
E-mail: gugu@saimm.co.za, Website: http://www.saimm.co.za

6–7 November 2017 — **Coal Preparation Society of India**
5 International Conference & Exhibition
'Coal Washing: a sustainable approach towards a greener environment'
Silver Oak Hall, India Habitat Centre, Lodhi Road,
New Delhi-110003, www.cpsi.org.in

2018

25–28 February 2018 — **Infacon XV: International Ferro-Alloys Congress**
Century City Conference Centre and Hotel, Cape Town, South Africa
Contact: Gugulethu Charlie
Tel: +27 11 834-1273/7, Fax: +27 11 838-5923/833-8156
E-mail: gugu@saimm.co.za, Website: http://www.saimm.co.za

12–14 March 2018 — **Society of Mining Professors 6th Regional Conference 2018**
Overcoming challenges in the Mining Industry through sustainable mining practices
Birchwood Hotel and Conference Centre, Johannesburg, South Africa
Contact: Camielah Jardine
Tel: +27 11 834-1273/7, Fax: +27 11 838-5923/833-8156
E-mail: camielah@saimm.co.za, Website: http://www.saimm.co.za

11–14 June 2018 — **SAIMM: Diamonds — Source to Use 2018 Conference**
Birchwood Conference Centre (Jet Park)
Contact: Camielah Jardine
Tel: +27 11 834-1273/7, Fax: +27 11 838-5923/833-8156
E-mail: camielah@saimm.co.za, Website: http://www.saimm.co.za

8–11 July 2018 — **Copper Cobalt Africa In Association with The 9TH Southern African Base Metals Conference**
Avani Victoria Falls Resort, Livingstone, Zambia
Contact: Gugulethu Charlie
Tel: +27 11 834-1273/7, Fax: +27 11 838-5923/833-8156
E-mail: gugu@saimm.co.za, Website: http://www.saimm.co.za

15–17 October 2018 — **Furnace Tapping 2018 Conference**
Nombolo Mdhluli Conference Centre, Kruger National Park, South Africa
Contact: Gugulethu Charlie
Tel: +27 11 834-1273/7, Fax: +27 11 838-5923/833-8156
E-mail: gugu@saimm.co.za, Website: http://www.saimm.co.za

Company Affiliates

The following organizations have been admitted to the Institute as Company Affiliates

3M South Africa (Pty) Limited
AECOM SA (Pty) Ltd
AEL Mining Services Limited
Air Liquide (PTY) Ltd
AMEC Foster Wheeler
AMIRA International Africa (Pty) Ltd
ANDRITZ Delkor(pty) Ltd
Anglo Operations (Pty) Ltd
Anglo Operations Proprietary Limited
Anglogold Ashanti Ltd
Arcus Gibb (Pty) Ltd
Atlas Copco (SA) (Pty) Limited
Aurecon South Africa (Pty) Ltd
Aveng Engineering
Aveng Mining Shafts and Underground
Axis House Pty Ltd
Bafokeng Rasimone Platinum Mine
Barloworld Equipment -Mining
BASF Holdings SA (Pty) Ltd
BCL Limited (BCL001)
Becker Mining (Pty) Ltd
BedRock Mining Support Pty Ltd
Bell Equipment Limited
BHP Billiton Energy Coal SA Ltd
Blue Cube Systems (Pty) Ltd
Bluhm Burton Engineering Pty Ltd(BLU003)
Bouygues Travaux Publics
CDM Group
CGG Services SA
Chamber of Mines
Concor Opencast Mining
Concor Technicrete
Council for Geoscience Library
CRONIMET Mining Processing SA Pty Ltd
CSIR Natural Resources and the Environment (NRE)
Data Mine SA
Department of Water Affairs and Forestry
Digby Wells and Associates
DMS Powers
DRA Mineral Projects (Pty) Ltd
Duraset
Elbroc Mining Products (Pty) Ltd
eThekwini Municipality
Expectra 2004 (Pty) Ltd
Exxaro Coal (Pty) Ltd
Exxaro Resources Limited
Filtaquip (Pty) Ltd
FLSmidth Minerals (Pty) Ltd (FFE001)
Fluor Daniel SA (Pty) Ltd
Franki Africa (Pty) Ltd-JHB
Fraser Alexander (Pty) Ltd
Geobrugg Southern Africa (Pty) Ltd
Glencore
Hall Core Drilling (Pty) Ltd
Hatch (Pty) Ltd
Herrenknecht AG
HPE Hydro Power Equipment (Pty) Ltd
Impala Platinum Limited
IMS Engineering (Pty) Ltd
Ivanhoe Mines SA
Joy Global Inc.(Africa)
Kudumane Manganese Resources
Leco Africa (Pty) Limited
Longyear South Africa (Pty) Ltd
Lonmin Plc
Lull Storm Trading (Pty) Ltd
Magnetech Pty Ltd
Magotteaux (Pty) Ltd
MBE Minerals SA Pty Ltd
MCC Contracts (Pty) Ltd
MD Mineral Technologies SA (Pty) Ltd
MDM Technical Africa (Pty) Ltd
Metalock Engineering RSA (Pty)Ltd
Metorex Limited
Metso Minerals (South Africa) Pty Ltd
Minerals Operations Executive (Pty) Ltd
MineRP Holding (Pty) Ltd
Mintek
MIP Process Technologies (Pty) Limited
Modular Mining Systems Africa (Pty) Ltd
MSA Group (Pty) Ltd
Multotec (Pty) Ltd
Murray and Roberts Cementation
Nalco Africa (Pty) Ltd
Namakwa Sands(Pty) Ltd
Ncamiso Trading (Pty) Ltd
New Concept Mining (Pty) Limited
Northam Platinum Ltd - Zondereinde
PANalytical (Pty) Ltd
Paterson & Cooke Consulting Engineers (Pty) Ltd
Perkinelmer
Polysius A Division Of Thyssenkrupp Industrial Sol
Precious Metals Refiners
Rand Refinery Limited
Redpath Mining (South Africa) (Pty) Ltd
Rocbolt Technologies
Rosond (Pty) Ltd
Royal Bafokeng Platinum
Roytec Global (Pty) Ltd
RungePincockMinarco Limited
Rustenburg Platinum Mines Limited
Salene Mining (Pty) Ltd
Sandvik Mining and Construction Delmas (Pty) Ltd
Sandvik Mining and Construction RSA(Pty) Ltd
SANIRE
Sasol Mining
Sebilo Resources (Pty) Ltd
SENET (Pty) Ltd
Senmin International (Pty) Ltd
Smec South Africa
SMS group Technical Services South Africa (Pty) Ltd
Sound Mining Solution (Pty) Ltd
SRK Consulting SA (Pty) Ltd
Technology Innovation Agency
Time Mining and Processing (Pty) Ltd
Timrite Pty Ltd
Tomra (Pty) Ltd
Ukwazi Mining Solutions (Pty) Ltd
Umgeni Water
Webber Wentzel
Weir Minerals Africa
Worley Parsons RSA (Pty) Ltd

CM solutions

metallurgical consultancy & laboratories

maximizing metallurgy

Our four-in-one solution.

We do your test work,
interpret it,
model it
and integrate the results
in metallurgical designs.

Our laboratory areas of expertise

- Mineral processing
- Hydrometallurgy
- Chemical analysis
- Process development
- Solid liquid separation
- Pyrometallurgy

CM SOLUTIONS IS AN
ISO 9001:2008
ACCREDITED COMPANY
Certificate 91215729,
audited by DEKRA GmbH, Stuttgart

T 011 608 0019
F 011 608 4067
C 082 441 2788
E consultants@cm-solutions.co.za

Pinelands Office Park
Unit T5, 1 Ardeer Road
Modderfontein, 1609
South Africa

Find us on www.cm-solutions.co.za

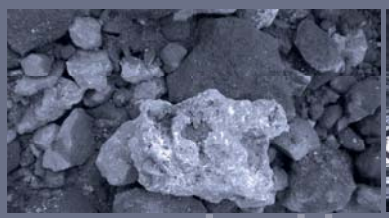


conductivity leaching test rig calcining wet chemistry sulfides shaking agitation electrowinning filtration furnace ion exchange open tanks roasting solvent extraction batch tests milling DMS pressure oxidation TCLP cyclone Isotherms PSD pilot plant cathode kinetics cell design flocculant screening flotation crushing ICP-OES crushing pyrometallurgy cyanidation attritioning water analysis thickening pressure oxidation heap pH control solid liquid separation

New Concept Mining

Support for the World's Deepest Mines

Next Generation Yielding Support

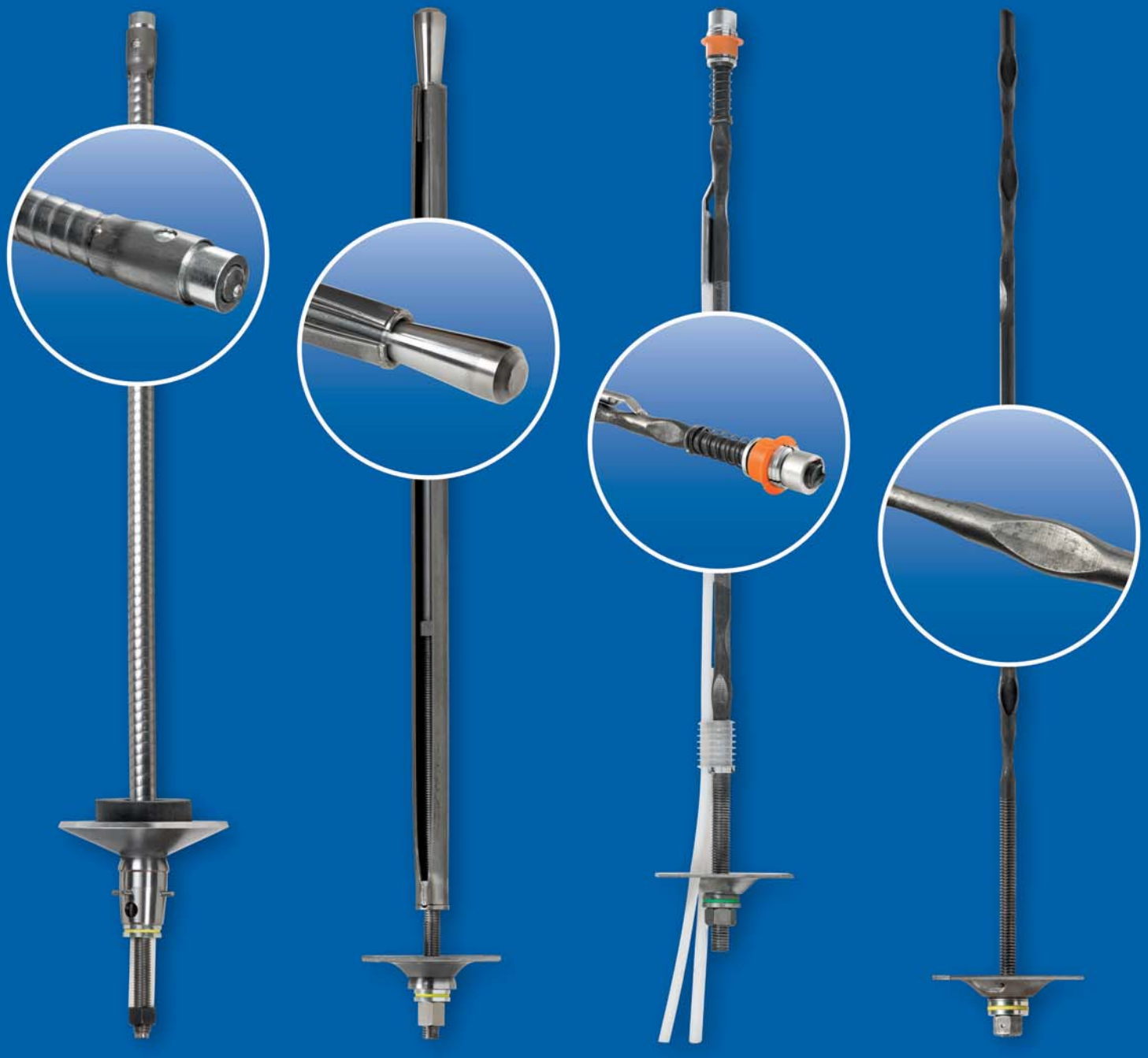

MP1 Bolt. Vulcan Bolt. Par1 Bolt. Par1 Resin Bolt.

+27 11 494 6000 www.ncm.co.za